

THE MEASUREMENT OF WIND TUNNEL FLOW QUALITY AT TRANSONIC SPEEDS

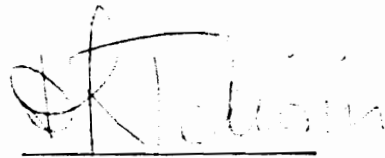
(Ph.D. Dissertation)

by

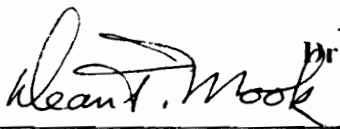
Gregory Stephen Jones

Dissertation submitted to the Faculty of the
Virginia Polytechnic Institute and State University
in partial fulfillment of the requirements for the degree of
Doctor of Philosophy
in
Department of Engineering Science and Mechanics


APPROVED



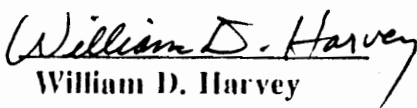
Dr. Demetrios P. Telionis



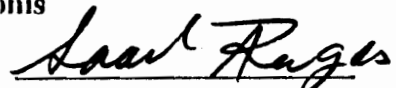
Dr. Dean T. Mook



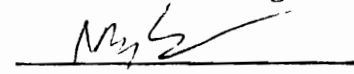
Dr. Daniel Frederick



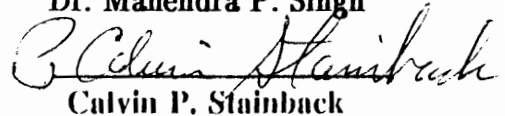
William D. Harvey



Dr. Saad A. Ragab



Dr. Mahendra P. Singh



Calvin P. Stainback

April 10, 1991
Blacksburg, Virginia

LD

5655

V856

1991

J662

C.2

The Measurement of Wind Tunnel
Flow Quality at Transonic Speeds

by

Gregory Stephen Jones

Committee Chairman: Demetri P. Telionis
Engineering Science and Mechanics

(ABSTRACT)

The measurement of wind tunnel flow quality for the transonic flow regime has been plagued by the inability to interpret complex unsteady flow field information obtained in the free stream. Traditionally hot wire anemometry and fluctuating pressure techniques have been used to quantify the unsteady characteristics of a wind tunnel. This research focuses on the application of these devices to the transonic flow regime.

Utilizing hot wire anemometry, one can decompose the unsteady flow field with a three sensor technique, to obtain fluctuations associated with the velocity, density, and total temperature. Implementing thermodynamic and kinematic equations, new methods for expanding the measured velocity, density, and total temperature fluctuations to obtain additional fluctuations are investigated. The derived static pressure fluctuations are compared to the static pressure fluctuations obtained with a conventional fluctuating static pressure probe. The results of this

comparison are good, which implies that the individual velocity, density, and total temperature components are time accurate.

In the process of obtaining a high quality fluctuating flow field information, it was necessary to evaluate the calibration of the hot wire sensors. A direct calibration approach was compared to a conventional non-dimensional technique. These two calibration techniques should have resulted in the same hot wire sensitivities. There were significant differences in the hot wire sensitivities as obtained from the two approaches. The direct approach was determined to have less errors due to the added heat transfer information required of the indirect approach. Both calibration techniques demonstrated that the velocity and density sensitivities were in general not equal. This suggests that the velocity and density information cannot be combined to form a mass flow. A comparison of several hot wire techniques was included to highlight the errors obtained when assuming that these sensitivities are the same.

An evaluation of the free stream flow quality associated with a Laminar Flow Control experiment was carried out in the Langley Research Center 8-Foot Transonic Pressure Tunnel (8' TPT). The facility was modified with turbulence manipulators and a liner that provided a flow field around a yawed super-critical airfoil that is conducive to transition research. These devices are evaluated to determine the sources of disturbances associated with the LFC experiment.

Acknowledgments

The author wishes to express his gratitude and sincere appreciation to P. Calvin Stainback for his dedication and resourcefulness throughout this project. Cal's expertise in hot wire anemometry techniques have spanned the low subsonic through hypersonic regimes which has made him a valuable resource in this research. His friendship and technical assistance have been the key to the success associated with this work.

I also find myself deeply indebted to Dr. Demetri Telionis for his patience, persistence, and technical guidance during the past decade. His friendship and guidance have encouraged me to reach beyond my limitations, and to pursue the unknown with authority.

I would also like to thank Bud Bobbitt for his vision and willingness to support the transonic hot wire efforts during the past decade. The author would also like to thank the engineering and technical staff of the 8'TPT for their resourcefulness and dedication to this effort.

Without the loving support of my wife, Doris, none of this would have been possible. Her patience and ability to hold me and my family together during the long hours required of this effort are greatly appreciated.

At last I would like to thank my mother and father, Joan & Zumie, for their encouragement and gentle persuasions that helped me finish this effort.

TABLE OF CONTENTS

1.0 INTRODUCTION	1
1.1 Background of Transonic Flow Quality Measurements	4
1.2 Hot-wire anemometer History	5
1.2.1 Indirect Hot-Wire Calibration Techniques	5
1.2.2 Direct Hot-wire Calibration Techniques	9
1.3 Application of Flow Quality to a Laminar Flow Control experiment	11
2.0 THEORETICAL CONSIDERATIONS.....	13
2.1 Theory of Flow Field Perturbations for Compressible Flows	13
2.1.1 Vorticity Analysis assuming no Sound or Entropy	18
2.1.2 Sound Analysis assuming no Velocity or Entropy	18
2.1.3 Entropy Analysis assuming no Vorticity or Sound.....	20
2.1.4 Extension of Velocity, Density, and Total Temperature fluctuations.....	21
Derivation of Mass Flow Fluctuations	23
Derivation of Static Temperature Fluctuations.....	24
Derivation of Static Pressure fluctuations.....	24
Derivation of Total Pressure fluctuations.....	25
2.1.5 Extension of Mass Flow, Pressure, and Total Temperature fluctuations	26
Derivation of Velocity and Density fluctuations	26
Extension of Single Element Fluctuating Theory	29
2.2 Theoretical Considerations of Hot-Wire Anemometry	31
2.2.1 Hot Wire Calibration Process.....	33
Direct Correlation Technique.....	35
Three-Element Calibration Theory	36
Two Element Calibration Theory	40
Single Sensor Calibration Theory	42
Indirect Correlation Technique.....	42
2.2.2 Determination of Fluctuating Parameters.....	46
Correlation of the Flow Variables	48
Three Element Fluctuation Theory.....	49
Two Element Fluctuation Theory.....	50
Single Element Fluctuating Theory	51
2.3 Theoretical Considerations for Fluctuating Pressure Probe	53
2.4 Wind Tunnel Flow Quality Manipulator Theory	62
2.4.1 Anti-Vorticity Devices.....	62
2.4.2 Anti-Sound Devices	64
2.4.3 Anit-Entropy Devices	66
2.5 LFC Theoretical Considerations	67
3.0 FACILITY AND INSTRUMENTATION	72
3.1 8'TPT Empty Wind Tunnel Configuration	72
3.2 8'TPT LFC Wind Tunnel Configuration	78
3.3 Instrumentation	84

3.3.1 Hot Wire Probes	84
3.3.2 Probes used for Fluctuating Pressure	90
3.3.3 Electronic Configuration	94
4.0 FLOW QUALITY RESULTS.....	98
4.1 Probe Calibration.....	98
4.1.1 Hot Wire Calibration Data	99
Non-dimensional Calibration Approach.....	100
Direct Calibration Approach.....	110
Comparison of the Calibration Techniques	114
Evaluation of the Hot wire sensitivities	
when $S_u = S_p$	114
Two Element Calibration.....	116
Single Element Calibration.....	119
4.1.2 Fluctuating Pressure Probe Calibration.....	123
4.2 Hot Wire Flow Field Fluctuation Data	126
4.2.1 Fluctuations vs. Mach Number	126
4.2.2 Fluctuations vs. Unit Reynolds Number.....	132
4.2.3 Correlation Coefficients	137
Extension of Measured Quantities	143
4.2.4 Hot Wire Spectra	148
4.2.5 Alternate Analysis of	
different Hot Wire Techniques.....	157
4.3 Effect of Wind Tunnel Turbulence Manipulators	168
4.4 Fluctuating Pressure Data.....	181
4.4.1 Empty Tunnel Results	181
4.4.2 LFC Fluctuating Pressure Results	197
4.4.3 Hot wire and Pressure Probe comparison.....	202
4.5 LFC Results.....	204
5.0 CONCLUSTIONS	213
5.1 Flow quality measurement techniques	213
5.2 Flow quality results.....	216
5.3 General Comments	217
6.0 REFERENCES	218
Appendix A Useful Relationships in Hot wire anemometry	223
Appendix B Derivation of Linearized Hot wire equations	229
Appendix C Derivation of Hot wire sensitivity relationships	236
Appendix D Hot wire sensitivity relationships for a cross wire	245
Appendix E Examples of different Hot wire voltages	246
Appendix F Example of heat transfer information	
required for indirect calibration	254
Vita	257

List of Figures

Figure 1.1	NASA Langley 8 Foot Transonic Pressure Tunnel	3
Figure 1.2	Heat transfer effects in the free molecular flow, slip flow, and continuum flow regime, (reference Baldwin 1958)	8
Figure 2.1	Sketch of transonic wind tunnel test section and potential sources of disturbances	15
Figure 2.2	Example of a hot wire calibration matrix for the 8'TPT	38
Figure 2.3	Theoretical Helmholtz cavity effects on the amplitude and phase of the pressure field for a typical fluctuating static pressure probe under flow conditions	58
Figure 2.4	Theoretical Helmholtz cavity effects on the amplitude and phase of the pressure field for a typical fluctuating static pressure probe under flow conditions	61
Figure 2.5	Typical boundary layer instabilities that can occur on a swept super-critical LFC airfoil	67
Figure 2.6	Calculated incompressible n-factors at transition for a swept super-critical LFC airfoil	68
Figure 3.1	Schematic of the 8'TPT	73
Figure 3.2	Empty tunnel flow quality configuration of the 8'TPT	75
Figure 3.3	Photograph of the Supercritical Laminar Flow Control Airfoil (SCLFC(1)-0513F) and Custom liner mounted in the 8'TPT Test section	77
Figure 3.4	Sketch of the LFC predicted sonic zones	80
Figure 3.5	Sketch of the Flow quality measurement locations for the LFC experiment	82
Figure 3.6	Photograph of the side wall flow quality strut and the LFC model	83
Figure 3.7	Three sensor hot wire probe and single sensor probe with shorting sensors	85

Figure 3.8	End view of sensor orientation for a typical Three sensor hot wire probe	87
Figure 3.9	Simplified diagram of a constant temperature bridge network	89
Figure 3.10	Fluctuating total pressure probe	92
Figure 3.11	Fluctuating static pressure probe	93
Figure 3.12	Fluctuating static pressure transducer natural frequency	94
Figure 3.13	Block diagram of flow quality electronic system	95
Figure 4.1	Reynolds number effect on Nusselt number at a constant Mach number	102
Figure 4.2	Comparison of corrected Nusselt number data to Baldwin's Nusselt number results (reference 1958)	103
Figure 4.3	Mach number effect on Nusselt number for constant Reynolds number in the slip flow regime, Sensor diameter 0.00015 inches.	105
Figure 4.4	Mach number effect on Nusselt number for constant Reynolds number in the continuum flow regime, Sensor diameter 0.001 inches.	106
Figure 4.5	Recovery temperature ratio	108
Figure 4.6	Comparison of the velocity and density sensitivities using the indirect calibration technique	109
Figure 4.7	Comparison of the velocity and density sensitivities using the direct calibration technique	111
Figure 4.8	Hot wire voltage correlation to mass flow for different total pressures	117
Figure 4.9	Free stream rms flow quality variations with Mach number for a LFC model configuration, P_o 1725 psf, T_o 540 R, Bandwidth $1 < \text{Hz} < 5000$	127

Figure 4.10	Free stream rms flow quality variations with Mach number for a LFC model Po: 1430 psf, To: 540 R, Bandwidth $1 < \text{Hz} < 5000$	128
Figure 4.11	Free stream rms flow quality variations with Mach number for a LFC model Po: 860 psf, To: 540 R, Bandwidth $1 < \text{Hz} < 5000$	129
Figure 4.12	Free stream rms flow quality variations with Mach number for a LFC model configuration, Po 710 psf, To 540 R, Bandwidth $1 < \text{Hz} < 5000$	130
Figure 4.13	Free stream rms velocity variations with Reynolds number for a LFC model configuration, To 540 R, Bandwidth $1 < \text{Hz} < 5000$	133
Figure 4.14	Free stream rms density variations with Reynolds number for a LFC model configuration, To 540 R, Bandwidth $1 < \text{Hz} < 5000$	134
Figure 4.15	Free stream rms total temperature variations with Reynolds number for a LFC model configuration, To 540 R, Bandwidth $1 < \text{Hz} < 5000$	135
Figure 4.16	Free stream rms mass flow variations with Reynolds number for a LFC model configuration, To 540 R, Bandwidth $1 < \text{Hz} < 5000$	136
Figure 4.17	Velocity & density correlations, velocity & total temperature correlations, and density & total temperature correlations for different Mach numbers, Po 1725 psf and To 540 R, Bandwidth $1 < \text{Hz} < 5000$	138
Figure 4.18	Velocity & density correlations, velocity & total temperature correlations, and density & total temperature correlations for different Mach numbers, Po 1430 psf and To 540 R, Bandwidth $1 < \text{Hz} < 5000$	139
Figure 4.19	Velocity & density correlations, velocity & total temperature correlations, and density & total temperature correlations for different Mach numbers, Po 860 psf and To 540 R, Bandwidth $1 < \text{Hz} < 5000$	140

Figure 4.20	Velocity & density correlations, velocity & total temperature correlations, and density & total temperature correlations for different Mach numbers, Po 710 psf and To 540 R, Bandwidth $1 < \text{Hz} < 5000$	141
Figure 4.21a	Comparison of the static temperature fluctuations due to entropy and sound, Po 1725 psf, To 540 R, Bandwidth $1 < \text{Hz} < 5000$	144
Figure 4.21b	Comparison of the static temperature fluctuations due to entropy and sound, Po 1430 psf, To 540 R, Bandwidth $1 < \text{Hz} < 5000$	145
Figure 4.21c	Comparison of the static temperature fluctuations due to entropy and sound, Po 860 psf, To 540 R, Bandwidth $1 < \text{Hz} < 5000$	146
Figure 4.21d	Comparison of the static temperature fluctuations due to entropy and sound, Po 710 psf, To 540 R, Bandwidth $1 < \text{Hz} < 5000$	147
Figure 4.22a	Mass flow spectra for a Mach number of 0.82 Po: 1430 psf, To 540 R, Bandwidth $1 < \text{Hz} < 5000$	149
Figure 4.22b	Velocity spectra for a Mach number of 0.82 Po: 1430 psf, To 540 R, Bandwidth $1 < \text{Hz} < 5000$	150
Figure 4.22c	Density spectra for a Mach number of 0.82 Po: 1430 psf, To 540 R, Bandwidth $1 < \text{Hz} < 5000$	151
Figure 4.22d	Total temperature spectra for a Mach number of 0.82 Po: 1430 psf, To 540 R, Bandwidth $1 < \text{Hz} < 5000$	152
Figure 4.23	Velocity spectra for different Mach numbers Po: 1430 psf, To 540 R, Bandwidth $1 < \text{Hz} < 5000$	154
Figure 4.24	Comparison of mass flow fluctuations for various hot wire techniques, Po 860 psf, To 540 R, Bandwidth $1 < \text{Hz} < 5000$	159
Figure 4.25	Comparison of velocity fluctuations for various hot wire techniques, Po 860 psf, To 540 R, Bandwidth $1 < \text{Hz} < 5000$	160
Figure 4.26	Comparison of density fluctuations for various hot wire techniques, Po 860 psf, To 540 R, Bandwidth $1 < \text{Hz} < 5000$	161

Figure 4.27	Comparison of total temperature fluctuations for various hot wire techniques, Po 860 psf, To 540 R, Bandwidth $1 < \text{Hz} < 5000$	162
Figure 4.28	Comparison of mass flow fluctuation for various hot wire techniques, Po 860 psf, To 540 R, Bandwidth $1 < \text{Hz} < 5000$	163
Figure 4.29	Comparison of velocity fluctuations for various hot wire techniques, Po 1430 psf, To 540 R, Bandwidth $1 < \text{Hz} < 5000$	164
Figure 4.30	Comparison of density fluctuations for various hot wire techniques, Po 1430 psf, To 540 R, Bandwidth $1 < \text{Hz} < 5000$	165
Figure 4.31	Comparison of total temperature fluctuations for various hot wire techniques, Po 1430 psf, To 540 R, Bandwidth $1 < \text{Hz} < 5000$	166
Figure 4.32	Photograph of flow quality measurement location upstream of the heat exchanger	169
Figure 4.33	Photograph of flow quality measurement location between the heat exchanger and the honeycomb	170
Figure 4.34	Photograph of the flow quality measurement location between the honeycomb and the first anti-turbulence screen	171
Figure 4.35	Photograph of the flow quality measurement location downstream of the anti-turbulence screens	172
Figure 4.36	Summary of the performance of the turbulence manipulators in the 8'TPT wind tunnel	173
Figure 4.37	Performance of the heat exchanger when acting as a anti-vorticy device, Po 1725 psf	175
Figure 4.38	Performance of the heat exchanger when acting as a anti-vorticy device, Po 710 psf	176
Figure 4.39	Performance of the anti-turbulence screens, Po 1725 psf	177
Figure 4.40	Performance of the anti-turbulence screens, Po 710 psf	178

Figure 4.41	Static pressure fluctuations at different locations in the empty wind tunnel for different Mach numbers Po 2125 psf	182
Figure 4.42	Static pressure fluctuations at different locations in the empty wind tunnel for different Mach numbers Po 1060 psf	183
Figure 4.43	Static pressure fluctuations at different locations in the empty wind tunnel for different Mach numbers Po 3180 psf	184
Figure 4.44	Comparison of 8'TPT static pressure fluctuations to other large scale transonic wind tunnels	186
Figure 4.45	Total pressure spectra for different Mach numbers Po 2125	187
Figure 4.46	Static pressure spectra for different Mach numbers Po 2125	188
Figure 4.47	Comparison of the total and static pressure spectra Mach number: 0.4, Po 2125 psf	189
Figure 4.48	The effect of choking the tunnel on wall static pressure spectra for different Mach numbers, Po 1060 psf	191
Figure 4.49	The effect of choking the tunnel on wall static pressure spectra for different Mach numbers, Po 2125 psf	192
Figure 4.50	The effect of choking the tunnel on wall static pressure spectra for different Mach numbers Po: 3180 psf	193
Figure 4.51	Comparison of wall static pressure fluctuations at different total pressures at Mach number of 0.2	194
Figure 4.52	Comparison of wall static pressure fluctuations at different total pressures at Mach number of 0.9	195
Figure 4.53	Effect of wind tunnel spoiler on static fluctuation pressure measurement at Mach number of 0.4	196
Figure 4.54	Static pressure spectra for different Mach numbers with the LFC model, Po 1430 psf	198

Figure 4.55	Static pressure spectra for different Mach numbers with the LFC model, Po 710 psf	199
Figure 4.56	Comparison of static pressure levels for the empty tunnel configuration and the LFC configuration, Po 2125 psf	200
Figure 4.57	Comparison of the static pressure spectra for different locations in the wind tunnel with the LFC model, Po 710 psf, Mach number of 0.827	201
Figure 4.58	Comparison of static pressure fluctuations derived from hot wire probe and fluctuating pressure probe	203
Figure 4.59	Theoretical and experimental pressure distributions on the supercritical LFC model	205
Figure 4.60	Calculated incompressible n-factor at transition for a swept LFC airfoil	207
Figure 4.61a	Transition detection gage location	208
Figure 4.61b	Transition detection scheme	209
Figure 4.62	Examples of transition distribution for the LFC model	210
Figure 4.63	Identified spectral velocity signatures that may instigate transition.	212

List of Tables

Table 1.1	Summary of velocity, density, and total temperature correlation coefficients using a single mode assumption	22
Table 4.1	Examples of velocity, density, and total temperature sensitivities for a three element hot wire	113
Table 4.2	Summary of correlation coefficients used in evaluating the different hot wire techniques	114
Table 4.3	Examples of Mass flow and total temperature sensitivities for a two element hot wire	118
Table 4.4	Description of assumptions for different single hot wire techniques	120
Table 4.5	Summary of single element mass flow sensitivities	122
Table 4.6	Example of fluctuating pressure transducer calibration	124
Table 4.7	Spectral signatures identified for different Mach numbers	156

Nomenclature

A	Correlation equation coefficients
C_p	Pressure coefficient
e'	Fluctuating voltage
E	Mean voltage
E	Heat stored by a hot wire sensor
H	Rate of heat loss by a hot wire sensor
h	Heat transfer coefficient
Kn	Knudsen number
k_t	Thermal conductivity
m	Mass flow
M	Mach number
Nu	Nusselt Number
r^2	Coefficient of determination
Re	Reynolds number
R_{up}	Velocity and density correlation
R_{uT_0}	Velocity and temperature correlation
R_{pT_0}	Density and temperature correlation
R_{mp}	Mass flow and pressure correlation
R_{mT_0}	Mass flow and total temperature correlation
R_{pT_0}	Pressure and total temperature correlation
R_{pu}	Pressure and velocity correlation
S_u	Velocity sensitivity
S_p	Density sensitivity

S_{T_0}	Total temperature sensitivity
S_m	Mass flow sensitivity
T_0	Total temperature
T_w	Temperature of heated wire
u	Velocity
W	Rate of heat generation of a hot wire sensor
ϵ	Calibration error
ρ	Density
γ	Ratio of specific heats
θ	Hot wire over heat parameter
θ	Angle between sound wave and axis of probe
η	Hot wire recovery temperature ratio

Subscripts

p	pressure
s	sound
v	vorticity
σ	entropy

Superscripts

'	Instantaneous values
\sim	rms values
$-$	Mean value

1.0 INTRODUCTION

During the past decade there has been an increased interest in improving the efficiency of our nation's transportation vehicles. This interest has opened up areas of research associated with transition to turbulence, turbulence, and turbulence control. One form of turbulence control is to retard transition to turbulence and maintain a laminar flow through laminar flow control. In the area of large transport aircraft design, advances in materials and aerodynamic techniques have made laminar flow control an attractive mechanism for reducing drag, thereby improving aerodynamic performance. Yet with this renewed interest in laminar flow and the transition process, the ability to set up controlled conditions in a wind tunnel environment is often limited by the quality of the flow in the wind tunnel.

The effects of the fluctuations in the free stream and their influence on the details of the boundary layer are still not clearly understood, particularly at transonic speeds. On the other hand, advances in Computational Fluid Dynamics (CFD) are producing a greater understanding of the physics of transitional flows. While the advances in CFD look promising, they must be verified through wind tunnel and/or flight experiments. One of the important flow characteristics which must be quantified to support CFD is the measurement of wind tunnel free stream flow quality at transonic speeds. Attempts to understand these physical characteristics are futile without some understanding of the measurement technique itself.

It is disappointing that wind tunnel testing has often been conducted in test-section environments that have not been adequately or consistently documented. This is particularly true when discussing flow disturbances in the freestream of transonic wind tunnels. The ability to obtain high quality flow disturbance information or "flow quality" data at transonic speeds is severely limited by the sparse measurement techniques available. Hot-wire anemometry and pressure fluctuation instrumentation have been the basis for most of the flow quality data base obtained to date. Yet these techniques have severe limitations in this speed regime, due to the inability to separate the fluctuating flow variables, such as vorticity, sound and entropy. **This dissertation focuses on the measurement and analysis of wind tunnel flow quality for the transonic flow regime using both hot-wire anemometry and fluctuating pressure probes.** This work was performed in the NASA Langley 8 Foot Transonic Pressure Tunnel (TPT), figure 1.1, which is considered to have good flow quality.

In the process of this investigation it was discovered that to date, hot-wire measurement practices in transonic flows have lead to inaccurate results. It is demonstrated here that a multiple sensor hot-wire measurement technique proposed by Stainback (1983) and expanded upon here, can overcome difficulties associated with the complex flow characteristics of the transonic flow regime. A large number of earlier methods and corresponding results are indeed largely inaccurate due to the assumptions made in the data acquisition or interpretation of the hot-wire data.

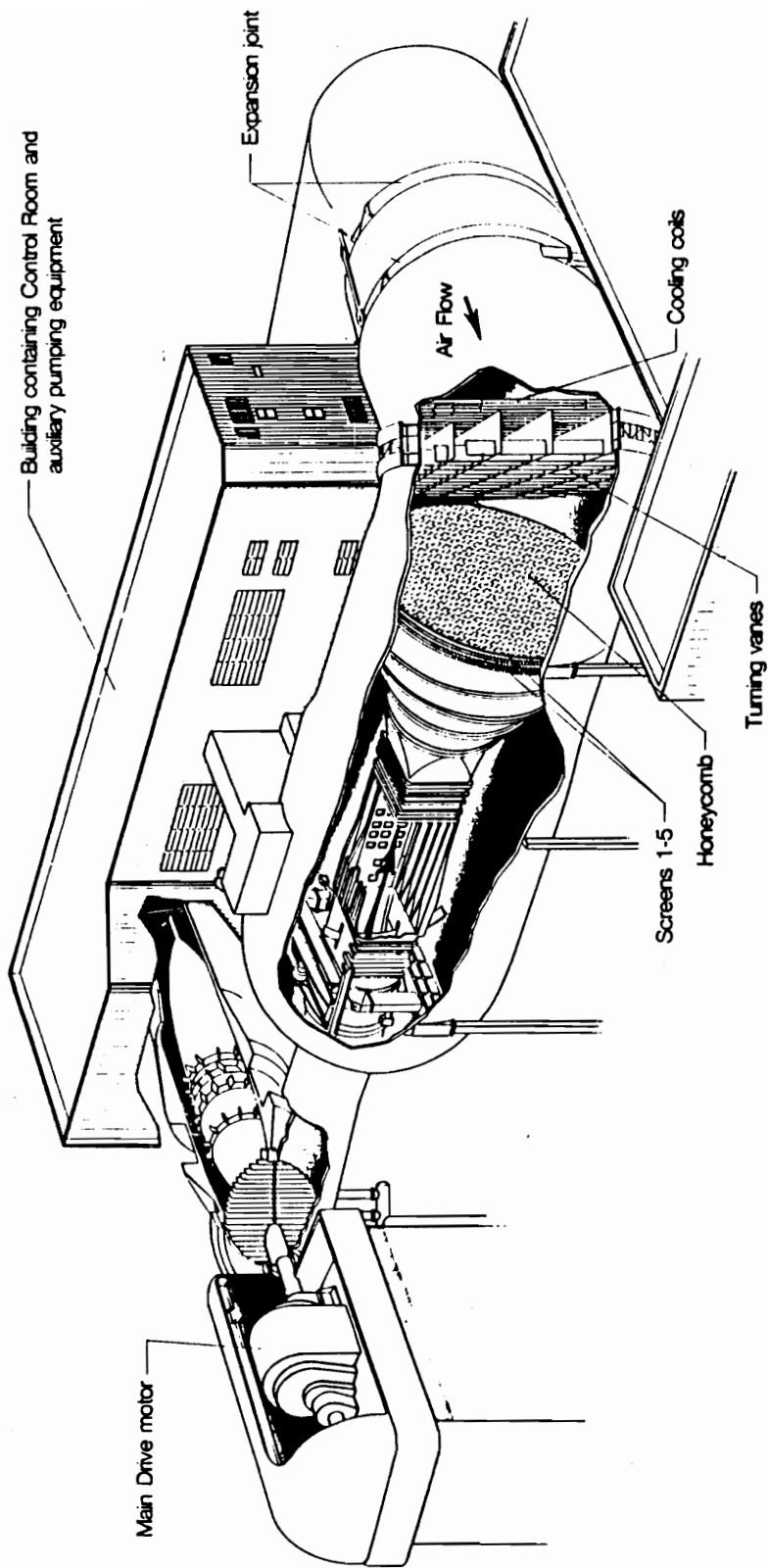


Figure 1.1 NASA Langley 8 Foot Transonic Pressure Tunnel

1.1 Background of Transonic Flow Quality Measurements

To understand flow quality at transonic speeds, it is important to define the fluctuating variables to be investigated. Historically these quantities have been described in terms of thermodynamic and kinematic variables. Kovasznay (1950) identifies the existence and nature of three "modes" for compressible flows; *vorticity, entropy, and sound*. While these three "modes" are used to define a general fluctuating flow field, it is important to recognize that the experimentalist is generally limited to hot-wire techniques which only measure velocity, density, and total temperature fluctuations. None of these quantities can be easily related to the mode variables, unless some knowledge of the sound mode is known or assumed. Morkovin (1956) indicated that certain factors or assumptions can be made concerning the sound mode and determined the relationships of the measured variables to the mode variables. In general, it is necessary for the experimentalist to measure the velocity, density, and total temperature fluctuations in the free stream, and then relate these measurements to vorticity, entropy and sound fluctuations.

Since comparisons to CFD stability or boundary layer transition results are desired, careful consideration of the influence of vorticity, entropy, and sound in the computations must be made. The CFD analyst must also consider both the level and length scales of the perturbations and relate them to the stability of the laminar boundary layer of interest. The effects of traditional assumptions, such as those made for boundary layer stability, on predicted transition results are not fully understood and are

complicated by relying on experimental data bases which do not properly account for the three co-existing modes described above.

The requirements established by theoretical and CFD specialists for experimental data bases indicate that the magnitude, frequency content, and relationship of the different fluctuating flow variables are essential. This dissertation will focus on the acquisition of this information in a transonic wind tunnel, and the evaluation of the outer flow perturbation as related to a laminar flow control experiment. The emphasis of this study will therefore be on the accuracy and repeatability of the flow quality measurements and will require an evaluation of both the hot-wire and pressure measurement techniques. It is understood that these measured flow variables are related and can be manipulated to make it possible to compare the results from both techniques.

1.2 Hot-wire anemometer History

While the theoretical developments for hot-wire measurements in the transonic flow regime were completed some 30 years ago, it is only recently that implementation of these concepts has become practical. It became possible with the advances in electronics and data reduction techniques.

1.2.1 Indirect Hot-Wire Calibration Techniques - Historically there have been two approaches in determining the hot-wire sensitivities for compressible flows. The first is an indirect approach which correlates the output of the anemometer to non-dimensional heat transfer and flow

properties. The second is a direct correlation of the anemometer outputs to velocity, density, and total temperature. Both of these approaches depend heavily on whether the sensor is being operated in the continuum flow, slip flow, or free molecular flow regimes.

The first approach or indirect technique was established for hot-wire anemometry in incompressible flows by King in 1914. His large diameter sensor was assumed to be operated in the continuum regime; therefore it was possible to correlate the heat transfer parameter with the Reynolds number and Prandtl number. King's analysis can be simplified for a constant temperature anemometer at a fixed total temperature as follows:

$$E^2 = A + BU^n$$

This is commonly referred to as "King's Law" and is used for application in low speed incompressible flows. There have been several modifications to this form which deal with the determination of the calibration coefficients A and B and the exponent n.

Kovasznay & Tormarck (1950) and Lowell (1950), independently made attempts to extend the use of hot-wire anemometry to transonic and supersonic speeds. Kovasznay (1953) first proposed the decomposition of the flow perturbation into three modes; *vorticity*, *entropy*, and *sound*. Both of the aforementioned groups related the heat transfer characteristics of a hot-wire to Reynolds number and Mach number. This suggested that King's law did not correctly express the rate of heat loss from a fine wire for compressible flows. Spangenberg (1954) confirmed this conclusion but

extended the functional variables to include Reynolds number, Mach number, and Knudsen number. McAdams (1954) correlated the data of several researchers and developed a heat transfer law that was related to Reynolds number alone.

Morkovin (1956) derived the relationships which relate the change in voltage across the wire to changes in velocity, density, and total temperature in terms of Reynolds number, Mach number, and the wire overheat ratio. Baldwin (1958) then derived the same relationships but in terms of Mach number, Knudsen number, and thermal loading characteristics of the wire. He also obtained extensive data in the slip-flow regime which extended the heat transfer data base. This work became extremely important to researchers who were able to use smaller diameter sensors which resulted in the operation of the sensor in the slip-flow regime. Figure 1.2 illustrates the relationship of the heat transfer and Reynolds number for hot-wires operated in the free molecular, slip, and continuum flow regimes. Baldwin (1958) defined the boundaries of these regimes based on the Knudsen number which correspond to:

Continuum flow : $Kn < 0.001$

Slip flow : $0.001 < Kn < 2.000$

Free Molecular flow: $Kn > 2.000$

where Knudsen number is defined as the ratio of the mean free path of the gas to the sensor diameter.

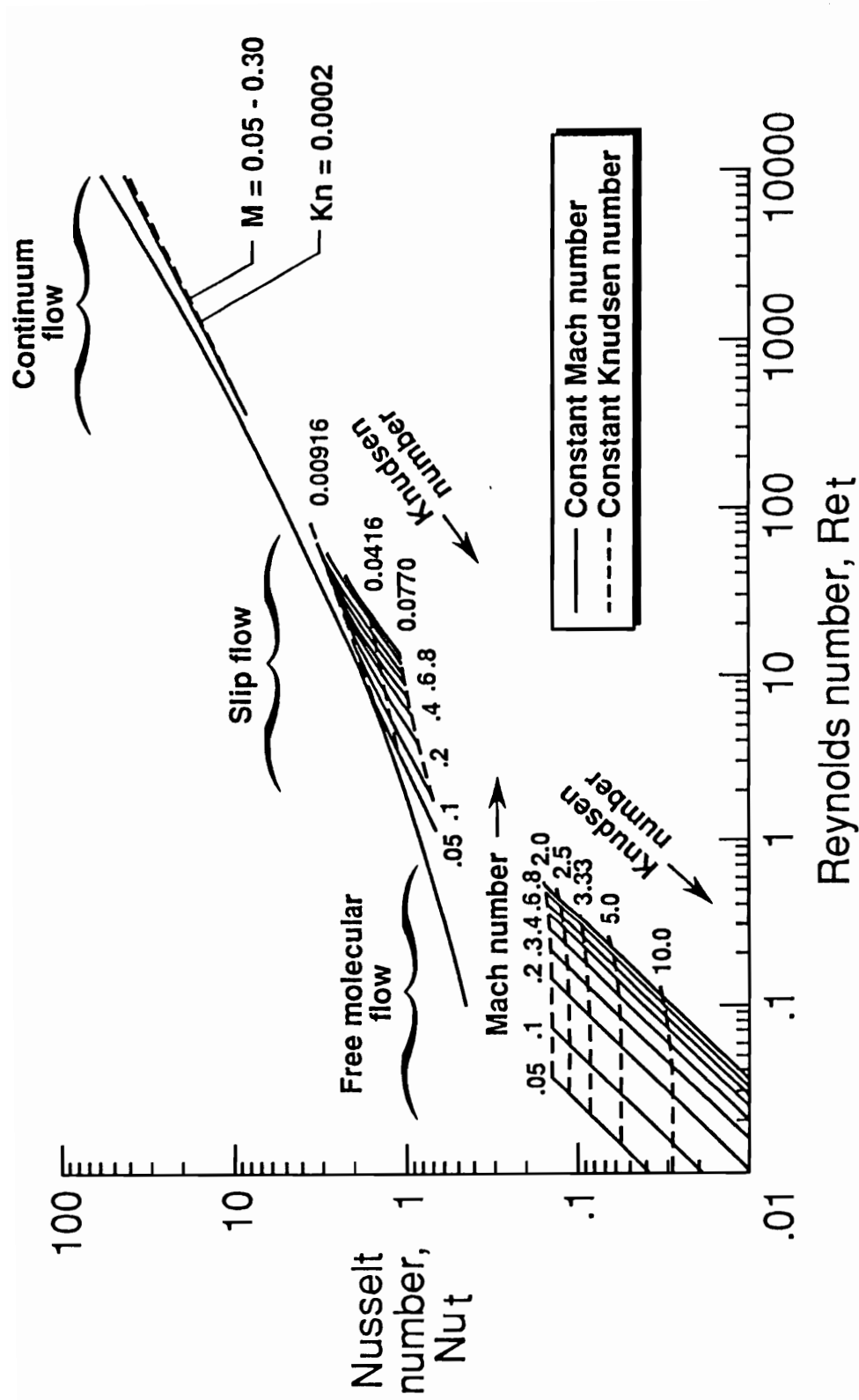


Figure 1.2 Heat transfer effects in the free molecular flow, slip flow, and continuum flow regime, (reference Baldwin 1958)

All of these indirect calibration techniques relied on similitude considerations of the heat transfer from a small heated cylinder which can be accurately correlated to the Nusselt number. In many of the early heat transfer theories used in hot-wire anemometry it was assumed that an infinite cylinder would model the characteristics of a typical hot-wire sensor. However, the relationship of Nusselt number to Reynolds number, Mach number, and Knudsen number for a heated finite wire is complicated by the heat loss to the support needles. To compare hot-wire results from different experiments, it is necessary to correct the Nusselt number data for these end losses. Even though end losses can be theoretically accounted for, it is essential to use the uncorrected data to obtain hot-wire sensitivities. The corrected data are normally only implemented when comparisons with other heat transfer data are necessary.

1.2.2 Direct Hot-wire Calibration Techniques - From 1958 until 1976 transonic hot-wire anemometry remained inactive due to difficulties in determining accurate sensitivity coefficients, as well as wire breakage and other mechanical problems associated with the high dynamic pressures incurred at transonic speeds. It was not until 1976, when a resurgence in transonic hot-wire anemometry occurred. Rose and McDaid (1976) suggested that the velocity and density sensitivities would be equal for hot-wires run at a high overheat ratio and Reynolds numbers greater than 20. This observation simplifies the transonic hot-wire equations to the well-

known supersonic hot-wire formulation where mass flow and total temperature are the measurable fluctuations .

Using a similar approach for a single element hot-wire, Horstman & Rose (1977), were able to obtain measured values for mass flow perturbation. Subsequently Otten, Pavel, Finley, & Rose (1981) extended this effort in a flight test to include measurements of mass flow and total temperature fluctuations. Resolving the two independent variables required a two element hot-wire probe. One of the critical assumptions employed for this hot-wire technique was that the velocity and density sensitivities of the sensors were equal.

Experiments by Stainback, Johnson, & Basnett (1983). utilized a three element hot-wire technique to obtain velocity, density, and total temperature perturbation. These investigations *did not* assume that the velocity and density sensitivities were equal, but attempted to calibrate the wire to determine the velocity and density sensitivities. While the differences in velocity and density sensitivities were not large, the investigators were able to calculate fluctuations in velocity, density, and total temperature. Stainback's subsequent results at transonic speeds (1986) showed that the density sensitivities were always substantially larger than the velocity sensitivities throughout the speed range. These results did not agree with results obtained by Rose & McDaid. This significant contradiction implies that further investigation into the calibration process of transonic hot-wire sensors is necessary and this issue is addressed later in this text.

Because of the above differences, transonic wind tunnel flow quality has been quantified using several different hot-wire techniques, which can

result in extremely different answers. This dissertation will address the assumptions of each of the techniques and relate them to potential problems associated with the operation of these instruments. Particular attention will be given to resolving velocity and density fluctuations from mass flow fluctuations and noting the differences in the measurements as a result of the assumptions made. The least number of assumptions related to the measurement of free stream flow quality are made by the three element technique described by Stainback, et.al (1983). As will become evident later, this technique will be used as a standard for comparison of other hot-wire results. To gain confidence in the three element hot-wire data, the three flow variables, velocity, density, and total temperature will be manipulated to obtain static pressure fluctuations which compared to the static pressure fluctuations obtained with an acoustic pressure probe.

1.3 Application of Flow Quality to a Laminar Flow Control experiment

The importance of wind tunnel flow quality is dependent on the type of testing being performed in the wind tunnel. Even in research associated with force and moments, small changes of lift and drag are often masked by adverse wind tunnel flow quality. In the area of laminar flow control research, the influence of the outer flow is thought to play a major role in the transition process. It is critical to assure that the outer flow does not contain perturbation that will cause premature transition. An evaluation of the outer flow characteristics was made with a complex laminar flow control model installed in a transonic wind tunnel.

Two laminar flow control (LFC) experiments were conducted to investigate active laminar flow control techniques on advanced supercritical airfoils. These experiments evaluated two boundary-layer suction concepts on the airfoils at conditions typical of high-performance transports with swept wings. One suction concept removed part of the boundary layer through discretely spaced, spanwise slots, and the other accomplished this by suction through perforated, spanwise strips. These concepts were investigated to determine which device was more efficient in reducing the total drag by delaying the transition of the laminar boundary with minimum suction. It is important to recognize that the physics of the transition process is extremely complicated and extends beyond the scope of this dissertation. Therefore, this research will concentrate on wind-tunnel flow quality as related to the LFC experiments. The details of the LFC experiments themselves are described by Harris & Brooks (1988), Harris, Harvey, & Brooks (1988), and Harris, Brooks, Clukey, & Stack (1989).

2.0 THEORETICAL CONSIDERATIONS

The following theoretical considerations are intended to give the reader the ability to interpret the flow quality results associated with the measurements made in the free stream of a transonic wind tunnel. Since the measurements consist of both hot-wire anemometer data and fluctuating pressure data, each technique will be discussed independently. These sections will be preceded by a general theoretical discussion on the sources of flow disturbances associated with the transonic flow regime. The last sub-section contains a brief theoretical description of the flow quality associated with a laminar flow control experiment.

2.1 Theory of Flow Field Perturbations for Compressible Flows

Before one can begin to evaluate the perturbations in a generalized flow field, it is necessary to understand the potential sources of the perturbations. It should be recognized that the velocity, density, and total temperature fluctuations are not independent, but related through the first law of thermodynamics, the mass balance equation, and the constitutive equation of the fluid. Kovasznay (1953) first proposed the decomposition of the flow perturbations into three modes: the *vorticity*, *sound*, and *entropy*. He decomposed the general velocity field into irrotational, solenoidal, and harmonic vector components. Identifying these modes in a complex flow field is extremely difficult; therefore, the following discussion is generalized for compressible flows.

The *Vorticity Mode* is characterized by the solenoidal and harmonic components of the velocity field, and therefore includes only the effect of velocity and is convected frozen-like in the streamwise direction. Potential sources for this mode, which can be found in a conventional closed circuit wind tunnel, are eddy like structures created by velocity differences in the circuit and are reduced but not eliminated by the anti-turbulence screens and honeycomb, (figure 2.1).

The *Sound Mode* is characterized by the purely irrotational velocity and includes the isentropic effect of velocity, density, and temperature, and is the only mode that involves pressure variations to the first order. This mode is radiated in all directions; therefore, pressure fluctuations in the test section can occur from both upstream and downstream sources. Typically related to acoustics, the sound generated in a closed circuit wind tunnel can be attributed to the fan, model support, shocks, heat exchangers, wall boundary layers, model wakes, wall slots, orifices or cavities in the test section or model, electric motors, and pumps or compressors connected to the operation of the facility.

The *Entropy Mode* is manifested by temperature spottiness or density fluctuations and is convected frozen-like in the streamwise direction. The potential sources for this mode are generally related to heat generating sources such as the fan and motor assembly. The cooling system is normally designed to maintain a nominal wind tunnel temperature. Yet if there are differences in heat transfer across the face of the cooler, the cooler itself may become a source for temperature spottiness.

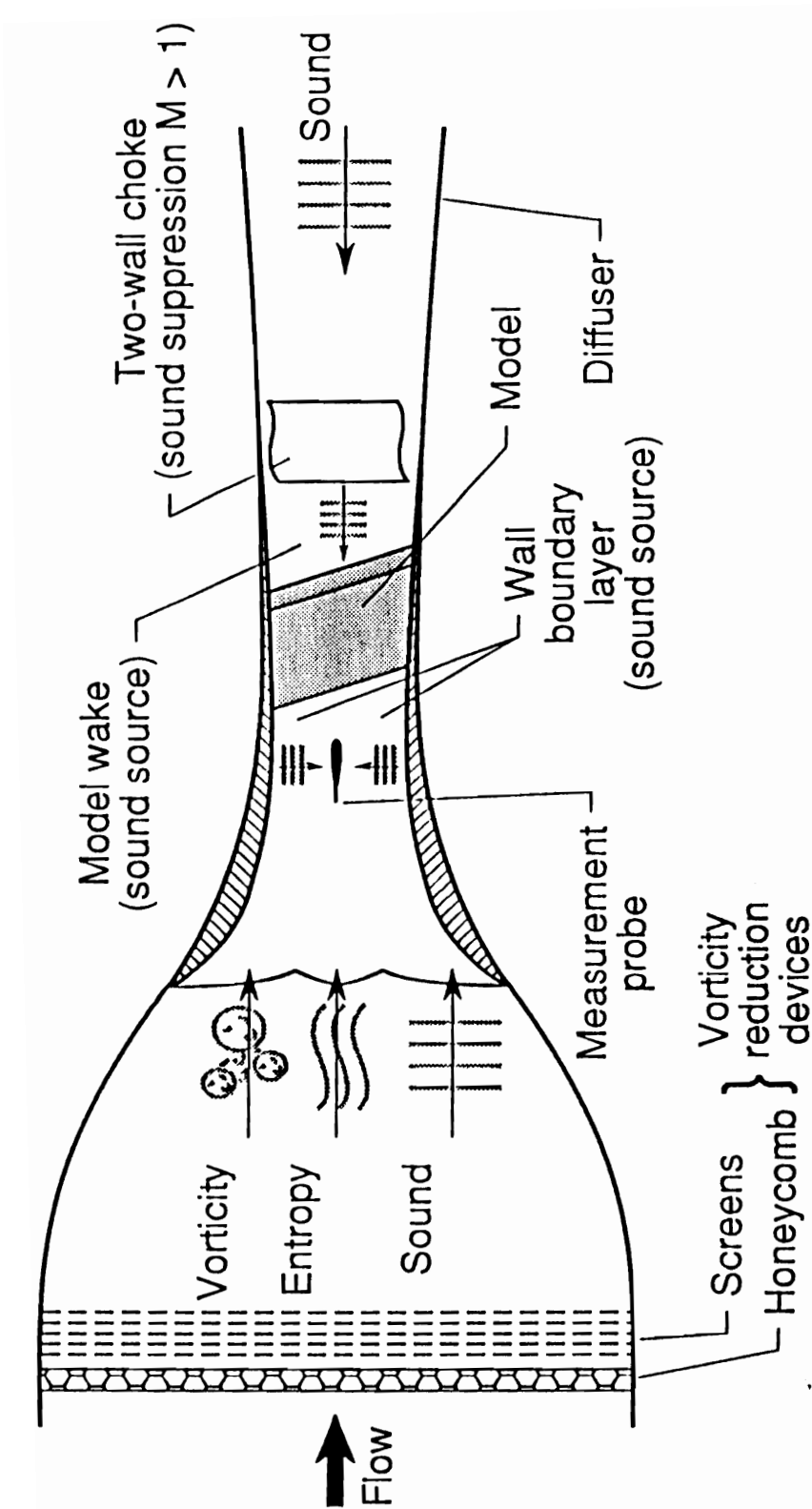


Figure 2.1 Sketch of transonic wind tunnel test section and potential sources of disturbances

Since these modes cannot be measured directly, it is necessary to relate them to the variables that can be measured. Morkovin (1956) expanded the mode concept in an elaborate derivation which related these three modes to the measured quantities of velocity, density, and total temperature fluctuations. The following section is intended to overview the relationships of measured velocity, density, and total temperature to vorticity, sound, and entropy. A small perturbation of a measured quantity will be denoted in this dissertation by a prime. It will be necessary to assume that the velocity in the streamwise direction dominates the flow field, and that the cross flow components can be neglected. This assumption affects the analysis of variables that contain total temperature and or pressure.

The velocity fluctuating field can be decomposed into perturbations due to *vorticity* and perturbations due to *sound*:

$$\frac{u'}{U} = \left(\frac{u'}{U} \right)_v + \left(\frac{u'}{U} \right)_s \quad (2.1)$$

Likewise the density fluctuating field can be decomposed into velocity perturbations due to *sound* and static temperature perturbations due to *entropy*:

$$\frac{\rho'}{\rho} = \frac{M}{\cos \theta} \left(\frac{u'}{U} \right)_s + \left(\frac{T'}{T} \right)_\sigma \quad (2.2)$$

where the angle θ is related to the direction of the sound perturbation.

Total temperature fluctuations are made up of all three perturbations, *vorticity, sound, and entropy*:

$$\frac{T_o'}{T_o} = \left(\frac{1}{1 + \frac{\gamma-1}{2} M^2} \right) \left[(\gamma-1) M^2 \left(\frac{u'}{U} \right)_v + \left(\frac{(\gamma-1) M (1 + M \cos \theta)}{\cos \theta} \right) \left(\frac{u'}{U} \right)_s + \left(\frac{T'}{T} \right)_\sigma \right] \quad (2.3)$$

Manipulating the above equations to obtain vorticity, entropy, and sound modes in terms of the measured variables of velocity, density, and total temperature fluctuation will result in:

$$\left(\frac{u'}{U} \right)_v = \left[1 + \left(\frac{\gamma-1}{\gamma} \right) (M \cos \theta) \right] \left(\frac{u'}{U} \right) - \left[\frac{\cos \theta}{\gamma M} \right] \left(\frac{\rho'}{\rho} \right) - \left[\left(1 + \frac{\gamma-1}{2} M^2 \right) \left(\frac{\cos \theta}{\gamma M} \right) \right] \left(\frac{T_o'}{T_o} \right) \quad (2.4)$$

$$\left(\frac{u'}{U} \right)_s = - \left[\left(\frac{\gamma-1}{\gamma} \right) (M \cos \theta) \right] \left(\frac{u'}{U} \right) + \left[\frac{\cos \theta}{\gamma M} \right] \left(\frac{\rho'}{\rho} \right) + \left[\left(1 + \frac{\gamma-1}{2} M^2 \right) \left(\frac{\cos \theta}{\gamma M} \right) \right] \left(\frac{T_o'}{T_o} \right) \quad (2.5)$$

$$\left(\frac{T'}{T} \right)_\sigma = - \left[\left(\frac{\gamma-1}{\gamma} \right) M^2 \right] \left(\frac{u'}{U} \right) - \left[\left(\frac{\gamma-1}{\gamma} \right) \right] \left(\frac{\rho'}{\rho} \right) + \left[\left(\frac{1}{\gamma} \right) \left(1 + \frac{\gamma-1}{2} M^2 \right) \right] \left(\frac{T_o'}{T_o} \right) \quad (2.6)$$

These equations can be used to determine the magnitude of the disturbances in the measured flow field if the sound perturbation angle is known or can be assumed. It is also possible to use the correlations of velocity, density, and temperature to gain some understanding of the sound perturbation angle which can help locate possible disturbance sources. However to do this, each mode must be analyzed individually while assuming that the other modes are zero.

2.1.1 Vorticity Analysis assuming no Sound or Entropy Effects - If all of the *fluctuations are due to vorticity*, then the cross product terms $\overline{u'\rho'}$ and $\overline{\rho'T_o'}$ are zero. Here the overbar denotes a time average of the product of the fluctuating quantities. The correlation coefficient R_{uT_o} then becomes:

$$R_{uT_o} = \frac{\overline{u'T_o'}}{\widetilde{\widetilde{u'T_o'}}} \quad (2.7)$$

which can also be expressed in terms of vorticity as:

$$R_{uT_o} = \frac{(\gamma - 1) M^2 \left(1 + \frac{\gamma - 1}{2} M^2 \right) \overline{\left(\frac{u'}{U} \right)_v^2}}{(\gamma - 1) M^2 \left(1 + \frac{\gamma - 1}{2} M^2 \right) \widetilde{\widetilde{\left(\frac{u'}{U} \right)_v^2}}} \quad (2.8)$$

This would suggest that R_{uT_o} will be +1 when the vorticity mode exists alone.

2.1.2 Sound Analysis assuming no Vorticity or Entropy Effects - Next assume that the *fluctuations are only due to sound* and that $R_{u\rho}$ can be expressed as:

$$R_{u\rho} = \frac{\overline{u'\rho'}}{\widetilde{\widetilde{u'\rho'}}} \quad (2.9)$$

which can be expressed in terms of sound fluctuation:

$$R_{u\rho} = \left[\frac{M |\cos \theta|}{M \cos \theta} \right] \frac{\left(\frac{u'}{U} \right)_s^2}{\overline{\left(\frac{u'}{U} \right)_s^2}} \quad (2.10)$$

or

$$R_{u\rho} = \frac{|\cos \theta|}{\cos \theta} \quad (2.11)$$

This expression shows that the sign of $R_{u\rho}$ depends on the value of the cosine of θ . For $0^\circ < \theta < 90^\circ$ then $R_{u\rho}$ is equal to +1. This would correspond to sound being generated in the wind tunnel settling chamber or at the wall. When $90^\circ < \theta < 180^\circ$ then $R_{u\rho}$ equals -1. This corresponds to upstream moving sound being generated by the diffuser or wind tunnel drive system. It should also be noted that R_{uT_o} too can be written in terms of sound:

$$R_{uT_o} = \left[\frac{(\gamma - 1) M (1 + M \cos \theta) |\cos \theta|}{(\gamma - 1) M (\cos \theta) (1 + M \cos \theta)} \right] \frac{\left(1 + \frac{\gamma - 1}{2} M^2 \right) \overline{\left(\frac{u'}{U} \right)_s^2}}{\left(1 + \frac{\gamma - 1}{2} M^2 \right) \overline{\left(\frac{u'}{U} \right)_s^2}} \quad (2.12)$$

or

$$R_{uT_o} = \left[\frac{(1 + M \cos \theta) |\cos \theta|}{(\cos \theta) (1 + M \cos \theta)} \right] \quad (2.13)$$

Here the sign of R_{uT_0} depends on both the value of θ and the Mach number.

For subsonic flows the quantity $(1 + M \cos \theta)$ is always > 0 and the sign of R_{uT_0} depends only in θ . Therefore for $0^\circ < \theta < 90^\circ$ R_{uT_0} is equal to +1 and when $90^\circ < \theta < 180^\circ$ R_{uT_0} is equal to -1.

The correlation of density and temperature can also be written in terms of the sound variables:

$$R_{\rho T_0} = \left[\frac{(\gamma - 1) M^2 (1 + M \cos \theta) |\cos^2 \theta|}{(\gamma - 1) M^2 (\cos \theta) (1 + M \cos \theta)} \right] \frac{\left(1 + \frac{\gamma - 1}{2} M^2\right) \overline{\left(\frac{u'}{U}\right)_s^2}}{\left(1 + \frac{\gamma - 1}{2} M^2\right) \overline{\left(\frac{u'}{U}\right)_s^2}} \quad (2.14)$$

or

$$R_{\rho T_0} = \left[\frac{(1 + M \cos \theta)}{(1 + M \cos \theta)} \right] \quad (2.15)$$

Again the sign of $R_{\rho T_0}$ depends on both the value of θ and the Mach number. For subsonic flows the quantity $(1 + M \cos \theta)$ is always positive and the sign of $R_{\rho T_0}$ depends only in θ . Therefore for $0^\circ < \theta < 90^\circ$, $R_{\rho T_0}$ is +1.

2.1.3 Entropy Analysis assuming no Vorticity or Sound Effects - If we

assume that *the fluctuations are only entropy*, then the cross product terms $\overline{u'\rho'}$ and $\overline{u'T_0'}$ are zero. The correlation coefficient related to density and total temperature become:

$$R_{\rho T_o} = \frac{\overline{\rho' T_o'}}{\widetilde{\rho T_o}} \quad (2.16)$$

or

$$R_{\rho T_o} = - \frac{\left(1 + \frac{\gamma - 1}{2} M^2\right) \overline{\left(\frac{T'}{T}\right)_\sigma^2}}{\left(1 + \frac{\gamma - 1}{2} M^2\right) \left(\widetilde{\frac{T'}{T}}\right)_\sigma^2} \quad (2.17)$$

This would suggest that $R_{\rho T_o}$ will be -1 when entropy exists. The results for R_{ρ} , R_{uT_o} , and $R_{\rho T_o}$ are summarized in Table I.

2.1.4 Extension of Velocity, Density, and Total Temperature fluctuations

Assuming that the time histories of velocity, density, and total temperature can be obtained, they can be combined to calculate quantities such as mass flow fluctuations, static temperature fluctuations, entropy, total and static pressure fluctuations. In addition, numerous cross product information can be obtained. This sub-section will provide brief derivations of these and other useful equations referred to in the text. Recall that the basic assumption required for these derivations is that the velocity fluctuations are represented by the u-component alone which has ignored the effect of the v-component and w-component of the velocity field.

Table I. Summary of Velocity, Density, and Total Temperature
Correlation Coefficients using a single mode assumption

	$R_{u\rho}$	R_{uT_o}	$R_{\rho T_o}$
Sound	$\theta = 0$	1	1
	$\theta = 180$	-1	1
Vorticity	0	1	0
Entropy	0	0	-1

Mass Flow Fluctuations expressed in terms of Velocity and Density

fluctuations - The mass flow fluctuation can be derived by differentiating the following equation:

$$m = \rho U \quad (2.17)$$

to obtain the instantaneous perturbation equation:

$$\frac{m'}{m} = \frac{\rho'}{\rho} + \frac{u'}{U} \quad (2.18)$$

Squaring equation 2.18 and taking the mean results in:

$$\left(\frac{\widetilde{m'}}{\widetilde{m}}\right)^2 = \left(\frac{\widetilde{\rho'}}{\widetilde{\rho}}\right)^2 + \left(\frac{\widetilde{u'}}{\widetilde{U}}\right)^2 + 2 \text{Ru}\rho \left(\frac{\widetilde{u'}}{\widetilde{U}}\right)\left(\frac{\widetilde{\rho'}}{\widetilde{\rho}}\right) \quad (2.19)$$

The mass flow fluctuations can be obtained from either equation 2.18 or 2.19, however, if spectra are desired equation 2.18 must be used. These results will be valid for other equations derived in this section. Note that the correlation coefficients for the velocity and density fluctuations were established by equation 2.11.

Derivation of Static Temperature Fluctuations described in terms of Velocity, and Total Temperature fluctuations - The static temperature fluctuations can be obtained from the Energy equation:

$$T_o = T + \frac{1}{2} \left(\frac{U^2}{C_p} \right) \quad (2.20)$$

Differentiating and normalizing gives:

$$\frac{T'}{T} = \frac{T_o}{T} \frac{T_o'}{T_o} - (\gamma - 1) M^2 \left(\frac{u'}{U} \right) \quad (2.21)$$

and squaring and taking the mean results in the static temperature equation as follows:

$$\left(\frac{\tilde{T}}{T} \right)^2 = \left(\frac{T_o}{T} \right)^2 \left(\frac{\tilde{T}_o}{T_o} \right)^2 + (\gamma - 1)^2 M^4 \left(\frac{\tilde{u}}{U} \right)^2 - 2(\gamma - 1) M^2 \frac{T_o}{T} R_u T_o \left(\frac{\tilde{u}}{U} \right) \left(\frac{\tilde{T}_o}{T_o} \right) \quad (2.22)$$

Derivation of Static Pressure fluctuations described in terms of Velocity, Density, and Total Temperature fluctuations - The static pressure fluctuations can be obtained from the equation of state ($P = \rho RT$) again by differentiation theory:

$$\frac{p'}{P} = \frac{\rho'}{\rho} + \frac{T'}{T} \quad (2.23)$$

Substituting the above equation into equation 2.21 gives the instantaneous static pressure:

$$\frac{p'}{\bar{P}} = \frac{\rho'}{\bar{\rho}} + \frac{T_o}{\bar{T}} \frac{T_o'}{\bar{T}_o} - (\gamma - 1) M^2 \frac{u'}{\bar{U}} \quad (2.24)$$

Squaring and taking the mean results in:

$$\begin{aligned} \left(\frac{\tilde{p}}{\bar{P}}\right)^2 &= \left(\frac{\tilde{\rho}}{\bar{\rho}}\right)^2 + (\gamma - 1)^2 (M)^4 \left(\frac{\tilde{u}}{\bar{U}}\right)^2 + \left(\frac{T_o}{\bar{T}}\right)^2 \left(\frac{\tilde{T}_o}{\bar{T}_o}\right)^2 + 2 \left(\frac{T_o}{\bar{T}}\right) (R\rho T_o) \left(\frac{\tilde{\rho}}{\bar{\rho}}\right) \left(\frac{\tilde{T}_o}{\bar{T}_o}\right) \\ &\quad - 2(\gamma - 1)(M)^2 (R\rho u) \left(\frac{\tilde{\rho}}{\bar{\rho}}\right) \left(\frac{\tilde{u}}{\bar{U}}\right) - 2(\gamma - 1)(M)^2 \left(\frac{T_o}{\bar{T}}\right) (Ru T_o) \left(\frac{\tilde{u}}{\bar{U}}\right) \left(\frac{\tilde{T}_o}{\bar{T}_o}\right) \end{aligned} \quad (2.25)$$

Derivation of Total Pressure fluctuations described in terms of Velocity,

Density, and Total Temperature fluctuations - The total pressure fluctuation can be obtained from the following equation by differentiation followed by the use of equations 2.21 and 2.22.

$$\frac{P_o}{P} = \left[1 + \left(\frac{\gamma - 2}{2} \right) (M)^2 \right]^{\frac{\gamma}{\gamma - 1}} \quad (2.26)$$

to give the equation for the instantaneous total pressure fluctuation equation:

$$\left(\frac{P_o'}{\bar{P}_o}\right) = \left(\frac{\rho'}{\bar{\rho}}\right) + \left(\frac{2 - M^2}{2}\right) \left(\frac{T_o'}{\bar{T}_o}\right) + (M)^2 \left(\frac{u'}{\bar{U}}\right) \quad (2.27)$$

Squaring and taking the mean of equation 2.27 gives:

$$\begin{aligned} \left(\frac{\widetilde{P_o}}{P_o}\right)^2 = & \left(\frac{\widetilde{\rho}}{\rho}\right)^2 + (M)^4 \left(\frac{\widetilde{u}}{U}\right)^2 + \left(\frac{2-M^2}{2}\right)^2 \left(\frac{\widetilde{T_o}}{T_o}\right)^2 + (2-M^2)(R\rho T_o) \left(\frac{\widetilde{\rho}}{\rho}\right) \left(\frac{\widetilde{T_o}}{T_o}\right) \\ & + 2(M)^2(R\rho u) \left(\frac{\widetilde{\rho}}{\rho}\right) \left(\frac{\widetilde{u}}{U}\right) + 2(2-M^2)(M)^2(RuT_o) \left(\frac{\widetilde{u}}{U}\right) \left(\frac{\widetilde{T_o}}{T_o}\right) \end{aligned} \quad (2.28)$$

2.1.5 Extension of Mass Flow, Pressure, and Total Temperature

fluctuations - For some applications of hot-wire anemometry, the mass flow and total temperature fluctuation data have been reported. Once the mass flow, static pressure, and total temperature fluctuations have been obtained, they can be combined to calculate quantities such as velocity fluctuations and density fluctuations. This sub-section will provide brief derivations of these and other useful equations referred to in the text.

Derivation of Velocity and Density fluctuations expressed in terms of mass flow, static pressure, and total temperature - The following derivation is applicable for one and two sensor hot-wire techniques. It should be recognized that the phase relationship of velocity and density play a major role in the formulation of mass flow fluctuations, see equation 2.18. If one can establish this relationship, by either making assumptions about density fluctuations or by making an independent measurement of pressure which can be related to the density fluctuations, then it is possible to separate the components of mass flow perturbations. The phase relationship of velocity and density is in general related to the sound sources of the wind tunnel. For most wind tunnels it is reasonable to expect sound being generated in the diffuser and heat exchangers which is often located in the settling

chamber region of the facility. The diffuser noise is most apparent and can often be identified when fan blade passing frequency is found in the test section or when a sonic region exists in the test section and the sound levels are reduced. Since these sound sources vary from wind tunnel to wind tunnel, it is difficult to generalize about the phase relationship of velocity and density.

Once the instantaneous mass flow, total temperature, and static pressure information are obtained, the velocity and density fluctuating components can be written as.

$$\frac{u'}{U} = \left[\frac{1}{1 + (\gamma - 1) M^2} \right] \frac{m'}{m} + \left[\frac{1 + \frac{(\gamma - 1)}{2} M^2}{1 + (\gamma - 1) M^2} \right] \frac{T_o'}{T_o} - \left[\frac{1}{1 + (\gamma - 1) M^2} \right] \frac{p'}{P} \quad (2.29)$$

and

$$\frac{\rho'}{\rho} = \left[\frac{(\gamma - 1) M^2}{1 + (\gamma - 1) M^2} \right] \frac{m'}{m} - \left[\frac{1 + \frac{(\gamma - 1)}{2} M^2}{1 + (\gamma - 1) M^2} \right] \frac{T_o'}{T_o} + \left[\frac{1}{1 + (\gamma - 1) M^2} \right] \frac{p'}{P} \quad (2.30)$$

Squaring and taking the mean gives:

$$\left(\frac{\tilde{u}}{U} \right)^2 = \frac{\left(\frac{\tilde{m}}{m} \right)^2 + \left(\frac{\tilde{p}}{P} \right)^2 + \left(\frac{T_o}{T} \right)^2 \left(\frac{\tilde{T_o}}{T_o} \right)^2}{[1 + (\gamma - 1) M^2]^2} \quad (2.31)$$

and

$$\left(\frac{\widetilde{\rho}}{\overline{\rho}}\right)^2 = \frac{((\gamma-1)^2 M^4 \left(\frac{\widetilde{m}}{\overline{m}}\right)^2 + \left(\frac{\widetilde{p}}{\overline{p}}\right)^2 + \left(\frac{T_o}{T}\right)^2 \left(\frac{\widetilde{T_o}}{\overline{T_o}}\right)^2)}{[1 + (\gamma-1) M^2]^2} \quad (2.32)$$

where the correlations R_{mp} , R_{mT_o} , R_{pT_o} have been neglected.

While Harvey, Stainback, & Owen (1980) have used equations 2.31 and 2.32, it should be noted that equation 2.29 can be re-written for the instantaneous mass flow fluctuations which would be a function of velocity, total temperature and static pressure. Squaring, taking the mean, and solving for the mean square velocity term would result in the following equation:

$$\left(\frac{\widetilde{u}}{\overline{U}}\right)^2 = \frac{\left(\frac{\widetilde{m}}{\overline{m}}\right)^2 - \left(\frac{\widetilde{p}}{\overline{p}}\right)^2 - \left(\frac{T_o}{T}\right)^2 \left(\frac{\widetilde{T_o}}{\overline{T_o}}\right)^2}{[1 + (\gamma-1) M^2]^2} \quad (2.33)$$

where it is assumed that $R_{pu} = R_{uT_o} = R_{pT_o} = 0$. A similar approach to the density equation (equation 2.30) will result in:

$$\left(\frac{\widetilde{p}}{\overline{p}}\right)^2 = \frac{((\gamma-1)^2 M^4 \left(\frac{\widetilde{m}}{\overline{m}}\right)^2 - \left(\frac{\widetilde{p}}{\overline{p}}\right)^2 - \left(\frac{T_o}{T}\right)^2 \left(\frac{\widetilde{T_o}}{\overline{T_o}}\right)^2)}{[1 + (\gamma-1) M^2]^2} \quad (2.34)$$

where the cross product terms were neglected.

Comparing equations 2.31 and 2.32 with equations 2.33 and 2.34, and noting the sign change on the pressure and temperature terms, illustrates the significance of neglecting the cross product terms in the equations. It is assumed that this cross product information, which is typically disregarded, compensates for the sign changes in the equations above. Since the two equation sets are theoretically equivalent the importance of the correlations terms are highlighted by the difference in the equations above. The major impact that these assumptions will have on the results obtained with a two element hot-wire probe is described later in the text.

Extension of Single Element Fluctuating Theory: - The ability to extend single element hot-wire data beyond mass flow information also requires the assumption that the static pressure fluctuations vanish or the pressure fluctuation must be measured. It is also necessary to assume that the temperature contribution, i.e. the product of the temperature sensitivity and the total temperature fluctuation, is much smaller than the mass flow contribution, i.e. the product of the mass sensitivity and the mass flow fluctuation. This allows equations 2.29 and 2.30 to be rewritten as:

$$\left(\frac{\tilde{u}}{\bar{U}}\right)^2 = \frac{\left(\frac{\tilde{m}}{\bar{m}}\right)^2 + \left(\frac{\tilde{p}}{\bar{P}}\right)^2}{[1 + (\gamma - 1) M^2]^2} \quad (2.35)$$

$$\left(\frac{\tilde{p}}{\bar{p}}\right)^2 = \frac{(\gamma - 1)^2 M^4 \left(\frac{\tilde{m}}{\bar{m}}\right)^2 + \left(\frac{\tilde{p}}{\bar{P}}\right)^2}{[1 + (\gamma - 1) M^2]^2} \quad (2.36)$$

It should be noted that equations 2.33 and 2.34 can be manipulated in a similar manner resulting in the subtraction of the pressure term. The validity of these equations and assumptions as related to interpreting flow quality physics will be discussed later.

2.2 Theoretical Considerations of Hot-Wire Anemometry - It is important to recognize that the operation of the hot wire anemometer is dependent on the flow regime in which it is being operated. There are three basic regimes in which the hot wire can operate and they are identified as "*continuum flow*", "*slip flow*", and "*free molecular flow*" regimes. They are defined in terms of the relative size of the hot wire sensor to the mean free path of molecules of the flow. For incompressible, continuum flow conditions and for supersonic flow, ($M > 1.2$), the hot wire heat loss can be related to mass flow and the total temperature. The intermediate case of subsonic slip flow and/or free molecular flow is complex and difficult to correlate to any single flow variable. The Knudsen number is a dimensionless flow parameter, defined as the ratio of the molecular mean free path to wire diameter, and used to determine which flow regime the wire is being operated. The boundaries for these different regimes are not well defined and conditions exists when testing in the "transonic flow regime" to warrant investigation in both the "continuum flow" regime and the "slip flow" regime.

It is generally accepted that the hot wire anemometer responds to any changes in the variables characterizing the kinematic or thermodynamic properties of the fluid in which it is immersed. These changes alter the rate of heat transfer between the hot wire element and the surrounding fluid. For correct interpretation of the mean and fluctuating electronic signals from the anemometer it is necessary to consider the influence of:

- (1) the effects of vorticity, sound, and entropy**
- (2) the laws of heat transfer between the fluid and the wire**
- (3) the laws governing the variation of resistance of the given wire with temperature and air loading**
- (4) the response of the associated electrical system.**

The variables in category one are in general the parameters that the researcher is exploring. Since the signals from the anemometer are sensitive to all of the variables mentioned in these four categories it is necessary to understand the relationship of the last three categories to the first. The remainder of this section will focus on these relationships and assumptions that make it possible to interpret anemometer outputs.

The general theory of operation of a heated wire is based not only upon the sensitive elements dependence on electrical resistivity, but also upon the laws of thermodynamics and heat transfer. There are some differences between the derivation of the theory for "constant temperature" and "constant current" anemometry. The focus of this work will be directed to the "constant temperature" approach. The basic, linearized hot wire equation for constant temperature anemometry can be represented by the relationship of output voltage to sensor sensitivities and flow variables as:

$$\frac{e'}{E} = S_u \frac{u'}{U} + S_\rho \frac{\rho'}{\rho} + S_{T_o} \frac{T_o'}{T_o} \quad (2.54)$$

where S_u , S_ρ , and S_{T_0} are the sensitivities of the sensor and the primed quantities represent the fluctuating flow variables or variations in voltages from the anemometer, (see appendix B for derivation).

This equation indicates that the fluctuating voltage output depends only on fluctuations in velocity, density, and total temperature and their corresponding sensitivities. Before one can combine the information of any multiple-element hot wire system it is essential to evaluate the sensitivities of each individual sensor. The sensitivity coefficients S_u , S_ρ , and S_{T_0} can be obtained using several different approaches. Two approaches will be addressed in this text, a "Direct" approach and "Indirect" approach.

2.2.1 Hot Wire Calibration Process - Regardless of the number of hot wire sensors utilized in any given probe *each sensor must be calibrated independently*. As shown in Appendix B the mean voltage measured across a heated wire mounted normal to the flow and operated with a constant temperature anemometer in compressible flows is governed by the following functional relationship:

$$E = f(U, \rho, T_o) \quad (2.55)$$

This may be represented in the non-dimensional form by:

$$E = f(Nu, Re, M, \theta) \quad (2.56)$$

where Nusselt number is related to the convective heat transfer characteristics of a fine wire; Reynolds number related to the ratio of inertial forces to the viscous forces of the local fluid surrounding the wire; Mach number is related to the compressibility effects on the wire; and the

overheat ratio is related to the temperature difference of the wire and the fluid surrounding the wire.

The ability to calibrate a hot wire element using one approach or the other will be determined by the flexibility of the calibration facility. To determine the sensitivities it is paramount to be able *to independently control each of the aerodynamic variables* on the right side of equation 2.54, which represents the foundation for the "Direct Correlation" approach promoted by Stainback, et al (1983). This is being termed a "Direct" approach since the required variables are obtained directly from classic wind tunnel information and subsequently correlated to measured mean anemometer voltages. This is believed to minimize the errors in the final analysis due to the simplicity of the correlation. The formulation utilizing equation 2.3 has been promoted by Kovasznay (1954), Morkovin (1958), and Anders (1974) for constant current anemometry and Morkovin & Phinney (1958), Rose (1973) for constant temperature anemometry. This approach was developed primarily for general compressible flows and took it's form because of the limitations of the wind tunnel calibration facilities. *Since the relationships of equations 2.55 and 2.56 represent the heat loss laws for hot wire anemometry, the resulting velocity, density, and total temperature sensitivities should be the same as derived from either approach.* The focus of this research utilizes the "Direct Correlation" method unless otherwise noted. The "Indirect Correlation" approach will be used as a check on the calibration accuracy of the "Direct Correlation" method.

Direct Correlation Technique - The total change in the voltage due to changes in the flow variables for a constant temperature anemometer is:

$$dE = \left(\frac{\partial E}{\partial U} \right)_{\rho, T_o, T_w} dU + \left(\frac{\partial E}{\partial \rho} \right)_{U, T_o, T_w} d\rho + \left(\frac{\partial E}{\partial T_o} \right)_{U, \rho, T_w} dT_o \quad (2.57)$$

If the application of the above equation is limited to small perturbations and normalized the following instantaneous equation results:

$$\frac{e'}{\bar{E}} = S_u \frac{u'}{\bar{U}} + S_\rho \frac{\rho'}{\bar{\rho}} + S_{T_o} \frac{T_o'}{\bar{T_o}} \quad (2.58)$$

where the coefficients on the right hand side depend on derivatives of voltage as described below. The three unknown variables in this equation are velocity fluctuations, density fluctuations, and total temperature fluctuations. All of the other parameters are measured or can be calculated. To simplify this equation the product of the sensitivity and flow variable must be negligible for one or two of the terms. Before one can make any simplifying assumptions it is necessary to evaluate the three sensitivity coefficients. For the direct calibration approach the sensitivities can be written:

$$S_u = \left[\frac{\partial(\log E)}{\partial(\log U)} \right]_{\rho, T_o, T_w} \quad (2.59)$$

$$S_\rho = \left[\frac{\partial(\log E)}{\partial(\log \rho)} \right]_{U, T_o, T_w} \quad (2.60)$$

$$S_{T_o} = \left[\frac{\partial(\log E)}{\partial(\log T_o)} \right]_{U, \rho, T_w} \quad (2.61)$$

Thus the hot wire sensitivities are related to the change in voltage across the heated wire as a function of the three flow variables, velocity, density, and total temperature. The velocity sensitivity can be obtained by measuring the mean voltage and correlating it to the velocity while holding density and total temperature constant. Similarly the density sensitivity can be obtained by measuring the mean voltage and correlating it to the density while holding velocity and total temperature constant. In like manner the total temperature sensitivity can be obtained by measuring the mean voltage and correlating it to the total temperature while holding velocity and density constant.

Since the voltage across a single hot wire element is a function of velocity, density, and total temperature, it is necessary to make simplifying assumptions or to utilize additional elements if fluctuations are to be measured. The following sections will address both of these options. In the experiments described here we will utilize two different types of hot wire probes, one which contains three elements and the other having just a single element. We also include a comparison of the results obtained with these probes, in addition to a two element case derived from utilizing two of the three sensors on the three element probe. The theory to support these comparisons is as follows.

Three-Element Calibration Theory - The three-element approach is the most general of the hot wire techniques and requires the fewest assumptions. The basic concept is to utilize three hot wire sensors to solve for the three unknown variables, velocity, density, and total temperature identified in equation 2.58. Therefore the most critical requirement of this

technique is a calibration facility that can independently vary velocity, density, and total temperature. The assumptions required for this technique are related to the general hot wire theory as noted above.

To utilize expressions given by equations 2.59 - 2.61 the test data must be obtained at very specific conditions, i.e.. constant velocity, constant density, and constant total temperature. Such a test matrix would require timely changes in the density, total temperature, and Mach number of the facility. This tedious process extends the wind tunnel time required to calibrate a hot wire probe, which increases the possibility of breaking a sensor. Figure 2.2 shows an example of a wind tunnel test matrix where the total pressure is varied to change density. In general this does not result in a data set where density has been held constant for a given Mach number or total temperature. While this is more efficient from the wind tunnel operational point of view, it does not satisfy the requirements for the sensitivity equations. However, the data can be correlated by using a multiple linear regression analysis technique to satisfy the constraints placed on the sensitivity equations.

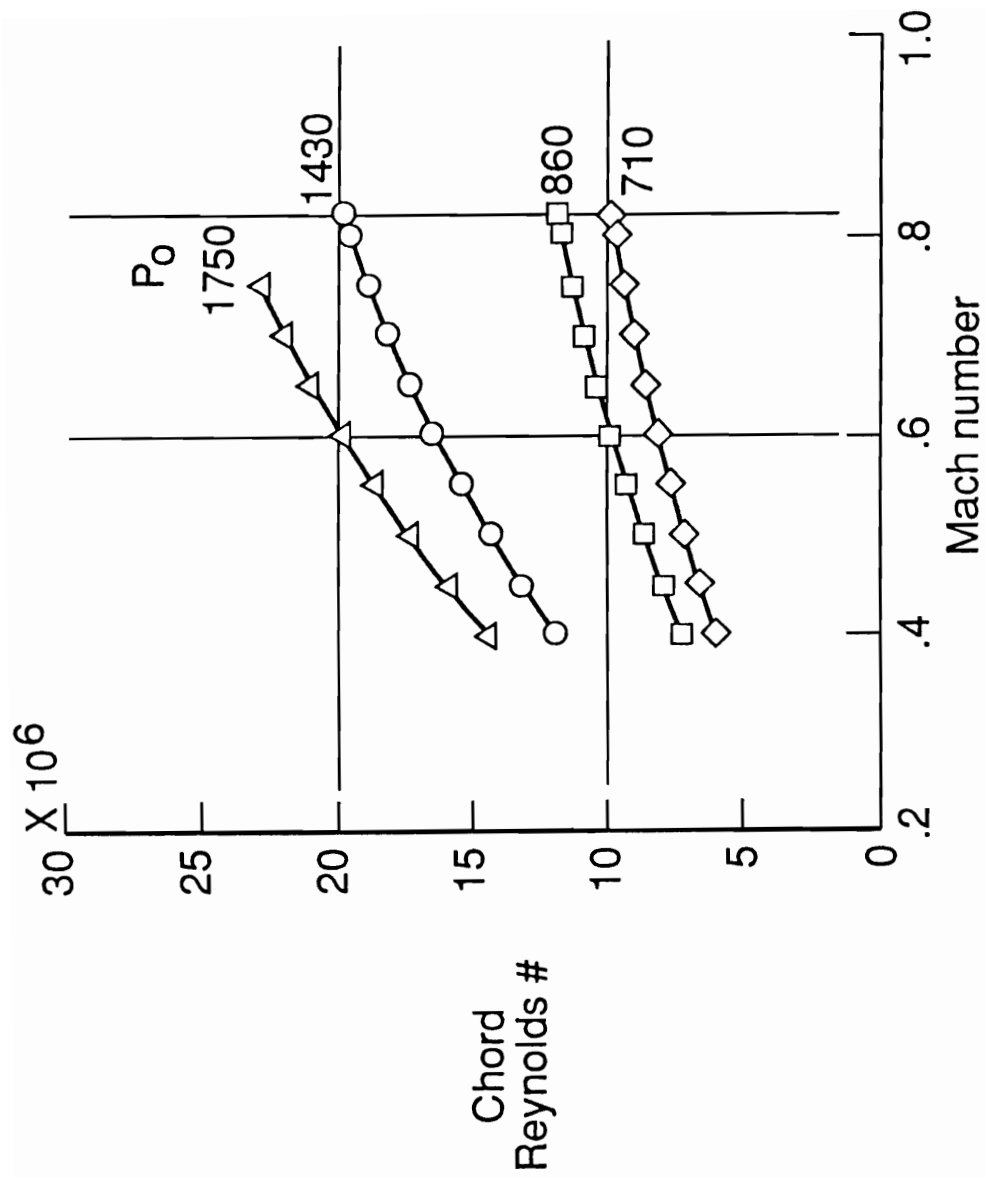


Figure 2.2 Example of a hot wire calibration matrix for the 8'TPT

The mean voltages for each of the sensors of the hot-wire probe, as measured over a range of velocity, density, and total temperature, were independently correlated using a multiple linear regression technique. The criterion for selecting the best regression equation from the set of all possible regression equations is to compute an estimate of the error. Statistically this error can be evaluated by examining the coefficient of determination, r^2 . By examining in detail the models that have the highest r^2 values, it can be seen that there was some consistent pattern that suggested the number and identity of the variables to include in the model. One problem with using r^2 as a criterion for the best-fitting regression equation is that r^2 itself increases for each independent variable. While r^2 values were always greater than 0.99 there could still be a possible formulation that would result in a better correlation and reduce errors.

Choosing the proper form of the correlation equation to be used with the multiple linear regression technique can be tedious, however, an equation that appears to be adequate is:

$$\begin{aligned} \log (E) = & A_1 + A_2 \log (U) + A_3 \log (\rho) + A_4 \log (T_o) \\ & + A_5 [\log (U) \log (\rho)] + A_6 [\log (U) \log (T_o)] \\ & + A_7 [\log (\rho) \log (T_o)] + A_8 [\log (U) \log (\rho) \log (T_o)] \end{aligned} \quad (2.62)$$

Using equation 2.62 as the correlation model, the sensitivity equations can be computed from equations 2.59, 2.60, and 2.61, resulting in:

$$S_u = A_2 + A_5 \log(\rho) + A_6 \log(T_o) + A_8 \log(\rho) \log(T_o) \quad (2.63)$$

$$S_p = A_3 + A_5 \log(U) + A_7 \log(T_o) + A_8 \log(U) \log(T_o) \quad (2.64)$$

$$S_{T_o} = A_4 + A_6 \log(U) + A_7 \log(\rho) + A_8 \log(U) \log(\rho) \quad (2.65)$$

Two Element Calibration Theory - As noted in the previous section, the hot wire will respond to changes in three flow variables; velocity, density, and total temperature. **To be able to combine the velocity and density and form a mass flow sensitivity**, it is necessary to show that the *velocity sensitivity equals the density sensitivity*, $S_u = S_p$. This has been experimentally determined for supersonic flow and assumed for low subsonic flows. To prove for each individual sensor that $S_u = S_p$, an elaborate calibration scheme which can independently control the three flow variables is necessary. The calibration requirements for the two element would therefore be the same as the calibration requirements for the individual elements of the three element probe.

In general $S_u \neq S_p$, as will be shown later. However, when the researcher can experimentally determine or assume that $S_u = S_p$ then equation 2.58 can be simplified for a two sensor probe to:

$$\left(\frac{e'}{E}\right) = S_m \left(\frac{m'}{m_\infty}\right) + S_{T_o} \left(\frac{T_o'}{T_o}\right) \quad (2.66)$$

where mass flow fluctuation is sum of the velocity and density fluctuations, (equation 2.18). The sensitivities in the above equation are:

$$S_m = \left[\frac{\partial \log E}{\partial \log (\rho U)} \right]_{T_o, T_w} \quad (2.67)$$

$$S_{T_o} = \left[\frac{\partial \log E}{\partial \log (T_o)} \right]_{m, T_w} \quad (2.68)$$

Correlation equations for the two element calibration will utilize the same form as described by equation 2.62 with the exception that the mean voltages will be correlated with mass flow and total temperature. This results in:

$$\log (E) = A_1 + A_2 \log (m) + A_3 \log (T_o) + A_4 \log (m) \log (T_o) \quad (2.69)$$

The sensitivities can then be obtained from equation 2.67 and 2.68:

$$S_m = A_2 + A_4 \log (T_o) \quad (2.70)$$

$$S_{T_o} = A_3 + A_4 \log (m) \quad (2.71)$$

The mean voltages can also be correlated with mass flow and total temperature without using the cross product term in equation 2.69. This results in:

$$S_m = A_2 \quad (2.72)$$

$$S_{T_o} = A_3 \quad (2.73)$$

Single Sensor Calibration Theory - To develop the compressible flow theory for a single element hot wire may seem somewhat arbitrary since one must reduce the three flow variables to just one. In an effort to couple the low subsonic and transonic regimes with the single sensor theory, several assumptions are necessary. It is the opinion of the author that most of these assumptions have no physical bases and in general will result in misguided efforts.

Making the same assumptions as for the two sensor theory ($S_u = S_p$) and ignoring all temperature terms, equation 2.69 becomes:

$$\log (E) = A_1 + A_2 \log (m) \quad (2.75)$$

The mass flow sensitivity then is constant and given by the following equation:

$$S_m = A_2 \quad (2.76)$$

This creates a dilemma when trying to correlate the data set as will be seen later.

Indirect Correlation Technique - Throughout the early days of hot wire anemometry the ability to calibrate a wire accurately depended on the calibration facility available. This was particularly true for researchers working in higher speed flows or with gases other than air. Morkovin (1955) developed a very elegant non-dimensional theory for constant current anemometry in terms of Nusselt number, Mach number, Reynolds

number and hot wire temperature parameters. Following Morkovin's analogy the hot wire sensitivities for a constant temperature anemometer become:

$$S_u = \frac{1}{2} \left[\left(\frac{\partial \log Nu}{\partial \log Re} \right)_{M,\theta} + \left(\frac{1}{\alpha} \right) \left(\frac{\partial \log Nu}{\partial \log M} \right)_{Re,\theta} - \left(\frac{\eta}{\tau \alpha} \right) \left(\frac{\partial \log \eta}{\partial \log M} \right)_{Re,\theta} - \left(\frac{\eta}{\tau} \right) \left(\frac{\partial \log \eta}{\partial \log Re} \right)_{M,\theta} \right] \quad (2.77)$$

$$S_p = \frac{1}{2} \left[\left(\frac{\partial \log Nu}{\partial \log Re} \right)_{M,\theta} - \left(\frac{\eta}{\tau} \right) \left(\frac{\partial \log \eta}{\partial \log Re} \right)_{M,\theta} \right] \quad (2.78)$$

$$ST_o = \frac{1}{2} \left[\chi_\mu \left(\frac{\partial \log Nu}{\partial \log Re} \right)_{M,\theta} + \left(\frac{1}{2\alpha} \right) \left(\frac{\partial \log Nu}{\partial \log M} \right)_{Re,\theta} - \left(\frac{\eta}{2\tau \alpha} \right) \left(\frac{\partial \log \eta}{\partial \log M} \right)_{Re,\theta} + \left(\frac{\eta}{\tau} \right) + \left(\frac{\partial \log Nu}{\partial \log \theta} \right) - \left(\frac{\partial \log k_t}{\partial \log T_o} \right) - \left(\chi_\mu \right) \left(\frac{\eta}{\tau} \right) \left(\frac{\partial \log \eta}{\partial \log Re} \right)_{M,\theta} \right] \quad (2.79)$$

A brief description and derivation of these sensitivities are found in Appendix C.

To evaluate these sensitivities it is important to recognize that the heat transfer has been characterized by Nusselt Number. Since heat loss due to radiation can generally be ignored for hot wire anemometry the convection and conduction must be analyzed. Many researchers, McAdams (1954), Van der Vijnen (1956), Kramer (1959), Collis & Williams (1959), Loch & Gartshore (1972) to name a few, have tried to experimentally relate these convection and conduction properties to form an empirical heat transfer relationship.

The character of the convective heat-transfer law for hot wire anemometry, the so-call generalized King's law, is expressed in terms of dimensionless variables:

$$Nu = f\left(M, Re, \theta, \phi, \frac{L}{d}, \text{wire properties}\right)$$

where ϕ is the flow angle relative the a yawed wire and L/d is used to relate the heat losses to the sensor supports. The Nusselt number is a dimensionless heat transfer parameter and is defined as:

$$Nu = \frac{hd}{k_t} \quad (2.80)$$

where h is the heat transfer coefficient, d is the characteristic length, and k_t is the thermal conductivity of the air defined at the total temperature.

For an infinitely long hot wire (no end conduction losses) that is heated electrically, the energy balance is as follows:

$$\frac{dE}{dt} = W - H \quad (2.81)$$

where E is defined as *Stored Heat* by the sensor, W is the rate of *Heat Generation* or the electrical power supplied to the sensor, and H is the *rate of Heat Loss* to the surrounding fluid. This energy balance formulation neglects heat conduction and radiation effects from the sensor.

The heat loss to the surrounding fluid, H , is normally given by the relation

$$H \equiv q = h A (T_w - T_{Adw}) \quad (2.82)$$

where A is the cylinder surface area and T_w is the wire temperature and T_{Adw} is the adiabatic wall temperature. Because of the aerodynamic heating of the sensor associated with compressible flows it is convenient to introduce the recovery factor, η . This factor relates the recovery temperature of the sensor due to aerodynamic heating to the total temperature. Re-writing the heat loss equation 2.82 in terms of Nusselt number and recovery temperature yields:

$$H \equiv q = Nu \pi L k_t (T_w - \eta T_o) \quad (2.83)$$

It should be noted that the recovery temperature ratio (η) is in general a function of Knudsen number (but could be expressed in terms of Reynolds number instead of Knudsen number) and Mach number. For the range of Knudsen numbers for the current research, η was determined to be independent of Reynolds number and only a function of Mach number. This simplifies the sensitivities equations 2.77, 2.78, 2.79. Data obtained from Vrebalovich (1962) was used to determine the recovery temperature ratio coefficients (See Appendix A).

The rate of Heat generation from equation 2.81 can be written in terms of the electrical power ($I^2 R_w$ or E^2 / R_w). Considering the steady state case, where $dE / dt = 0$, using equation 2.81 and 2.83 Nusselt number can be written:

$$Nu = \frac{\text{Electrical Power}}{[\pi L k_t (T_w - \eta T_o)]} \quad (2.84)$$

where the electrical power for a constant temperature bridge circuit is:

$$\text{Electrical Power} \equiv \frac{E^2 R_w}{(R_{\text{top}} + R_{\text{lead}} + R_w)^2} \quad (2.85)$$

This accounts for the circuit resistance which is the sum of the sensor resistance, R_w , lead resistance, R_{lead} , and fixed "top" resistor in the bridge, R_{top} .

The present approach therefore emphasizes that in any given calibration the primary information for the computation of the Nusselt numbers is contained in the measured voltages, resistances, and tunnel temperatures. In other words, at a given point in the flow, the basic information resides in the variation of wire resistance R_w .

If the researcher wants to compare his results with other researchers Nusselt number data, the end losses to the wire supports must be accounted for. However the uncorrected Nusselt number must be used to calculate the sensitivities. The reader is referred to page 219 of Sandborn (1972) for a description of the Nusselt number corrections due to conduction to the wire supports.

2.2.2 Determination of Fluctuating Parameters - Having determined the hot wire sensitivities we need to discuss how to use them to obtain the fluctuating flow field information. Before beginning the discussion on the fluctuating variables, we consider two important factors:

1. Frequency response (or length scale limitations)
2. Correlation of the flow variables (Vorticity, Sound, Entropy)

The concepts associated with frequency response of a hot wire system are associated with the electronic response of the anemometer, the processing bandwidth, and the wire geometry itself. The limitations for a typical hot wire system are related to the length scales of the flow field. The low frequency limit of the system is a function of the long length scales associated with the meandering of the flow. These length scales can be on the order of several feet. The high frequency limit is generally related to micro eddies or structures characterized by the Kolmogoroff length scale, (λ). The characteristic time related to the Kolmogoroff length scale (λ) is:

$$\tau_{\text{Kolmogoroff}} = \frac{\lambda}{\overline{U}} \quad (2.86)$$

The "System Time Constant", τ_{System} , is composed of two principle parts, a "Spatial Time Constant", τ_{Spatial} , and a "Electronic Time Constant", $\tau_{\text{Electronic}}$. In order to be capable of measuring the full spectrum of length scales the researcher must ensure that $\tau_{\text{System}} < \tau_{\text{Kolmogoroff}}$ where the system response will be the larger of the two aforementioned time constants.

The "Spatial Time Constant" can be defined by

$$\tau_{\text{Spatial}} = \frac{L_{\text{Sensor}}}{\overline{U}} \quad (2.87)$$

where the sensor length will be the maximum length of the wire. For a multiple element probe, the sensor length will be the diagonal dimension of

the wire supports. For a single element probe the sensor length will be the wire length itself.

The "Electronic Time Constant" ($\tau_{\text{Electronic}}$) of the hot wire is a function of the anemometer feedback amplifier and the wire geometry. According to Kovasznay (1954) the length scale resolution, or the smallest disturbance to be measured without attenuation is

$$\ell_{\text{Resolution}} = \frac{U}{2 n_{\text{max}}} \quad (2.88)$$

where n_{max} is the maximum frequency of the amplifier system at which there is no appreciable loss of response. The resolution length must be small compared to the micro scales of the flow. Since $\tau_{\text{Electronic}}$ is inversely proportional to n_{max} then $\ell_{\text{Resolution}}$ is proportional to $\tau_{\text{Electronic}}$.

In order to resolve a micro scale perturbation (0.070 inches) typical of the three element probes at Mach = 0.90 the dynamic frequency response of the electronic system must be compensated to 150 kHz.

Correlation of the Flow Variables - The measurements made with a hot wire are influenced by vorticity, sound, and entropy. In general, the researcher cannot measure these variables. The correlation coefficients, $R_{u\rho}$, R_{uT_0} , and $R_{\rho T_0}$, can sometimes be used to determine the major contribution of the basic fluctuations, vorticity, entropy, or sound, to the measured fluctuations of velocity, density, and total temperature. If it is assumed that the fluctuations are exclusively due to either vorticity,

entropy, or sound, the values for the correlation coefficients can be obtained as shown in Section 2.1.2 and as presented in Table I. Note that these measurements require the information of all three flow variables and thus this fact dictates the need for the three element hot wire system.

Three Element Fluctuation Theory - Attempts have been made to measure the fluctuations in U , ρ , and T_o by using a probe with three wires mounted normal to the flow and operated at different overheats to separate the sensitivities. This leads to the following system of equations:

$$\begin{bmatrix} \left(\frac{u'}{U_\infty} \right) \\ \left(\frac{\rho'}{\rho_\infty} \right) \\ \left(\frac{T_o'}{T_o} \right) \end{bmatrix} = \begin{bmatrix} (Su)_1 & (S\rho)_1 & (ST_o)_1 \\ (Su)_2 & (S\rho)_2 & (ST_o)_2 \\ (Su)_3 & (S\rho)_3 & (ST_o)_3 \end{bmatrix}^{-1} \begin{bmatrix} \left(\frac{e'}{E} \right)_1 \\ \left(\frac{e'}{E} \right)_2 \\ \left(\frac{e'}{E} \right)_3 \end{bmatrix} \quad (2.89)$$

where the sensitivity matrix has been predetermined for this particular wind tunnel condition. The voltage matrix represents the time histories of the three different sensors on the hot wire probe. To solve this set of simultaneous equations it is necessary to ensure the simultaneous digitization of the three instantaneous voltages across the three elements of the hot-wire probe. These three instantaneous voltages will be used to solve for the instantaneous velocity, density, and total temperature. This process will be repeated for the entire time history of the flow for that particular

condition. Standard statistical analysis can then be implemented to determine the rms magnitudes of the fluctuating flow variables .

The condition of the matrix can be determined by evaluating the condition number of the matrix. Haftka (1990) indicated that the condition number is representative of the upper bound of the amplification of errors through the matrix. What constitutes a good condition number seems to be somewhat arbitrary since for many structural applications the condition number may run into the millions. It is also necessary to ensure that the inverse of the sensitivity matrix is well conditioned. For the sensitivity matrices that were determined for the experiment described by this research a check of the sensitivity coefficient matrix revealed that the inverse of the inverse matrix resulted in the original matrix to within 2 parts in 10^{10} . A second check of the condition of the inverse matrix was to multiply the original sensitivity matrix by its inverse. This resulted in the unity matrix within 2 parts in 10^{10} . Therefore, the matrices of the sensitivity coefficients appeared to be very well conditioned. Once the above matrix operation is solved for the instantaneous velocity, density, and total temperature fluctuations, standard statistical techniques can be applied in both the time and frequency domain to obtain rms quantities, cross products, and spectral information.

Two Element Fluctuation Theory - As noted in section 2.2.1, before we can combine the velocity and density perturbation to form a mass flow perturbation it is necessary to show that the velocity sensitivity equals the

density sensitivity. $S_u = S_p$. Once this has been done then equations 2.66, 2.67 and 2.68 can be used for a two element probe to write:

$$\begin{bmatrix} \left(\frac{m'}{m_\infty} \right) \\ \left(\frac{T_o'}{T_o} \right) \end{bmatrix} = \begin{bmatrix} (S_m)_1 & (S_{T_o})_1 \\ (S_m)_2 & (S_{T_o})_2 \end{bmatrix}^{-1} \begin{bmatrix} \left(\frac{e'}{E} \right)_1 \\ \left(\frac{e'}{E} \right)_2 \end{bmatrix} \quad (2.90)$$

As in the three element case, special attention must be given to the simultaneous measurement of the instantaneous voltages required to solve the above set of equations. Time histories of mass flow and total temperature can be calculated. The rms values and cross product of the mass flow and total temperature can then be obtained.

Single Element Fluctuating Theory - To develop the compressible flow theory for single element hot wire anemometry, one must reduce the three flow variables, for which the wire will respond, to one flow variable. Some researchers have accomplished this by making the assumptions that:

$$S_m \left(\frac{m'}{m} \right) \gg S_{T_o} \left(\frac{T_o'}{T_o} \right) \quad (2.91)$$

in addition to $S_u = S_p$. This results in the wire voltage being a function of only one fluid variable:

$$\frac{m'}{m} = \frac{1}{S} \frac{e'}{E} \quad (2.92)$$

from which $\frac{m'}{m}$ can be obtained directly.

2.3 Theoretical Considerations for Fluctuating Pressure Probe

The measurement of time dependent pressure has been described in detail through the study of acoustics, or the science of sound, by many recognized experts. This section is not intended to review the history, or details of acoustics as related to the aerospace industry, but to highlight several factors that are important in the measurement of pressure fluctuations at transonic speeds. Sound can be thought of as mechanical vibrations in gaseous, fluid, or solid media. Such vibrations are characterized by their amplitude, their frequency, and their phase.

To characterize the magnitude of the vibration, several mathematical quantities may be considered. The RMS (root-mean-square) value is the most commonly used because of its direct relation with the energy content of the signal in linear systems. It is defined as:

$$A_{\text{RMS}} = \sqrt{\frac{1}{T} \int_0^T a^2(t) dt} \quad (2.93)$$

where $a(t)$ is the time varying amplitude of a pure tone signal. For a pure tone or a sinusoidal variation, the relationship of the RMS to the peak amplitude may be described by:

$$A_{\text{RMS}} = \frac{1}{\sqrt{2}} A_{\text{PEAK}} = \frac{1}{F_c} A_{\text{PEAK}} \quad (2.94)$$

where F_c is the crest factor.

Most sounds are generally complex and random in nature. This non-stationary condition has lead to the concept of amplitude density which is substituted for the single tone condition because the different possible amplitude values can occur with a certain "density" when the phenomenon is studied statistically over a period of time. The amplitude density can be related to the standard deviation (RMS deviation) from the mean and is and is integrated over the band width of interest

$$\sigma \equiv A_{\text{RMS}} = \sqrt{\frac{1}{T} \int_0^T x^2(t) dt} \quad (2.95)$$

If a medium is set into vibration, the disturbances propagate away from the place of their origin. Physically, the propagation may be thought of as the transfer of momentum from one molecule to the next. Due to the elastic bonds between the molecules, the propagation is considered to take the form an elastic motion. The time which the disturbance takes to propagate through the medium is defined as the *wave speed*. Plane sound waves propagate with a speed (U_p) that is proportional to the wind tunnel velocity (U) and the speed of sound (a):

$$U_p = U \pm a$$

Note that due to the finite speed which a disturbance can propagate through a medium, the disturbance can be defined as *wave* where the time scale of the original vibration is can be transformed into a length scale. This length

scale is define as the *wavelength* which corresponds to one period of vibration.

$$\lambda = cT$$

More often this relationship is given in the form of an equation connecting the wavelength to the vibration frequency.

$$\lambda = \frac{c}{f}$$

When dealing with broadband disturbances, such as those associated with wind tunnel noise, the wavelength is difficult to define because no single disturbance signature may occur at a frequency which can be easily distinguished from another.

Analyzing the power spectral density in the frequency domain of a typical free stream flow quality experiment, it can be easily seen that the data is broad band. Ideally the most accurate representation of the fluctuating flow field would be to include the frequency information from DC (or the average mean value) to an infinite frequency. This approach is impractical due to the limits of the electronic system used to acquire the fluctuating data. Electronic filtering of the data is necessary to optimize the signal to noise ratio of the transducer and can be critical to the amplitude and frequency information being analyzed. Integrating the power spectral density will result in the mean square magnitude of the disturbances.

The implementation of a high pass filter will eliminate the low frequency, high energy information associated with the flow. For subsonic and transonic wind tunnel applications the low frequency portion of the spectra contains the largest portion of the energy. The importance of this low frequency information may be associated with the lack of data repeatability of in some buffet, flutter, or other force and moment types of testing. For the experiments related to boundary layer or free shear layer the coupling of the low frequency information is not fully understood, yet it is believed to play a significant factor in the receptivity process. Because of the digitizing process it is necessary to use a low pass or anti-aliasing filter. Care must be used in setting this filter so the high frequency information that may be tied to boundary layer transition or other stability-related flow phenomena is not eliminated.

The construction and orientation of the fluctuating pressure probe will also play a role in determining the amplification or elimination of flow field pressure information being measured. The diaphragm, differential type pressure transducer can be configured to respond to a small changes in pressure with a linear electrical output. The frequency response of this transducer is primarily a function of the diaphragm diameter and membrane material. Assuming that these transducers have a flat amplitude response across the frequency range of interest, the other factors that significantly influence the transducer output is the support mechanism of the diaphragm and the orientation to the flow.

When the transducer is large with respect to the measurement probe, it is often necessary to relocate the transducer to an remote location.

For a typical total pressure or static pressure probe, recessing the transducer into a cavity and coupling the transducer to an orifice with a tube may be necessary. Ideally the pressure perturbation at the orifice would propagate through the coupling to the transducer membrane without any attenuation or amplification. However, there is a time delay and amplitude change at the transducer membrane due to the cavity which was created by the coupling. The cavity of the orifice and tubing, forms a Helmholtz resonator. The natural frequency of the cavity depends on the length and volume of the coupling to the transducer membrane and is described by Morse (1948) and Pierce (1981).

When the transducer and coupling is configured for static pressure fluctuation measurements, the Helmholtz cavity frequency response can be affected by the flow of air across or perpendicular to the orifice. Tijderman (1977) has developed a theory for calculating the response of a recess-mounted pressure transducer including the effects of flow over the static orifice. Marcolini, et.al. (1991) describe the application of this theory to recess-mounted static pressure transducers and showed that for the no flow condition, the Tijderman-Bergh calculation of probe frequency response was in good agreement with experimental amplitude ratio results. This favorable result gave some confidence that corrections could be implemented to compensate for the Helmholtz effects of the probes used in this experiment.

Figure 2.3 shows an example of a typical Helmholtz effect of a static pressure probe under flow conditions at atmospheric conditions. The overall effect resulting from the Helmholtz cavity would be to amplify

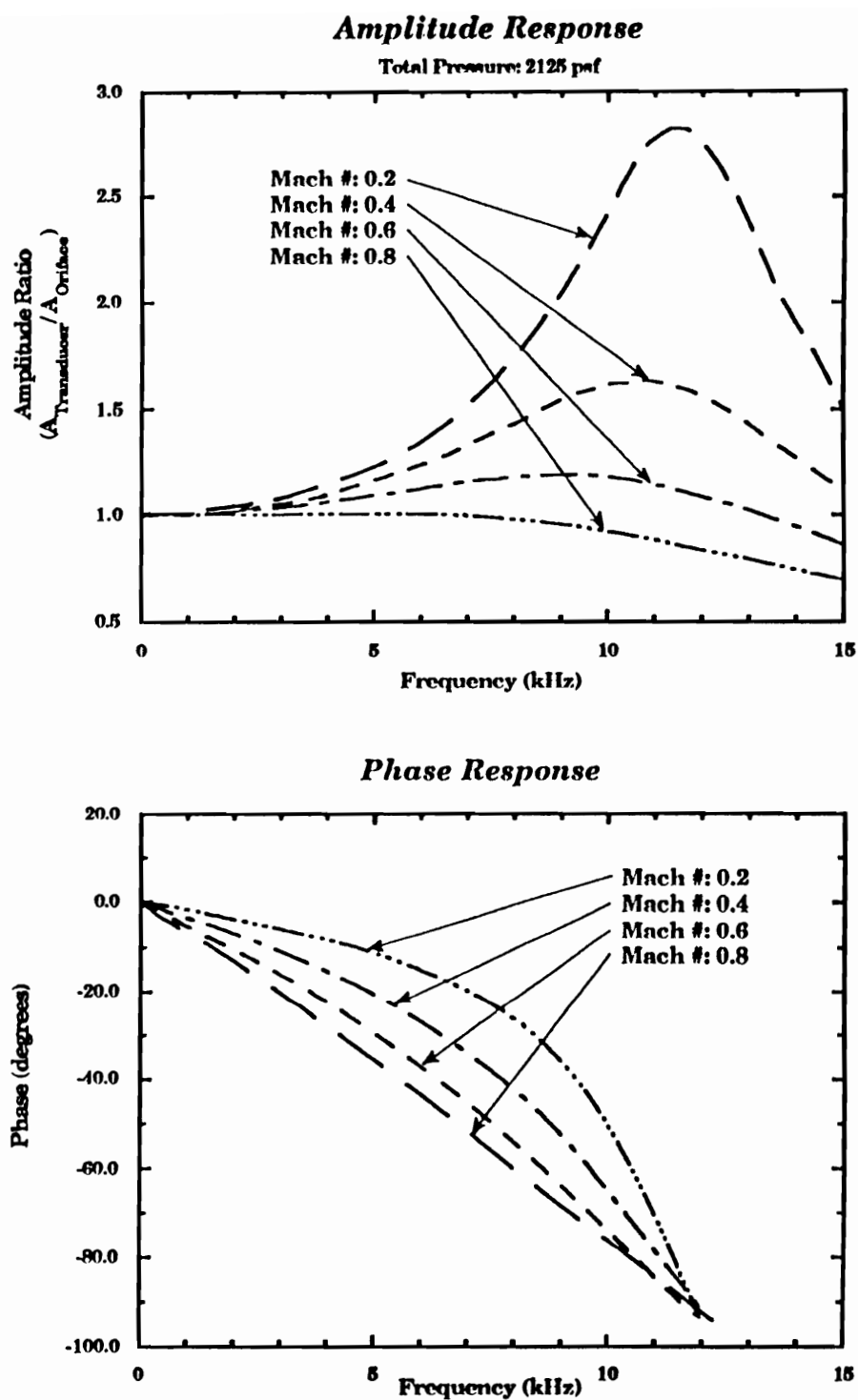


Figure 2.3 Theoretical Helmholtz cavity effects on the amplitude and phase of the pressure field for a typical fluctuating static pressure probe under flow conditions,

(or attenuate) and phase shift the pressure information, particularly at the higher frequencies. At the low Mach numbers there is an overall amplification of the pressure at the transducer membrane. This effect decreases as the Mach number increases, which corresponds to a lowering of the static pressure at the orifice face. At a Mach number of 0.8 the effect of the Helmholtz cavity was the attenuation of the pressure pressure field measured at the transducer membrane. This is expected to have an overall attenuation of the rms values at this Mach number. Figure 2.4 shows a similar effect of flow over the orifice for the same probe configuration but at a lower wind tunnel total pressure. The magnitude of the amplification is less for the lower static pressure condition.

To compensate for the Helmholtz effect, a pressure correction can be theoretically determined which is based on the amplitude ratios shown in figure 2.3 and 2.4, which would be applied to the data in the frequency domain. The power spectral density would then be integrated to determine the corrected RMS values. The results from figure 2.3 and 2.4 indicates that the fluctuating pressure measurements at low Mach numbers are too high and the measurements at higher Mach numbers are too low.

When these transducers are mounted to measure total pressure fluctuations, the membrane is flush to the edge of the probe. Therefore no cavity is formed and no Helmholtz correction is necessary. The ultimate desire of the acoustic measurement of the freestream is to define the fluctuating flow quality. Careful selection of electronic filtering and Helmholtz cavity corrections are necessary to avoid misrepresentation of the flow quality. At transonic speeds the fluctuating pressure can not only

be used to quantify the sound levels but also the direction. The fluctuation pressure information can also be coupled to hot wire data to determine fluctuating velocities and densities, see section 2.1.5, yet the phase lag through the Helmholtz cavity configuration must be accounted for to obtain accurate results.

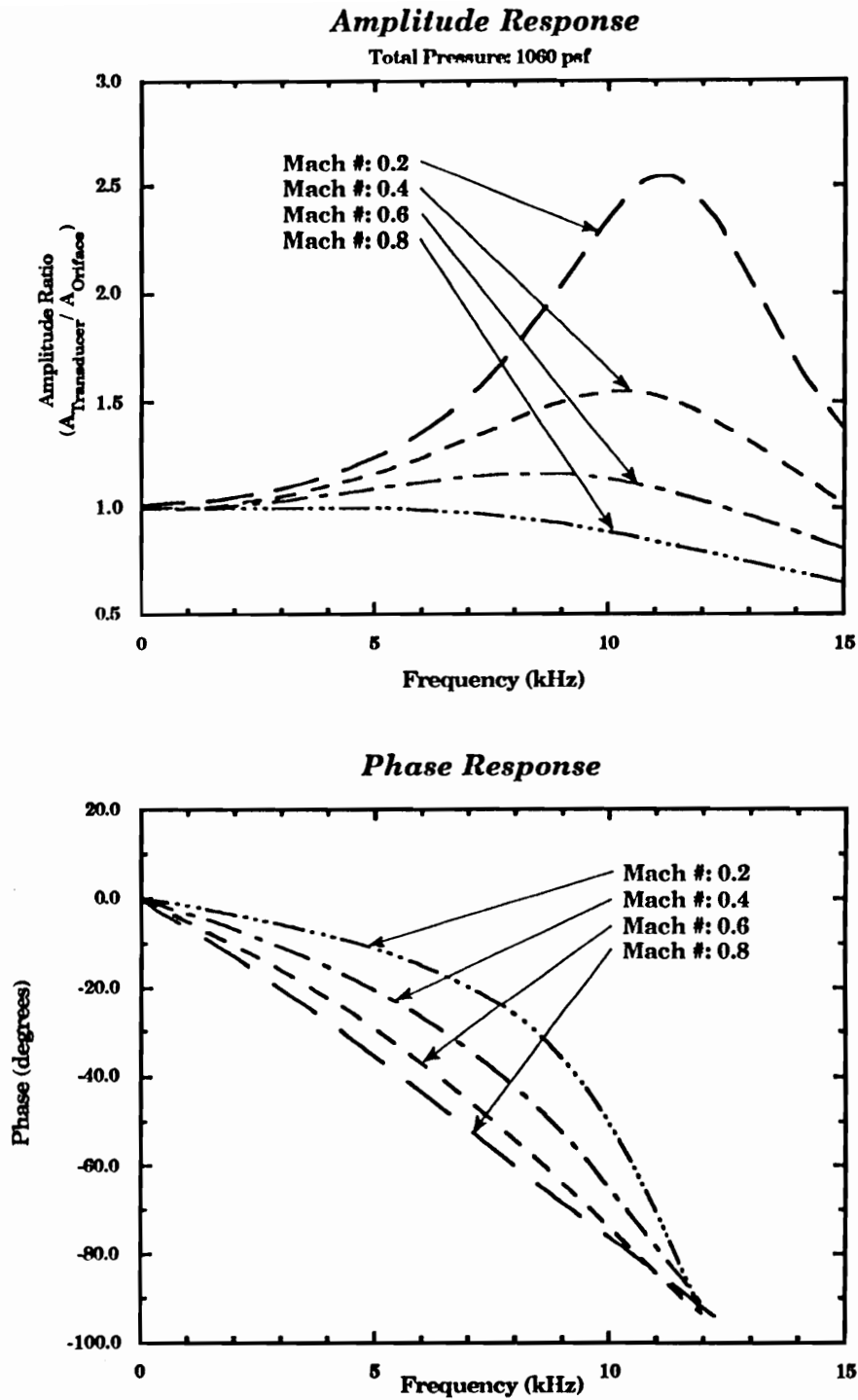


Figure 2.4 Theoretical Helmholtz cavity effects on the amplitude and phase of the pressure field for a typical fluctuating static pressure probe under flow conditions,

2.4 Wind Tunnel Flow Quality Manipulator Theory

In a study that focuses on wind tunnel flow quality, it is important to recognize the sources of disturbances measured in the test section. Once these disturbance sources have been identified it is possible to reduce the effect of the disturbance with the treatment of turbulence manipulators. It is also necessary to recognize that the efficiency of these manipulators vary with changes in the wind tunnel configuration and/or speed.

Wind tunnels have been designed in a variety of configurations but many of the disturbance sources can be found in all configurations. Common disturbance sources include; fans, drive motors, turning vanes, support struts, turbulent boundary layers, separated flows, tunnel wall vibration, slotted or perforated walls, diffuser flaps, blowing or suction systems, etc. There have been many attempts to reduce the disturbance levels in the test section which include removing the disturbance source itself or treating the results of the disturbance source. There are three classes of flow quality manipulators:

1. Anti-vorticity devices
2. Anti-sound devices
3. Anti-entropy devices

2.4.1 Anti-vorticity devices - The anti-vorticity devices are characterized by altering the scale and level of disturbances before they reach the test section. This is generally accomplished by placing screens and honeycomb in the low speed region of the tunnel. The screens reduce both the axial and lateral disturbances, but tend to reduce the axial perturbation more. The

amount of turbulence reduction is a function of both the pressure loss across the screen and the scale of the perturbation coming into the screen. Screens that have a relatively large pressure drop in the flow direction generally reduces the higher velocities more than the lower, thus promoting a more uniform axial velocity. When multiple screens are used, the turbulence reduction is a product of the individual screens. Batchelor (1953), Uberoi (1956), Tan-atichat, Nagib, & Loehrke (1972) have described this process in detail.

The use of honeycomb, having a minimum length of 6-8 times the cell size, operates on the large scale disturbances in the settling chamber. The small pressure drop tends to have a lesser effect on the axial velocities thus reducing only the lateral velocities.

The effect of the contraction on free-stream turbulence moving downstream into the test section is generally related to the contraction ratio and the change in local density as the disturbance propagates through the contraction. Prandtl (1933) developed a semi-quantitative theory to predict the resultant velocity perturbations in the test section after they had propagated through a wind tunnel contraction. He assumed that the velocity fluctuations in the axial direction are due to vortex filaments lying perpendicular to the axial direction. Similarly, the velocity fluctuations in the lateral direction are due to vortices lying perpendicular to the lateral axis. As the flow goes through the contraction, the vortex filament in the axial direction are elongated by a factor c , and those in the lateral directions are contracted by a factor \sqrt{c} , where c is the contraction ratio. Uberoi (1956) explains that when vorticity is the dominant perturbation in the settling

chamber, (for contraction ratios less than 10), the decay of the velocity perturbation through the contraction is consistent with Prandtl's prediction. However for contraction ratios similar to the 8'TPT ($c=20.25$) the magnitude of the velocity fluctuation in the axial direction initially decreases, (as in the contractions with $c < 10$), but then increases to a final value which is higher than the initial value measured at the contraction entrance. These values can be two to three times the initial magnitude. Most of the work done to date is for low speed incompressible applications, yet the limited work done for supersonic wind tunnels suggest that the influence of sound or density fluctuations have biased the measurements at the exit of the contraction.

Streamlining struts and wind tunnel supports reduce the effects of unsteady wakes which can be related to a reduction vorticity disturbances. Asymmetries in the flow through the diffuser often result in separations on the wall which drastically impact the fan efficiency. These separated regions often pulsate causing the mean velocity of the tunnel to meander. Vortex generators are often used to ensure the diffuser boundary layers remain attached. However the addition of the vortex generators become a source of sound being generated upstream into the diffuser.

2.4.2 Anti-sound devices - The sound field for a closed wind tunnel is complex as the tunnel interior is highly reverberant and noise sources from around the tunnel circuit will contribute to the noise levels in the test section. It has been suggested by Wilby & Scharton (1975), Hayden & Wilby (1984), and Soderman (1988) that for many wind tunnels the noise from the

drive and fan dominates the noise field in the test section. Fan noise is caused mainly by fluctuating lift forces on the blades. These fluctuating forces arise from a variety of reasons. Even if the flow into the fan were uniform and free from oncoming disturbances, noise would be generated by the vortex shedding and by the interaction between the turbulent boundary layer on the blades and the blade trailing edge. This vortex shedding can result in broadband or discrete frequency sound, depending on the Reynolds number and the shape of the blade trailing edge. The presence of random or non-uniform disturbances coming into the fan causes random variations in the blade angle of attack which, in turn, causes random fluctuations of the lift forces and, thus, random noise. This sound is propagated in all directions.

To reduce the sound levels in the test section one can acoustically treat the walls and/or for some wind tunnels locally increase the speed of the wind tunnel to a sonic level. This choking process is usually done between the test section and the diffuser which eliminates the upstream moving sound from the fan and diffuser. This approach is appropriate for transonic testing but usually requires a complex choking mechanism that can be manipulated to achieve any desired Mach number. Acoustically treating the walls reduces the noise reverberated from the walls, however is not generally implemented due to cost, except where cavities or slots can be filled. Streamlining struts and wind tunnel supports also can be used to reduce the sound being generated around the circuit.

2.4.3 Anti-entropy devices - The entropy typically generated in a wind tunnel is primarily from the non-uniform heating generated by the wind tunnel drive system. The treatment of this disturbance is normally handled by some type of heat exchanger, yet for some facilities there is no treatment at all. In general these heat exchangers are designed to produce a uniform temperature profile in the settling chamber. In addition they can have a relatively large pressure drop across them which results in the heat exchanger acting as a anti-vorticity device. This aids in the removal of vorticity in a manner similar to a honeycomb.

2.5 LFC Theoretical Considerations - (Boundary-Layer Stability)

The main objective of the LFC test series was to determine the effectiveness of active boundary-layer control at transonic speeds. Bobbitt, et al (1988) suggested that the physics of boundary-layer transition can be divided roughly into these stages:

- (1) the development of the laminar boundary layer,
- (2) the receptivity of this boundary layer to external disturbances,
- (3) the growth of linear disturbances,
- (4) nonlinear interaction of disturbances, and
- (5) the breakdown into turbulent flow.

It is not the intent of this paper to describe these processes, but to carefully document the oncoming outer flow unsteadiness which could trigger instabilities on the LFC model. The transition process is described by the nonlinear, time-dependent Navier-Stokes equations. Since solutions to these equations are not available for complex geometries, researchers usually rely on experimental and theoretical comparisons for the evaluation of receptivity on the boundary layer as defined by linearized stability theory.

The linear growth of disturbances in the boundary layer can be characterized by the presence of Tollmien-Schlichting (TS) waves, crossflow (CF) vortices, Gortler vortices, or some combination of these disturbances. The LFC model has the potential for all of these types of instabilities to be generated as seen by the pressure distributions in figure 2.5. Based on n-factor calculations performed by Berry (1986) the dominant source of

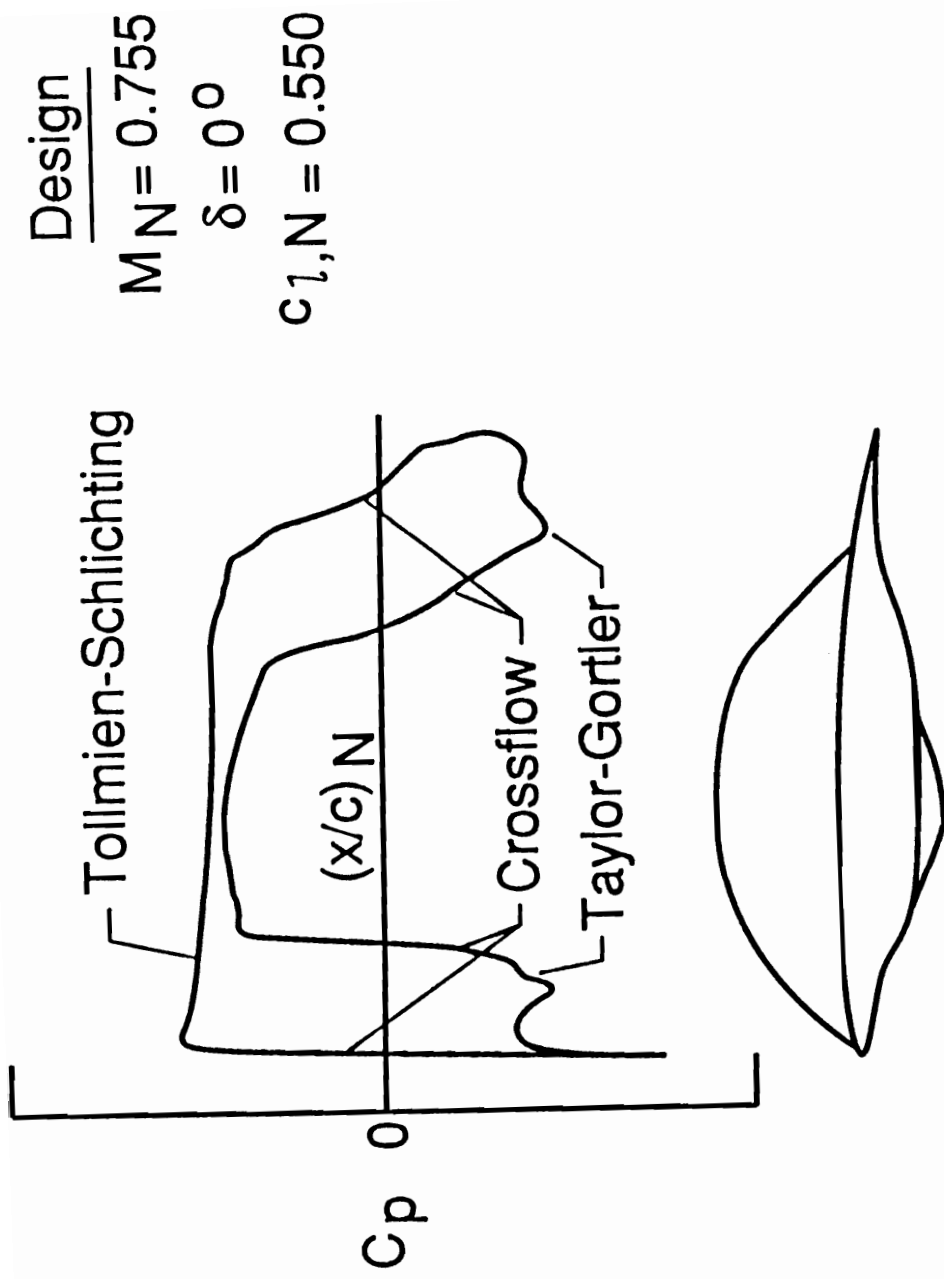


Figure 2.5 Typical boundary layer instabilities that can occur on a swept super-critical LFC airfoil

instabilities for the upper surface of this model is TS waves, figure 2.6. These instabilities are typically defined by the linearized Orr-Sommerfeld equation, (Betchov & Criminale, 1967). The linear stability theory provides a method for determining disturbance amplitudes relative to their initial values at the neutral stability point. Using linear stability theory, one can calculate, as a function of Reynolds number, the amplification factor "n". In general the n factor is "wave number" or frequency dependent. This quantity is related to the amplitude ratio via:

$$\frac{A}{A_0} = e^n$$

where A is the disturbance amplitude at some location x and A₀ is the initial amplitude of the disturbance in the boundary layer. It should be noted that the initial amplitude A₀ and the outer flow disturbances are thought to be coupled through the leading edge receptivity process. This process is complicated and goes beyond the scope of this study, however, some observations will be made concerning the frequencies of potential disturbances that might be amplified in the boundary layer.

The linear incompressible stability theory was used in the design of the LFC model and included calculations for the required suction levels, Harvey & Pride (1982), whereas compressible and incompressible theories were used to evaluate the experimental transition data, Harvey (1987). A wide range of values of "n" have been suggested for the transitional

$10 \leq R_c \leq 20$ million
 $\Lambda = 23^\circ$, upper surface

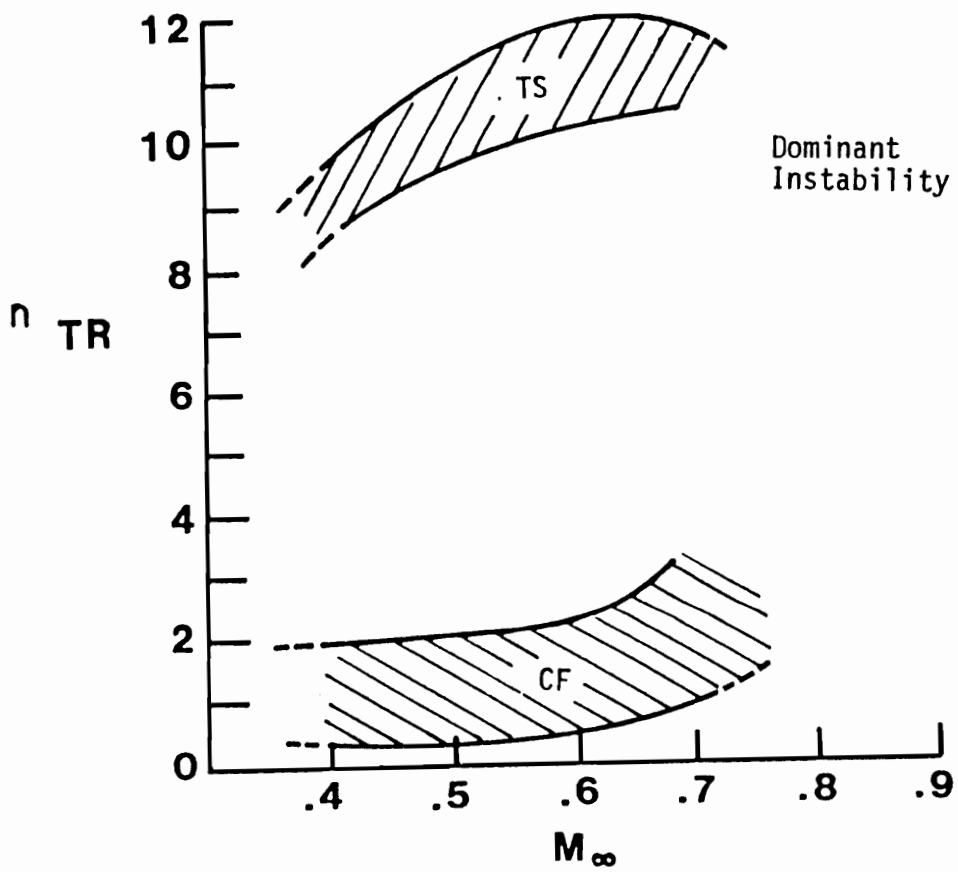


Figure 2.6 Calculated incompressible n -factors at transition for a swept super-critical LFC airfoil

amplification factor and are documented by Hefner & Bushnell (1979) and Harvey (1987). Reshotko (1987) suggested that caution should be exercised in the interpretation of n -factor results, due to the complexities of the computation, but that values of 10 to 11 hold up for good quality flight experiments. The calculation of " n " for a given transition location depends on many variables which are related to the boundary layer itself. The uncertainties in the calculation are functions of variables that include ability of the code to account for compressibility, shocks, enthalpy fluctuation, pressure gradients, acoustic noise, 3-D boundary-layer flows, etc. The remainder of this text will focus on disturbances which include velocity, density, temperature, pressure, and mass flow fluctuations. The amplitude of these disturbances and the phase relationship of the disturbances should be related to the variables controlling the transition process, however, this dissertation will only attempt to relate the transition process to the obvious influences of the free stream flow quality for the LFC experiment.

3.0 FACILITY AND INSTRUMENTATION

The facility utilized throughout this research was the NASA Langley 8-foot Transonic Pressure Tunnel (TPT). This section will describe the two configurations for the facility and the basic instrumentation used in this investigation. The first configuration was an empty tunnel configuration which was used primarily to establish the baseline wind tunnel flow quality. The second configuration was used as an evaluation of the flow quality of the facility with a complex model in place. Since there are drastic differences in these configurations, they will be described independently. This will be followed by a brief description of the instrumentation.

3.1 8'TPT Empty Wind Tunnel Configuration

The calibration of a hot wire sensor in transonic flows requires that the calibration facility have independent control of velocity, density, and total temperature. The 8'TPT is one of the few facilities in the world with such a capability. A schematic of the 8' TPT is shown in figure 3.1. The facility is a fan-driven, closed-circuit, continuous-flow, variable-pressure wind tunnel with controls that permit independent variations of Mach number, stagnation pressure, temperature, and humidity.

The facility is similar to most transonic tunnels except for the presence of a cooler, consisting of eight staggered rows of finned tubes. The cooler is located just upstream of the 36 foot diameter settling chamber. There is a set of five anti-turbulence screens that is preceded by a

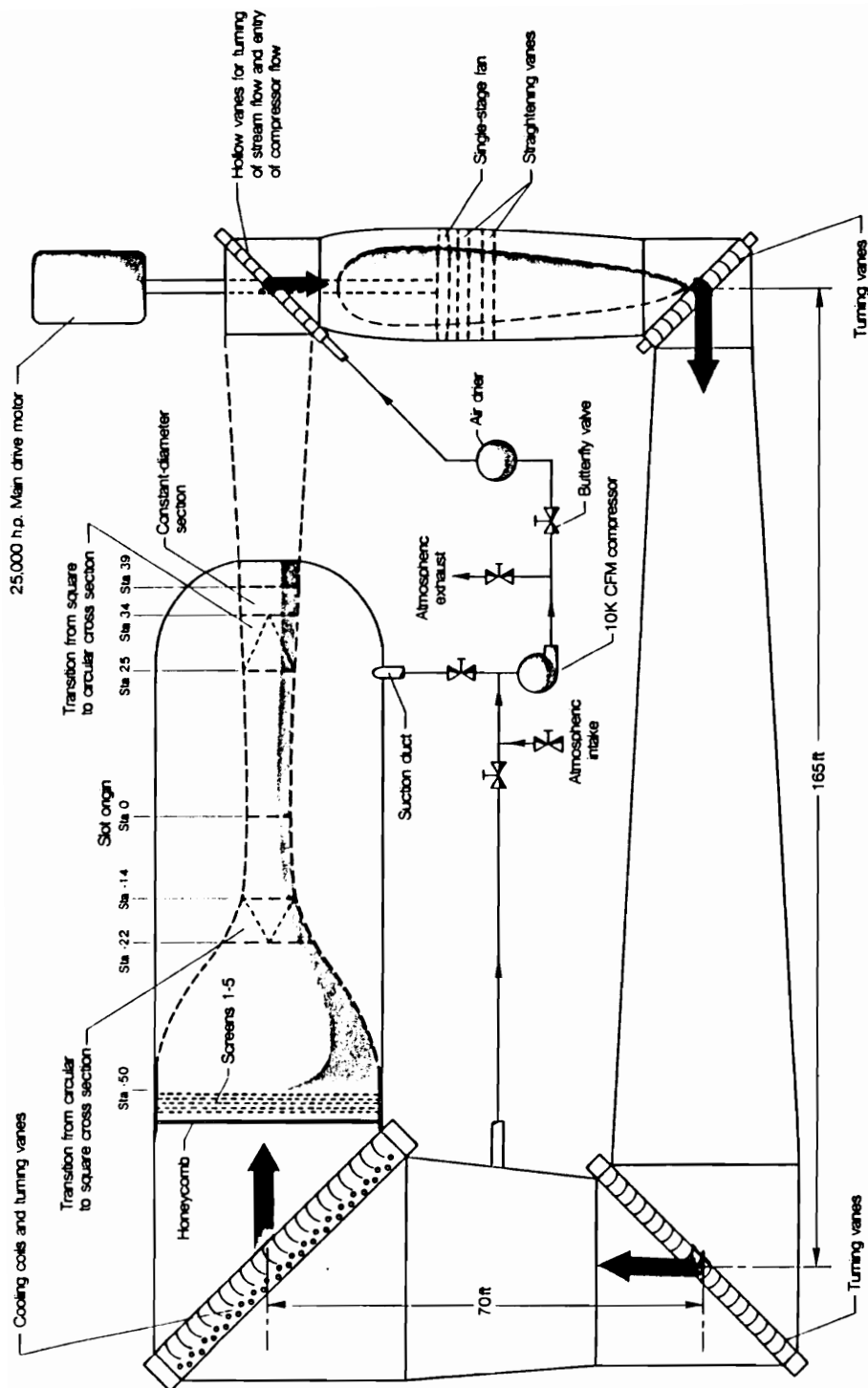


Figure 3.1 Schematic of the 8'TPT

honeycomb section, both of which are located in the settling chamber. The 20.25:1 contraction section is 50 feet long and couples to a rectangular test section with an equivalent diameter of 8 feet. The facility has specially designed "transonic slots" located at the top and bottom walls of the test section. The origin of these slots define the beginning of the test section and run the entire 25 foot length of the test section.

For the empty tunnel configuration, a sting mounted probe holder was mounted on the centerline of the test section, figure 3.2. This strut was originally designed for a flight test on a nose boom of an F-15, therefore named the "F-15 Strut". Five probes, (two three element hot wire probes, one fluctuating total pressure probe, one fluctuating static pressure probe, and a mean total and static pressure probe), were mounted in four forward swept airfoil sections and the nose cone of the F-15 strut as shown in figure 3.2b. The probes were located 106 inches from the slot origin which is typical of model locations for this facility. The F-15 strut itself was held at mean zero angle of attack with the use of guy wires and the arc sector. It should be noted that both the F-15 strut and guy wires are sources of sound which will be identified later in the text.

A secondary wall mounted strut was used for complementary hot wire data. A single element probe with two "dummy" elements or a three element probe could be mounted in this location. Local pressure and temperature measurements were obtained and used in the hot wire calibration process. Surface mounted pressure transducers were mounted in the side walls of the facility, as shown in figure 3.2, to measure the pressure fluctuations at the wall.

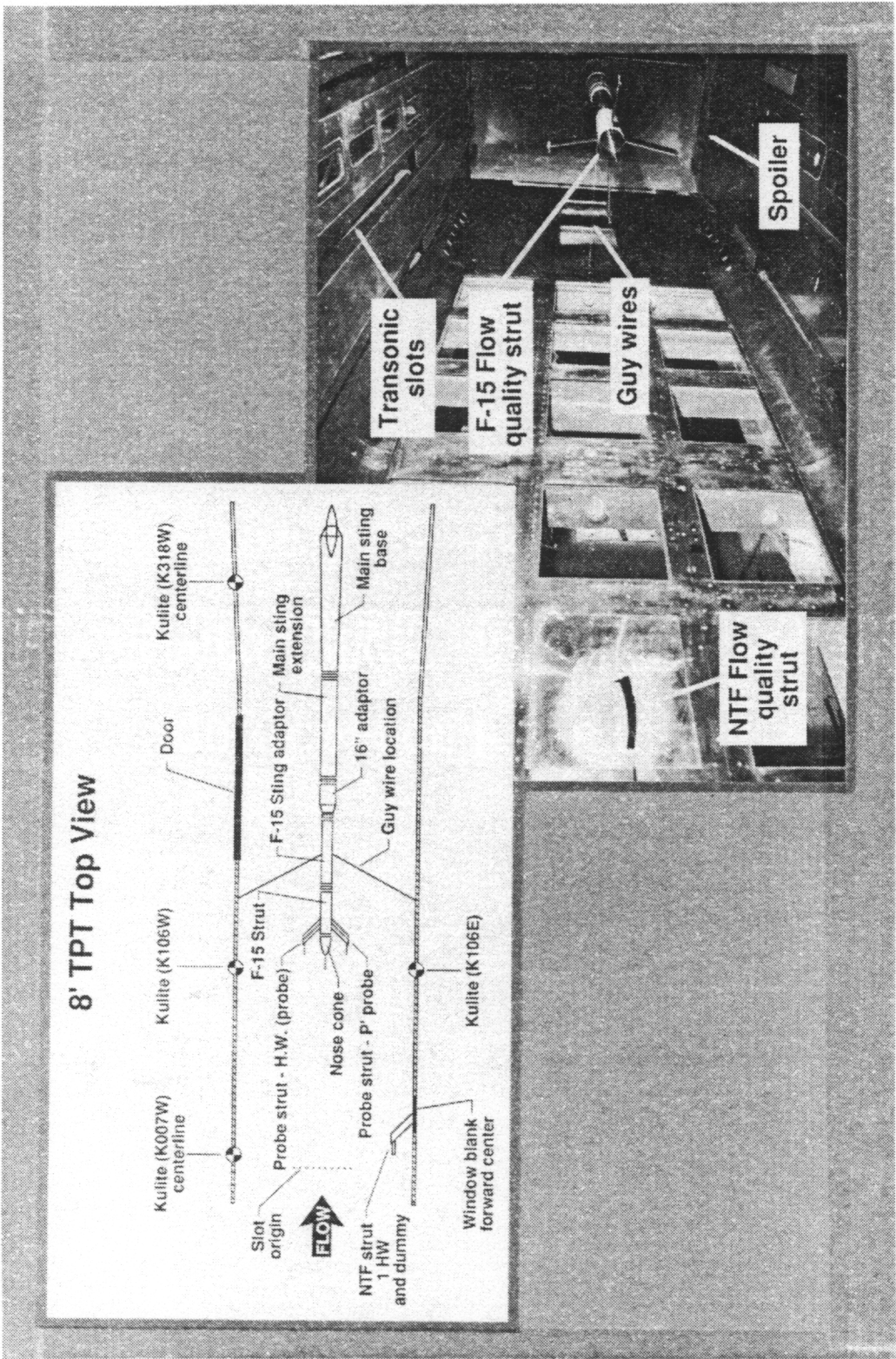


Figure 3.2 Empty tunnel flow quality configuration of the 8'TPT

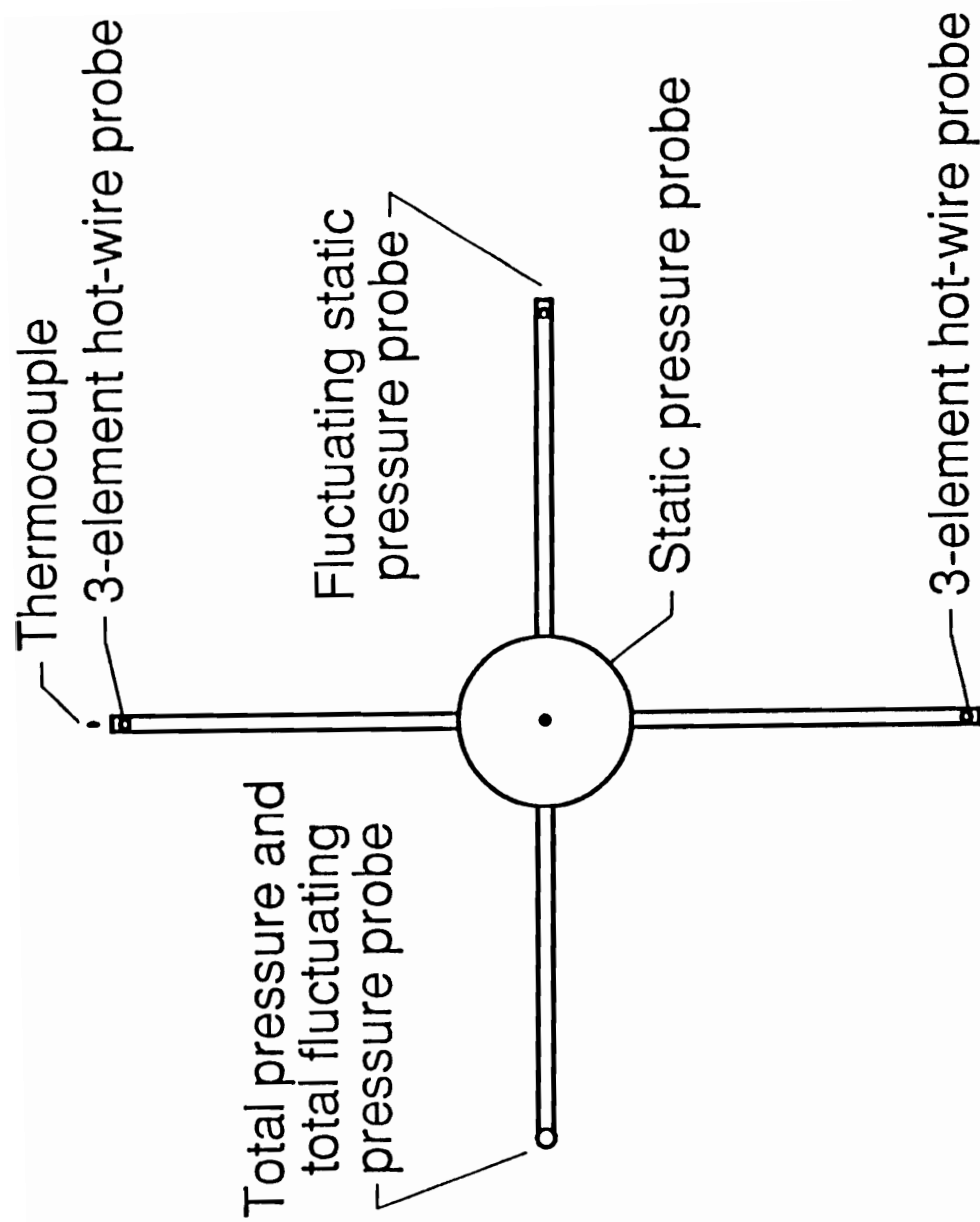


Figure 3.2b Flow quality probe orientation in the F-15 strut

The tunnel operated over the following conditions for the empty test section configuration:

$$0.333 < P_0,(\text{atm}) < 2.000$$

$$0.20 < \text{Mach no.} < 1.25$$

$$520 < T_0,(\text{R}) < 580$$

$$7 \times 10^5 < Re_{\text{foot}} < 9.5 \times 10^6$$

The emphasis of the fluctuating flow quality measurements focused on the operating range of the facility most often used in general testing.

3.2 8'TPT LFC Wind Tunnel Configuration

For the second configuration the test section was modified to accommodate the swept, large-chord (7.07 ft) Laminar Flow Control model, (SCLFC(1)-0513F) as shown in figure 3.3. Detailed descriptions of the facility modifications are made by Harris & Brooks (1988). The super-critical LFC airfoil model spanned the height of the test section and had a porous skin on the model's upper surface and a slotted skin on the lower surface. The airfoil was designed for a shock-free super-critical flow which would simulate the flow over a typical LFC aircraft wing. Details of the model design are described by Pfenniger, Reed, & Dagenhart (1979), Harvey & Pride (1982), and Allison & Dagenhart (1987). Boundary-layer suction was applied to both the upper and lower surfaces in an attempt to maintain a laminar boundary layer to the trailing edge of both surfaces.

To avoid blockage problems and to minimize wall interference over such a large-chord swept wing, a test section liner was designed and built to match the contours of the streamlines of an infinite span wing in free air. This liner design was optimized to provide a uniform flow into the LFC model. The contours of the walls of the tunnel were optimized for a single flow condition which was for Mach number of 0.82, a Reynolds number of 20×10^6 , and a lift coefficient of 0.47. Operation of the facility at any other condition resulted in reduced liner efficiency. Figure 3.4 illustrates the desired near shock-free supersonic regions on both the upper and lower

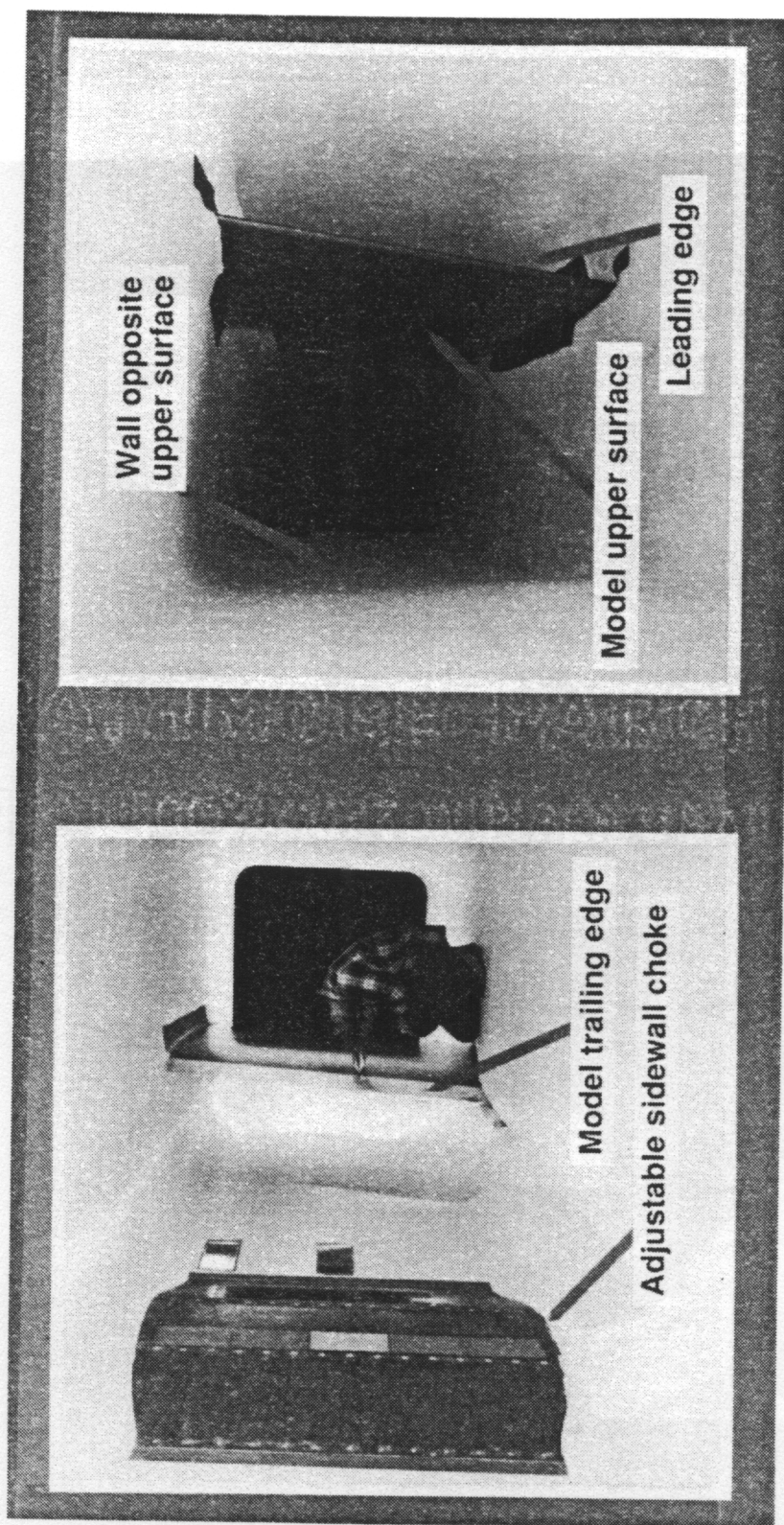


Figure 3.3 Photograph of the Supercritical Laminar Flow Control Airfoil (SCLFC(1)-0513F) and Custom liner mounted in the 8'TPT Test section

Figure 3.4 Photograph of the side wall flow quality strut and the LPT model

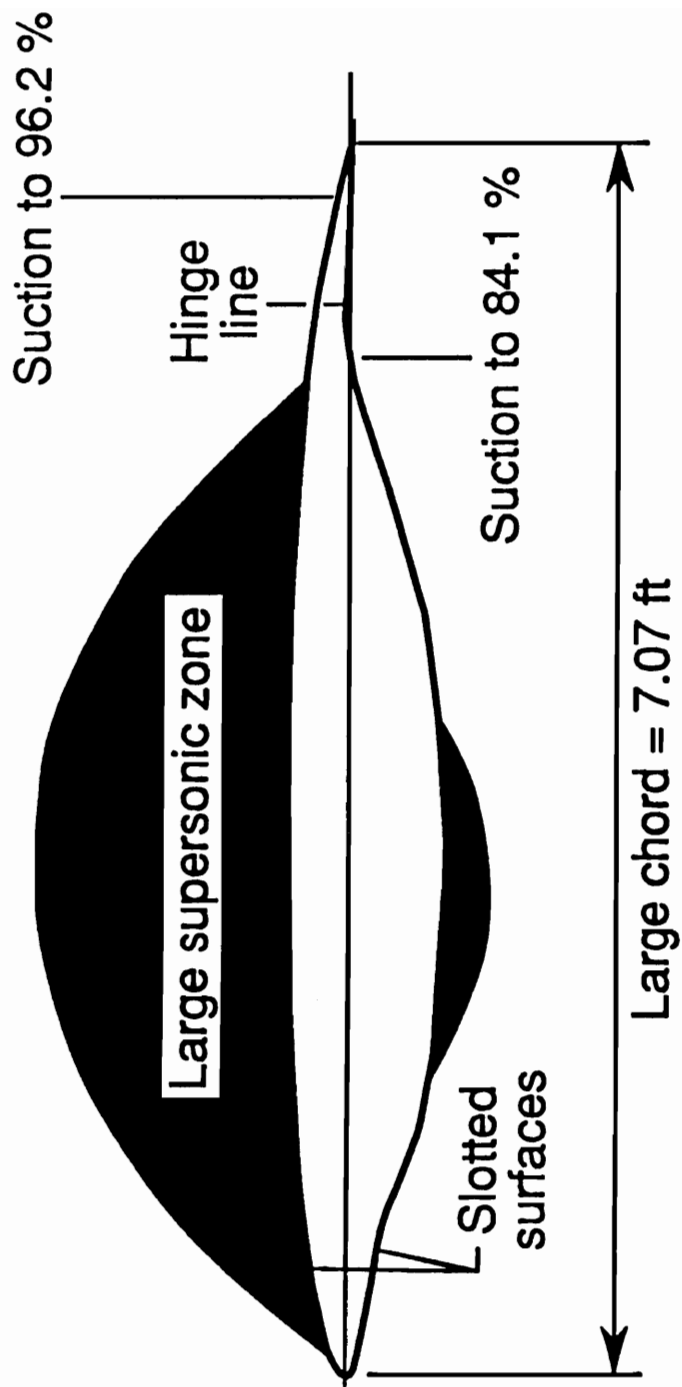


Figure 3.4 Sketch of the LFC predicted sonic zones

surfaces of the super-critical airfoil section at design conditions. For more details of the model performance see Harris & Brooks (1988), and Harris, Brooks, Stack, & Clukey (1989).

For the LFC tunnel configuration the limits of the flow quality test matrix were bound by safety considerations for both the model and the liner. In fact the flow quality was desired primarily for the point design condition of the LFC model. This is because the off design conditions are plagued with potential liner separation, ineffective boundary layer suction, and facility choking problems. Even though these problems may exist it was necessary to run the facility across a range of velocity, density, and temperature for hot wire calibration purposes. The tunnel was operated over the following conditions :

$$0.333 < P_o,(\text{atm}) < 1.000$$

$$0.40 < \text{Mach no.} < 0.82$$

$$520 < T_o,(\text{R}) < 580$$

$$5 \times 10^6 < \text{LFC } Re_{\text{chord}} < 23 \times 10^6$$

The flow quality measurement were made at two different locations as shown in figure 3.5. The presence of the liner made it necessary to measure local conditions at the probes. Wall mounted struts were fitted with a total pressure probe, a static pressure probe, a total temperature probe, a fluctuating static pressure probe, and a three element hot wire probe. The side wall strut was mounted one chord upstream of the LFC model along the theoretical stagnation streamline as shown in figure 3.6.

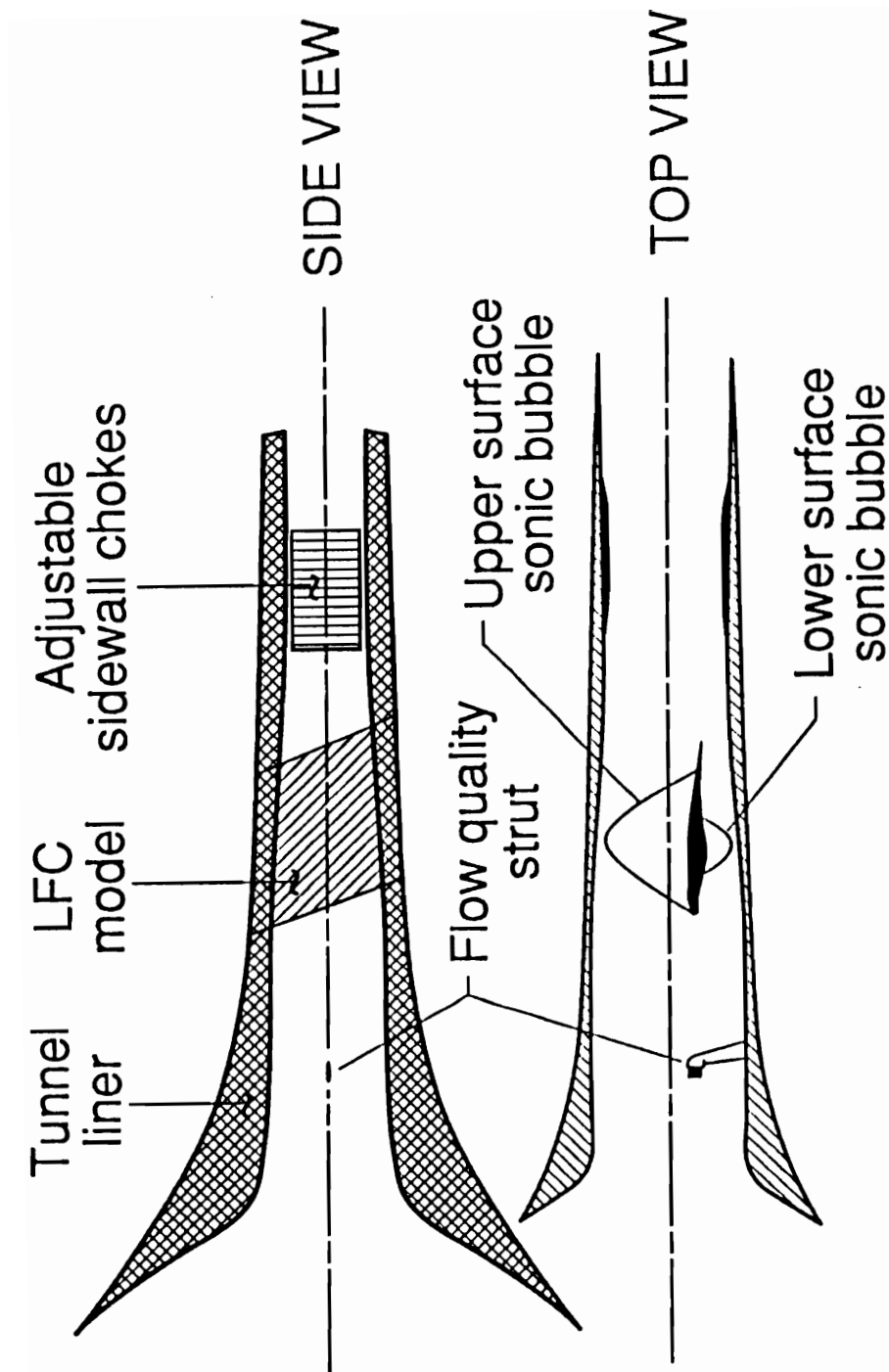


Figure 3.5 Sketch of the Flow quality measurement locations for the LFC experiment

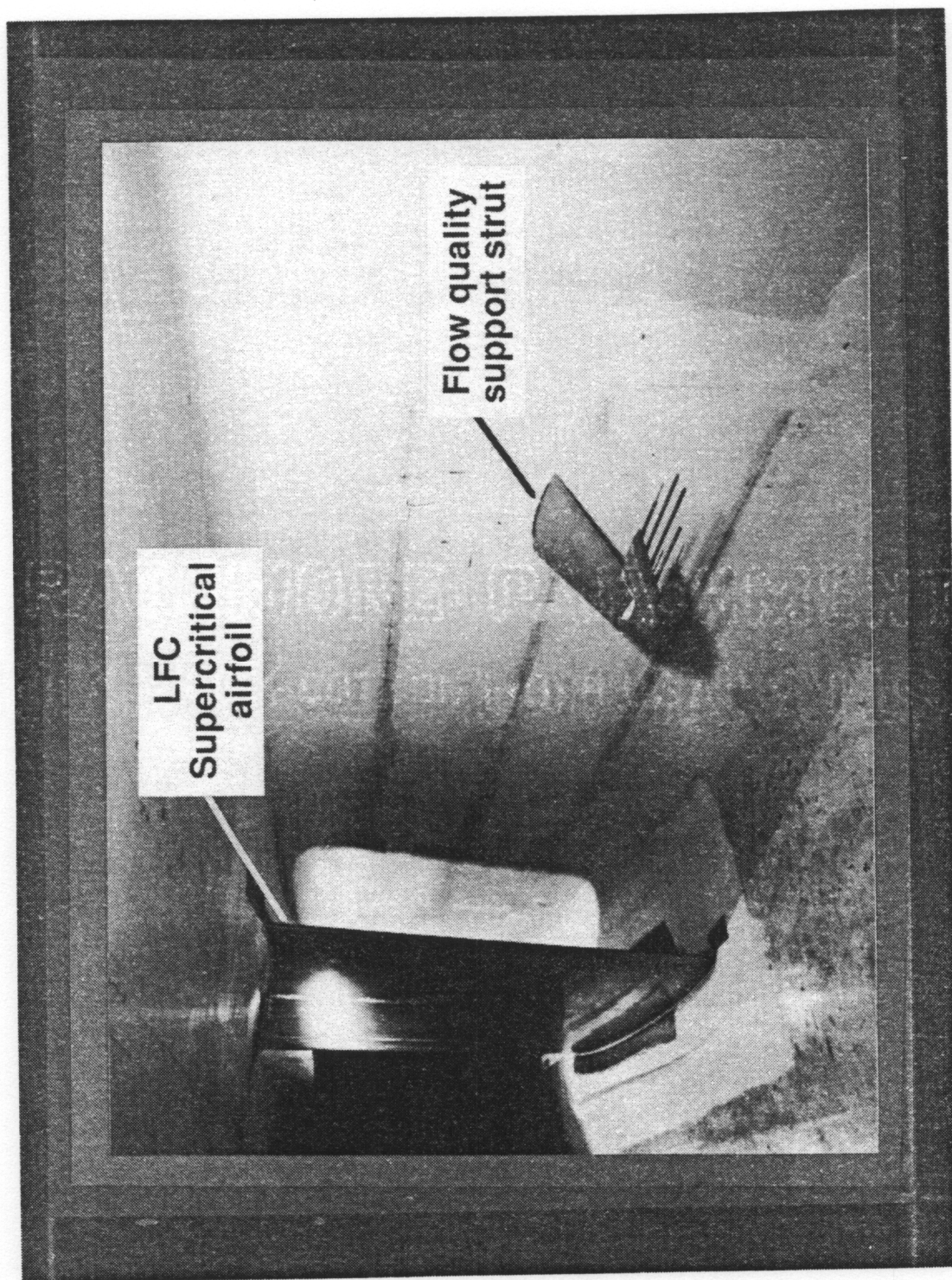


Figure 3.6 Photograph of the side wall flow quality strut and the LFC model

3.3 Instrumentation

The primary flow quality instruments (hot wire & fluctuating pressure) used for both the empty tunnel and LFC wind tunnel configuration were custom built for the large dynamic pressures associated with transonic applications. This section will describe the construction and electronic application of the hot wire probes and fluctuating pressure probes related to this study.

3.3.1 Hot Wire Probes - The specific design and construction of a hot wire is often dictated by the application in which it is used. The first requirement for most hot wire applications is to be able to make a point measurement at a known location in the flow field without disturbing the flow field which is to be measured. This requires the miniaturization of the probe. To achieve this, several electromechanics parameters must be considered. These consideration may include the influence of one sensor on another (cross-talk), the influence of non-uniform heating across the sensor (L/d ratio), the influence of mechanical vibration of the sensor supports, or unsteady motion of the sensor in the flow (strain-gaging).

Since the likelihood of wire breakage was good, several custom plug-in type probes were constructed, figure 3.7. The plug-in type of construction provided easy installation and replacement of the probe in the event of wire breakage. The three sensors were mounted normal to the flow and utilized either 0.0002 inch diameter or 0.00015 inch diameter platinum coated tungsten wires. The nominal wire length was 0.040 inches as

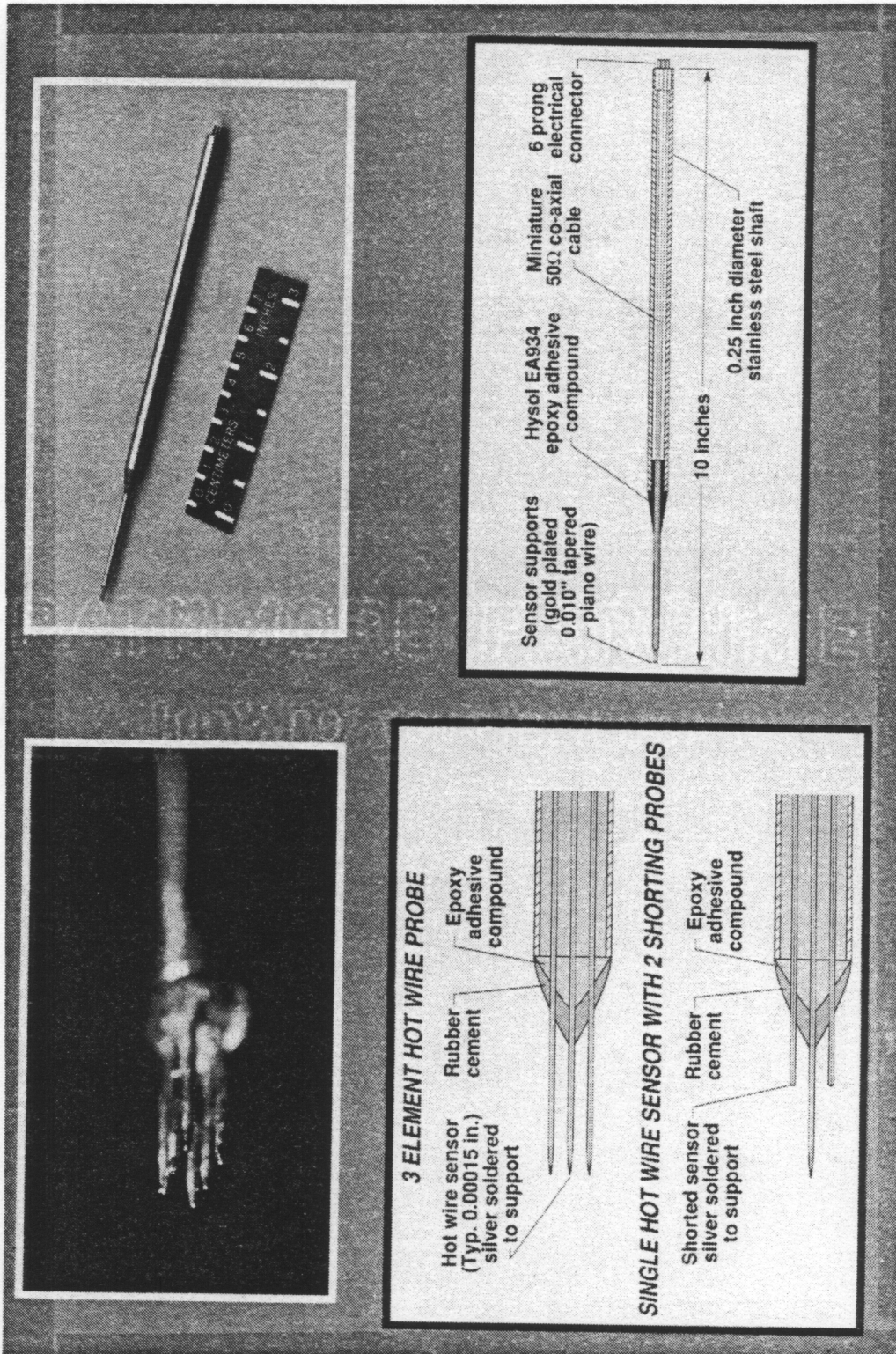


Figure 3.7 Three sensor hot wire probe and single sensor probe with shorting sensors

defined by the distance between the gold plated sensor supports. Since sensors were given a small amount of slack (to avoid strain gaging when the wires were aerodynamically loaded) the exact length of the sensor varied, figure 3.8.

To make point flow quality measurements that are time and scale accurate, it is necessary to make the probe measurement volume as small as possible. The miniaturization of multiple sensor hot wire probes are generally limited by the heat transfer parameters that have been previously discussed and the electronic cross-talk associated with the sensors being in close proximity to each other. In an effort to keep the measurement volume small and still avoid cross talk and interference between elements, the probe was designed for a minimum diagonal length of 0.065 inches.

Each of the three wires were operated with its own constant temperature anemometer. The cold resistance of each element was measured and adjusted to an "overheat" value. Nominal "overheats" of 1.5, 1.75, and 2.0 were used for the three elements, and these corresponding hot resistances were held constant throughout the test.

Three 50 meter tri-axial cables were required to couple the hot wire sensors to the anemometers. While the cables were not placed directly in the flow environment, they are run through the wind tunnel plenum which experienced temperature changes of 20° to 40° R. The resistance changes of the cables varied 2 to 4 ohms depending on the total temperature changes. The variations in resistance occurred over a long period which can be thought of as a baking in period. Even though this baking in period was long, it was necessary to compensate for these resistance changes.

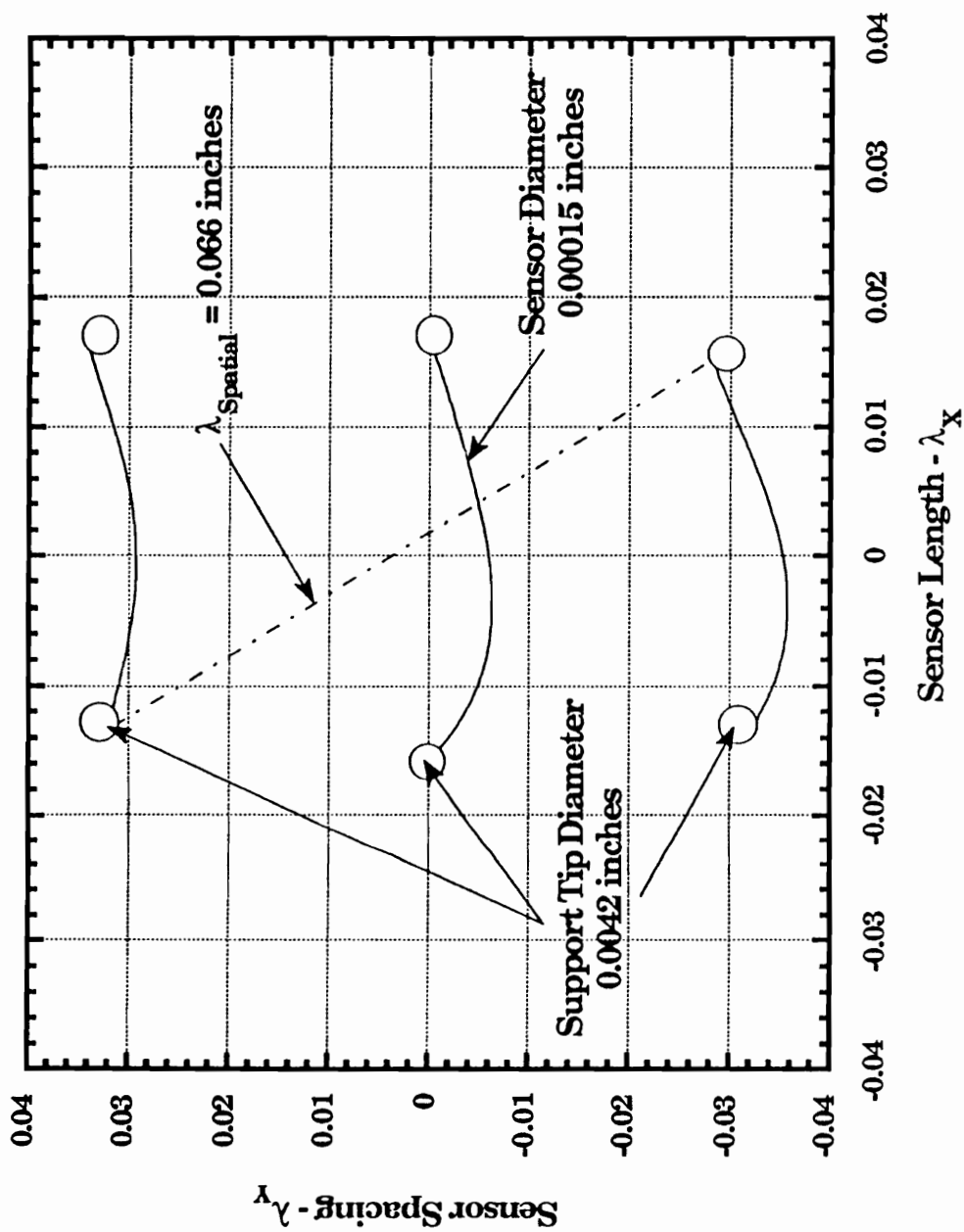


Figure 3.8 End view of sensor orientation for a typical Three sensor hot wire probe

This can be accomplished by shorting the hot wire sensor then balancing the bridge by adjusting a variable resistor in the bridge circuit. It was not practical to bring the facility to its operating condition then shut down the facility to short the hot wire sensor. Therefore a duplicate 50 meter cable was run parallel to a shorting probe which was located next to the active three-element probe. This shorted cable simulated the changes in resistances in the active hot wire circuit and was used when the tunnel conditions were changed. The difference in resistance of the two cables plus the shorting probe were matched to within a 0.001 ohm.

To optimize the "Electronic Time Constant" described in section 2.2.2 is accomplished by changing the impedance of the compensating network of the hot wire 20:1 bridge circuit, (figure 3.9). Normally a square wave input to the bridge circuitry is used to determine the electronic recovery of the feedback amplifier which is related to $\tau_{\text{electronic}}$. The impedance adjustments to the bridge circuitry are normally optimized at the maximum wind tunnel speed to ensure that the electronic feedback circuit will remain stable through the experiment.

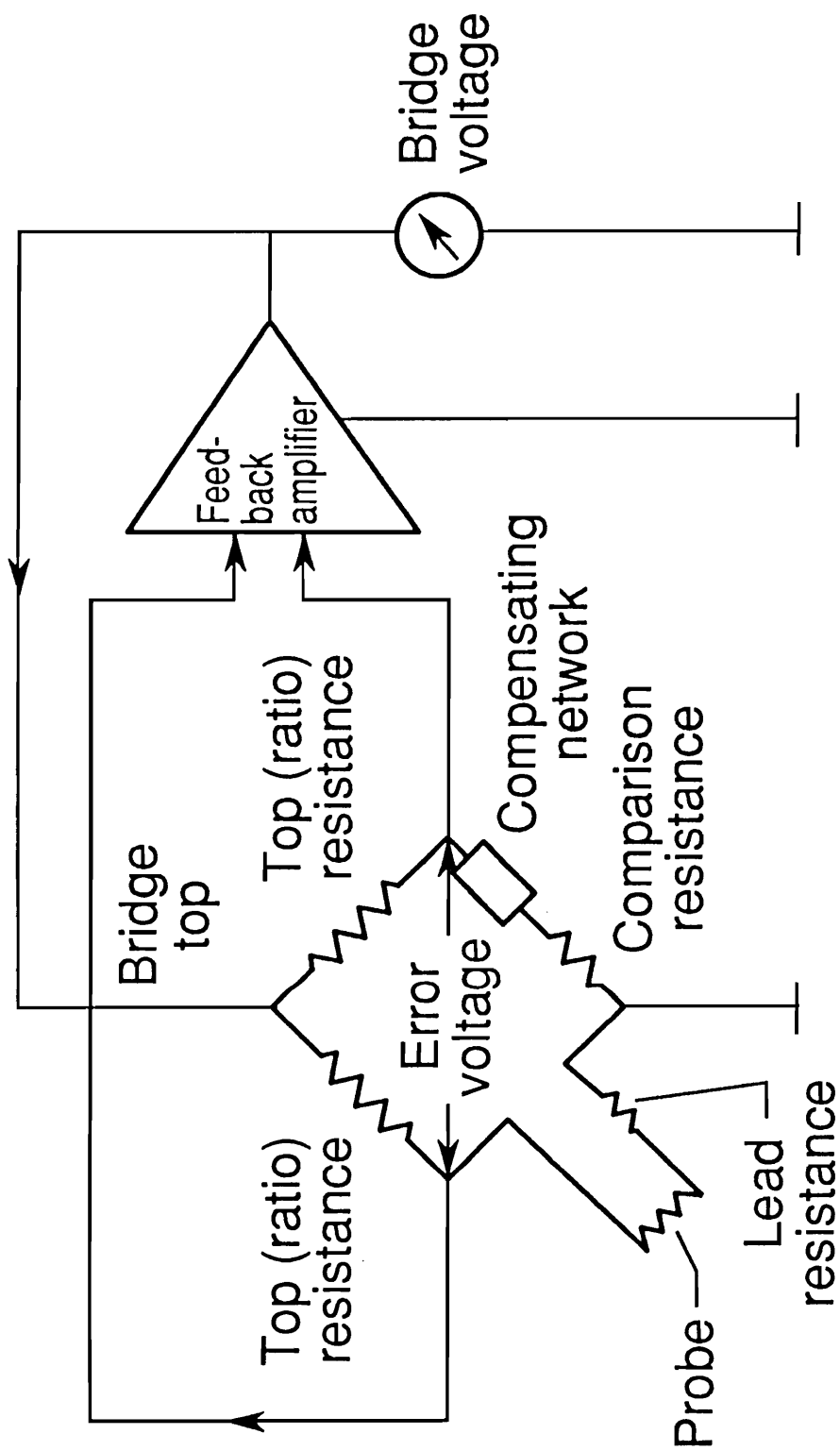


Figure 3.9 Simplified diagram of a constant temperature bridge network

3.3.2 Probes used for Fluctuating Pressure - There were two configurations of pressure probes used to determine the fluctuating pressure for this study. The fluctuating total pressure probe is shown in figure 3.10. The transducer is mounted along the centerline of the probe with four mean pressure orifices located outboard of the pressure transducer housing. This allows the mean and fluctuating pressure to be measured at the same location.

The fluctuating static pressure probe has one 0.020 inch orifice located 10 diameters from the nose of the probe, figure 3.11. The frequency response and natural resonance of the transducer are altered by presence of a "Helmholtz" cavity created by the orifice which couples the flow field to the transducer. The Helmholtz cavity volume was 0.00289 in^3 and the discussion of it's resonance is discussed in section 2.3. In addition to the natural frequency of the Helmholtz cavity the pressure transducer itself has a natural frequency. This resonance was excited at the higher Mach numbers and is shown in figure 3.12 to occur at approximately 70 kHz which corresponds to the manufacturer specifications. Based on this result the bandwidth of the fluctuating pressures were limited to the range of 1 Hz to 40 kHz.

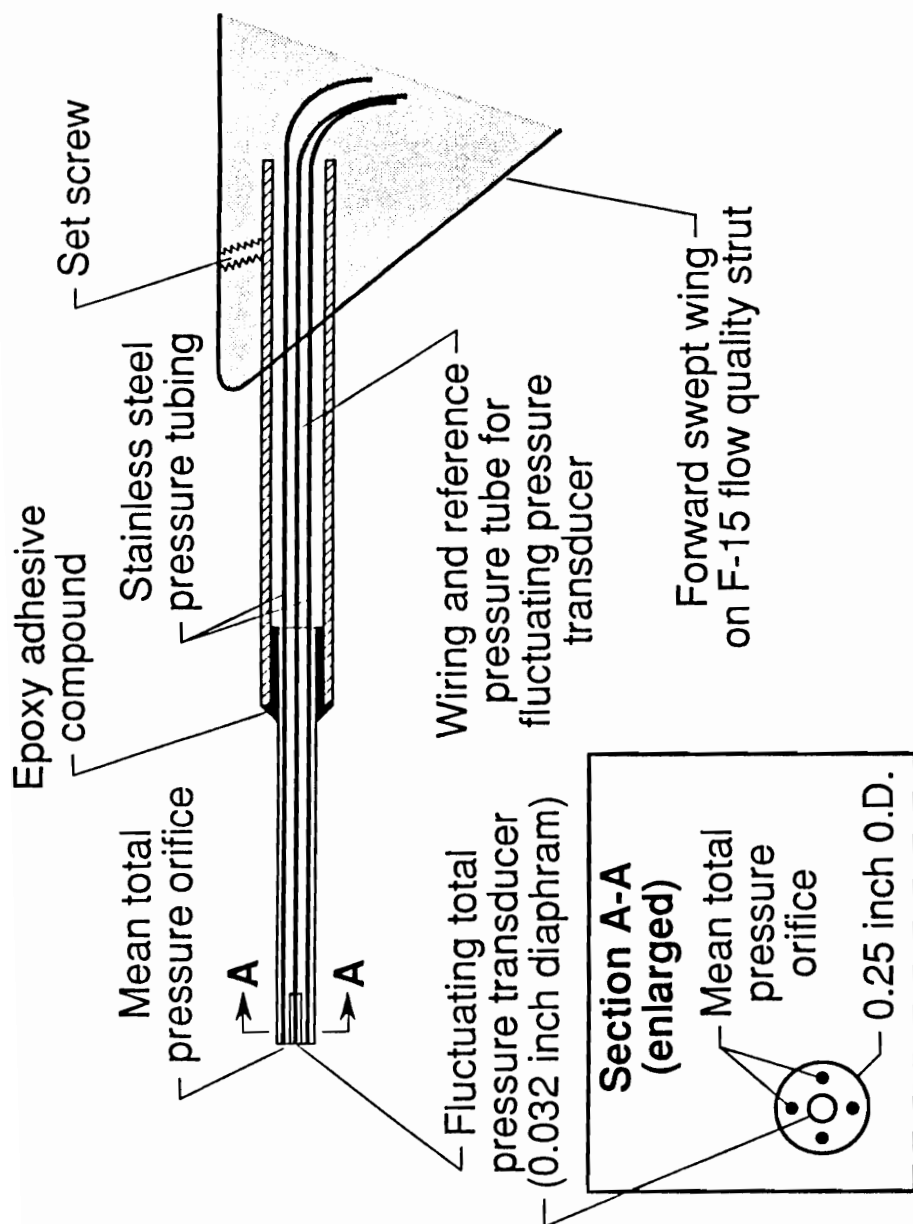


Figure 3.10 Fluctuating total pressure probe

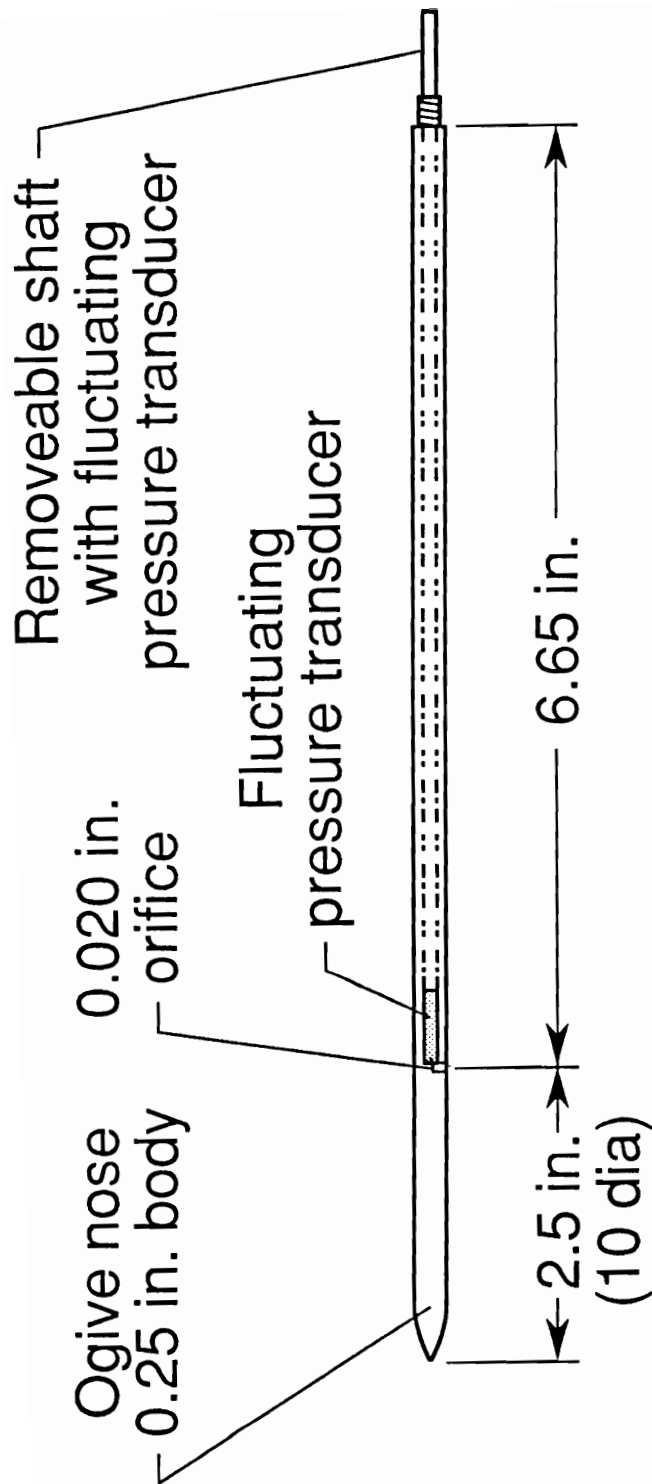


Figure 3.11 Fluctuating static pressure probe

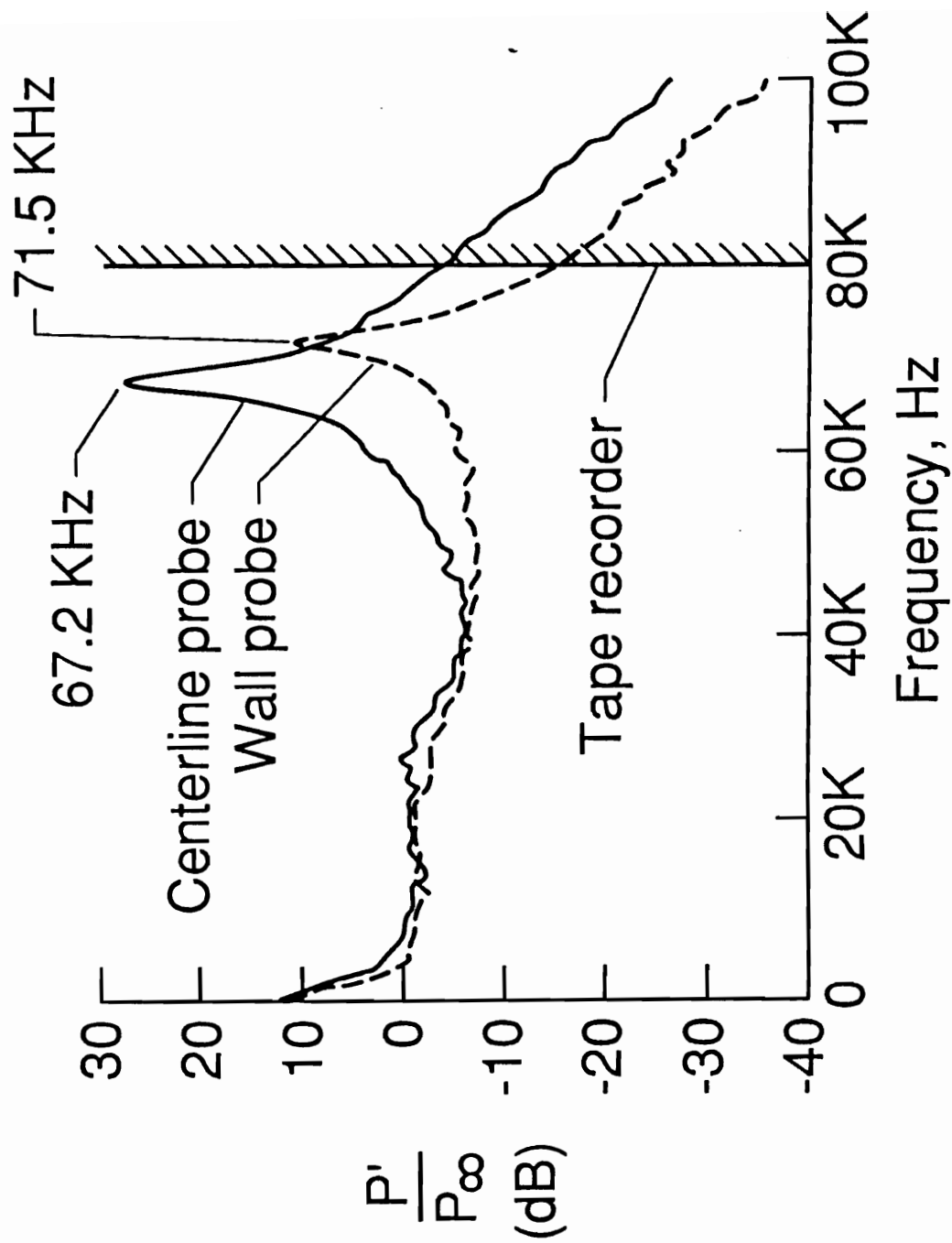


Figure 3.12 Fluctuating static pressure transducer natural frequency

3.3.3 Electronic Configuration - Separating the fluctuating portion of the flow quality signal from the mean level allows the researcher to increase the signal to noise ratio of the fluctuating signal by amplification. A block diagram of the data acquisition system shown in figure 3.13a highlights the filtering and amplification process used in these experiments. Figure 3.13b shows the electronic configuration setup in the 8'TPT control room. By acquiring both the mean and fluctuating data simultaneously, the tunnel run time was significantly reduced. The mean voltages were used to calibrate the probes, and both the mean and fluctuating voltages were used to calculate the velocity, density, and total temperature fluctuations in the flow. The data analysis techniques utilized in this report relied on digitization and post-processing of the data which were recorded on FM tape. A detailed description of the data acquisition and flow quality analysis is described by Clukey, Jones, and Stainback (1988).

The process of eliminating the DC or mean portion of the flow quality signal requires a high pass electronic filter. Ideally the bandwidth should begin a zero hertz (i.e. the mean) and go to infinity, yet this is impractical. The selection of the high pass filter sets the low frequency end of the bandwidth of the data to be analyzed. However, there are no "bandwidth standards" developed for flow quality measurements in wind tunnels, using either hot wires or fluctuating pressure instrumentation. Without such a standard, it is often difficult to compare results from one facility to another or for comparisons of one measurement technique to another. The impact of changing the high pass filtering in the low frequency range of the

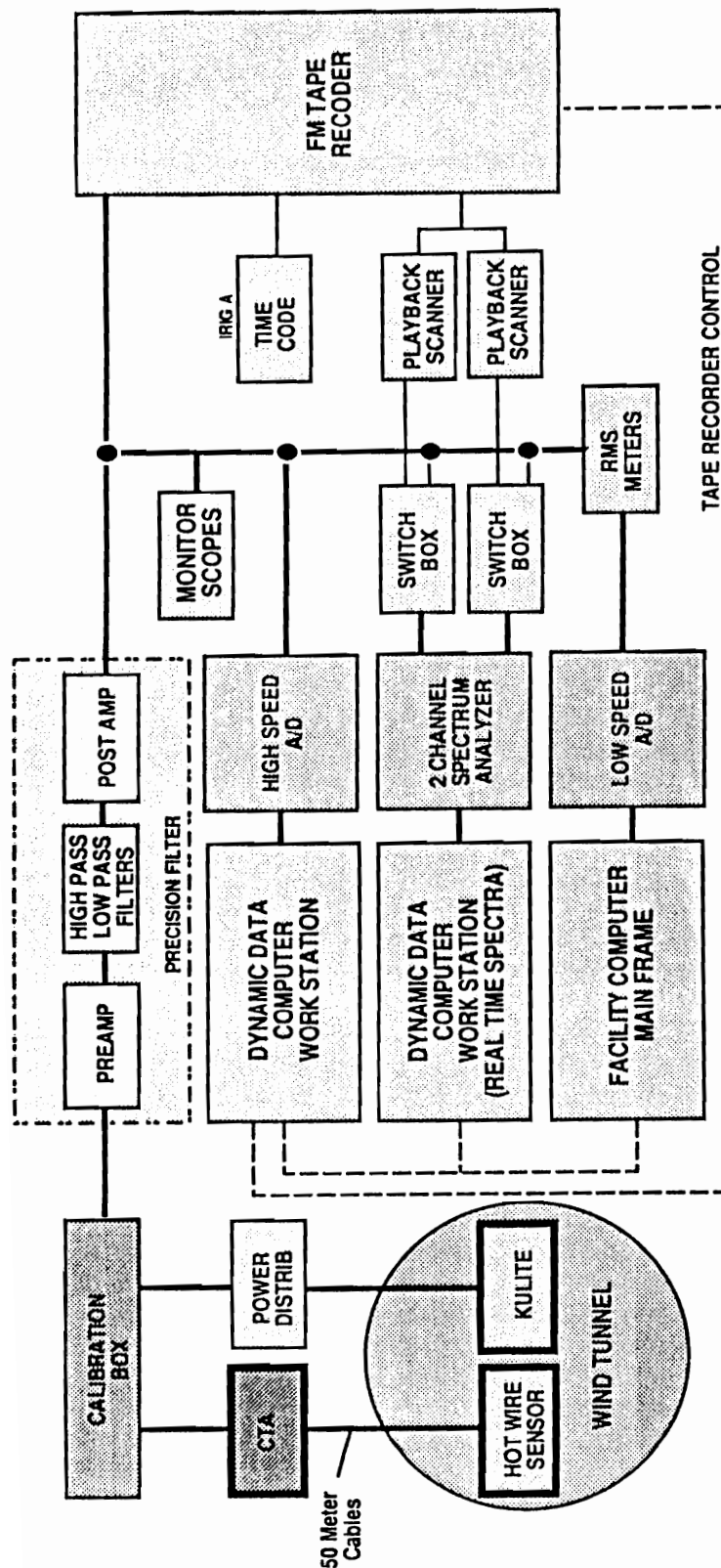


Figure 3.13a Block diagram of flow quality electronic system

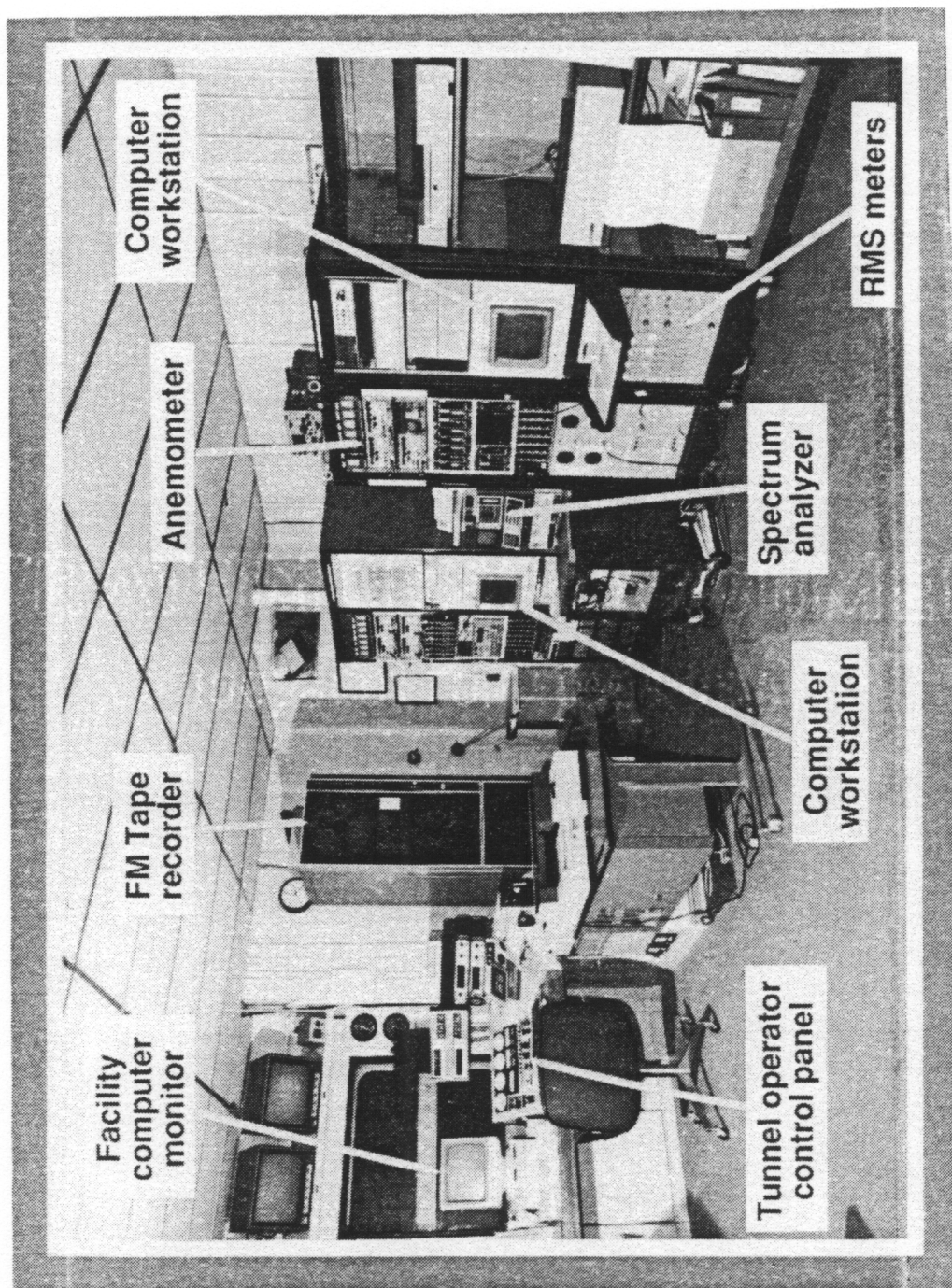


Figure 3.13b Photograph of the flow quality electronic system in the 8'TPT control room

measurement can be dramatic for subsonic flow quality analysis. As an example, to change the high pass filter from 1 hertz to 2 hertz can decrease the perceived pressure fluctuation levels as much as 30%. All fluctuating data was acquired to include information from 1 Hz to 80kHz. During the post-processing analysis the filters were optimized for the flow condition.

Spectral information suggested that the hot-wire data beyond 5 kHz was influenced by electronic noise, therefore, most of the rms data within this report were limited to 1 to 5 kHz. Some spectra were obtained to 25 kHz for comparison of the measured frequencies to the T-S frequencies obtained from linear stability theory. It should be noted that this bandwidth falls well within the frequency response of the hot-wire probe and pressure transducers.

4.0 FLOW QUALITY RESULTS

The application of any advanced measurement technique is always weighted by the ability of the technique to accurately represent the phenomena of interest being measured. Therefore before the flow quality data is presented the calibration results will be described. This will establish the limits of the data set, and determine what assumptions are valid. This will be followed by a description of the flow field fluctuation data associated with the LFC model. Data for several different hot wire techniques will also be analyzed and compared to the generalized, three element hot-wire results. The hot wire data has been extended to obtain fluctuating pressure data which will be compared to the fluctuating pressure probe data set.

4.1 Probe Calibration

This section will focus on the calibration process for hot wire anemometry and fluctuating pressure probes. Emphasis will be given to the hot wire calibration as it is the more complex instrument. The test matrix can become quite extensive and the time required to properly calibrate the hot wire probes can become lengthy. This is often compounded for the Three Element Technique because if any one of the three sensors break the calibration matrix must be restarted. If one can show that the velocity and density sensitivities for a hot wire sensor are the same, then the calibration matrix being reduced significantly and the flow quality

analysis can be simplified. Therefore the focus of this section is directed at the calibration sensitivities and the errors associated with simplified hot wire techniques.

4.1.1 Hot Wire Calibration Data - To begin the discussion of hot wire calibration, it is important to reiterate that the mean voltage output of the anemometer is generally a function of velocity, density, total temperature, and wire temperature, and regardless of the number of elements being used to extract flow information, each sensor must be calibrated independently. The following discussion will focus on the two calibration techniques described in section 2.2.1. It is anticipated that the results of the two calibrations approaches will be the same. An emphasis will be given to the velocity and density sensitivities because if it can shown that they are equal then they can be combined to form a mass flow sensitivity. This simplifies the acquisition of the fluctuating hot wire information from three variables (velocity, density, and total temperature) to two (mass flow, and total temperature). While this greatly simplifies the data analysis, it also limits the amount of information that can be extracted from the hot wire technique.

In general, to obtain the sensitivities of a hot wire, (see equations 2.63, 2.64, and 2.65 OR 2.77, 2.78, and 2.79), it is desired to operate the facility in the following manner:

(Vary Reynolds number): Mach number and Overheat Constant

(Vary Mach number): Reynolds number and Overheat Constant

(Vary Total Temperature): Reynolds number and Mach number Constant

While each of these variables can be changed independently, this process is very time consuming and the productivity of the facility diminishes. As is often the case in transonic testing, this approach must be modified due to the time constraints of the test schedule of the facility. The evaluation of this modified test matrix may require the interpolation of data and or the use of a multiple regression analysis technique.

Non-dimensional Calibration Approach - Based on data obtained by Vrebalovich (1962), the change in Recovery Temperature coefficient with Reynolds number can be neglected for the Knudsen number range of this study and equations 2.77 and 2.78 can be reduced to:

$$S_u = \left[\left(\frac{\partial \log Nu}{\partial \log Re} \right)_{M,\theta} + \left(\frac{1}{\alpha} \right) \left(\frac{\partial \log Nu}{\partial \log M} \right)_{Re,\theta} - \left(\frac{\eta}{\tau \alpha} \right) \left(\frac{\partial \log \eta}{\partial \log M} \right)_{Re,\theta} \right] \quad (4.1)$$

$$S_p = \left[\left(\frac{\partial \log Nu}{\partial \log Re} \right)_{M,\theta} \right] \quad (4.2)$$

The different components of the velocity, density, and total temperature sensitivities can be evaluated individually, then combined to form the appropriate sensitivity. If one can show that the last two terms of the

velocity sensitivity are negligible (or cancel) then the velocity sensitivity and density sensitivity are identically equal to:

$$\left(\frac{\partial \log \text{Nu}}{\partial \log \text{Re}}\right)_{\text{M},\theta}$$

The variation of Nusselt number with respect to Reynolds number, at a constant Mach number, has been shown to be a linear function in logarithmic space. This is illustrated by the curve fit of the data shown in figure 4.1. The straight line curve fit shows that for the Reynolds number range of this hot wire test, the following is true:

$$\left(\frac{\partial \log \text{Nu}}{\partial \log \text{Re}}\right)_{\text{M},\theta} = \text{Constant} \quad (4.3)$$

However Baldwin's data, (figure 1.2), clearly shows that for continuum flows and free molecular flows, the slopes change from 0.5 and 1, respectively. This would indicate that some non-linearity exists over a sufficiently large range of Reynolds numbers. The data shown in figure 4.1 is consistent with Baldwin's data (1958) over the limited Reynolds number range of the present data as shown in figure 4.2. Note that to compare to other results from different investigators the Nusselt number must be corrected for heat conduction to the sensor supports. The Nusselt number data shown in figure 4.2 has been corrected for these losses, using a technique described by Sandborn (1972). The agreement indicates that the heat transfer characteristics of the hot wires used throughout this study is consistent with other researchers data, yet the absolute magnitude of the corrected Nusselt number varied slightly from sensor to sensor. This is due to the small variations in wire length, resulting from slack added to the

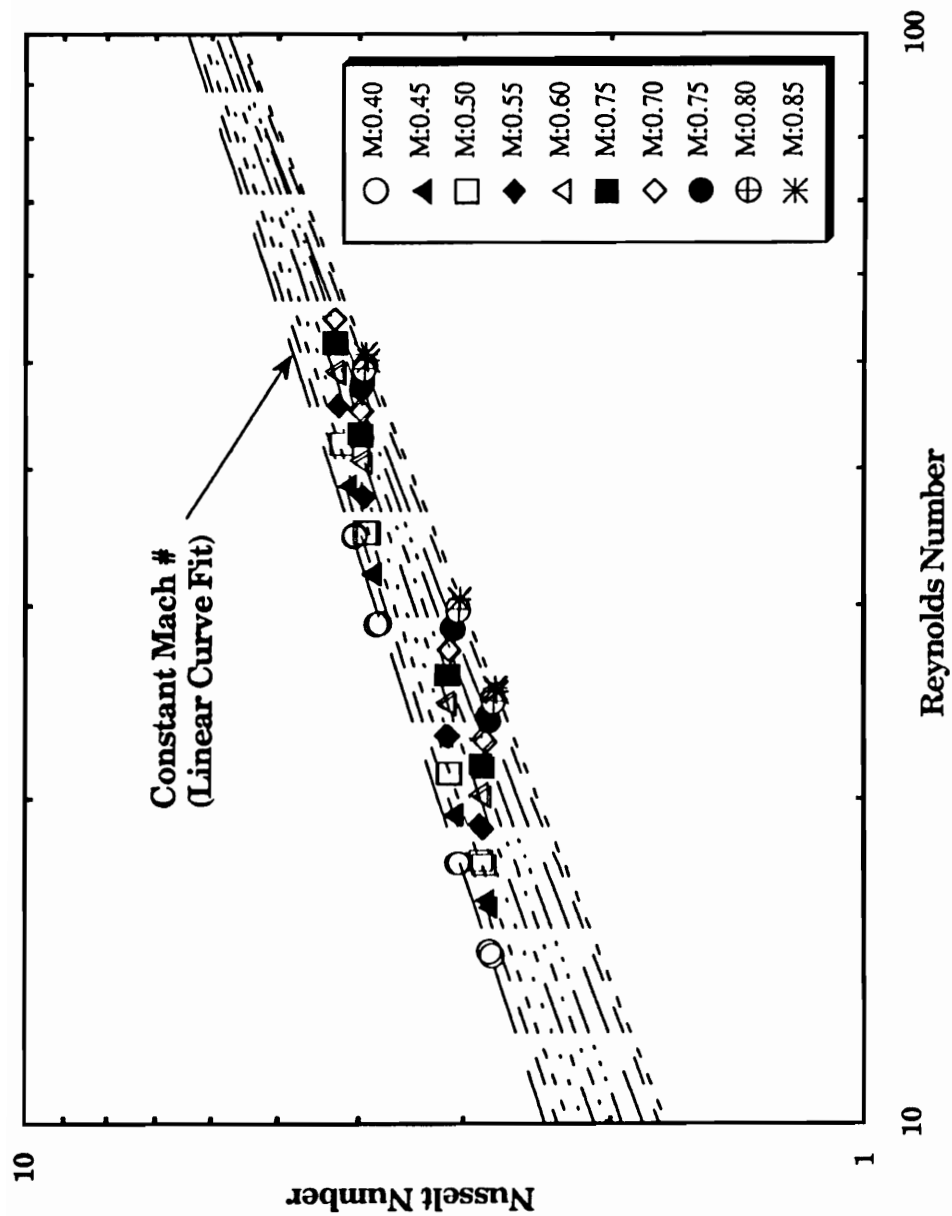


Figure 4.1 Reynolds number effect on Nusselt number at a constant Mach number

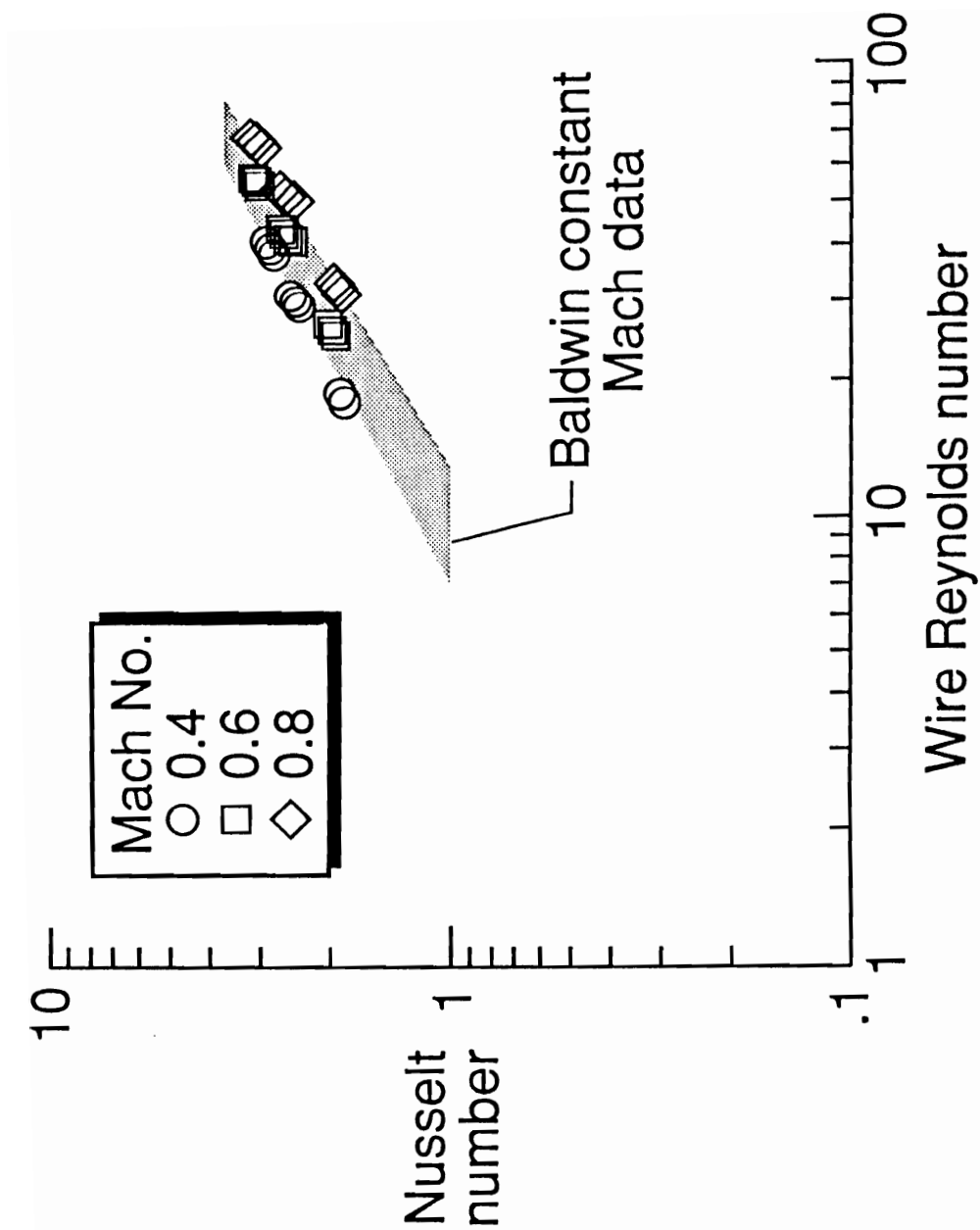


Figure 4.2 Comparison of corrected Nusselt number data to Baldwin's Nusselt number results (reference 1958)

sensor to avoid breakage or strain-gaging. Since the sensitivities required to obtain fluctuating quantities must be based on uncorrected Nusselt numbers, the remainder of this section will present only uncorrected Nusselt numbers.

To obtain the second term in the velocity sensitivity equation, (Nusselt number as a function of Mach number at a constant Reynolds number), the Nusselt number and Mach number data (figure 4.1) were extrapolated to the limits of the Reynolds number range of the present test. The Nusselt numbers were determined for constant Reynolds number, as shown in figure 4.3, by cross-plotting the data along a constant Reynolds number line from figure 4.1. Evaluating these data revealed that Nusselt number varied with Mach number as follows:

$$\left(\frac{\partial \log \text{Nu}}{\partial \log M} \right)_{\text{Re}, \theta} = f(\text{Mach number})^2 \quad (4.4)$$

Examining the extrapolated data in figure 4.3 indicates that as the Mach number was reduced to less than 0.3, the influence of this term diminishes and may be neglected. The data was grouped into constant Knudsen number arrays which were related to total pressure runs of the calibration matrix. While this information is not used in calculating the sensitivities it can be used to estimate whether the sensor is being affected by slip flow and/or compressibility effects. Note that the calculation of the velocity and density sensitivities used the local slopes of the actual Mach number and Reynolds number.

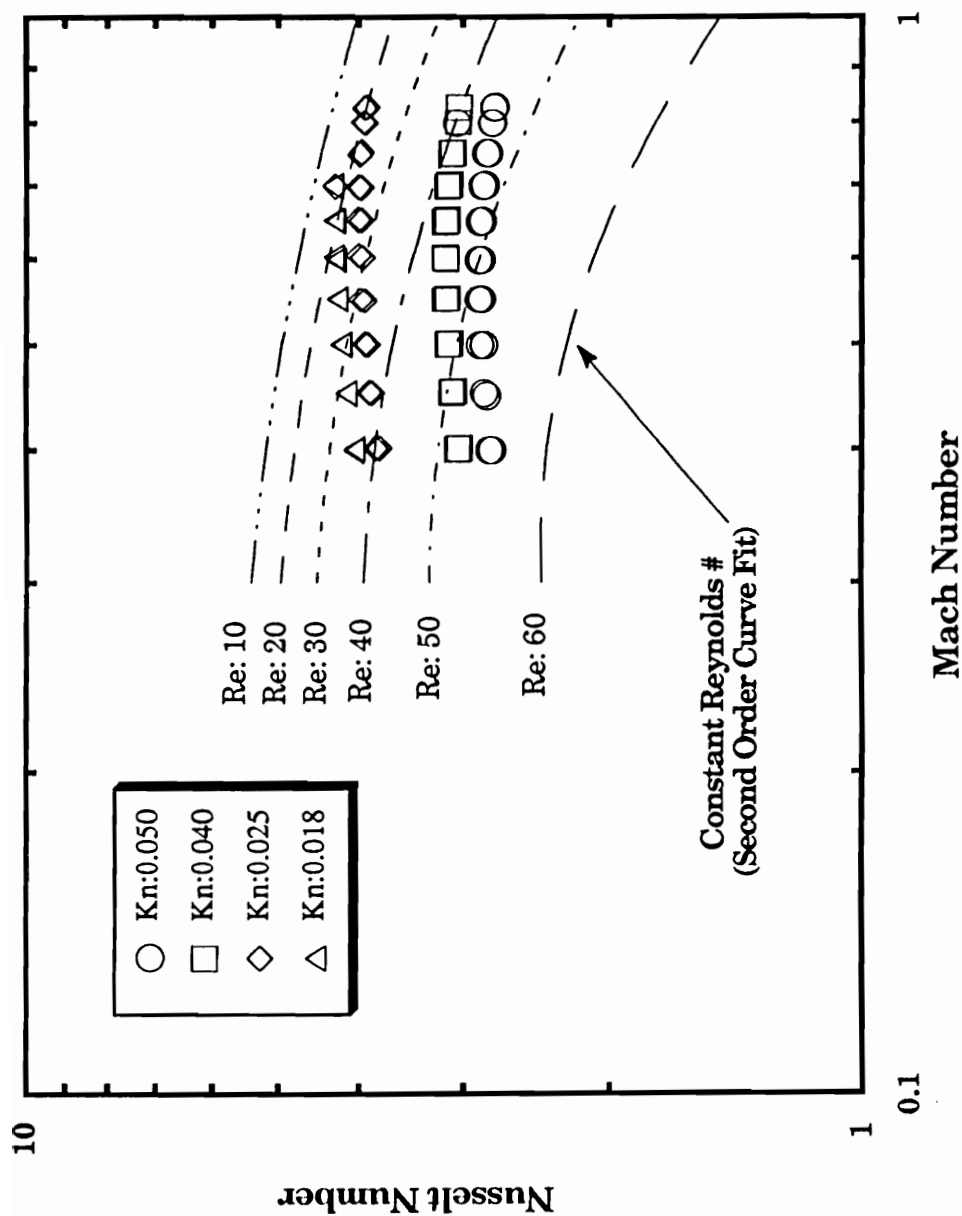


Figure 4.3 Mach number effect on Nusselt number for constant Reynolds number in the slip flow regime, Sensor diameter 0.00015 inches.

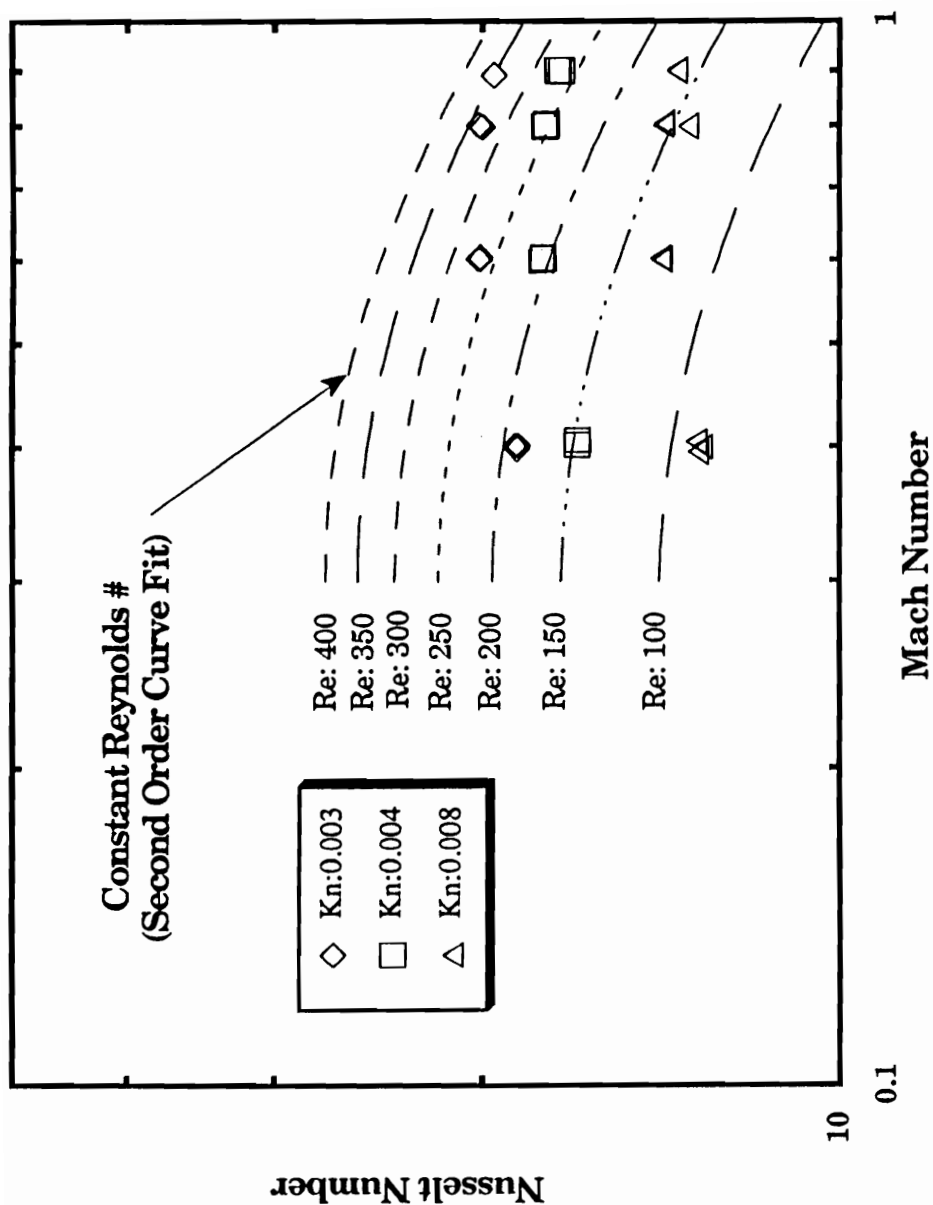


Figure 4.4 Mach number effect on Nusselt number for constant Reynolds number in the continuum flow regime, Sensor diameter 0.001 inches.

Separating the slip flow and the compressible effects is difficult and cannot be determined from the sensor data described in figure 4.1 alone. Figure 4.4 shows data obtained from a hot film sensor that is 10 times larger in diameter. This sensor was operating in the continuum regime based on Hinze's criteria (1975) ($Kn < 0.01$). However, if Baldwin's criteria ($Kn < 0.001$) is used the sensor is being operated in the upper regions of the slip flow regime. Comparing the high Mach number data from both probes demonstrates a Mach number effect. For the smaller sensor, the local slope decreases with increasing Reynolds number. The local slope of the film sensor evaluated at any given Mach number remains constant with increasing Reynolds number. It would be difficult to separate the effect of slip flow and compressibility using this data since it is not clearly in the continuum regime.

The third term of the velocity sensitivity is associated with the Recovery Temperature ratio relationship to Mach number. Data from Vrebalovich (1962) shown in figure 4.5, was used to obtain the following relationship (see Appendix A),

$$\left(\frac{\partial \log \eta}{\partial \log M} \right)_{Re, \theta} = f(Mach^6) \quad (4.5)$$

Evaluating the influence of this term and combining it with the results of the first two terms results in the velocity sensitivity and density sensitivity.

As seen in figure 4.6, the velocity and density sensitivities are not equal, $S_u \neq S_p$. There is a trend for S_u to approach S_p as Mach number decreases and or Reynolds number increases. This corresponds to a range in velocity sensitivities that change approximately 95% from the low Mach

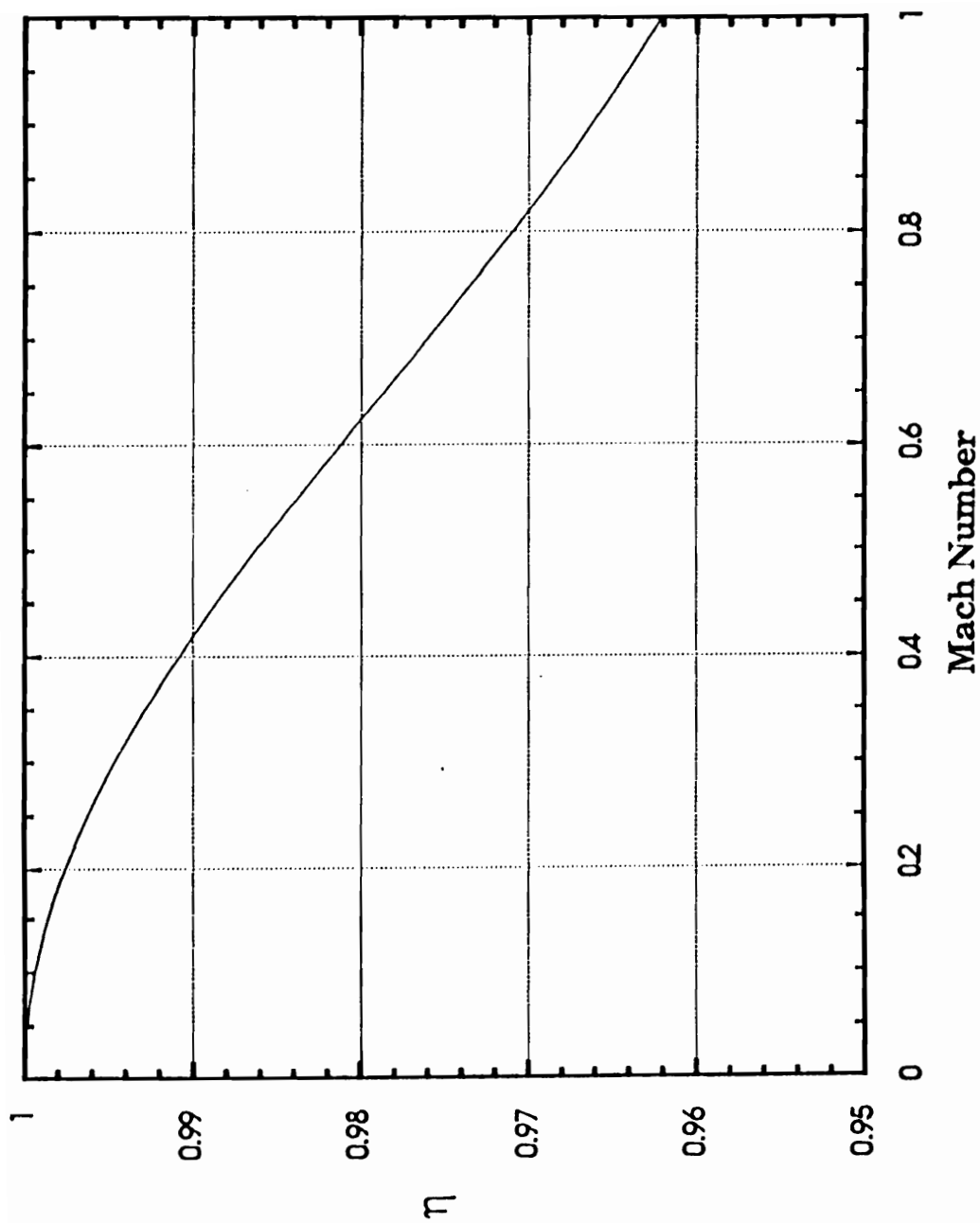


Figure 4.5 Recovery temperature ratio

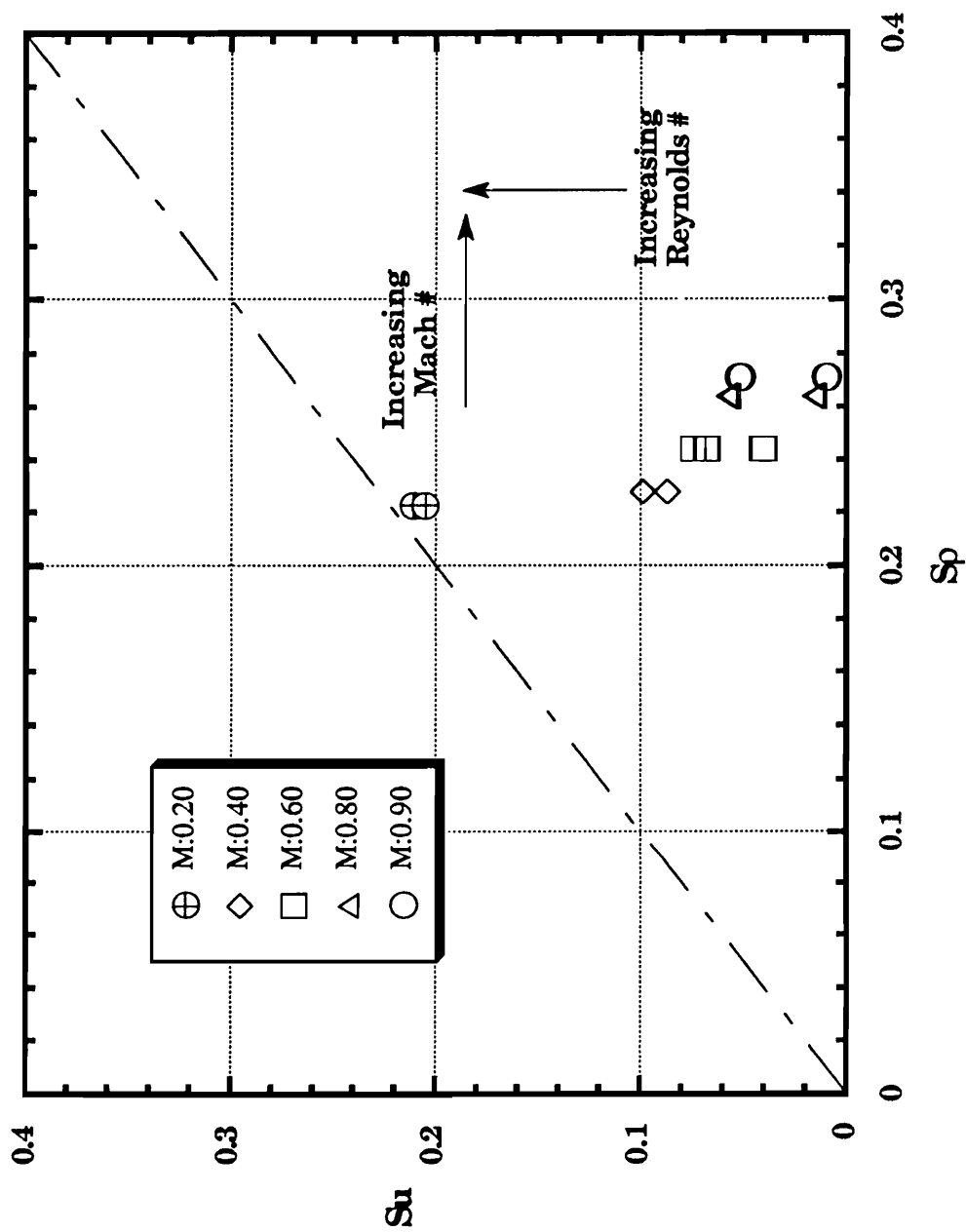


Figure 4.6 Comparison of the velocity and density sensitivities using the indirect calibration technique

numbers to the higher Mach numbers. The corresponding changes in density sensitivity is approximately 9% for the same range. The surprising result is that by obtaining the sensitivities using equations 4.1 and 4.2 the sensor is not very sensitive to velocity at high Mach numbers and low Reynolds numbers. This tendency is confirmed with several other sensors (See Appendix D). The general trends that $S_u = S_p$ for the conditions stated is also consistent with the assumptions that researchers who test in the low subsonic regime have been making. The trends at high Mach number and high Reynolds number are moving into the supersonic regime where it has been shown that $S_u = S_p$. It should be noted that the evaluation of the current results are made using data that is limited to three temperatures, four pressures, and ten Mach numbers. Even though there is a limited amount of data, the trends are consistent with Nusselt number being a function of Reynolds number and Mach number.

Direct Calibration Approach - The velocity, density, and total sensitivities can be obtained by correlating the mean voltage directly to velocity, density, and total temperature (See equations 2.63, 2.64, and 2.65). This greatly simplifies the calculation of the sensitivities. The velocity and density sensitivities for the same sensor described above is presented in figure 4.7. These data clearly show that $S_u \neq S_p$. In fact S_p is always greater than S_u for the conditions tested as was the case described above. In addition, the difference between S_u and S_p increased with Mach number at all total pressures, but decreased with increasing Reynolds number at a constant Mach number. This corresponds to a change in in velocity

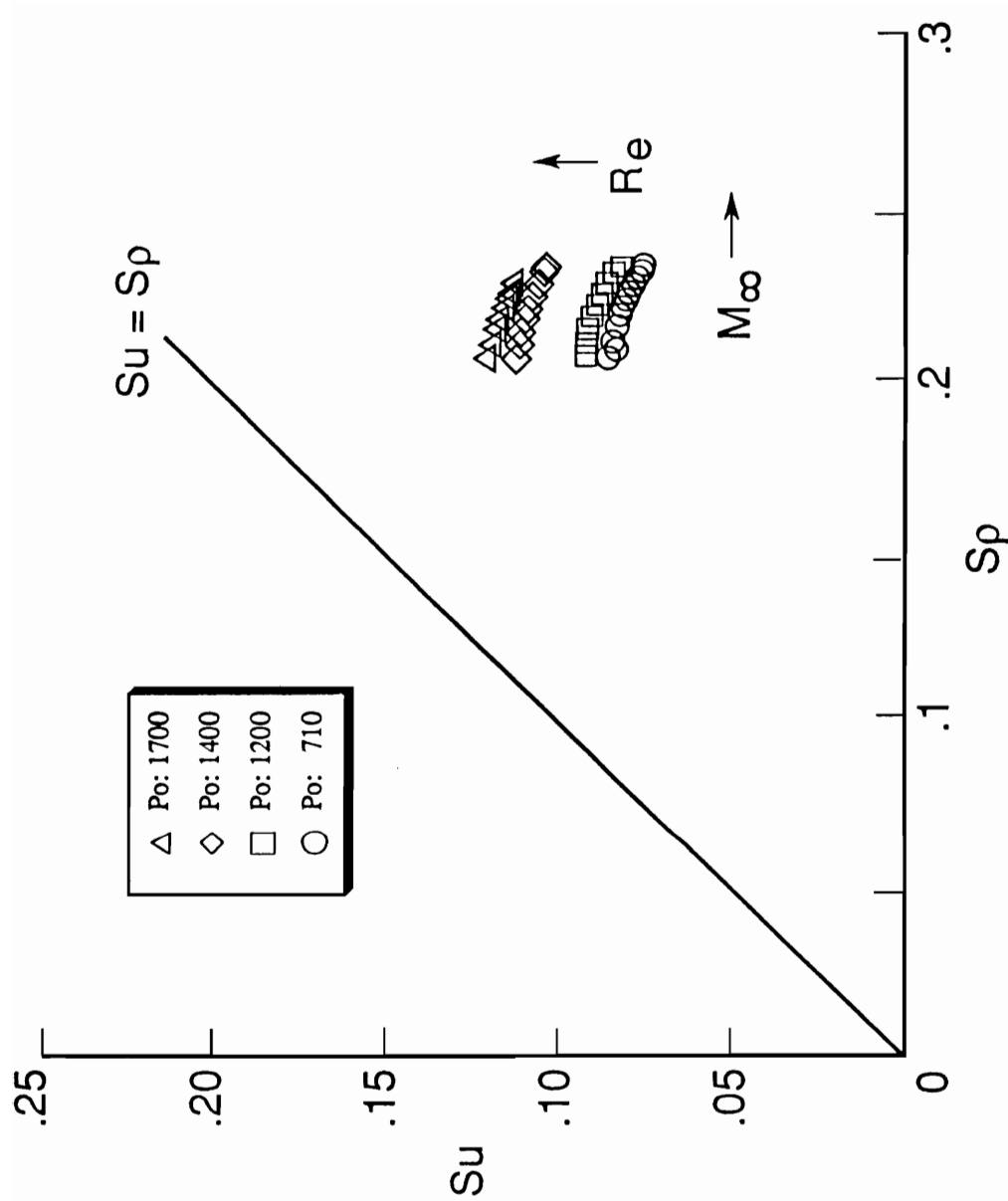


Figure 4.7 Comparison of the velocity and density sensitivities using the direct calibration technique

sensitivity of approximately 9% and a change in density sensitivity of 18%. Table 4.1 shows typical velocity, density, total temperature sensitivities and condition numbers for the three element probe used for this test at a fixed pressure and total temperature.

Table 4.1 Velocity, density, and total temperature sensitivities for three element hot wire.

THREE ELEMENT (CASE A)										
MACH	S _{U1}	S _{U2}	S _{U3}	S _{p1}	S _{p2}	S _{p3}	S _{T01}	S _{T02}	S _{T03}	Condition #
0.40	0.1301	0.1248	0.1115	0.2111	0.3930	0.2064	-0.4716	-0.8187	-0.5979	33.6
0.45	0.1291	9.1239	0.1108	0.2174	0.3985	0.2108	-0.4493	-0.8026	-0.5723	32.7
0.50	0.1280	0.1229	0.1100	0.2228	0.4032	0.2147	-0.4305	-0.7894	-0.5514	32.3
0.55	0.1267	0.1218	0.1091	0.2278	0.4075	0.2182	-0.4140	-0.7792	-0.5337	31.8
0.60	0.1252	0.1205	0.1080	0.2326	0.4117	0.2216	-0.3986	-0.7682	-0.5181-	31.7
0.65	0.1237	0.1192	0.1069	0.2365	0.4149	0.2244	-0.3872	-0.7612	-0.5073	31.7
0.70	0.1223	0.1180	0.1059	0.2400	0.4180	0.2269	-0.3773	-0.7556	-0.4989	31.7
0.75	0.1205	0.1165	0.1046	0.2434	0.4209	0.2293	-0.3685	-0.7511	-0.4925	31.8
0.80	0.1189	0.1151	-.1035	0.2468	0.4241	0.2319	-0.3608	-0.7480	-0.4884	31.9
0.82	0.1182	0.1143	0.1029	0.2484	0.4257	0.2332	-0.3576	-0.7470	-0.4873	31.9

Comparison of the Calibration Techniques - The most disturbing result of the hot wire calibration is that the actual magnitudes of S_u and S_p are **not consistent** between the two calibration methods. Comparing the results of the two calibration methods, there is a reversal in the trends in the sensitivities. That is to say the *Direct Calibration* method shows a greater variation in the density sensitivity compared to the velocity sensitivity, while the *Indirect Calibration* technique indicates that there is a larger variation in the velocity sensitivity compared to the density sensitivity. The one consistent factor for both calibration techniques is that in general $S_u \neq S_p$.

Evaluation of the Hot wire sensitivities when $S_u = S_p$ - In an effort to maintain consistency in the comparison of the three element, two element, and single element hot wire techniques, the data from the three element probe was used for the two element and single element cases. This was done to avoid differences in wind tunnel conditions from one location to another and/or potential differences in time histories from one point in time to the next. There were some concerns that there might be sensor to sensor interference or influence of the sensor supports. A special Y-configuration three wire probe was built and it was determined that the sensor to sensor interference was negligible. This is documented by Stainback, Nagabushana, Jones, and Clukey (1991).

Table 4.2 summarizes the correlation coefficients to be used in evaluating the different hot wire techniques. As noted in section 2.2.2, both the two-element and single-element techniques require that $S_u = S_p$. Since

Table 4.2 Calibration coefficients and error analysis for normal three-element hot-wire probe.

Coeff.	THREE ELEMENT			TWO ELEMENT			SINGLE ELEMENT				
	CASE A			CASE B			CASE C	CASE D	CASE E	CASE F	CASE G
	Wire 1	Wire 2	Wire 3	Wire 2	Wire 3	Wire 3	Wire 3	Wire 3	Wire 3	Wire 3	Wire 3
A1	17.2336	16.3569	32.7590	3.4376	2.0783	2.0783	2.0783	2.0972			
A2	-5.2289	-4.7608	-10.5261	-0.3306	0.2150	0.2150	0.2150	0.2002	0.1993	0.0445	0.0868
A3	9.4483	8.6217	20.6159	-1.0941	-0.5725	-0.5725	-0.5725	-0.5795			
A4	-6.2201	-5.8885	-11.8222	0.1918	-0.0054	-0.0054	-0.0054				
A5	-3.1833	-3.0315	-7.0881								
A6	2.0232	1.8416	3.9373								
A7	-3.5028	-3.1905	-7.0881								
A8	1.2113	1.1495	2.6272								
r2	0.9982	0.9990	0.9988	0.9126	0.9865	0.9865	0.9865	0.8865	0.8851	0.6102	0.9894
ϵ	0.0016	0.0011	0.0013	0.0100	0.0118	0.0118	0.0118	-.0117	0.0119	0.0025	0.0005

transonic hot wire data is sometimes obtained by assuming that $S_u = S_p$ without a suitable calibration, the present three element data was analyzed assuming $S_u = S_p$ for both the two element and single element techniques.

Two Element Calibration - The equations used for calibrating the two element probe had the same form as describe by equation 2.62 for the three element case. The primary difference is that the mean voltages was correlated with mass flow, total temperature, and the cross products. For a fixed total temperature the correlation of mass flow and anemometer voltage is shown in figure 4.8. Note that there is a voltage "roll over" at the higher mass flows, i.e. multi-valued mass flow for a single voltage. These non-linearities occurred at approximately a Mach number of 0.65 for each of the total pressures observed, and are thought to be a result of a combination of factors. These factors may include the differences in the rate of change in velocity and density with Mach number and the higher sensitivity of wire voltage with density.

To evaluate the S_m and S_{To} the data can be considered in two ways as described by equations 2.70 and 2.71 or equations 2.72 and 2.73. Since the two element equations (2.70 and 2.71) will theoretically account for the changes in velocity and density in the mass flow calculation, all of the calibration data can be used to compute S_m and S_{To} . This does not seem practical since none of the local slopes are represented by the curve fit, (table 4.3). The mean voltages can also be correlated with mass flow and total temperature without using the cross product term.

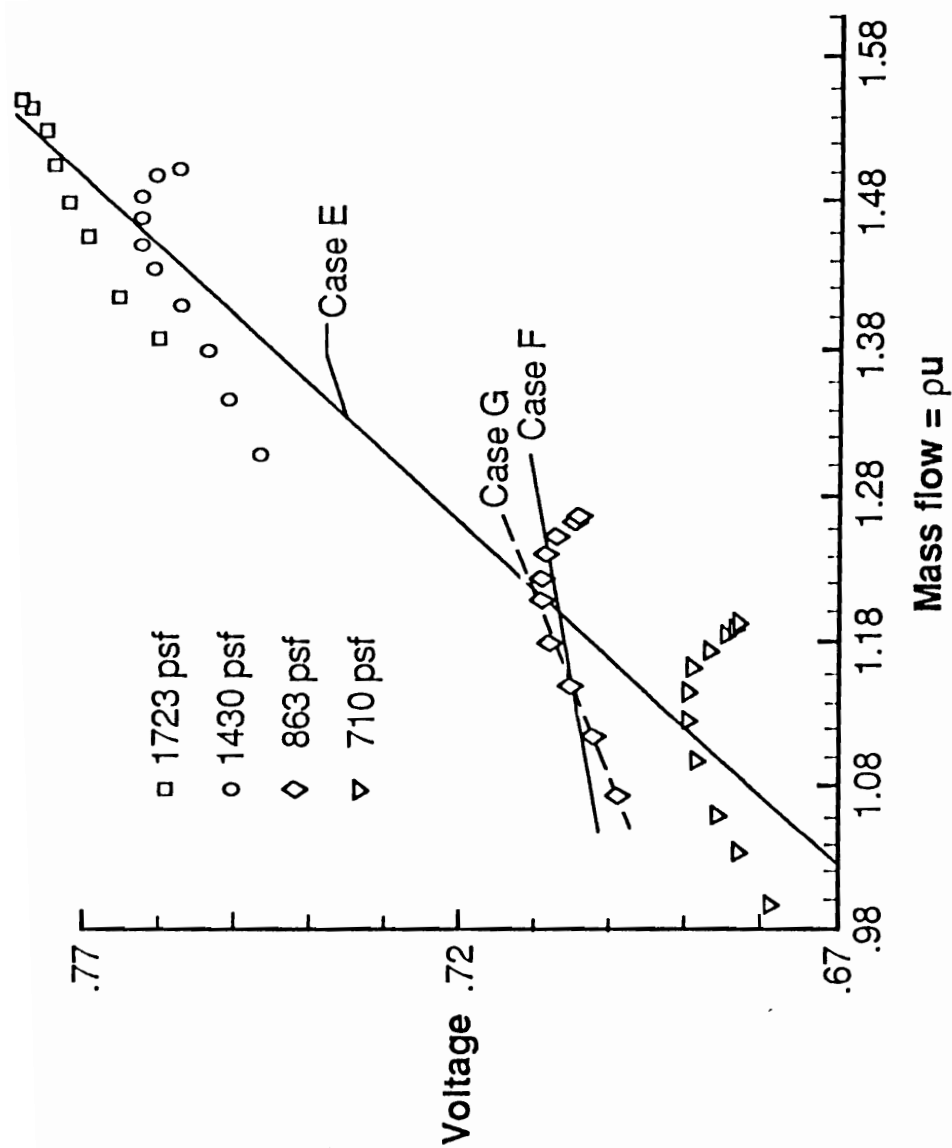


Figure 4.8 Hot wire voltage correlation to mass flow for different total pressures

Table 4.3 Mass Flow and total temperature sensitivities for two element hot wire.

MACH	TWO ELEMENT (CASE B)	
	S_m	S_{T_0}
0.40	0.20028	-0.5795
0.45	0.20028	-0.5798
0.50	0.20028	-0.5799
0.60	0.20028	-0.5801
0.70	0.20028	-0.5802
0.75	0.20028	-0.5803
0.80	0.20028	-0.5804
0.83	0.20027	-0.5805

Single Element Calibration - The calibration of a single element probe, which only requires the determination of S_m , can be performed in several ways, depending on the type of data available and the assumptions made. Table 4.4 summarizes the assumptions made for several single element hot wire techniques to be compared in this report. As in the calibration of the two element probe, the quality of the calibration will be a function of the amount of data used to obtain the sensitivity. Case "C" utilizes all of the calibration data and takes advantage of the cross product terms described in equation 2.69, but will use only the S_m determined by equation 2.70. The results obtained for case "D" utilized all of the data available but without the cross product term. Therefore, S_m was determined by equation 2.72.

The special case for conditions where the total temperature is fixed and cannot be varied will be identified as case "E". The mass flow sensitivity would be obtained by correlating the data over a Mach number and total pressure range. If the cross product and temperature terms of equation 2.69 are neglected, the calibration of a single element probe can be simplified by directly correlating the voltage as a function of mass flow only, (equation 2.75). The results for case "E" were therefore obtained by utilizing all of the data for a fixed total temperature, and uses S_m as determined by equation 2.76.

The second special case would be representative of facilities that operate at atmospheric or fixed total pressures. The mass flow sensitivity would be obtained for a Mach number sweep at a single total pressure, case "F". The third special case is an extension of the second special case

Table 4.4 Description of assumptions for cases A through G.

BASIC DATA								
CASE	NUMBER OF ELEMENTS	Su = Sp	$S_{T_0} \frac{\tilde{T}_0}{T_0} < S_m \frac{\tilde{m}}{m}$	\tilde{T}_0	T ₀ & P ₀	T ₀ & P ₀ & M < 0.7	EXTENSION OF DATA	
A	3						Rmp = Rm T ₀ = Rp T ₀	
B	2	X					X	
C	1	X	X				X	
D	1	X	X				X	
E	1	X	X	X			X	
F	1	X	X	X	X		X	
G	1	X	X	X	X	X	X	

which is to limit the calibration to the Mach number range that would give the best fit, i.e. eliminate the data beyond the non-linearity effects in the calibration data. For the data described in this report case "G" represents the conditions where the Mach number is less than 0.65. This value of the Mach number is in the general vicinity where the slope of the calibration data goes to zero.

Table 4.5 summarizes the single element mass flow sensitivities. One can clearly see from figure 4.8 that when all of the data are used for a fixed total temperature, case "E", the computed variation of voltage with mass flow does not agree very well with the measured data. Case "F", utilized a restricted amount of the data and appears to correlate to the data better than case "E". The correlation in case "G" is even better, because all of the non-linearity effects have been removed for the same restricted data set used in case "E". This is borne out by the r^2 values which represent the quality of curve fit and are listed in table 4.1.

Table 4.5 Mass Flow sensitivities for single element hot wire.

SINGLE ELEMENT				
MACH	CASE C	CASE D	CASE E	CASE F
0.40	0.0028	0.2002	0.1993	0.0445
0.45	0.0028			
0.50	0.0028			
0.55	0.0028			
0.60	0.0028			
0.65	0.0028			
0.70	0.0028			
0.75	0.0028			
0.80	0.0027			
0.83	0.0027			
				0.0868

4.1.2 Fluctuating Pressure Probe Calibration

For the pressure transducers used in the present test, there was a linear relationship of pressure to voltage which is typical of diaphragm type transducers. The transducer was calibrated by means of varying the pressure on one side of the diaphragm and correlating the mean pressure to the mean output voltage. Following this approach resulted in a voltage and pressure correlation or pressure transducer sensitivity. Table 4.6 shows a sample mean calibration matrix for a typical transducer.

It is recognized that the static calibration of a transducer does not address the frequency response of the probe under flow conditions. If the transducer is mounted to measure the total pressure fluctuations, figure 3.10, the frequency response of the probe can be directly related to the frequency response of the transducer. A "no flow" calibration was performed using both broad band noise and sinusoidal input for each transducer and has indicated a flat frequency response up to 10kHz. This was also used to validate the transducer sensitivity as determined by the mean static pressure calibration.

When the transducers are mounted to measure static pressure fluctuations, figure 3.11, there is normally a degradation of the probe frequency response, due to the effect of the Helmholtz cavity created at the transducer interface. This is compounded by the acoustic impedance of the orifice itself under flow conditions. The ability to evaluate

Table 4.6 Example of fluctuating pressure transducer calibration.

REFERENCE STANDARD	REF STD CORRECTED	TRANSDUCER OUTPUT	LEAST SQUARES STRAIGHT LINE	TRANSDUCER DEVIATION
MMHGD	PSID	MILLIVOLTS	MILLIVOLTS	MILLIVOLTS
X1	X	Y1	Y	(Y1-Y)
10.343	0.20000	8.436	8.448	-0.012
20.686	0.40001	11.275	11.293	-0.018
31.029	0.60001	14.128	14.138	-0.010
41.372	0.80001	16.980	16.983	-0.003
51.715	1.00001	19.833	19.828	0.005
-10.343	-0.20000	2.761	2.759	0.002
-20.686	-0.40001	-0.085	-0.086	0.001
-31.029	-0.60001	-2.936	-2.931	-0.005
-41.372	-0.80001	-5.772	-5.776	0.004
-51.715	-1.00001	-8.613	-8.621	0.008

SENSITIVITY 14.22394 MV/PSID

the orifice impedance is very restricted, (Marcolini, et al 1991), and therefore will be neglected.

4.2 Hot Wire Flow Field Fluctuation Data

Based on the calibration results of the probes $S_u \neq S_p$, it becomes apparent that to determine the flow field perturbations for the transonic flow regime, it is necessary to utilize a three element probe. The following data analysis will focus on the three element data and be followed by a section on alternate hot wire techniques to illustrate potential errors of such techniques.

4.2.1 Fluctuations vs. Mach Number - The velocity, density, total temperature, and mass flow fluctuations presented in this section were measured in the test section of the 8' TPT over a total pressure and Mach number range using a three-element hot-wire probe. The results at a fixed total temperature of 540° R are presented in figures 4.9 ($P_o=1725$ psf), figure 4.10 ($P_o=1430$ psf), figure 4.11 ($P_o=860$ psf), and figure 4.12 ($P_o=710$ psf). In general, all of the fluctuating rms amplitudes increased with Mach number. When the tunnel was choked the rms amplitudes should decrease. This occurs for the 8'TPT when the Mach numbers are greater than 0.75. The results for the total pressures of 710 psf and 860 psf conditions show such a decrease. However the results for the total pressures of 1430 psf and 1725 psf do not have such a trend. This cannot be explained at this time. The decrease in the rms level of the fluctuating quantities for the other two conditions occurred at $M > 0.75$ and was associated with a decrease in upstream moving sound which was being generated in the wind-tunnel diffuser.

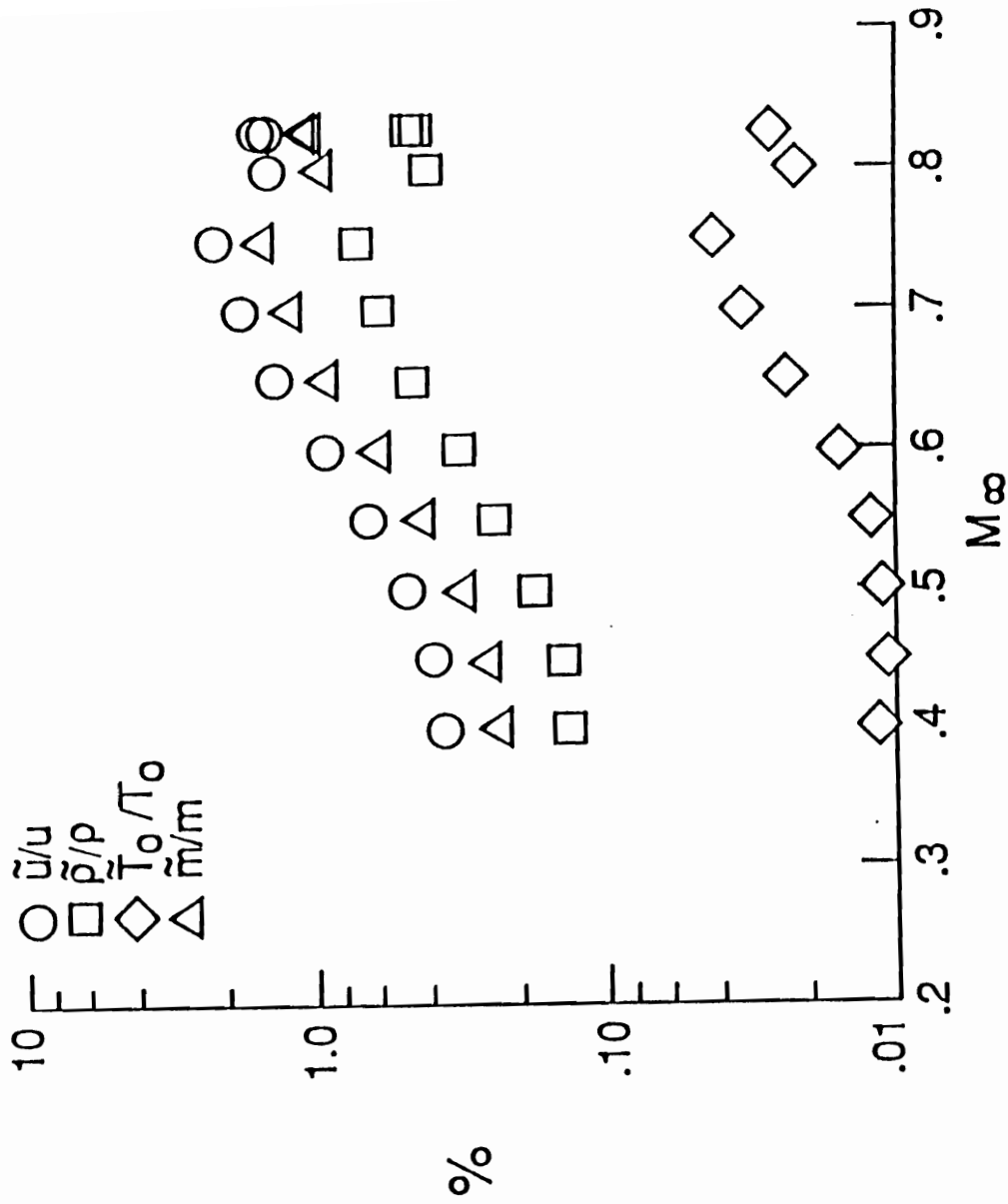


Figure 4.9 Free stream rms flow quality variations with Mach number for a LFC model configuration, Po710 psf, To 540 R, Bandwidth 1 < Hz < 5000

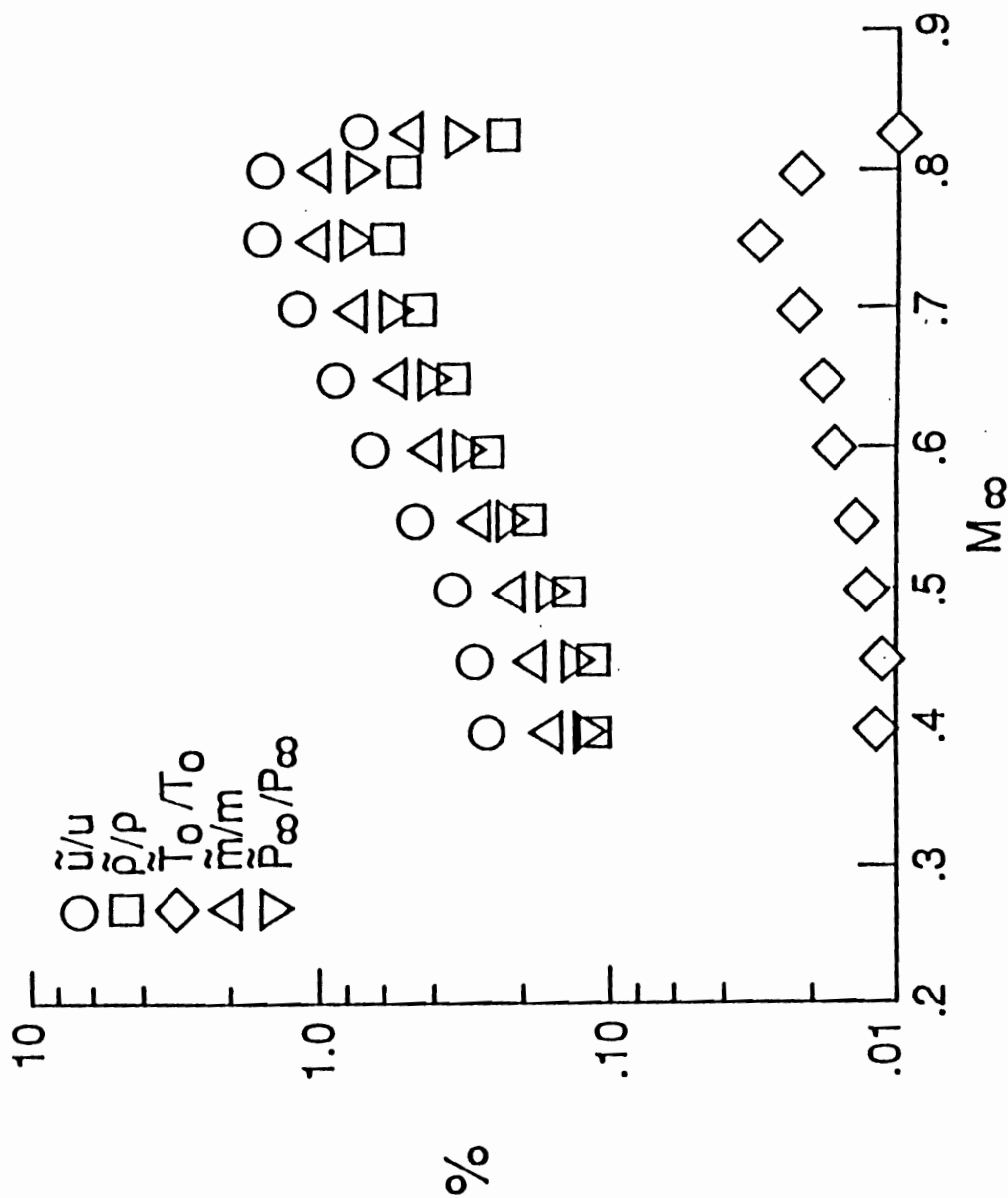


Figure 4.10 Free stream rms flow quality variations with Mach number for a LFC modelPo: 860 psf, To: 540 R, Bandwidth 1<Hz<5000

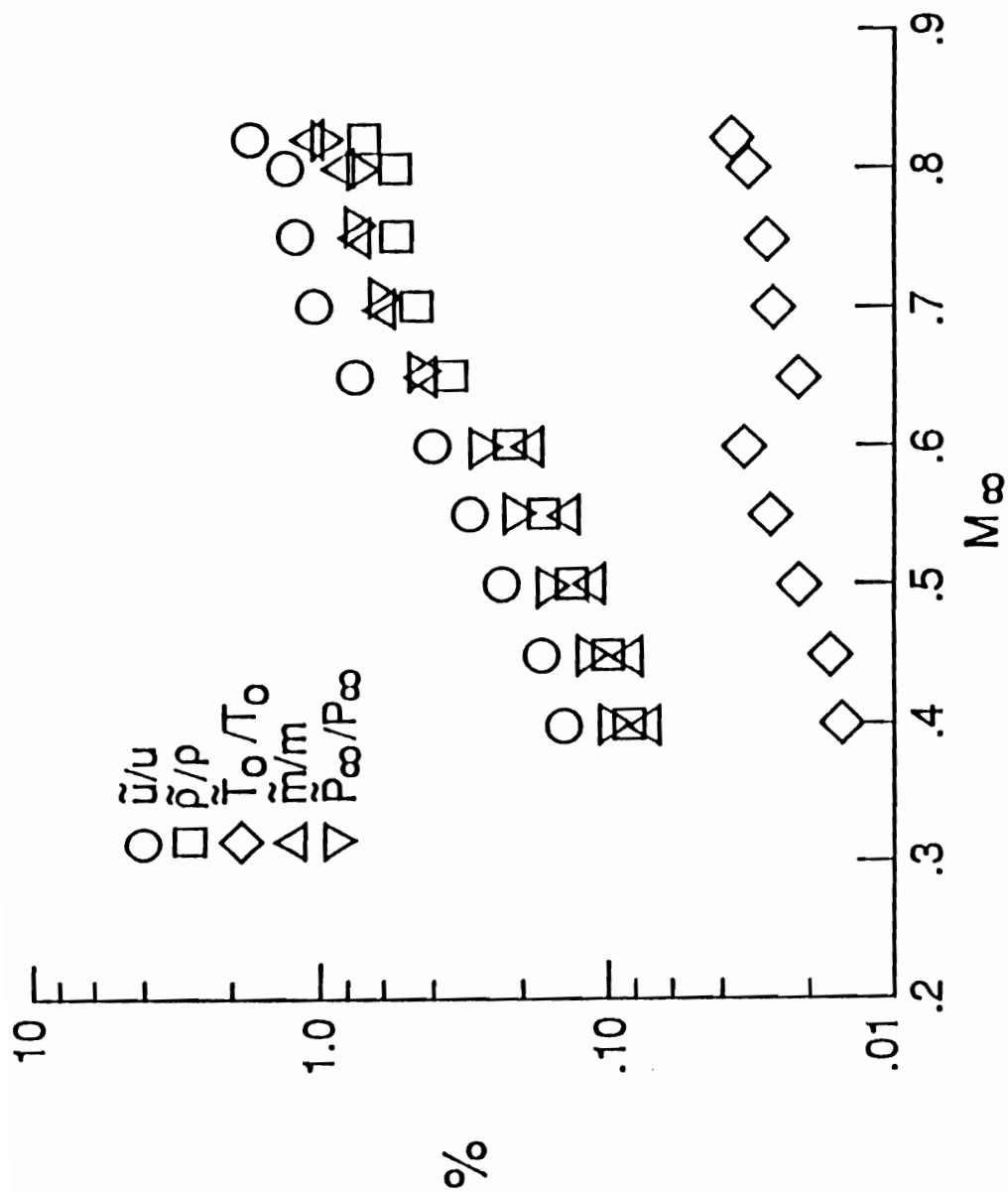


Figure 4.11 Free stream rms flow quality variations with Mach number for a LFC modelPo: 1430 psf, T_0 : 540oR, Bandwidth 1<Hz<5000

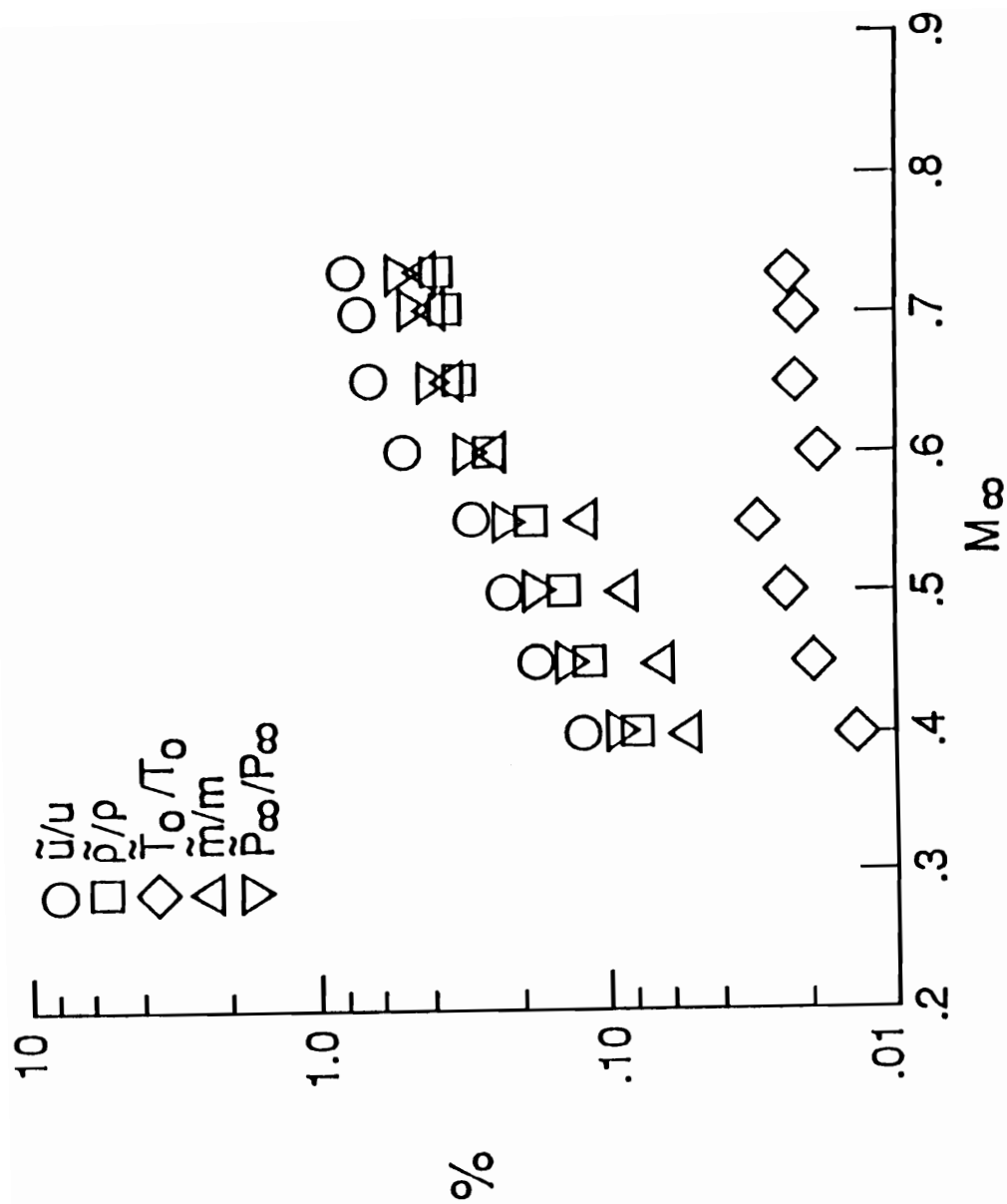


Figure 4.12 Free stream rms flow quality variations with Mach number for a LFC model configuration, P_o 1725 psf, T_o 540oR, Bandwidth 1 < Hz < 5000

The rms velocity fluctuations were higher than the rms values for density and total temperature fluctuations. The rms velocity fluctuations ranged from a lower level of 0.12 percent at $M = 0.4$ and a total pressure of 1725 psf to 2.2 percent at $M = 0.75$ and total pressure of 710 psf. The total temperature fluctuations had the lowest rms values and ranged from a lower level of 0.011 percent at $M = 0.45$ and total pressure of 710 psf to 0.044 percent at $M = 0.75$ and total pressure of 710 psf. The density and mass flow fluctuations had rms levels between those for the velocity and total temperature fluctuations. The density fluctuations ranged from a high value of 0.73 percent at $M = 0.75$ and total pressure of 710 psf to a low of 0.082 at $M = 0.4$ and total pressure of 1725 psf. The mass flow fluctuations ranged from a high value of 1.55 percent at $M = 0.75$ and total pressure of 710 psf to a low of 0.053 percent at $M = 0.4$ and total pressure of 1725 psf.

4.2.2 Fluctuations vs. Unit Reynolds Number

The data are replotted as a function of unit Reynolds number for constant values of Mach number in figure 4.13 through figure 4.16.

At a constant Mach number Figure 4.13 shows that there was a significant decrease in the velocity fluctuations with increasing Reynolds number when the tunnel was not choked. The slopes of the curves are about minus one. The variation of velocity fluctuations with Reynolds number changed markedly when the tunnel was choked at $M = 0.80$. Under choked conditions, the rms velocity fluctuations either remained unchanged with Reynolds number or increased slightly with an increase in Reynolds number.

Figure 4.14 shows that there was a reduced effect of Reynolds number on the density fluctuations compared with those of the velocity fluctuations. The slopes of the curves for density fluctuations with respect to Reynolds number were approximately minus 0.5 or less when the tunnel was not choked. When the tunnel was choked, the density fluctuations increased with increasing Reynolds number.

Figure 4.15 shows that there was no consistent variation of the temperature fluctuations with Reynolds number at constant Mach numbers. The wind tunnel has a cooler located in the fourth corner ahead of the settling chamber, and this could be responsible for the apparent inconsistency of the temperature fluctuations. For example, if the water flow through the cooler was being increased or decreased to maintain a

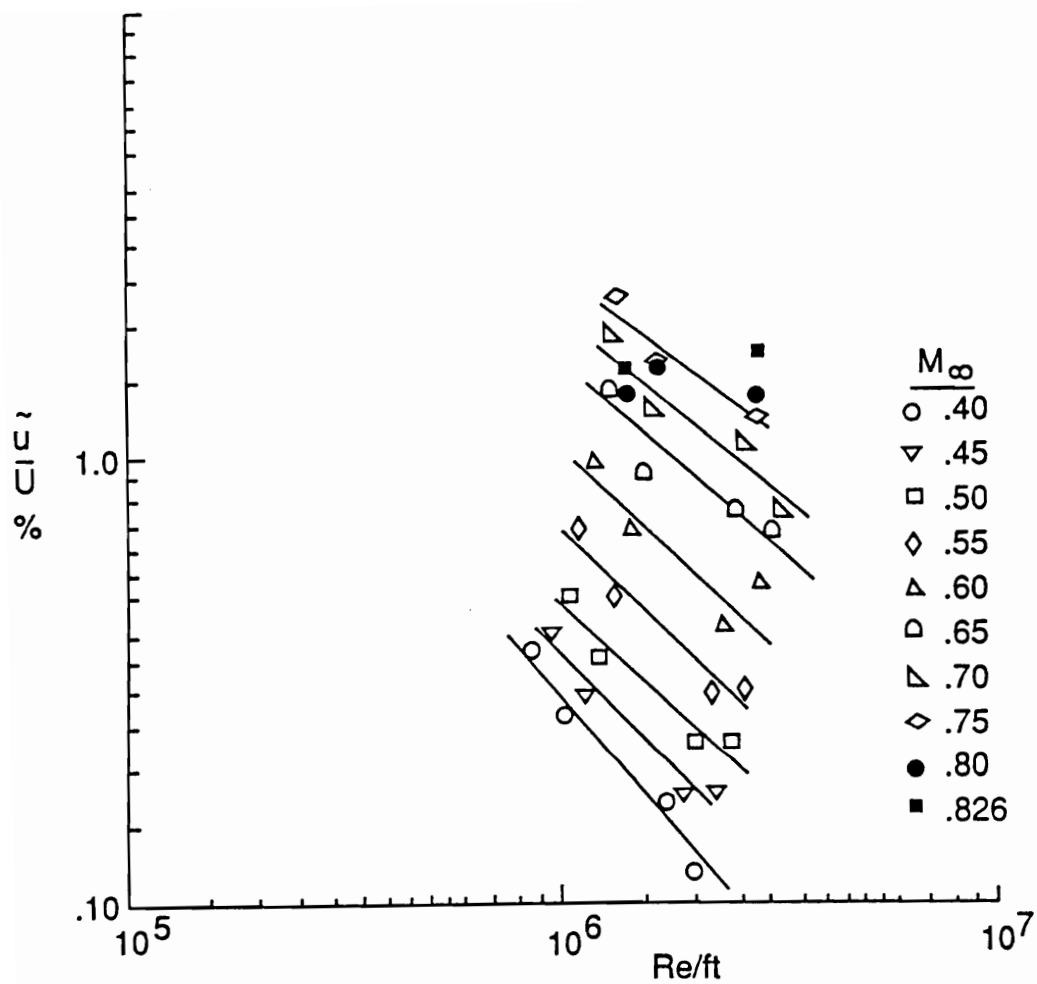


Figure 4.13 Free stream rms velocity variations with Reynolds number for a LFC model configuration, To 540oR, Bandwidth 1 < Hz < 5000

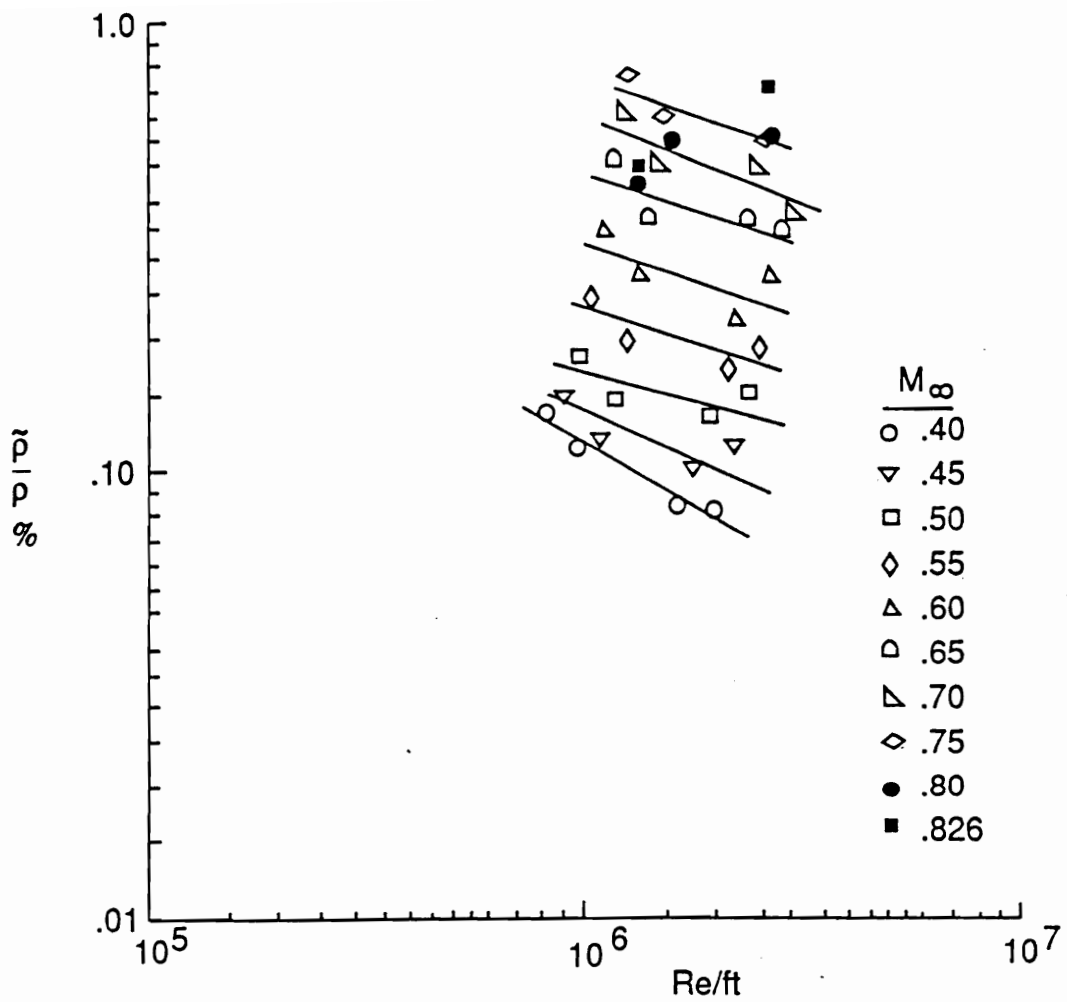


Figure 4.14 Free stream rms density variations with Reynolds number for a LFC model configuration, To 540oR, Bandwidth $1 < \text{Hz} < 5000$

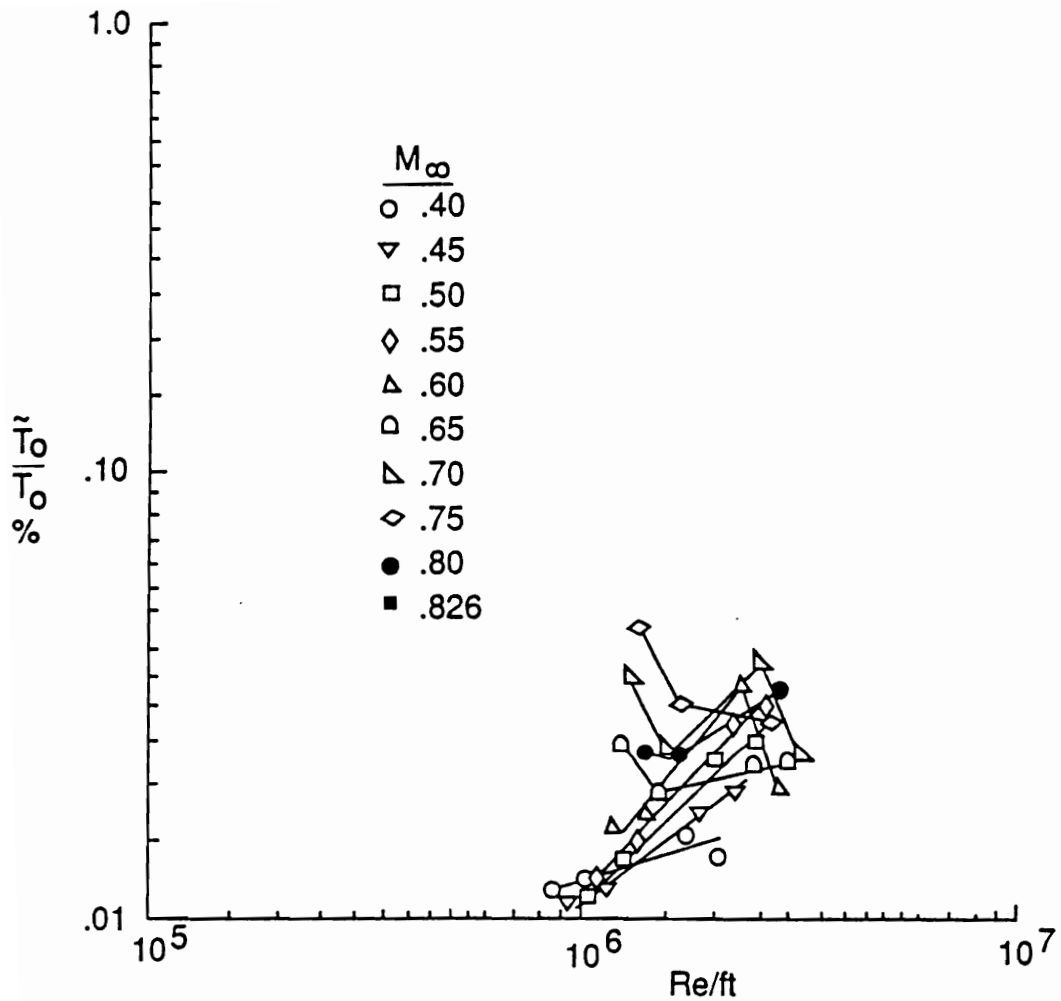


Figure 4.15 Free stream rms total temperature variations with Reynolds number for a LFC model configuration, T_0 540oR, Bandwidth $1 < \text{Hz} < 5000$

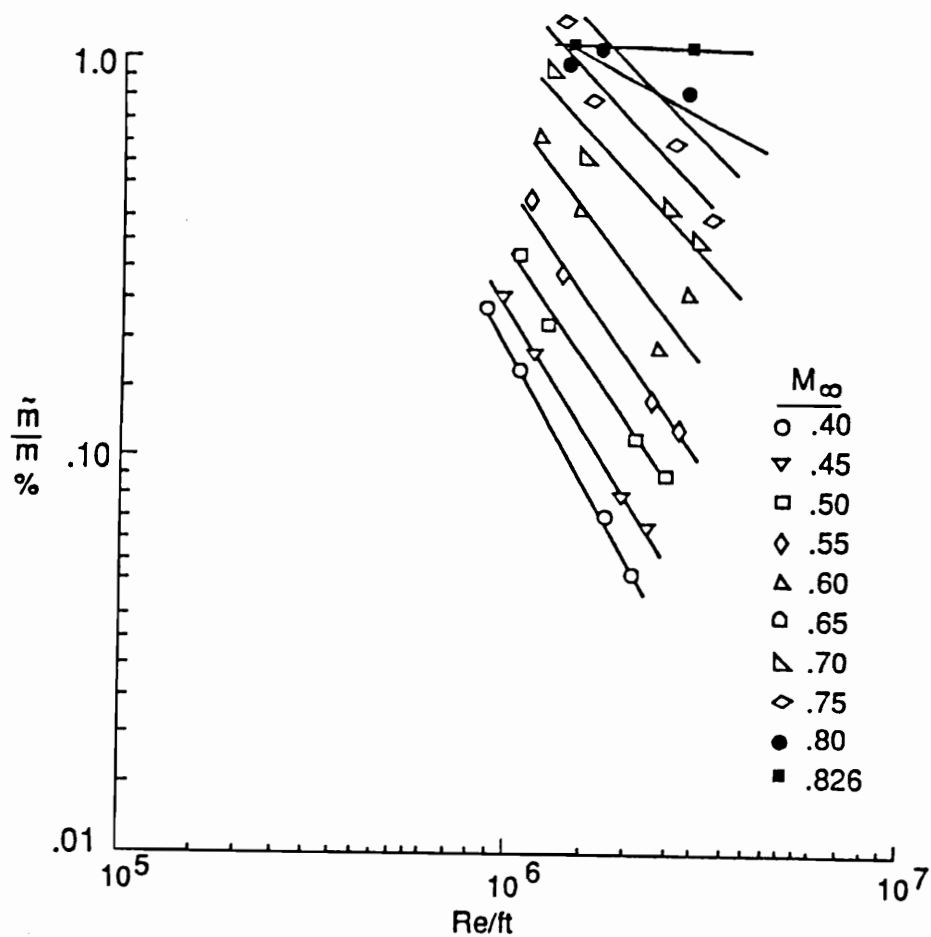


Figure 4.16 Free stream rms mass flow variations with Reynolds number for a LFC model configuration, To 540oR, Bandwidth $1 < \text{Hz} < 5000$

constant temperature in the test section while hot-wire data were being taken, the temperature fluctuations could increase or decrease with the flow rate of the coolant. It should be noted that the maximum rms value of total temperature during data acquisition corresponds to approximately 0.30°R .

The variation of the mass flow fluctuation with Reynolds number shown in figure 4.16 was similar to the variations for the velocity fluctuations. Mass flow fluctuations also increased with Reynolds number when the tunnel choked as did the velocity fluctuations. The magnitude of these measured fluctuating variables are higher than usually accepted when transition processes are being evaluated.

4.2.3 Correlation Coefficients - The correlation coefficients, R_{up} , R_{uTo} , and R_{pTo} , can sometimes be used to determine which of the basic fluctuations, vorticity, entropy, or sound, is being measured. If it is assumed that all the fluctuations are either vorticity, entropy, or sound, the values for the correlation coefficients can be obtained as shown in section 2.1 and as presented in Table 1.1. The correlations calculated from the present data are presented in figure 4.17 through figure 4.19.

First consider R_{up} and compare the data from figure 4.17 - 4.20 with the results in Table 1.1. If the fluctuations were either vorticity or entropy, R_{up} would be zero, but if the fluctuations were sound with $\theta = 0^{\circ}$, R_{up} would be +1. However, if the fluctuations were sound with $\theta = 180^{\circ}$, then R_{up} would be -1. The R_{up} data for all the pressures appear to confirm the latter condition. So from this comparison we might expect upstream

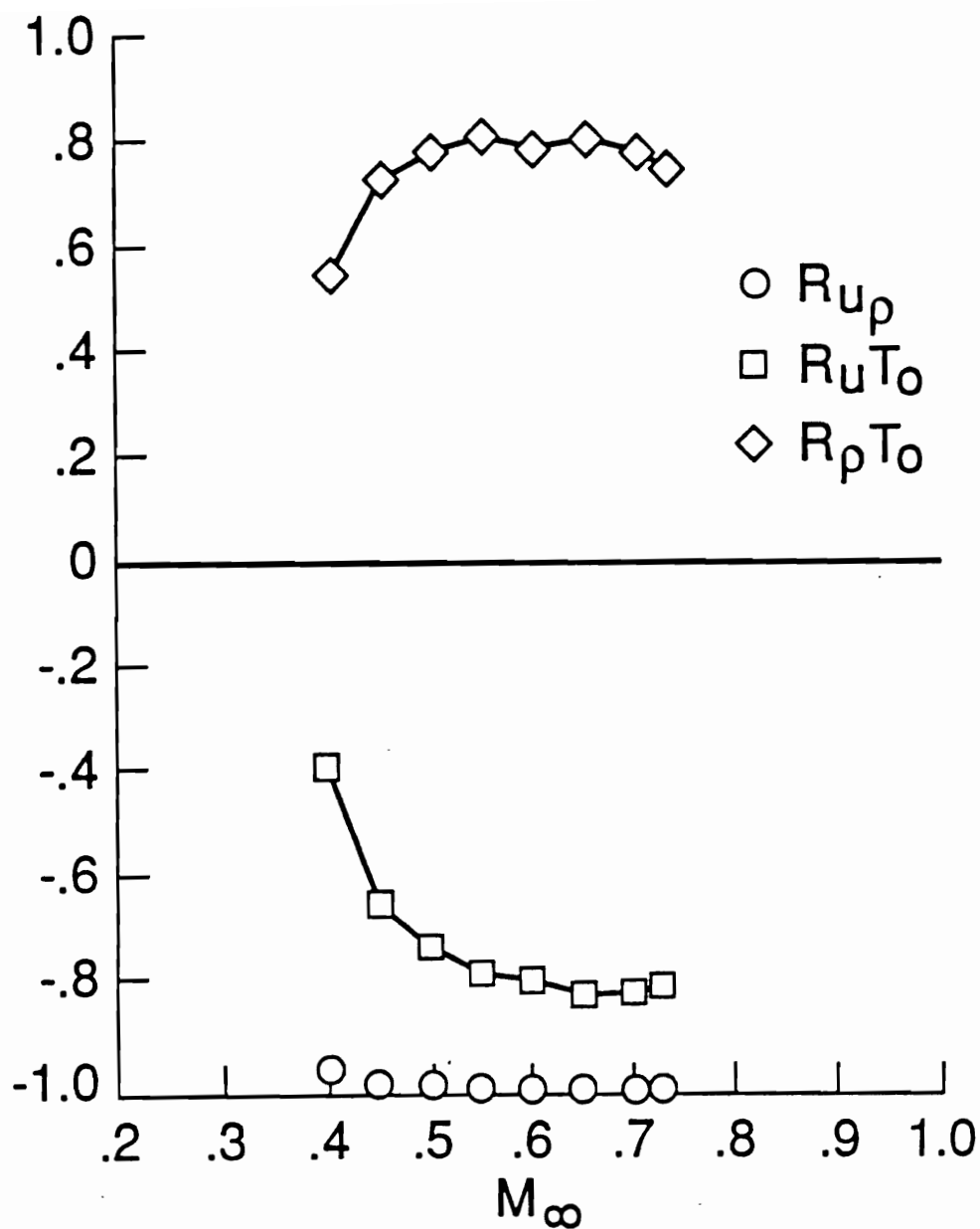


Figure 4.17 Velocity & density correlations, velocity & total temperature correlations, and density & total temperature correlations for different Mach numbers, P_o 1725 psf and T_o 540oR, Bandwidth $1 < \text{Hz} < 5000$

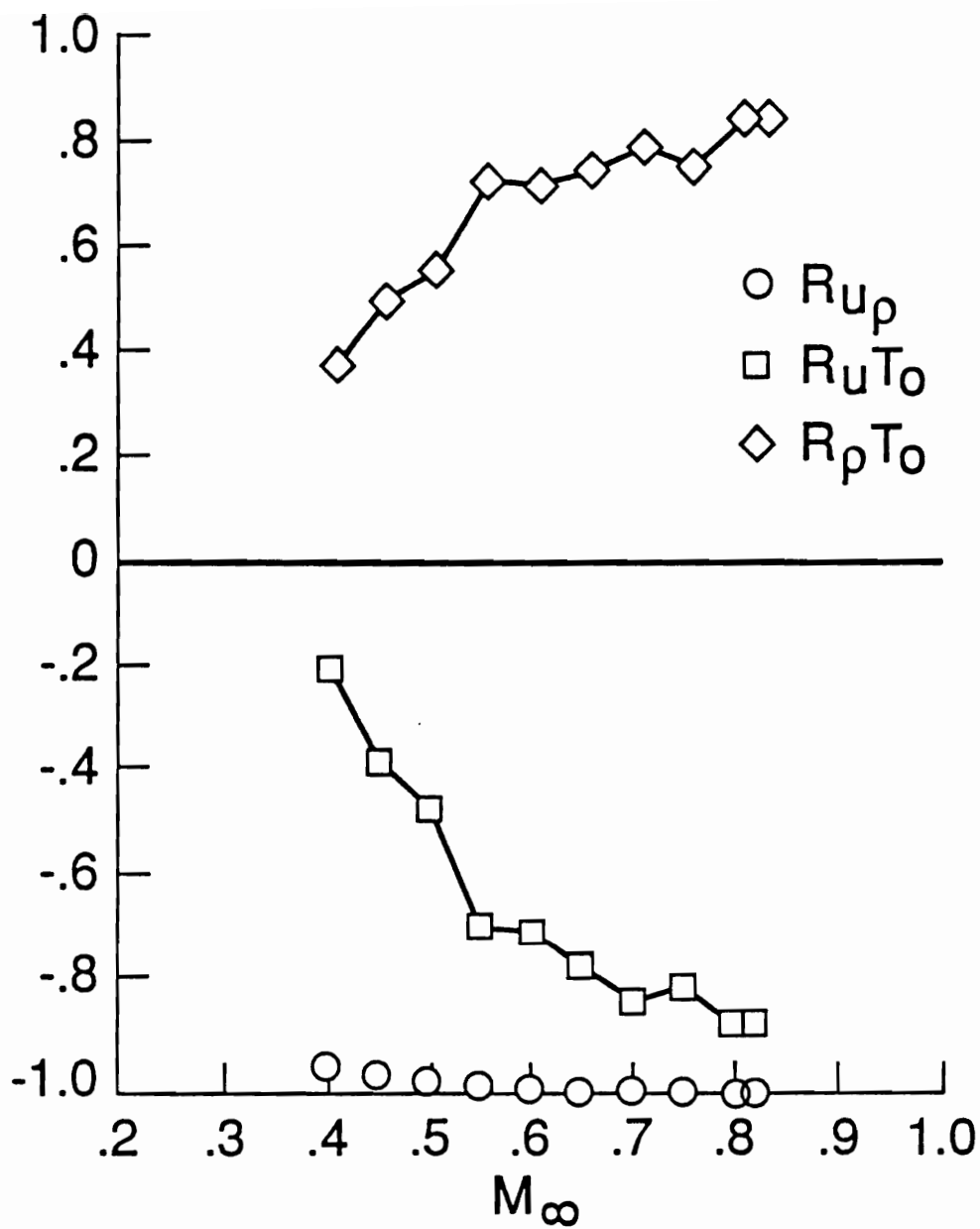


Figure 4.18 Velocity & density correlations, velocity & total temperature correlations, and density & total temperature correlations for different Mach numbers, P_o 1430 psf and T_o 540oR, Bandwidth $1 < \text{Hz} < 5000$

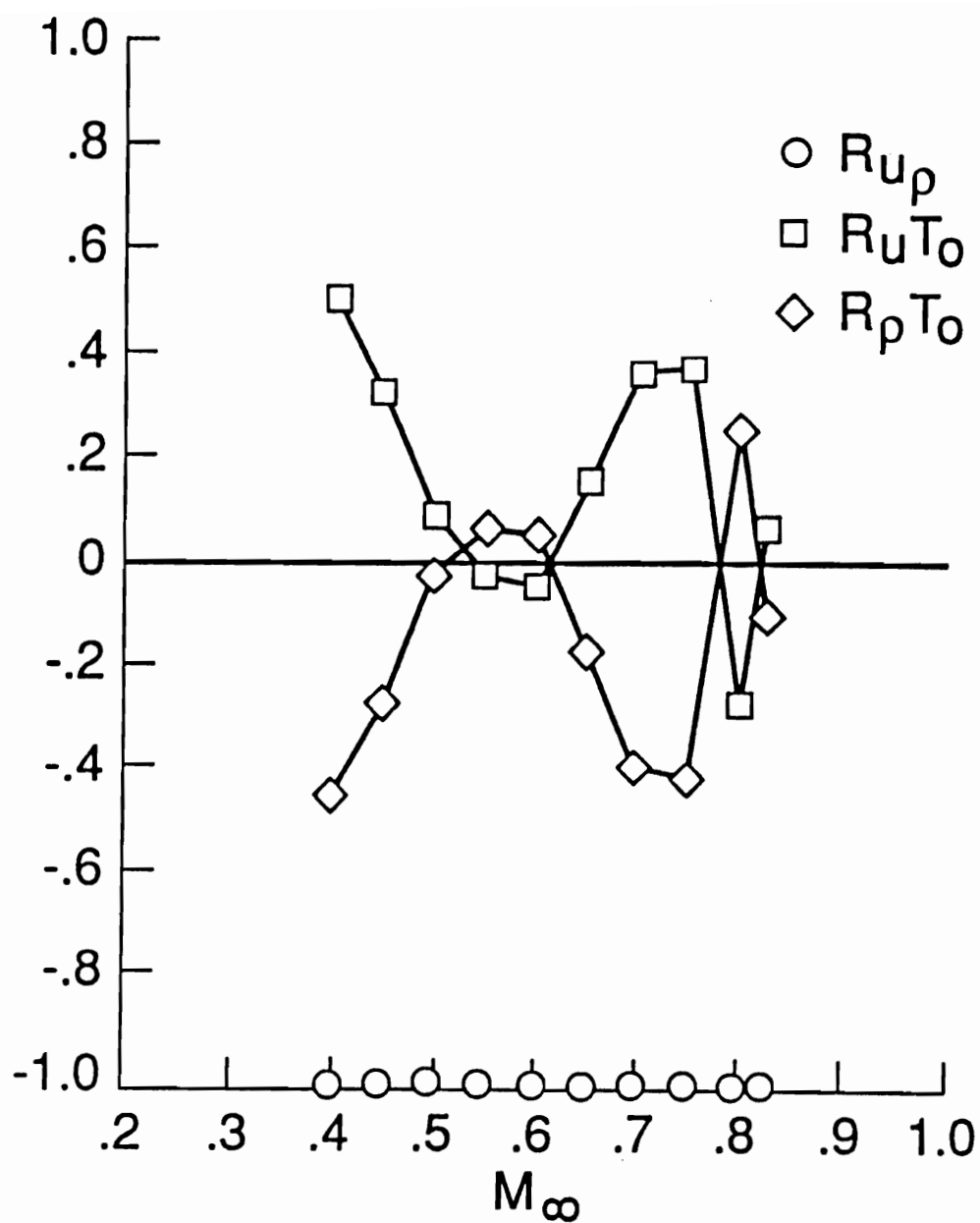


Figure 4.19 Velocity & density correlations, velocity & total temperature correlations, and density & total temperature correlations for different Mach numbers, P_o 860 psf and T_o 540oR, Bandwidth $1 < \text{Hz} < 5000$

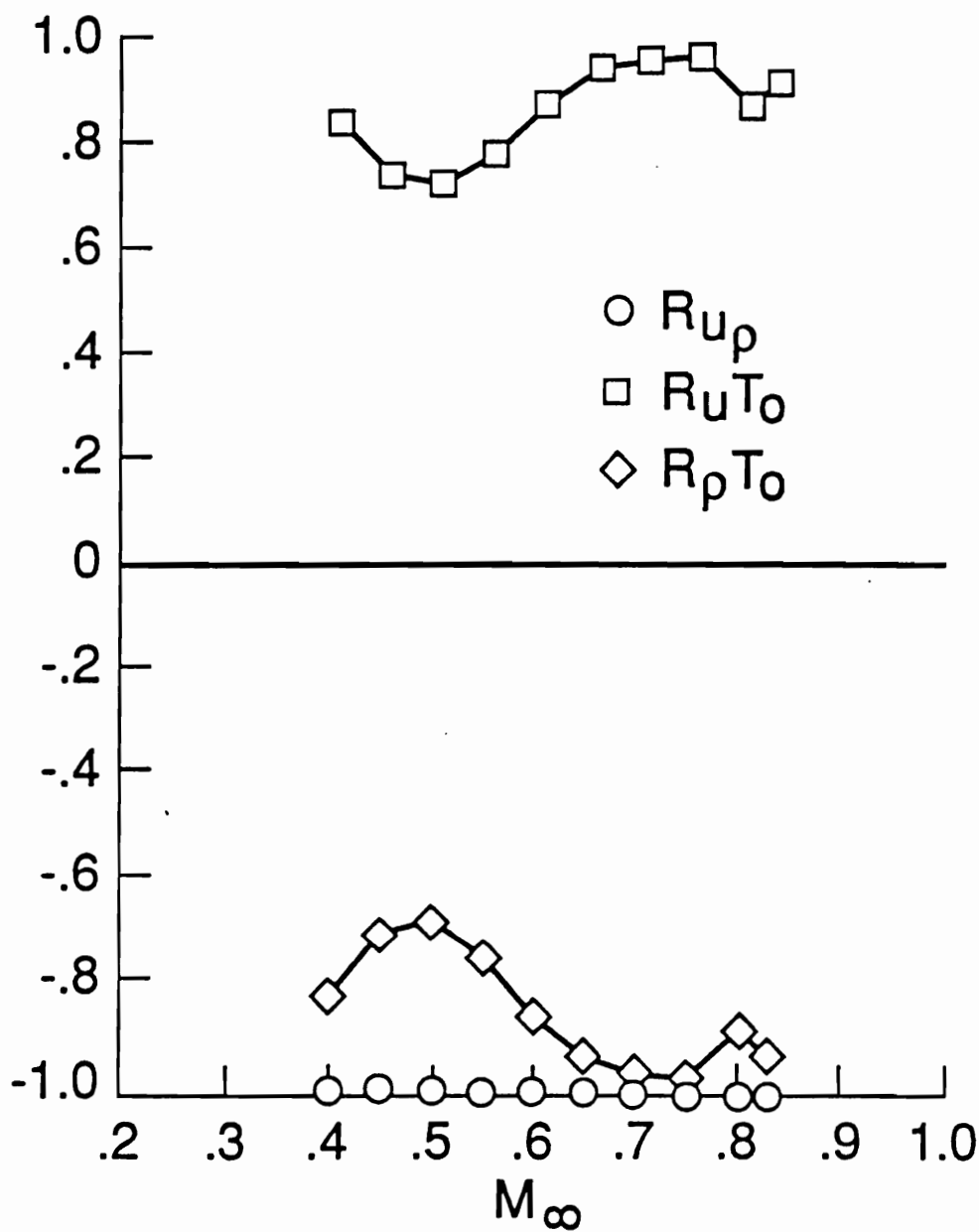


Figure 4.20 Velocity & density correlations, velocity & total temperature correlations, and density & total temperature correlations for different Mach numbers, P_o 710 psf and T_o 540oR, Bandwidth $1 < \text{Hz} < 5000$

moving sound to dominate the fluctuations in the 8' TPT for the condition of the present test.

Next, consider $RuTo$ and compare the data with the assumption of a single mode. If the dominant fluctuation were entropy, then $RuTo$ would be zero. There is some data at $P_0 = 860$ psf, (figure 4.19), which tend to agree with this assumption for some Mach numbers. If the dominant fluctuation was vorticity or downstream moving sound, ($\theta = 0^\circ$), then $RuTo$ would be +1. The data at $P_0 = 710$ psf, (figure 4.20), tend to agree with this assumption. Next, upstream moving sound ($\theta = 180^\circ$) would result in a value of $RuTo$ of -1. The data at $P_0 = 1430$ and 1725 psf, (figures 4.18 and 4.17 respectively), tends to approach this value at the higher Mach numbers of this test. Therefore, the quantity $RuTo$ indicates that each basic fluctuation might be expected in the flow depending on the total pressure and Mach number.

Finally, consider evaluate the values of $RpTo$. If the dominant disturbance were sound, moving upstream or downstream, then $RpTo$ would have a value of +1. It can be seen that the data at $P_0 = 1430$ and 1725 psf approach +1 at the higher Mach number, (figures 4.18 and 4.17 respectively). If vorticity is the major disturbance, then $RpTo$ would be zero. Some data at $P_0 = 860$ psf agrees with this assumption, (figure 4.19). Finally, if the dominant disturbance were entropy, then $RpTo$ would be -1. The data at $P_0 = 710$ psf tends to approach this value at the higher Mach number, (figure 4.20).

In summary, it appears that the only consistent result obtained from comparing the data with various assumptions of a single mode exist for

upstream moving sound but the comparison holds only for $P_0 = 1725$ and 1430 psf at the higher Mach numbers. For all other cases, it is highly likely that no one fundamental disturbance dominates the flow and vorticity, entropy, and sound coexist with comparable magnitudes.

Extension of the Measured quantities - There are several techniques which can be used to extend the velocity, density, and total temperature data. After the velocity, density, and total temperature fluctuations have been obtained, the equations 2.4, 2.5, and 2.6 can be solved for vorticity, entropy, and sound fluctuations if the direction of the sound mode (θ) is known or reasonable values can be assumed.

Based on the discussion in section 2.1, it appears that neither vorticity, entropy, nor sound dominated the fluctuations in the 8' TPT. Because of this, it is not clear what value can be assigned to θ . However, as seen from equation 2.6, the static temperature fluctuations due to entropy is not a function of the direction of sound. Therefore the values for the static temperature fluctuations due to entropy can be obtained even though we do not know the direction of sound. These results can then be compared with the static temperature fluctuations obtained by using equation 2.22. Once the static temperature fluctuations due to entropy have been obtained, equation 2.2 can be used to compute the pressure fluctuations due to sound using equation 2.25.

The static temperature fluctuations are presented in figures 4.21(a) through 4.21(d) for fluctuations due to entropy, sound, and for the combination or total magnitude of the static temperature fluctuations. As

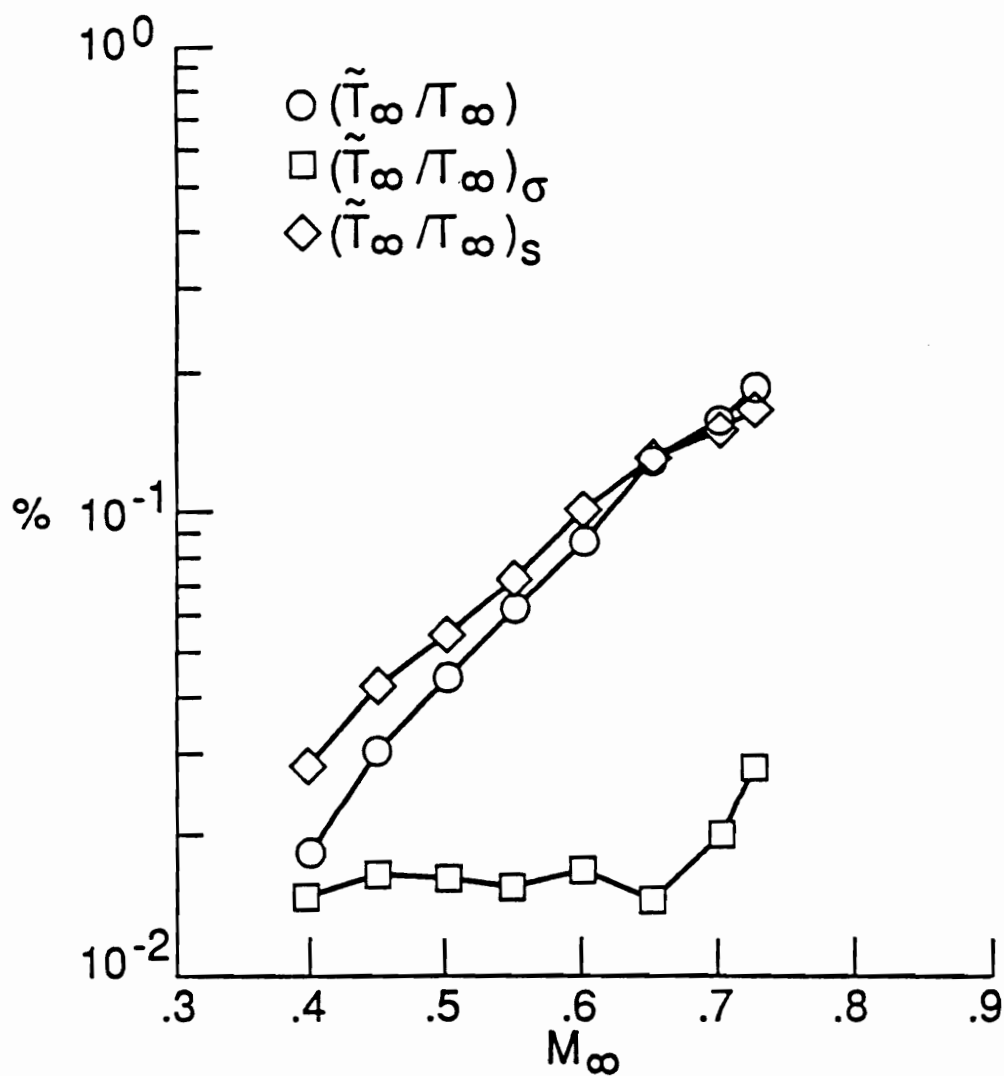


Figure 4.21a Comparison of the static temperature fluctuations due to entropy and sound, Po1725 psf, To540oR, Bandwidth 1 < Hz < 5000

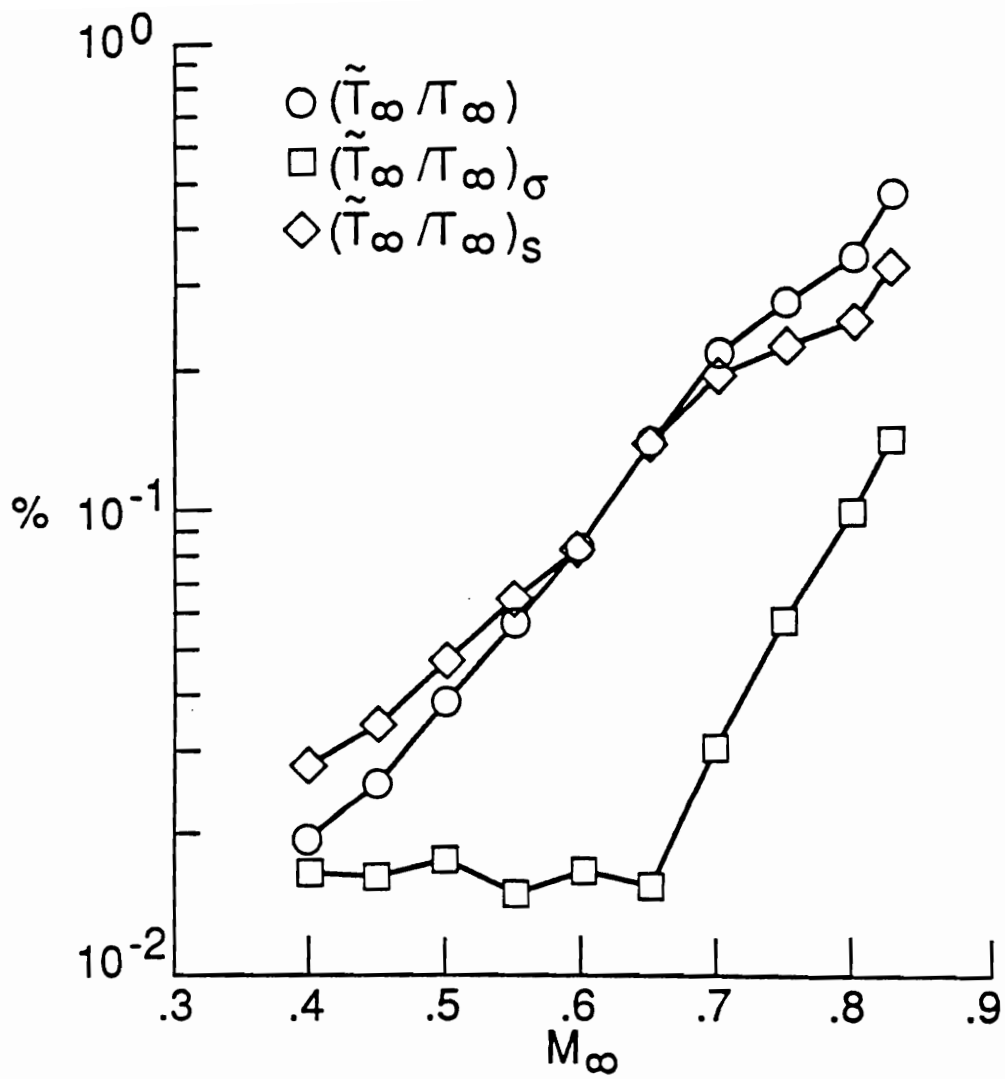


Figure 4.21b Comparison of the static temperature fluctuations due to entropy and sound, P_o 1430 psf, T_o 540oR, Bandwidth $1 < \text{Hz} < 5000$

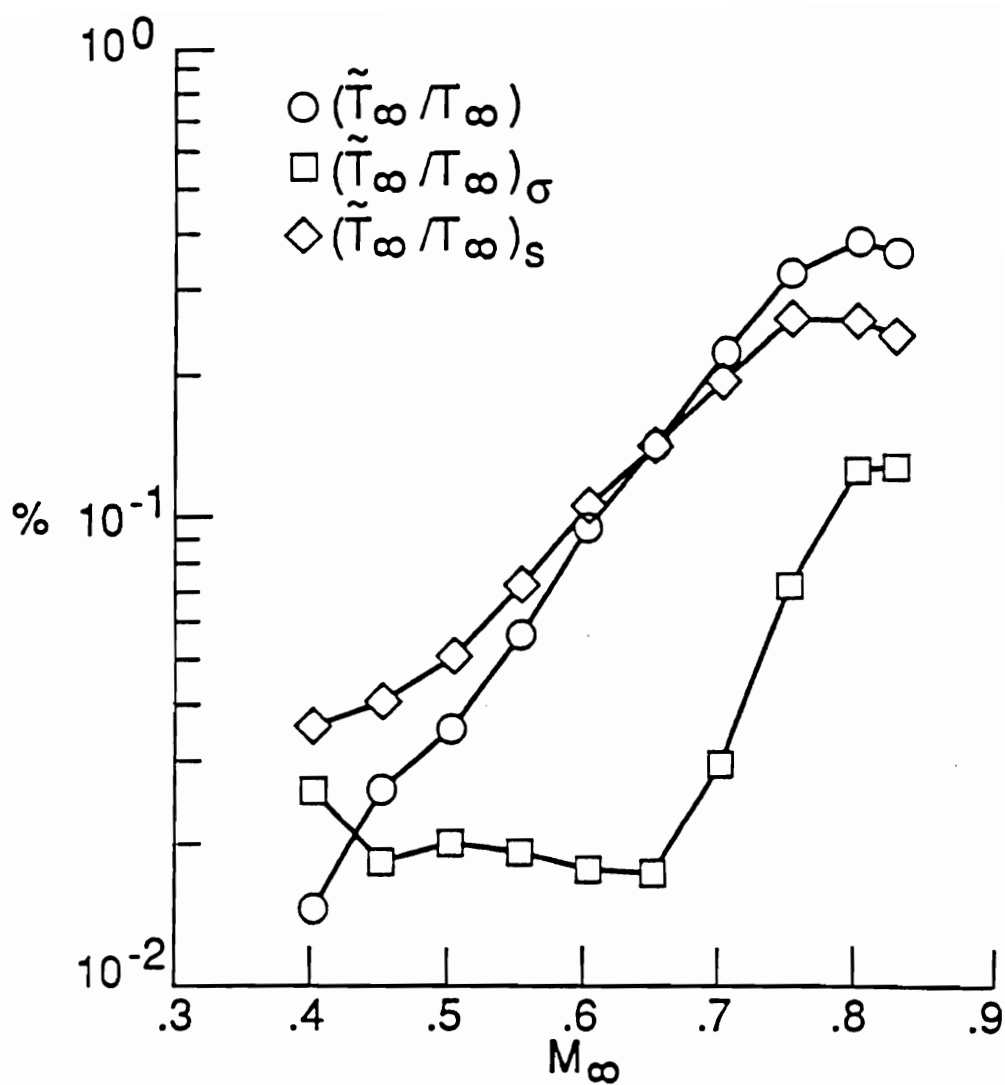


Figure 4.21c Comparison of the static temperature fluctuations due to entropy and sound, P_o 860 psf, T_o 540oR, Bandwidth $1 < \text{Hz} < 5000$

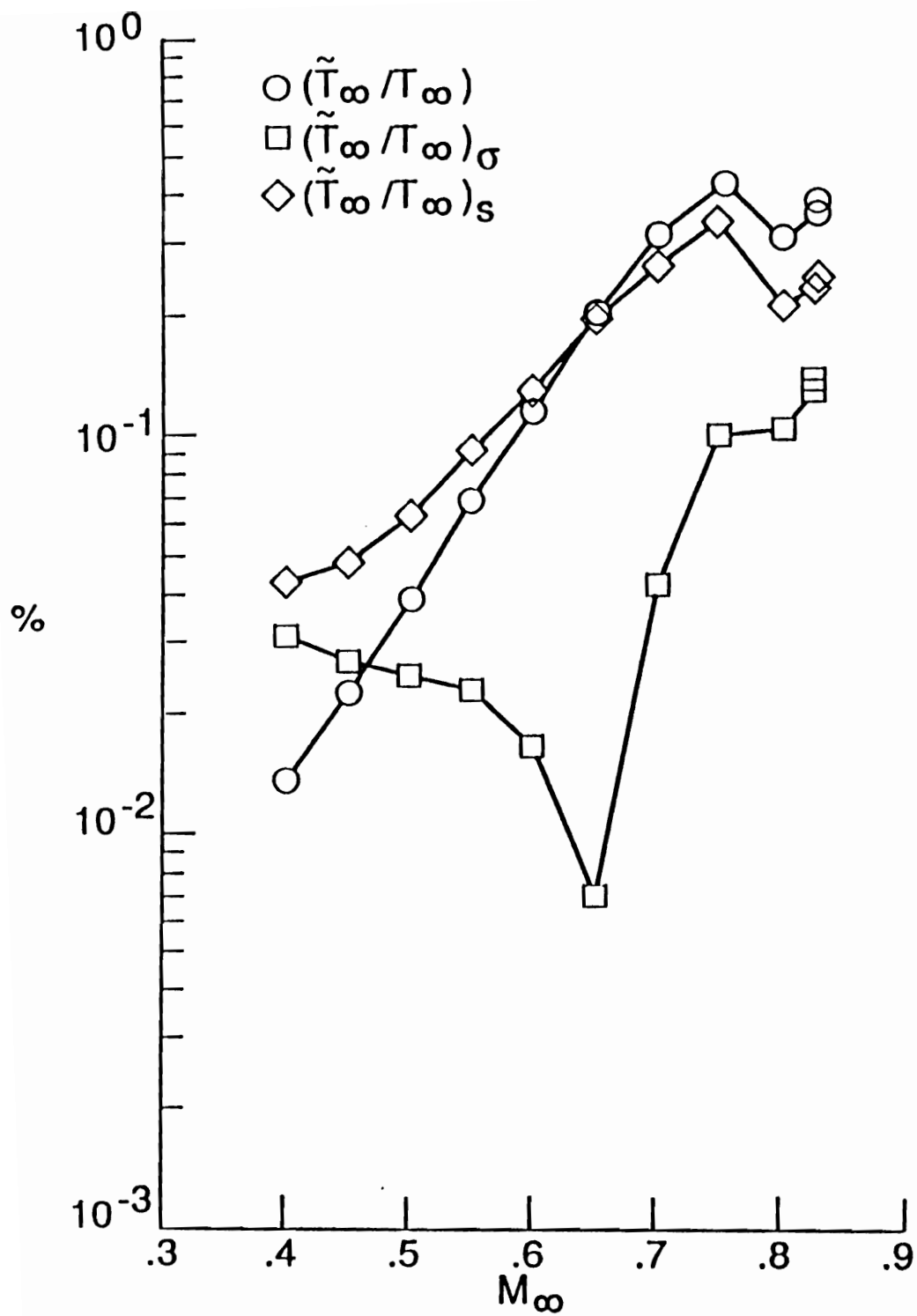


Figure 4.21d Comparison of the static temperature fluctuations due to entropy and sound, Po 710 psf, To 540oR, Bandwidth 1 < Hz < 5000

noted in figure 4.21, the static temperature fluctuations due to sound exceed the combination or total magnitude of the static temperature fluctuations at Mach numbers below 0.65 for all total pressures. Also, the static temperature fluctuations due to entropy exceeded the combination or total magnitude of static temperature fluctuations at low Mach numbers for $P_0 = 700$ and 860 psf. These results indicate that the data are only self-consistent at Mach numbers greater than 0.65, and there are errors in the data below this Mach number. The errors at low Mach numbers can probably be attributed to the reduced signal-to-noise ratio at these Mach numbers.

If we accept the data for $M > 0.65$, the static temperature fluctuations range from a low of 0.13 percent at $M = 0.65$ and $P_0 = 1725$ psf to a high of 0.49 percent at $M = 0.827$ at 1425 psf. The static temperature fluctuations due to entropy range from a low of 0.0071 percent at $M = 0.65$ at 710 psf to a high of 0.145 percent at $M = 0.827$ at 1425 psf. The static temperature fluctuations due to pressure range from a low of 0.145 at $M = 0.65$ at 1425 psf to a high of 0.345 at $M = 0.75$ at 700 psf.

4.2.4 Hot Wire Spectra - Examples of the spectra for the velocity, density, total temperature, and mass flow fluctuations are presented in figure 4.22. The data for this spectra was obtained for a Mach number of 0.82, total pressure of 1430 psf, and total temperature of 540° R. In general, all of the hot wire spectra were broad band with most of the energy below 100 Hz. However, there are two discrete frequencies that can be identified which are not related to 60 Hz electronic noise. The frequency component at

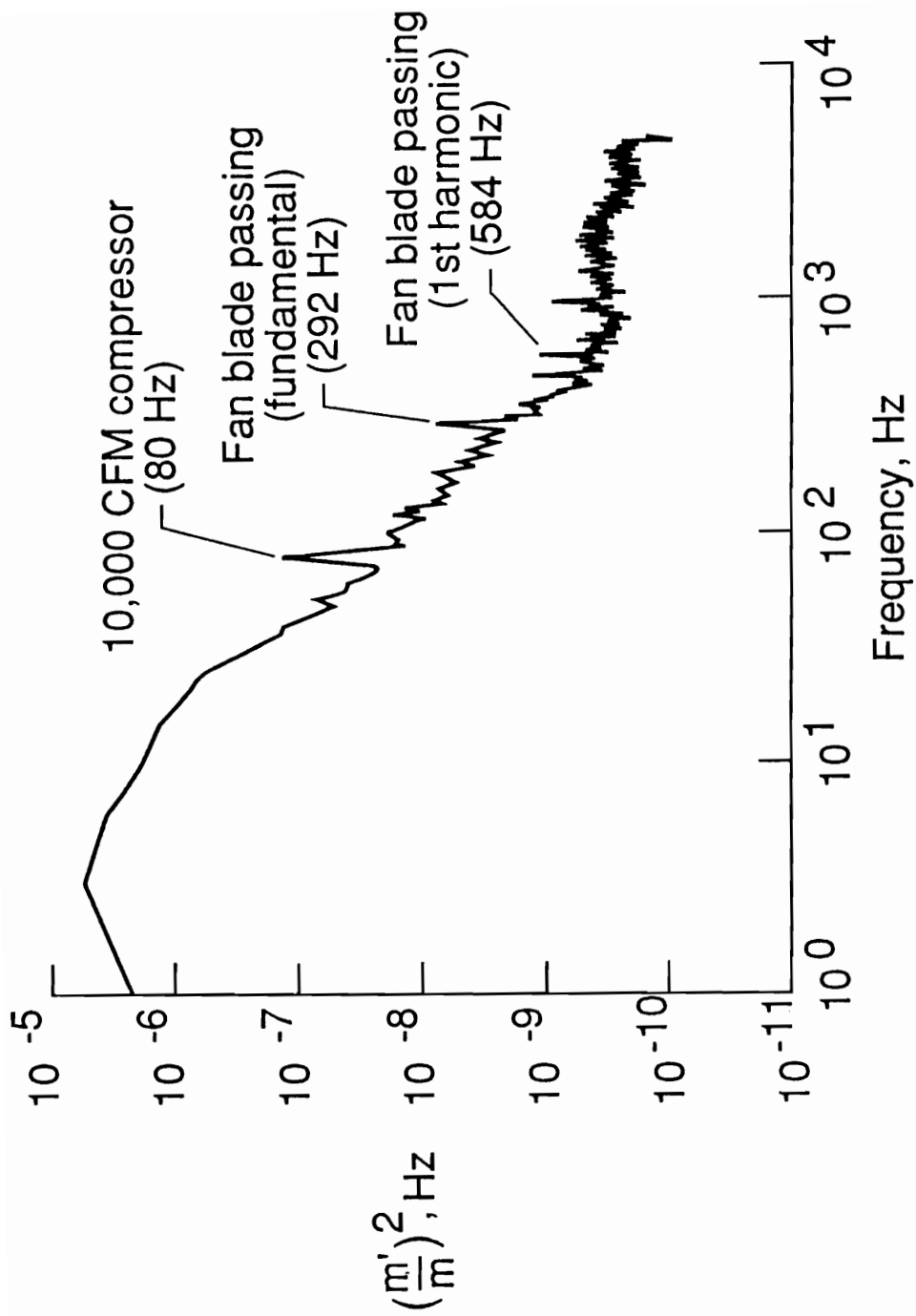


Figure 4.22a Mass flow spectra for a Mach number of 0.82
Po: 1430 psf, To 540oR, Bandwidth 1<Hz<5000

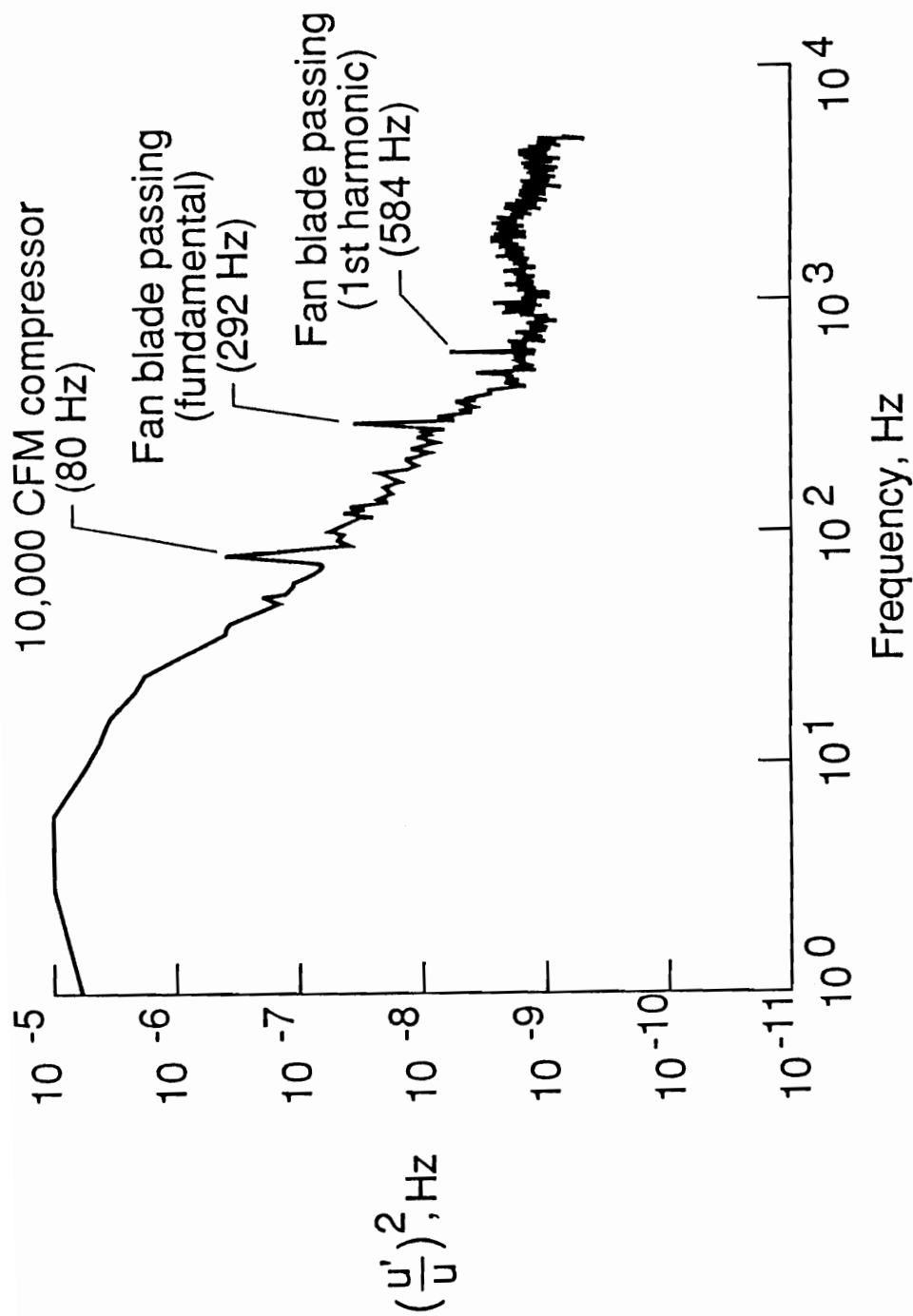


Figure 4.22b Velocity spectra for a Mach number of 0.82
Po: 1430 psf, To 540oR, Bandwidth 1<Hz<5000

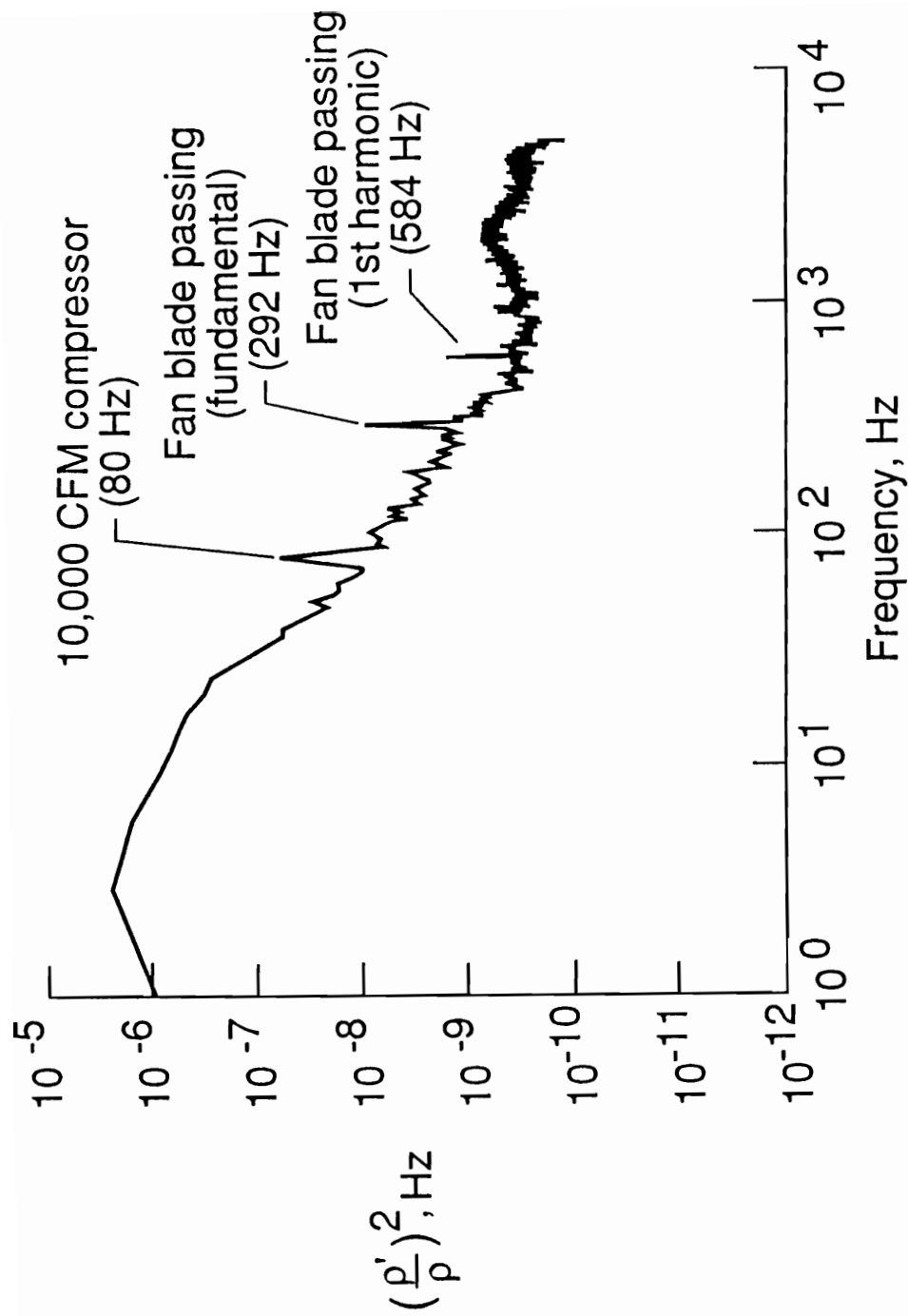


Figure 4.22c Density spectra for a Mach number of 0.82
 Po: 1430 psf, To 540oR, Bandwidth 1<Hz<5000

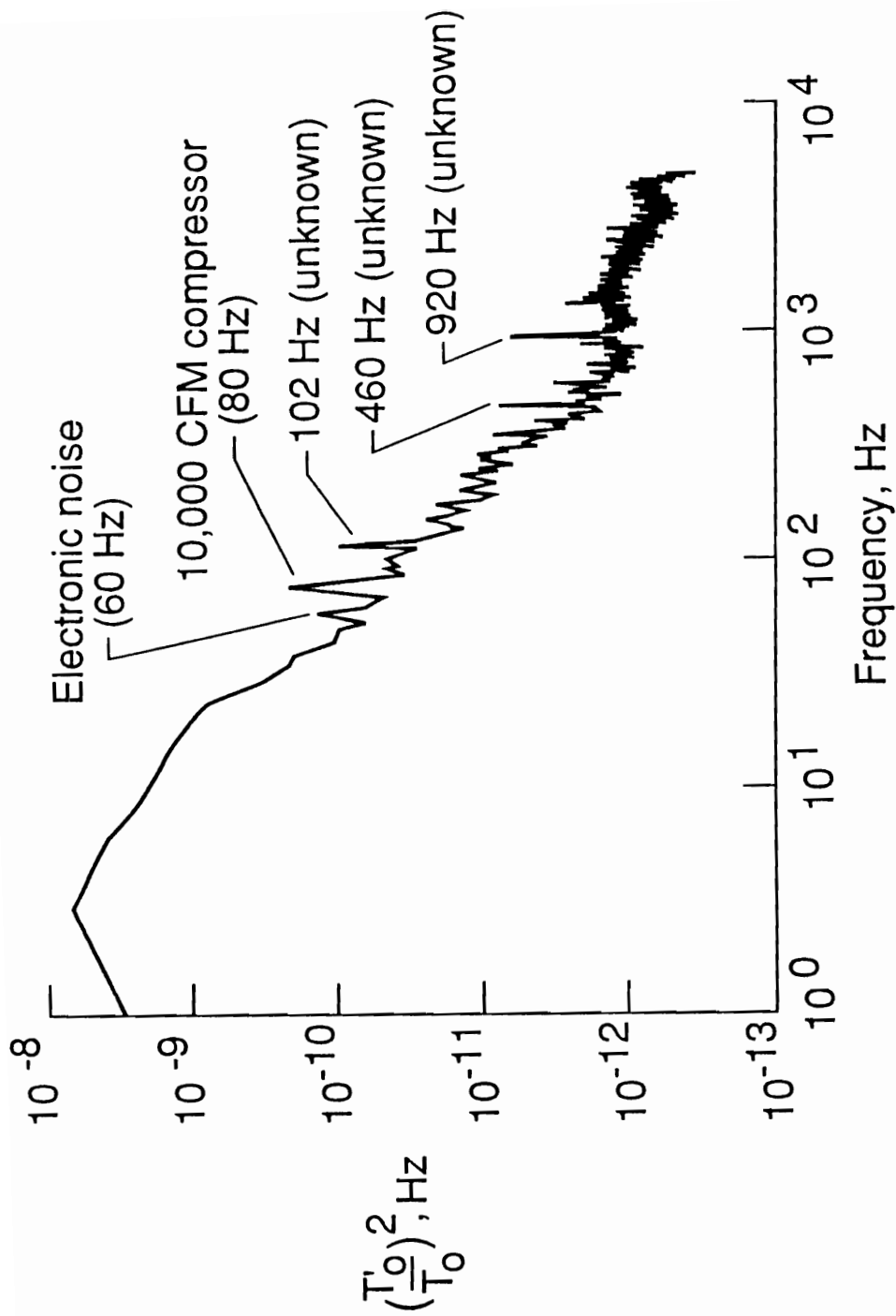


Figure 4.22d Total temperature spectra for a Mach number of 0.82
Po: 1430 psf, To 540oR, Bandwidth 1<Hz<5000

80 Hz was due to the 10,000 CFM compressor which operates at a constant RPM. This compressor was used to provide control of the total pressure in the tunnel when it was operated below atmospheric pressure. The 292 Hz and 584 Hz signatures are due to the fundamental and first harmonic fan blade passing frequency of the wind-tunnel. All three of these signatures are found in the velocity, density, and mass flow fluctuations. The fan blade signatures do not appear in the total temperature fluctuations. Sources for other spikes have not been identified.

Several observations can be made about the frequency signatures for u'/U , ρ'/ρ , T_o'/T_o and m'/m at the design conditions. There are distinct differences in the rate of decay of the level of the fluctuations with increasing frequency for the different perturbations. For example, the velocity fluctuation decayed at a faster rate with frequency than the density, but at about the same rate as the total temperature and mass flow fluctuations. The spectra for T_o'/T_o had larger magnitude discrete frequencies in its spectra which was probably due to the decrease in the signal-to-noise ratio for the temperature fluctuations.

A comparison of the velocity spectra signatures for a Mach number sweep at two different total pressure conditions are presented in figure 4.23. As the Mach number was reduced, more discrete frequencies appeared in both of the spectra due to the amplification of electronic noise at 60 Hz and its harmonics. Finally, as the Mach number was decreased, the shape of the spectra appeared to have two maxima. The two maxima are broad band in nature and occur at 20 kHz and less than 100 Hz. This result suggests the possibility of two dominant disturbance sources in the flow at the lower

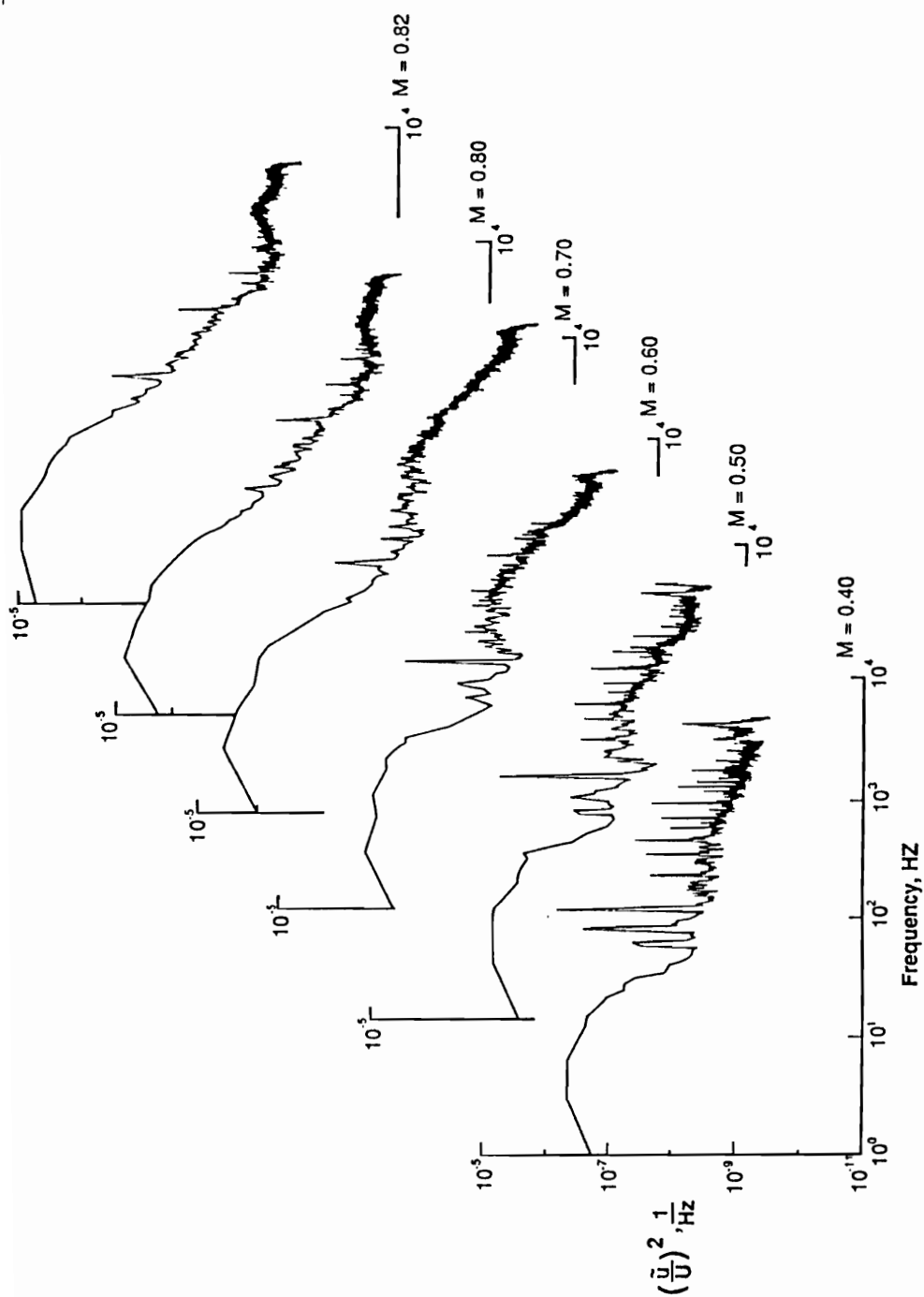


Figure 4.23 Velocity spectra for different Mach numbers
Po: 1430 psf, To 540oR, Bandwidth 1<Hz<5000

values of Mach number. The reason for this result is not known at the present time. The spectral signatures that can be easily identified are tabulated for each Mach number in Table 4.7.

Table 4.7 Spectral Signatures identified from the freestream velocity field
that are in the transition range for the LFC experiment.

MACH #	SPECTRAL SIGNATURES (Hz)				
0.50	80	6600	10000	19000	20000
0.55	80	5000	9500	18000	20000
0.65	80	4500	9000	17000	20000
0.70	80	3500	8500	16000	20000
0.75	80	2200	8000	14000	20000
0.80	80	1000	7000	14000	20000
0.82	80	920			

4.2.5 Alternate Analysis of different Hot Wire Techniques - Even though it has been established that $S_u \neq S_p$ this section is to provide the reader an understanding of the consequences of ignoring or assuming that $S_u = S_p$ when in fact they are not equal. The data described in the three element flow quality analysis section will be used as a reference for the other hot wire techniques. The three element data were assumed to be "more" correct since more flow physics information is accounted for, and the data reduction method required the least number of assumptions. This section will be limited to data taken only for Mach number sweeps at total pressures of 860 psf and 1430 psf at a fixed total temperature of 540°R.

Comparisons of flow quality data will be made for the three element, two element and five different single element cases described in the calibration section above. The pressure fluctuation data which was used to extend the two element and single element hot wire mass flow data to velocity and density fluctuations will be discussed in the next section. Figure 4.24 through 4.31 illustrates the differences in seven hot wire techniques for the mass flow, velocity, density, and total temperature fluctuations at total pressures of 860 psf and 1430 psf respectively.

The data denoted as case "A" represents the flow quality obtained with the three element probe. Using these results as a datum, the mass flow measurements, figure 4.24 and figure 4.28, can be compared to the two element method, case "B". Case "B" results are always significantly below those obtained using the three element technique. These differences also occur for the velocity, density, and total temperature fluctuations.

There are considerable differences in the measured results obtained with the five different single element hot wire techniques. These differences are caused by the different amount of data used as noted in the calibration procedure. Cases "C", "D", and "E" are similar in nature for mass flow, velocity, and density due to the negligible differences in the corresponding sensitivities.

For the mass flow fluctuations, all cases except case "F" resulted in lower measured values for mass flow fluctuations when compared to the three element case. Recall that the calibration for case "F" resulted in the best mass flow correlation for Mach numbers less than 0.65. Even so, at low Mach numbers the mass flow fluctuations obtained for case "F" are higher than those for case "A". The level of fluctuations for cases "A" and "F" begin to agree more closely at $M=0.65$ for the 1430 psf case and $M=0.55$ for the 860 psf case. The level of mass flow data for case "G" seems to approach the three element data for $M<0.65$ for the 1430 psf case.

The velocity fluctuation comparisons shown in figures 4.25 and 4.29, indicates a wide degree of differences except for case "F". Data for this case is converging with the three element data at low Mach numbers. Again data for cases "C", "D", and "E" are similar due to similarities in the sensitivities.

The density fluctuations shown in figures 4.26 and 4.30, are representative of all of the different pressure cases. For cases "B" through "G" the levels of the density fluctuations are nearly equal except for Mach numbers greater the 0.75. The level of the three element case is substantially greater than the data obtained using the other techniques.

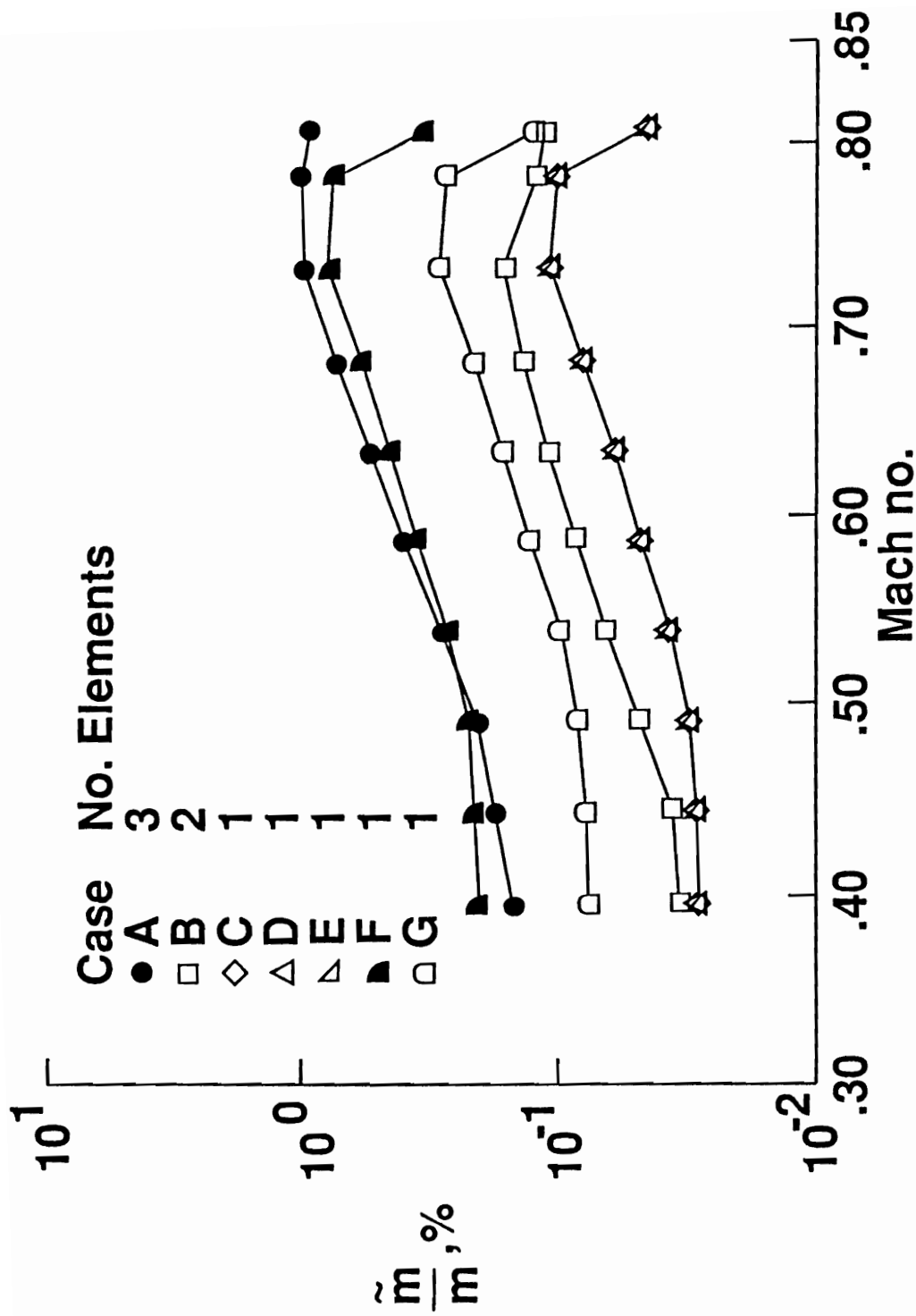


Figure 4.24 Comparison of mass flow fluctuations for various hot wire techniques, Po 860 psf, To 540oR, Bandwidth 1 < Hz < 5000

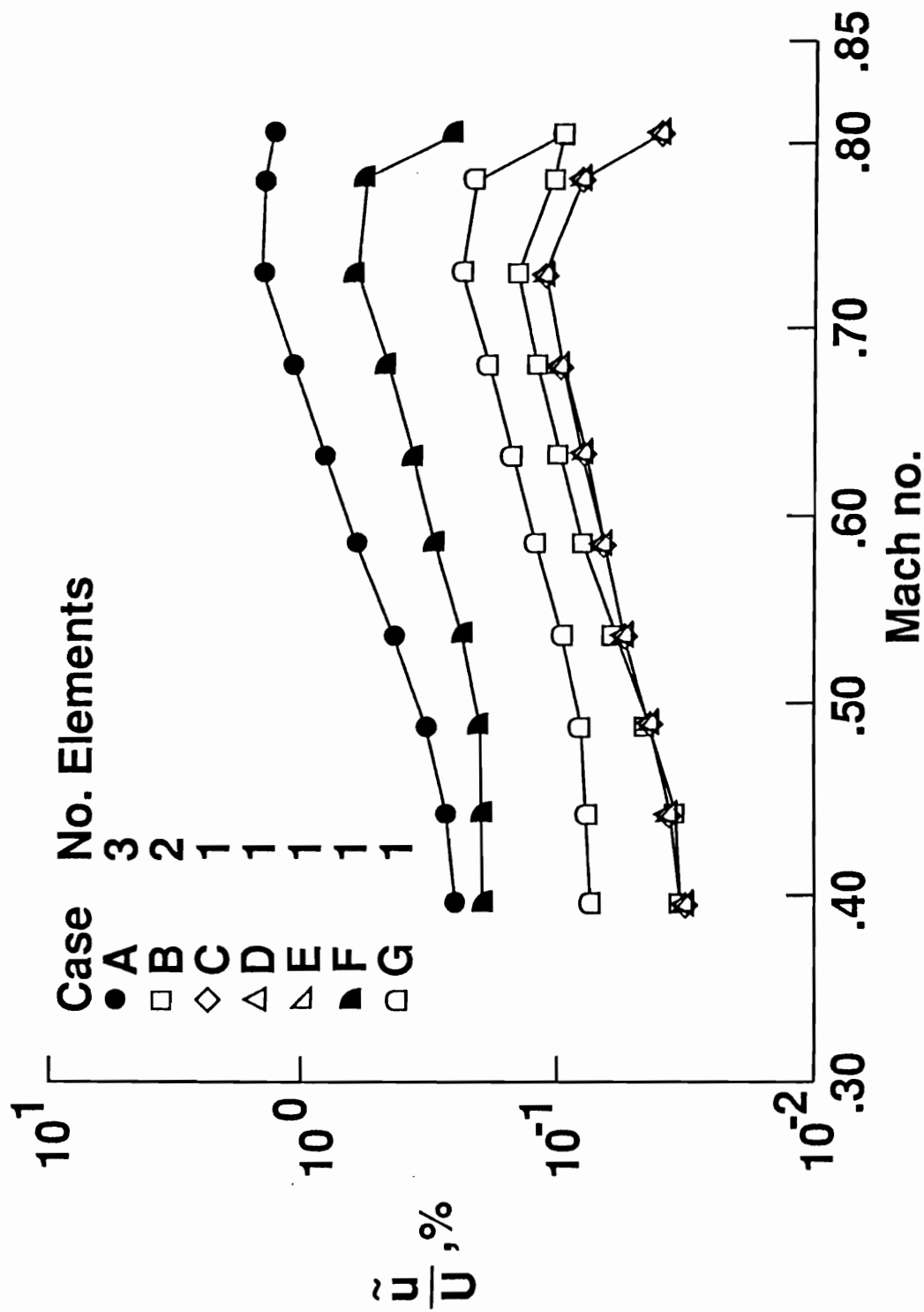


Figure 4.25 Comparison of velocity fluctuations for various hot wire techniques, Po 860 psf, To 540oR, Bandwidth 1 < Hz < 5000

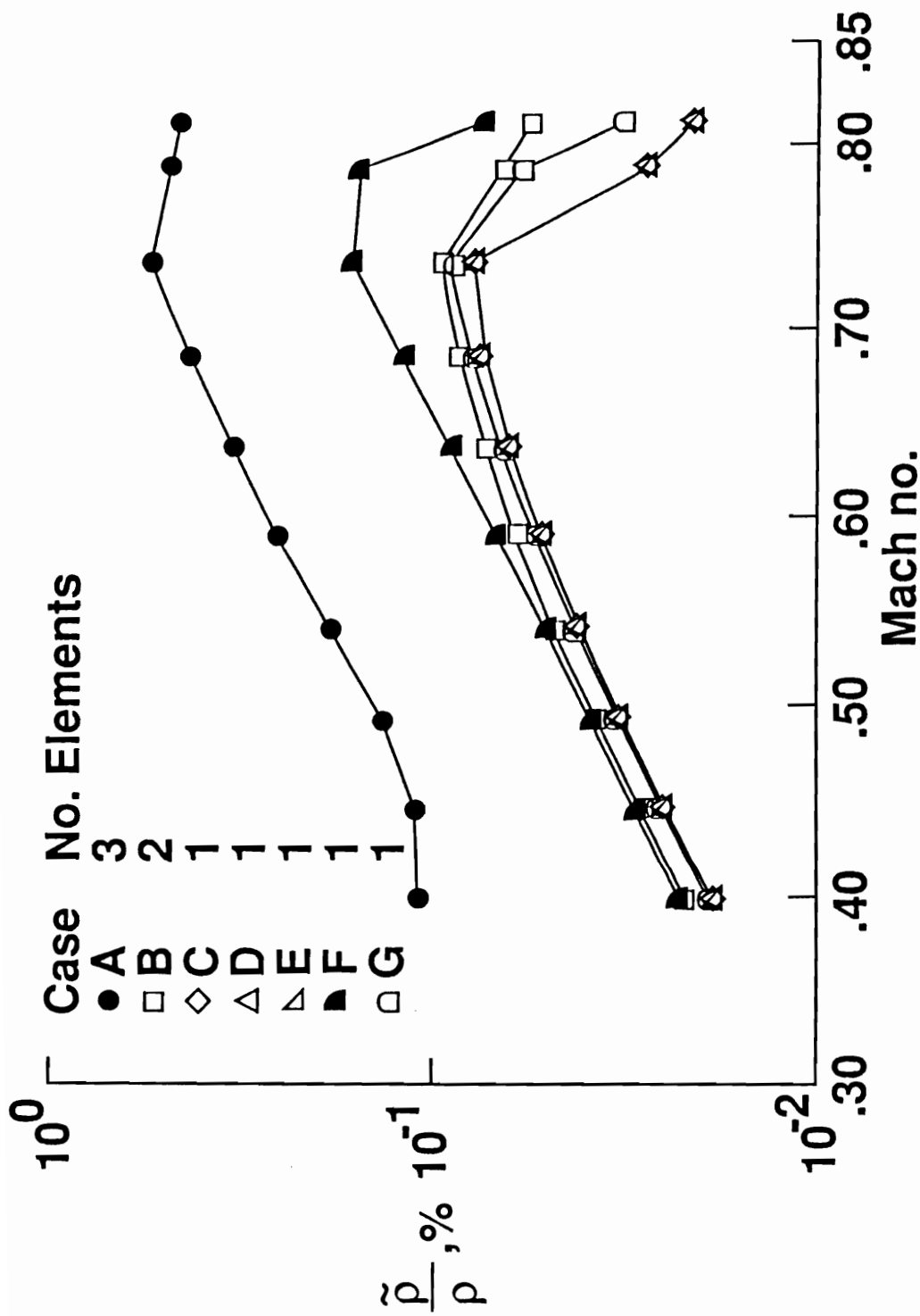


Figure 4.26 Comparison of density fluctuation for various hot wire techniques, Po 860 psf, To 540oR, Bandwidth $1 < Hz < 5000$

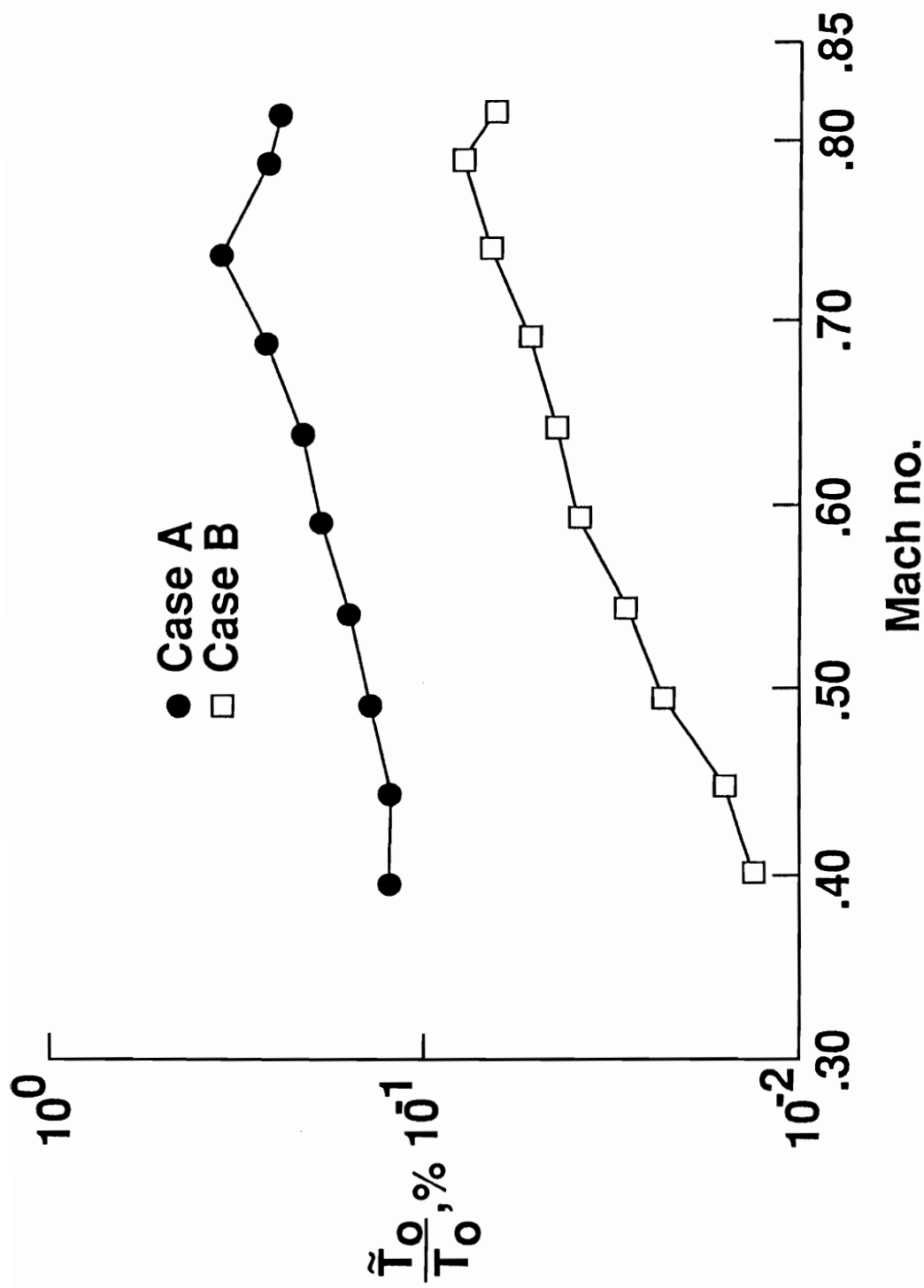


Figure 4.27 Comparison of total temperature fluctuations for various hot wire techniques, P_o 860 psf, T_o 540oR, Bandwidth $1 < \text{Hz} < 5000$

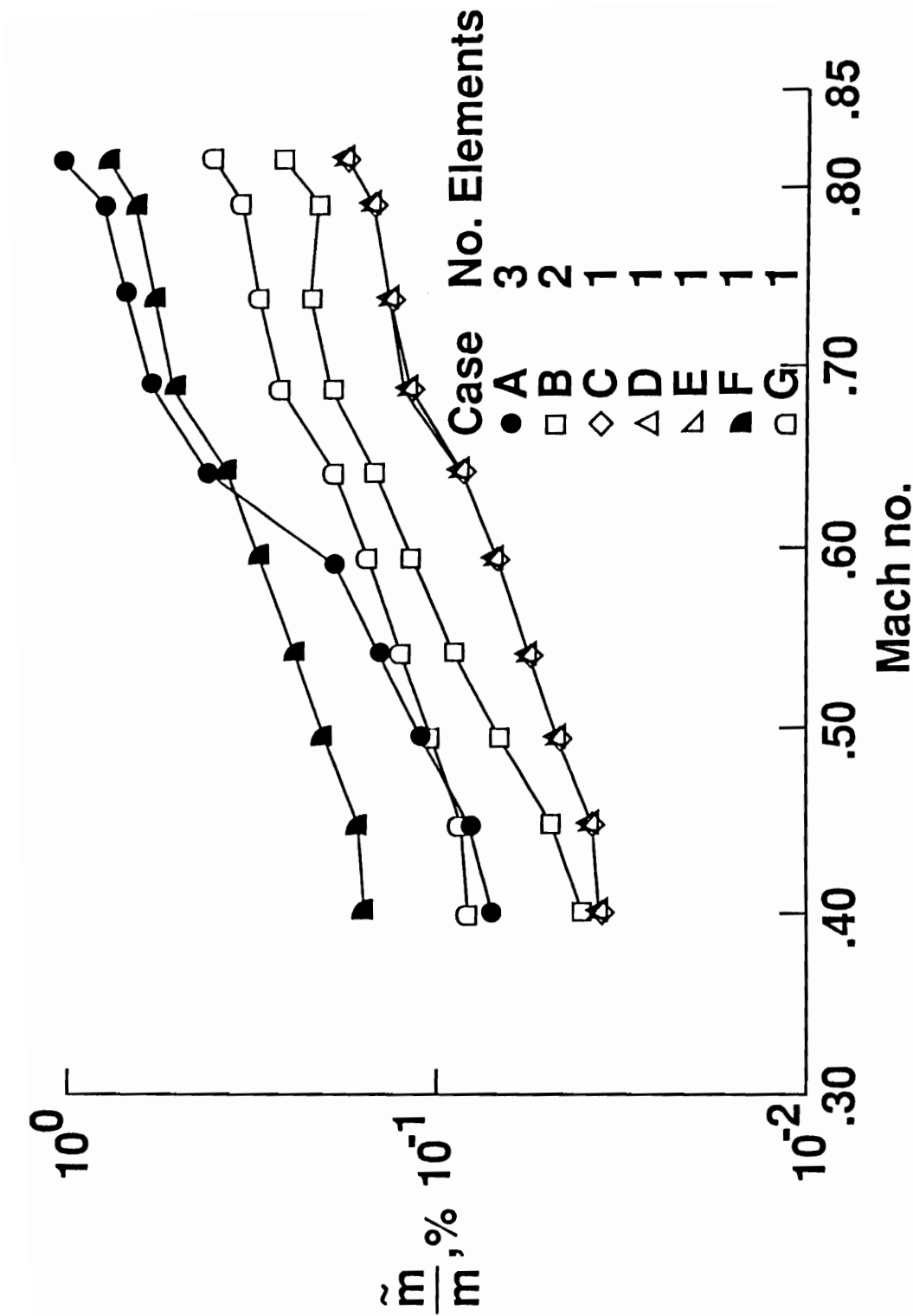


Figure 4.28 Comparison of mass flow fluctuation for various hot wire techniques, Po 860 psf, To 540oR, Bandwidth 1 < Hz < 5000

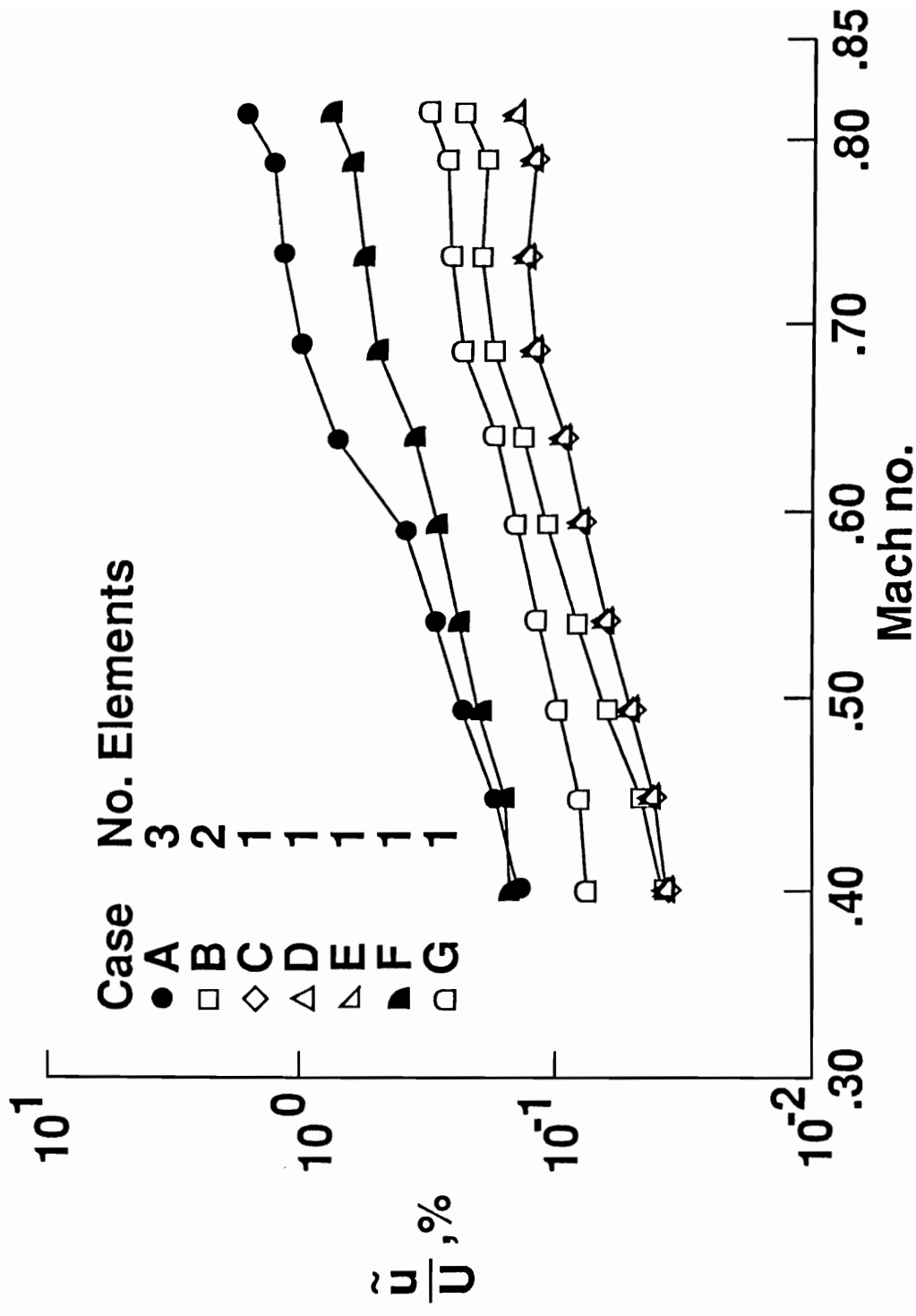


Figure 4.29 Comparison of velocity fluctuations for various hot wire techniques, Po 1430 psf, To 540oR, Bandwidth 1 < Hz < 5000

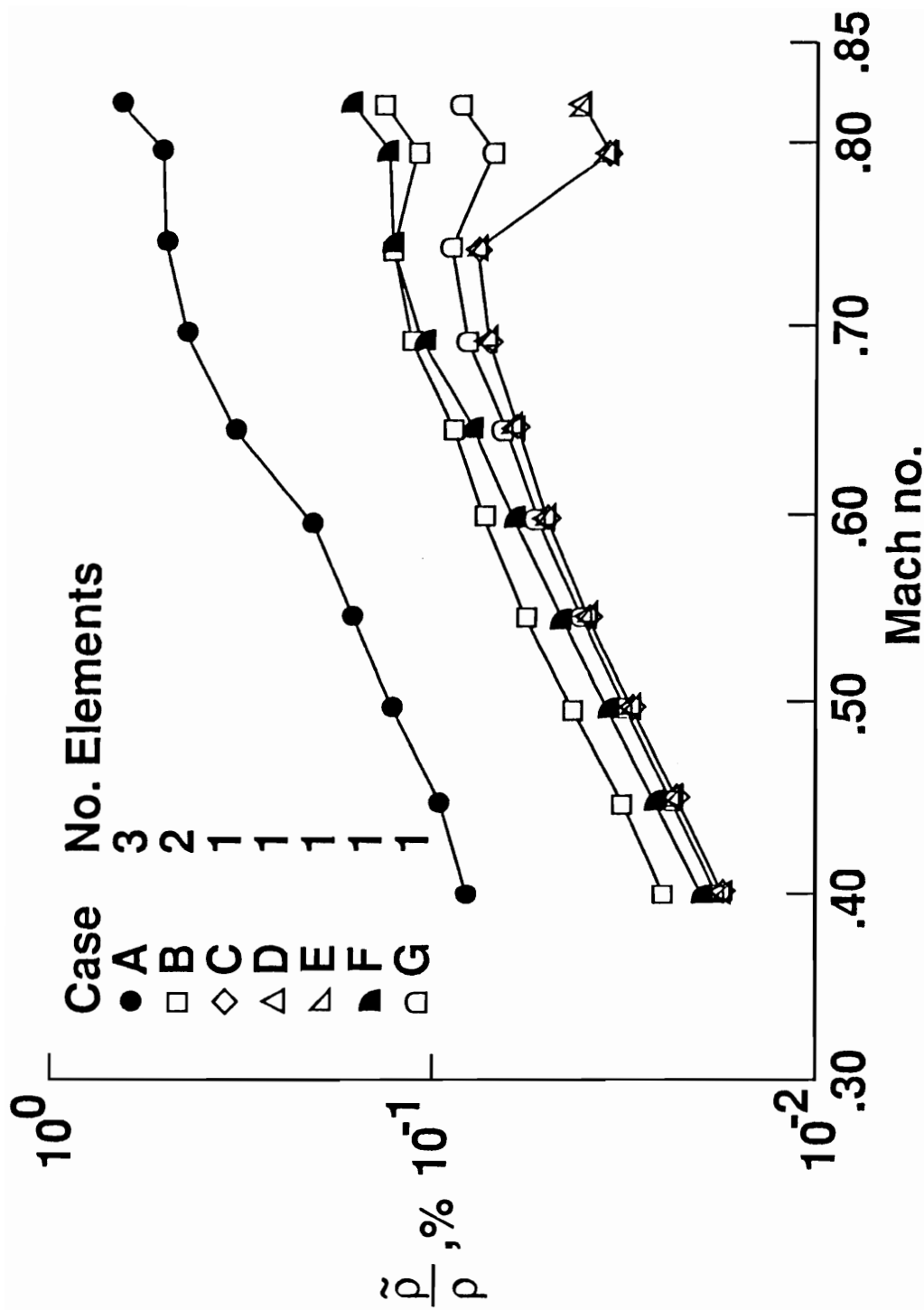


Figure 4.30 Comparison of density fluctuations for various hot wire techniques, P_o 1430 psf, T_o 540oR, Bandwidth 1 < Hz < 5000

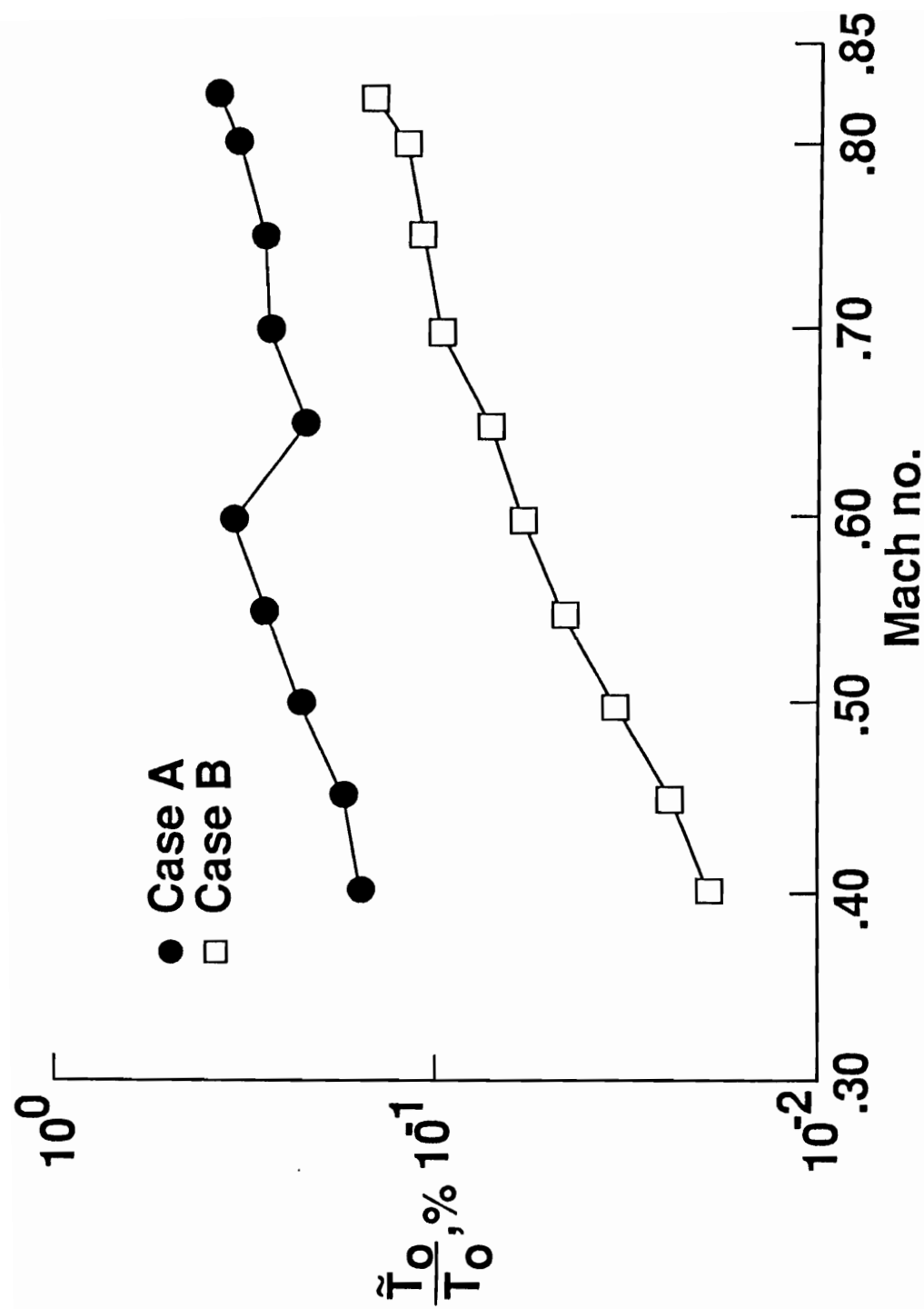


Figure 4.31 Comparison of total temperature fluctuations for various hot wire techniques, P_o 1430 psf, T_o 540oR,

Comparisons of total temperature fluctuations are limited to the three element and two element cases. As seen in figures 4.27 and 4.31, the two techniques results in levels of total temperature fluctuations that can differ by an order of magnitude. The discontinuity shown in figure 4.31 for the three element case cannot be explained at this time.

It should be noted that the limited results of the three-element hot-wire technique revealed magnitude levels that are in general higher than the two element and single element configuration. Attempting to optimize the calibration to mass flow improved this discrepancy, yet confidence wanes as these techniques are extended to velocity and density fluctuations.

4.3 Effect of Wind Tunnel Turbulence Manipulators

To assist in identifying the sources of disturbances in the test section, it is important to evaluate the perturbations at different locations in the wind tunnel circuit, particularly the settling chamber and the diffuser. Disturbances in the settling chamber can be characterized by using the same approach that was used in defining the disturbances in the test section. However several simplifying assumptions can be made which are related to the measurements of low speed flows. The most significant assumption to be made is based on the Mach = 0.4 data shown in figure 4.25 and figure 4.29 which indicates that the single sensor velocity fluctuations are representative of the three sensor velocity fluctuation data. If the single sensor data trends for the velocity fluctuations at low speed can be assumed to be consistent with these Mach 0.4 data then X-wire techniques described by Sandborn (1972), can be applied in the settling chamber region where the maximum velocity is 25 feet per second.

Velocity measurements were obtained at four locations in the settling chamber: upstream of the heat exchanger (figure 4.32), between the heat exchanger and the honeycomb (figure 4.33), between the honeycomb and the anti-turbulence screens (figure 4.34), and downstream of the anti-turbulence screens at the entrance to the contraction (figure 4.35). Figure 4.36 summarizes the magnitudes of the velocity fluctuations at these locations. The 10% to 40% velocity fluctuations upstream of the heat exchanger are reduced to approximately 2% to 3% through the cooler at a total pressure of 1725 psf, figure 4.37. In addition to controlling the

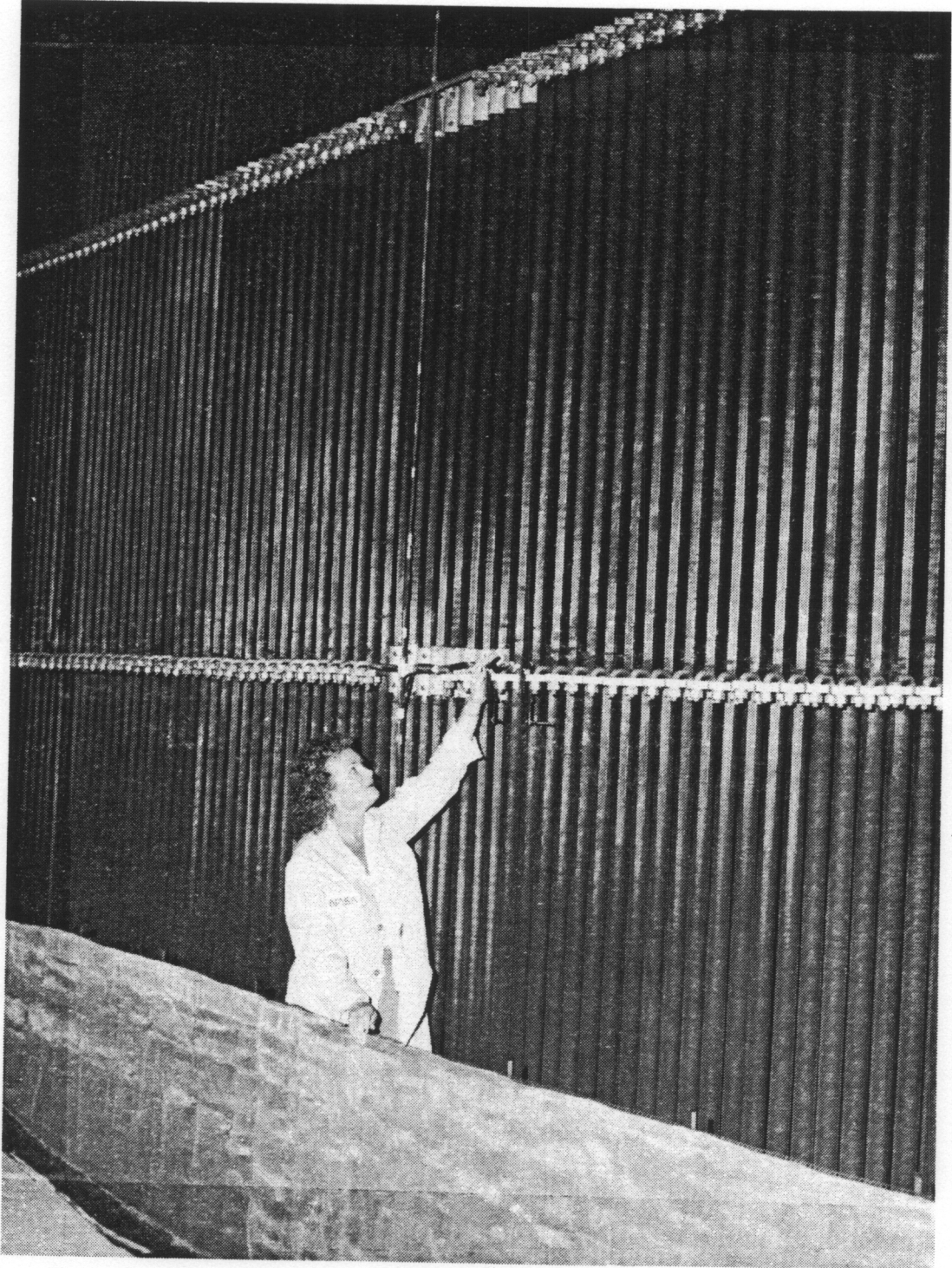


Figure 4.32 Photograph of flow quality measurement location upstream of the heat exchanger

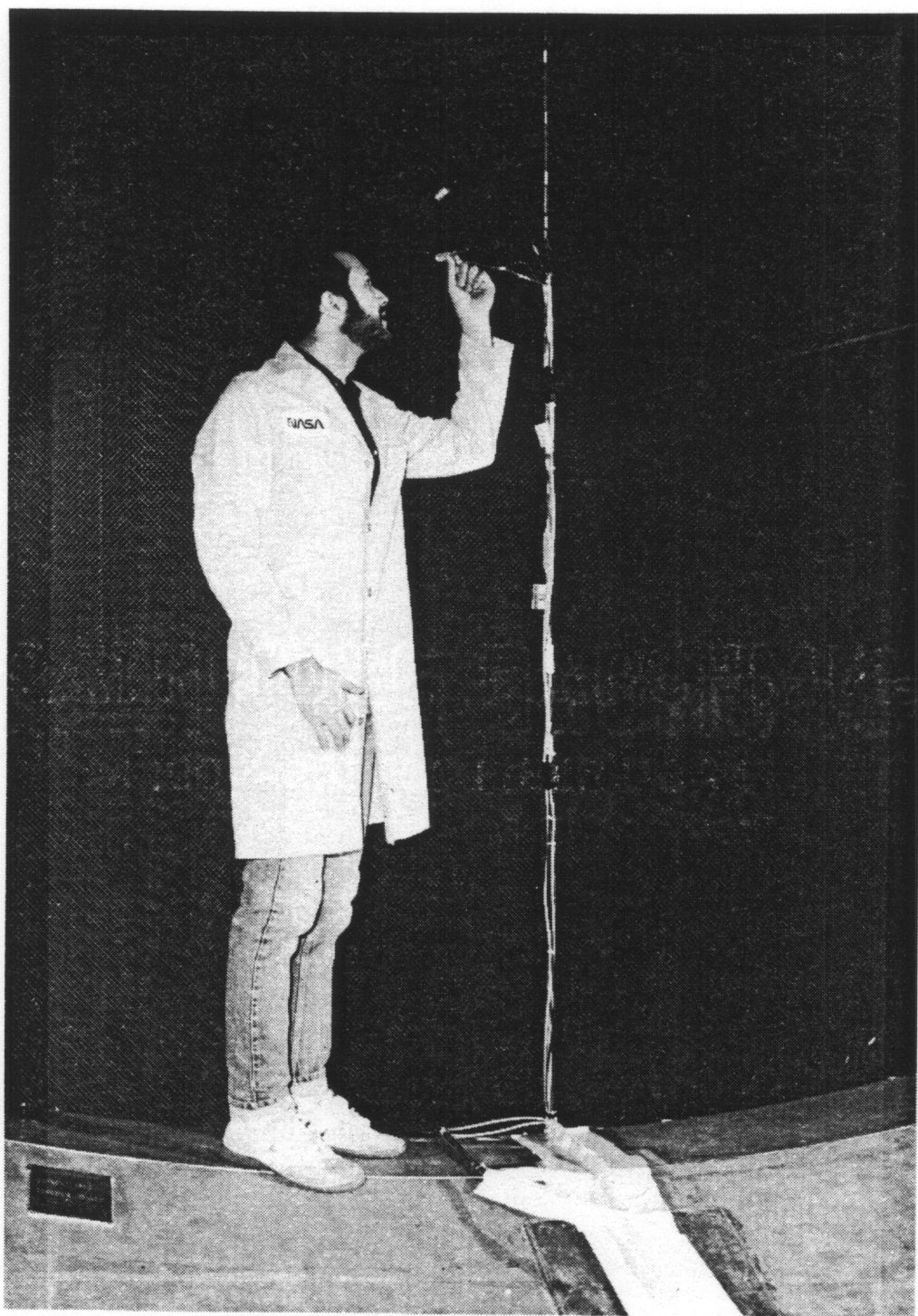


Figure 4.33 Photograph of flow quality measurement location between the heat exchanger and the honeycomb

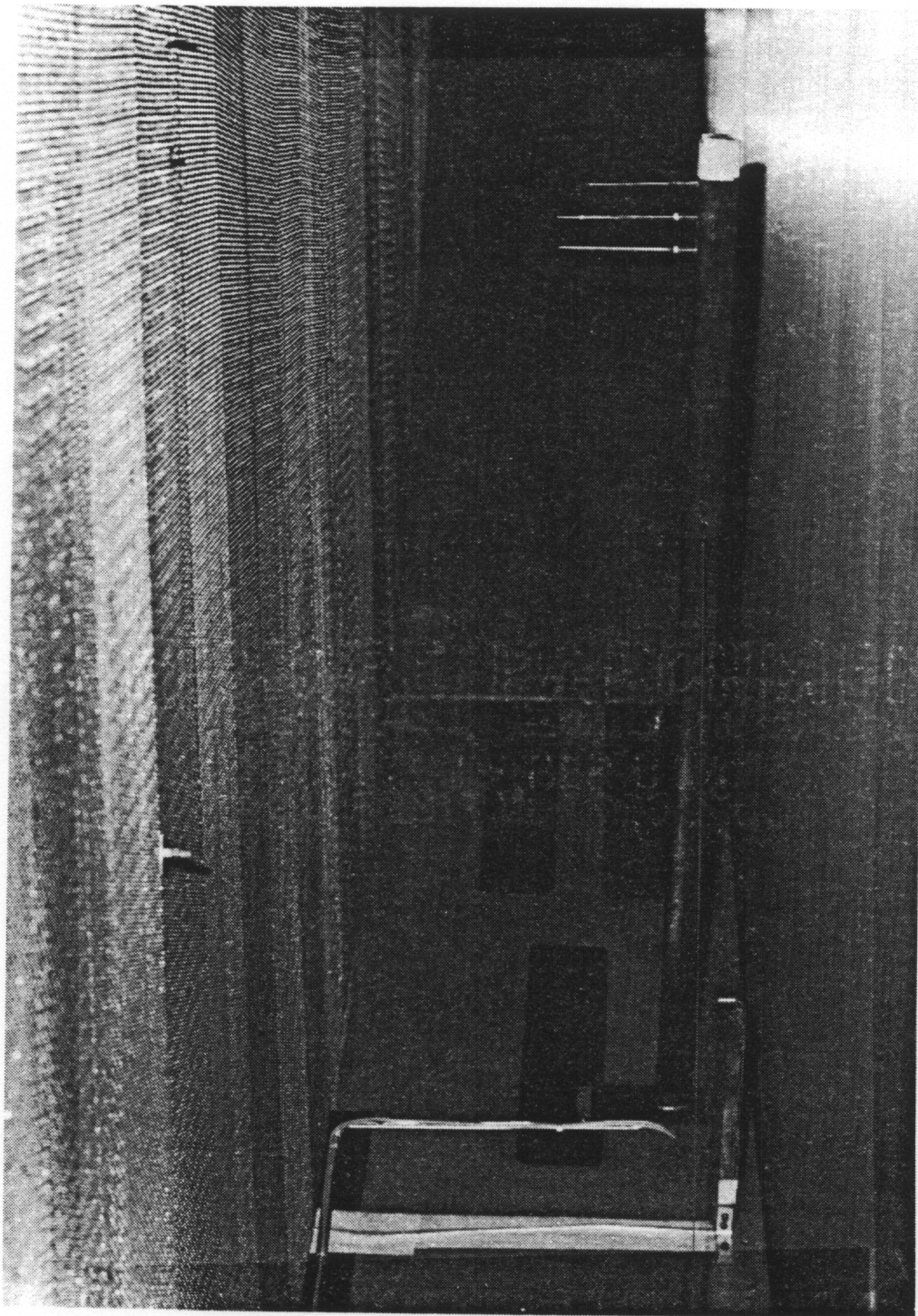


Figure 4.34 Photograph of the flow quality measurement location between the honeycomb and the first anti-turbulence screen

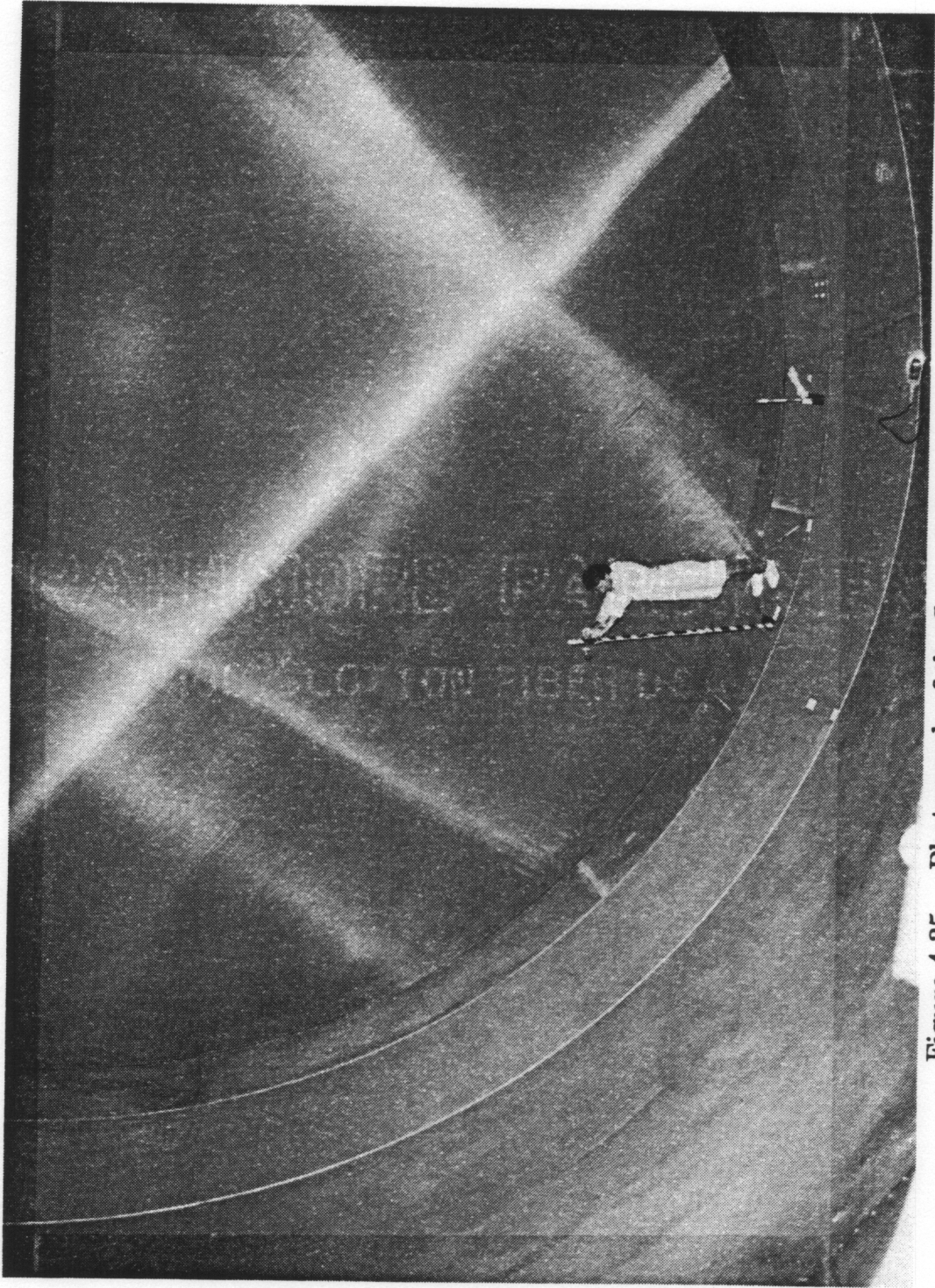


Figure 4.35 Photograph of the flow quality measurement location downstream of the anti-turbulence screens

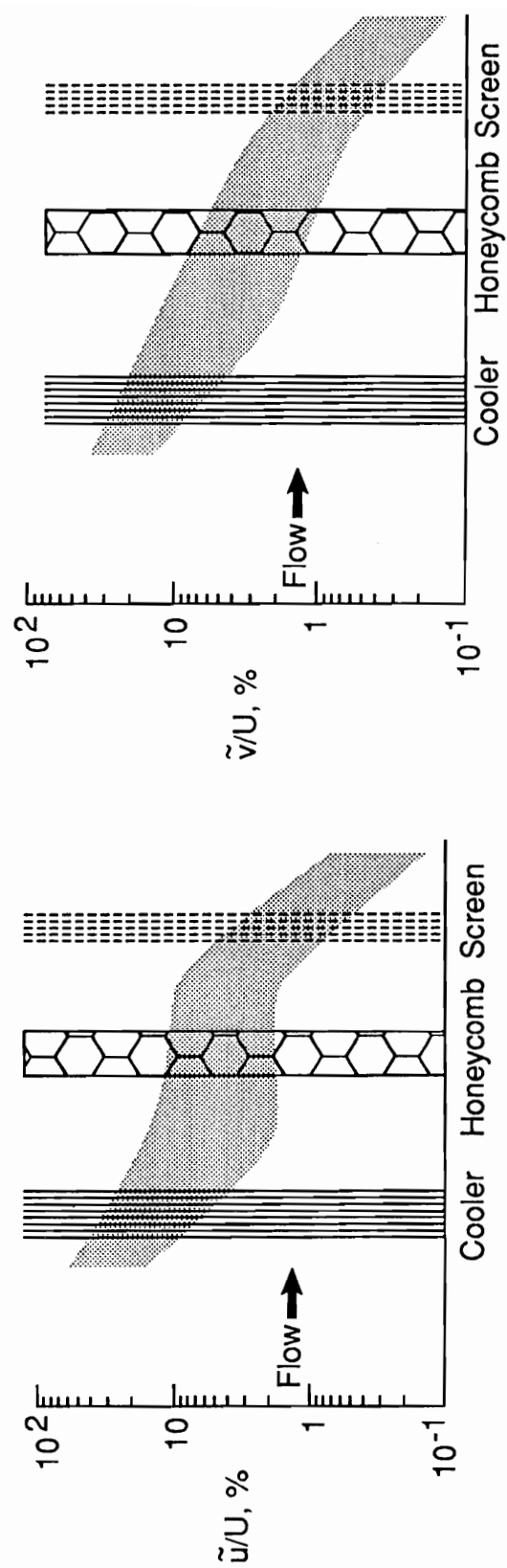


Figure 4.36 Summary of the performance of the turbulence manipulators in the 8'TPT wind tunnel

temperature of the wind tunnel, the eight stages of cooling tubes with fins also act as flow straighteners to reduce the large scale eddies. The velocity fluctuations are reduced through the heat exchanger to approximately 10%, at a total pressure of 710 psf, figure 4.38, indicating a reduction in the efficiency of the cooler when acting as a flow straightener. Since most large scale eddies have been significantly reduced by the heat exchanger, the honeycomb has little effect on the remaining turbulence. This can be seen by comparing the results measured downstream of the heat exchanger and results upstream of the anti-turbulence screens, figures 4.37 and 4.39 respectively. The reduction of the velocity fluctuations through the five anti-turbulence screens are similar for the different total pressures observed as shown in figures 4.39 and 4.40. There is a trend for the fluctuating velocity magnitudes to increase with wind tunnel speed downstream of the final anti-turbulence screen. This may be attributed to the upstream moving sound being generated from the test section.

The velocity fluctuations at the entrance of the settling chamber ranges from 0.15% to 0.60%. To determine how these disturbances propagate into the test section is not trivial for large transonic wind tunnels. The effect of the contraction on free-stream turbulence moving downstream into the test section is generally related to the contraction ratio and the change in density as the disturbance propagates through the contraction. Prandtl (1933) developed a semi-quantitative theory to predict the resultant velocity perturbations after they had propagated through a wind tunnel contraction. He assumed that the velocity fluctuations in the x direction are due to vortex filaments lying perpendicular to the x direction.

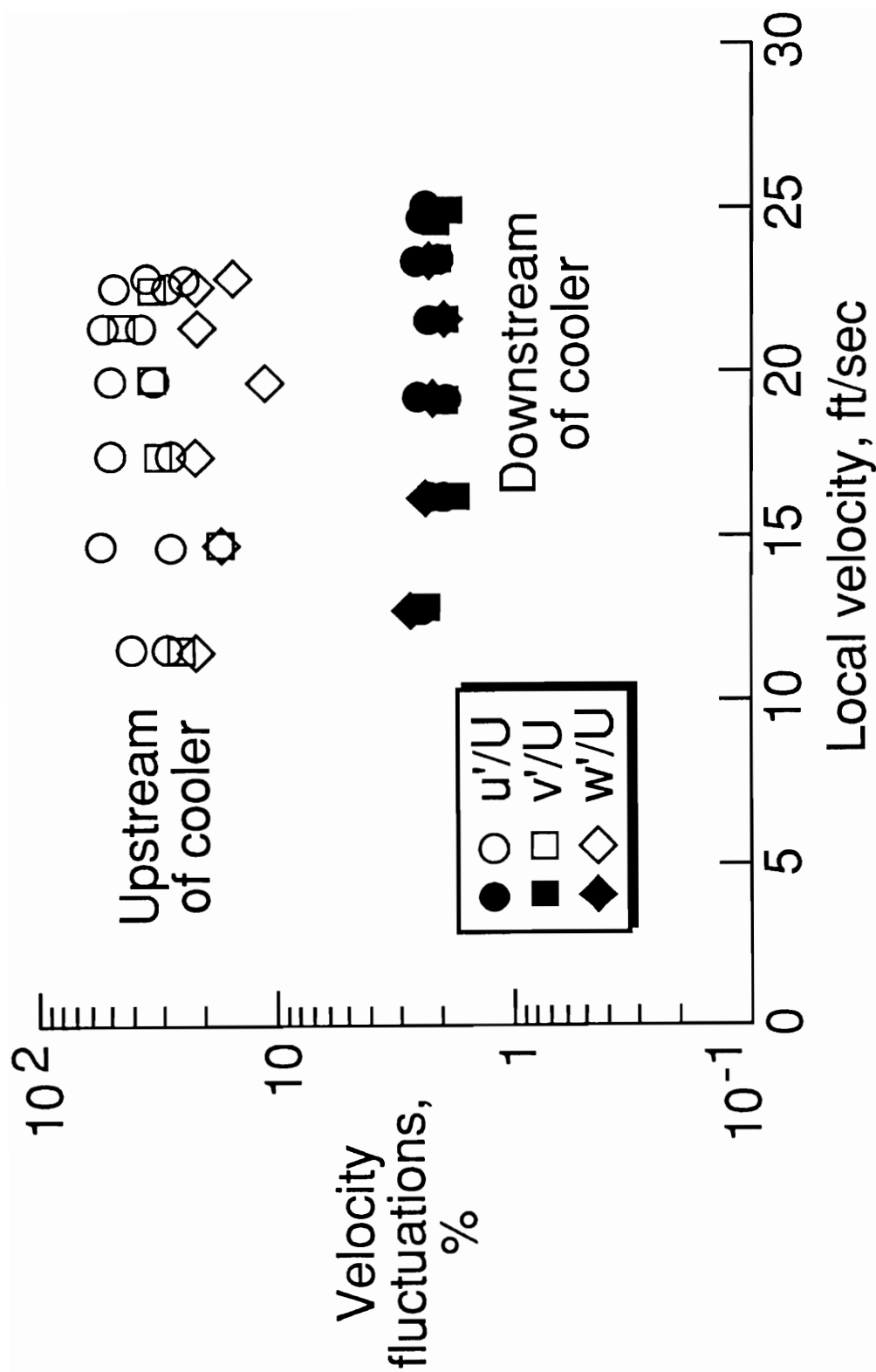


Figure 4.37 Performance of the heat exchanger when acting as a anti-vorticity device, Po 1725 psf

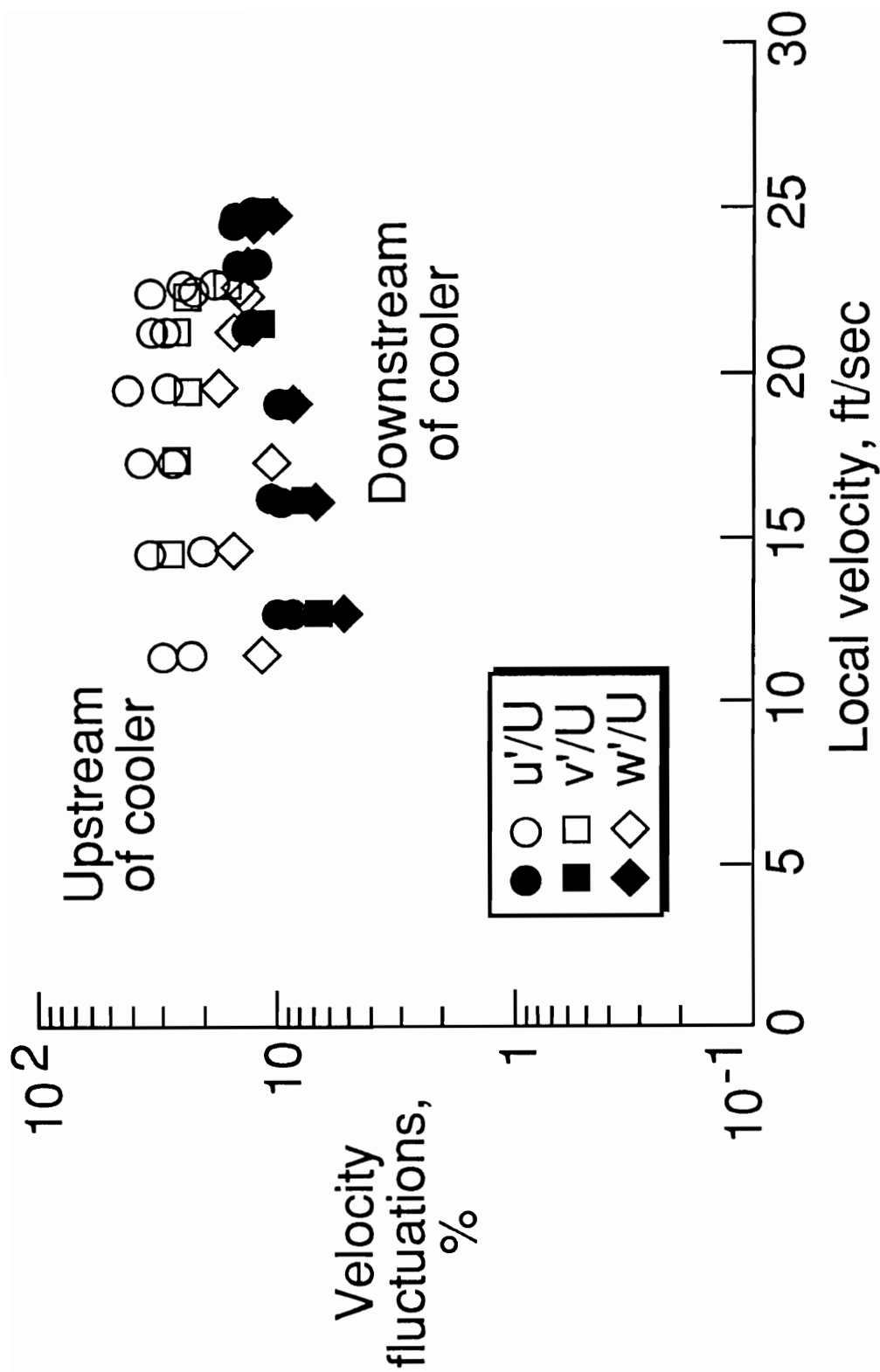


Figure 4.38 Performance of the heat exchanger when acting as a anti-vorticity device, Po 710 psf

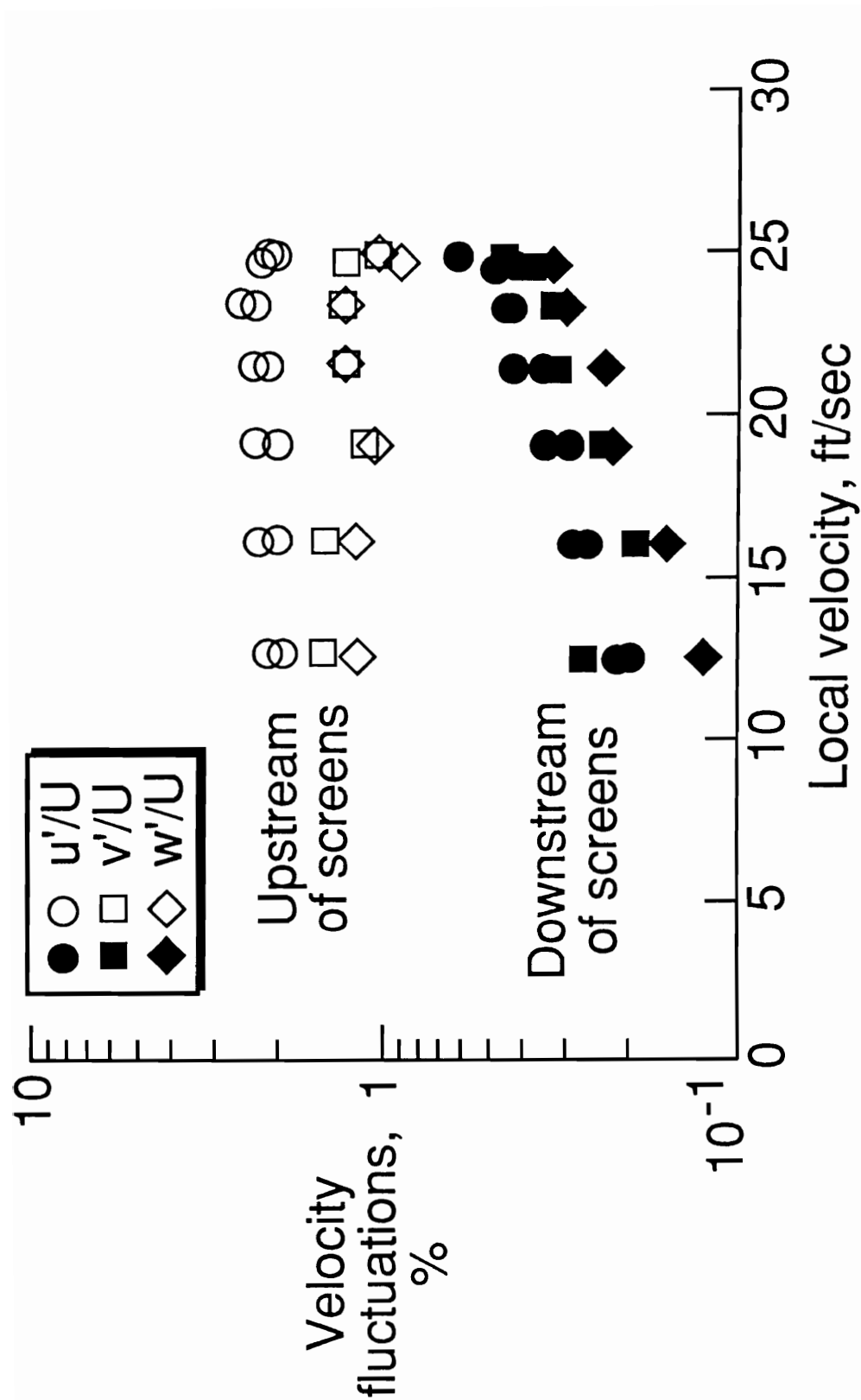


Figure 4.39 Performance of the anti-turbulence screens, Po 1725 psf

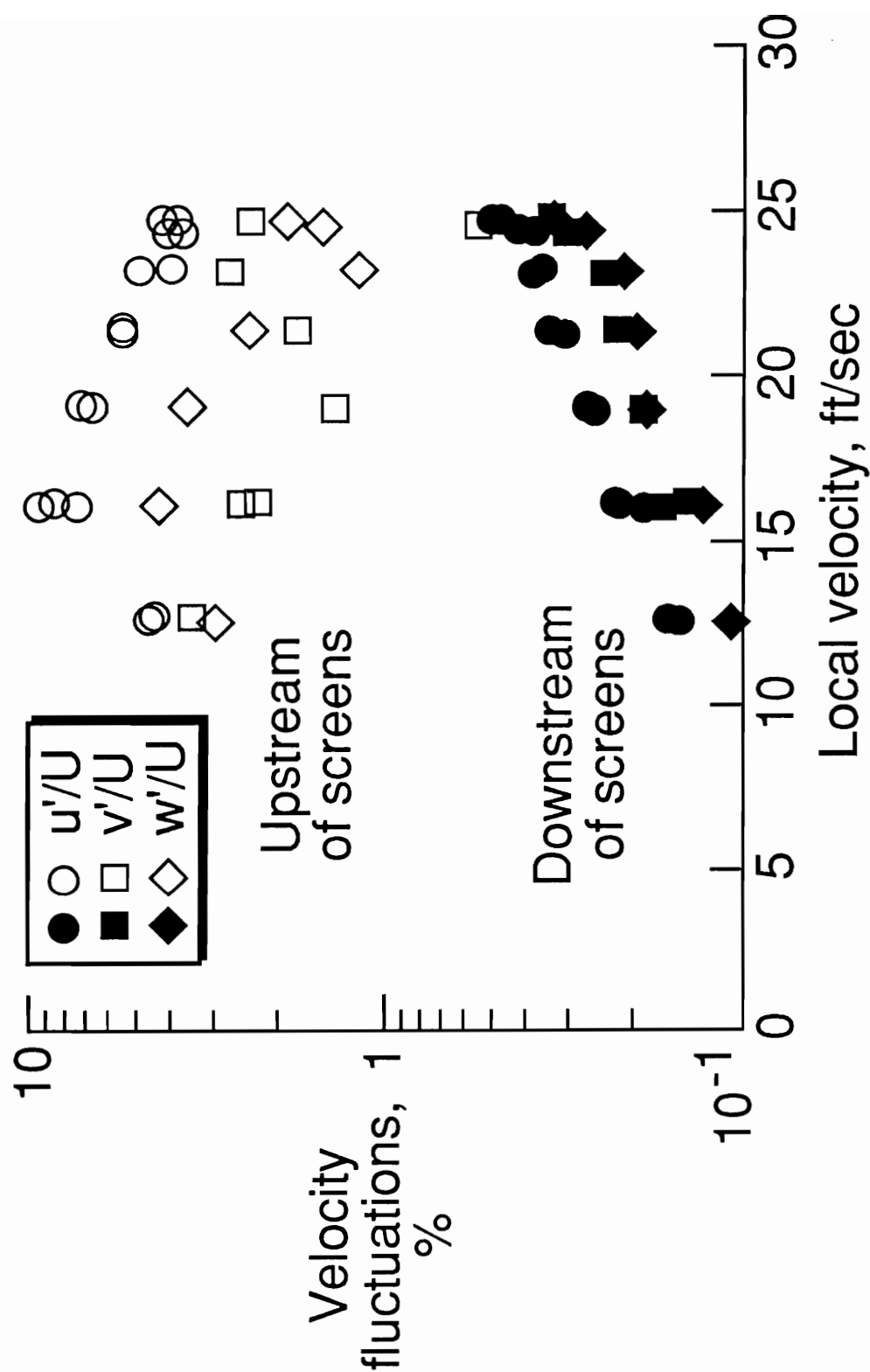


Figure 4.40 Performance of the anti-turbulence screens, Po 710 psf

Similarly, the velocity fluctuations in the y direction are due to vortices lying perpendicular to the y axis. As the flow goes through the contraction, the vortex filament in the x direction are elongated by a factor c, and those in the y and z directions are contracted by a factor \sqrt{c} , where c is the contraction ratio. Uberoi (1956) obtained data which showed that for contraction ratios less than 10 the velocity perturbations are consistent with Prandtl's prediction. However for contraction ratios similar to the 8'TPT (c=20.25) the magnitude of the velocity fluctuation in the x direction initially decreases, (as in the contractions with $c < 10$), but then increases to a final value which is higher than the initial value measured at the contraction entrance. Uberoi had measurements that indicated the velocity fluctuations in the x direction were larger than the y direction. He suggested that these were due to sound coming from the fan.

The following exercise of extending the velocity fluctuation information measured in the settling chamber to the test section of the 8'TPT will assume that the velocity perturbations are dominated by vorticity at the beginning of the settling chamber. The justification to assume that only vorticity is present in the settling chamber is questionable, which makes this particular analysis suspect to large error. The analysis is intended to give the reader a sense of the order of magnitude of disturbances transported from the settling chamber to the test section. It should be noted that it may be reasonable to assume that there are no local sound sources present in the settling chamber or that the amplitude of sound is small and can be neglected, but it is not a good assumption to assume that no temperature fluctuations exist.

Applying a linear extrapolation to the velocity perturbation data obtained by Uberoi (1956) for a large contraction ratio facility, the absolute magnitude of the longitudinal disturbance can increase 2.6 times the initial value through the contraction. This corresponds to a Mach number of 0.8 in the test section and a mean velocity of 25 feet per second at the contraction inlet. Scaling the expected increase in longitudinal disturbances to an initial disturbance of 0.6% measured in the settling chamber (or the absolute magnitude of 0.15 feet per second) will result in a test section velocity fluctuation of 0.0275% (or an absolute magnitude of 0.242 feet per second). Comparing the projected value of 0.0275% to the typical 0.8% velocity fluctuations measured in the test section, would suggest that only 3% of the measured velocity fluctuations in the test section originated in the settling chamber. The remainder of the velocity fluctuations are implied to result from sound sources from the test section and/or diffuser.

4.4 Fluctuating Pressure Data

The influence of Sound on the flow quality of a wind tunnel can be represented utilizing one of several different approaches. The results of this study will focus on free stream fluctuating total pressure, fluctuating static pressure, and fluctuating wall pressures using a miniature diaphragm type pressure transducer. The data will be used to gain a better understanding of the disturbance environment of the wind tunnel in addition to assisting in the interpretation of hot wire information. This section will be broken into two primary sections, Empty Tunnel, and LFC Configuration.

4.4.1 Empty Tunnel Results - The primary purpose of analyzing the fluctuations in the freestream of an empty wind tunnel test section is to establish the baseline disturbance levels that occur in the facility. It is also useful to determine the disturbance levels at locations other than the freestream, since freestream measurements may not always be possible with a model in place. This will allow the researcher to correlate the influence of the model on freestream disturbances with data measured at locations other than the freestream. Figure 4.41 is a summary of the rms pressure fluctuations for several different locations in the empty test section at atmospheric pressure. All of the fluctuating pressure data were normalized by the local mean static pressure. The corresponding sound pressure levels for the data shown in figure 4.41, range from 106 dB to 135 dB in the test section and 112 dB to 152 dB in the diffuser. When compared

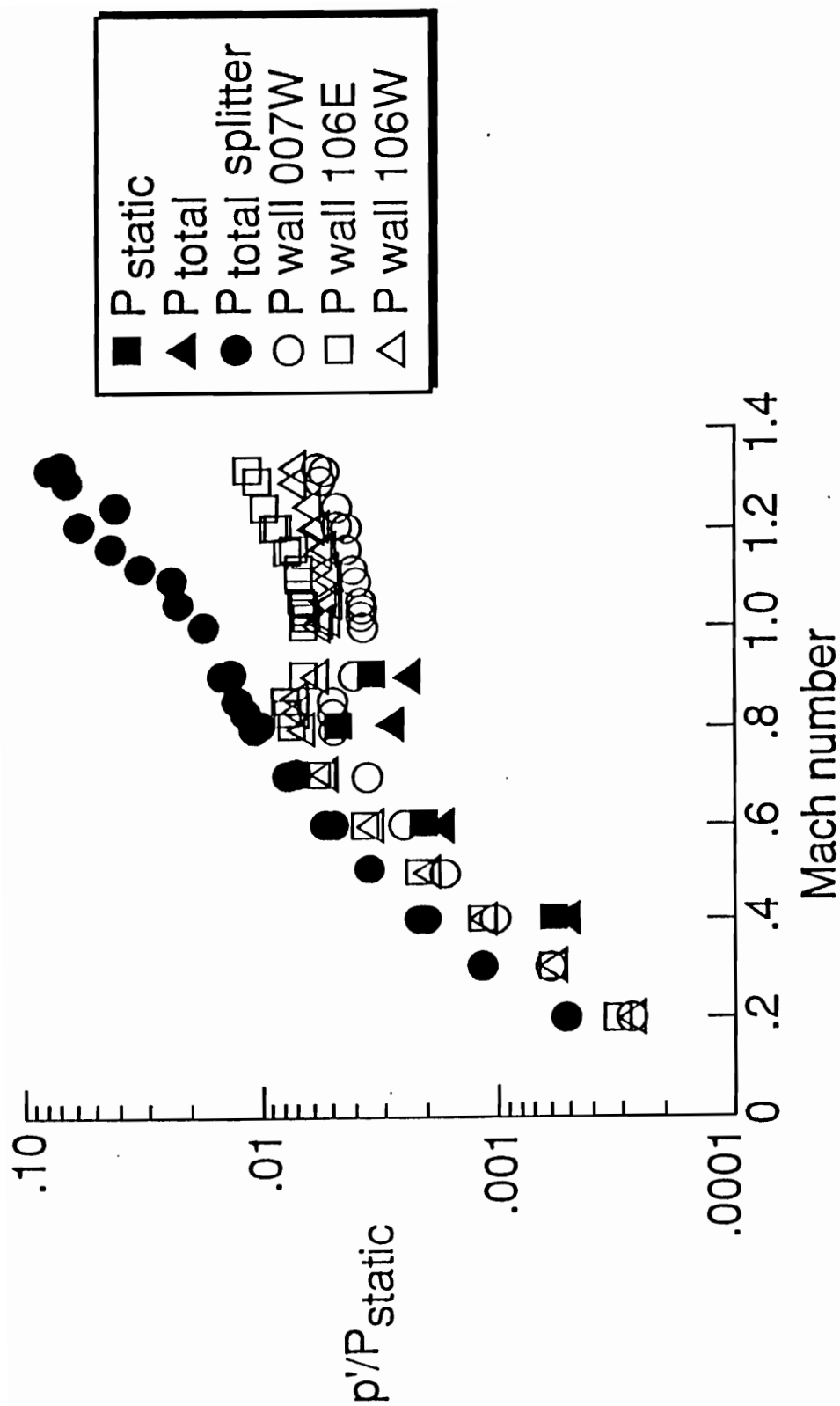


Figure 4.41 Static pressure fluctuations at different locations in the empty wind tunnel for different Mach numbers
Po 2125 psf

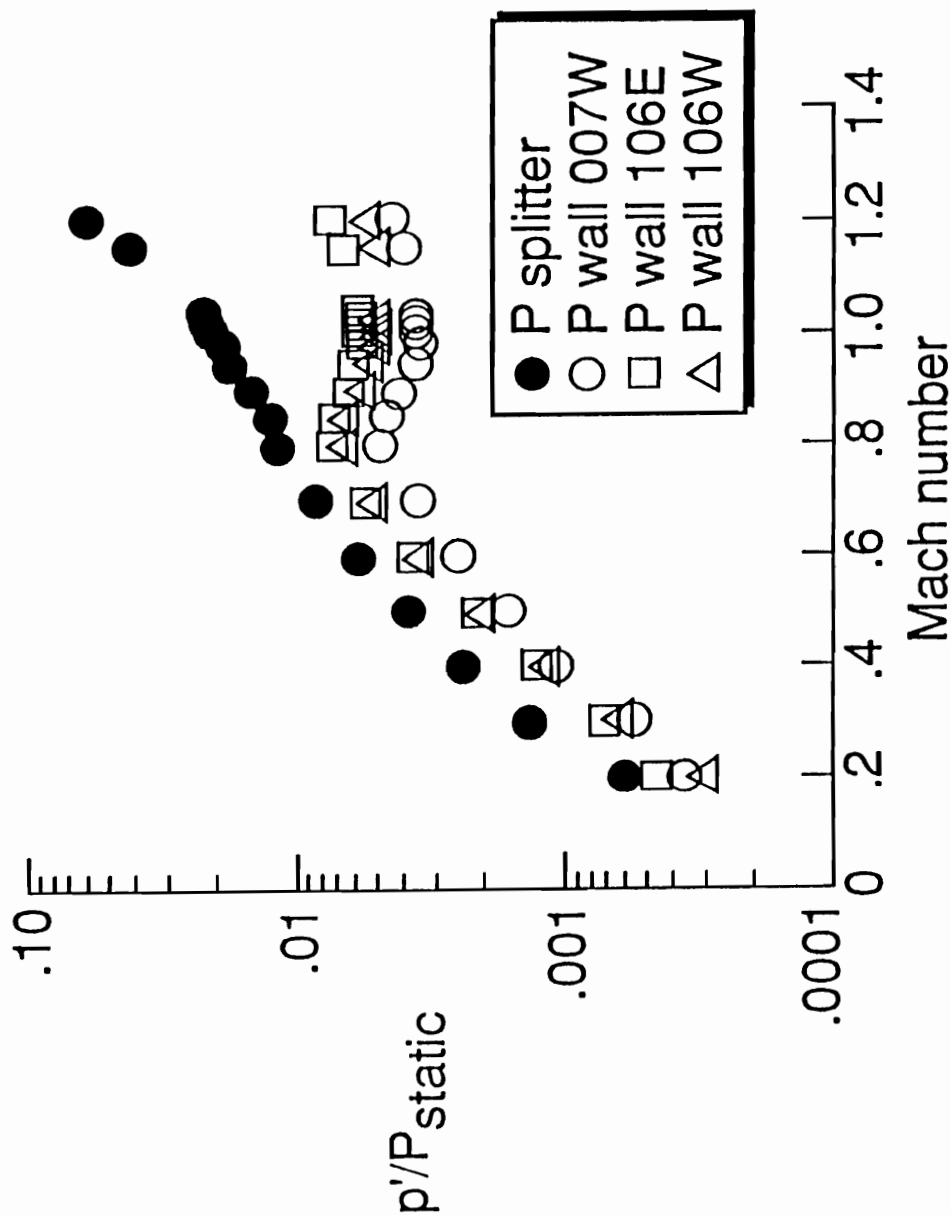


Figure 4.42 Static pressure fluctuations at different locations in the empty wind tunnel for different Mach numbers
 P_0 1060 psf

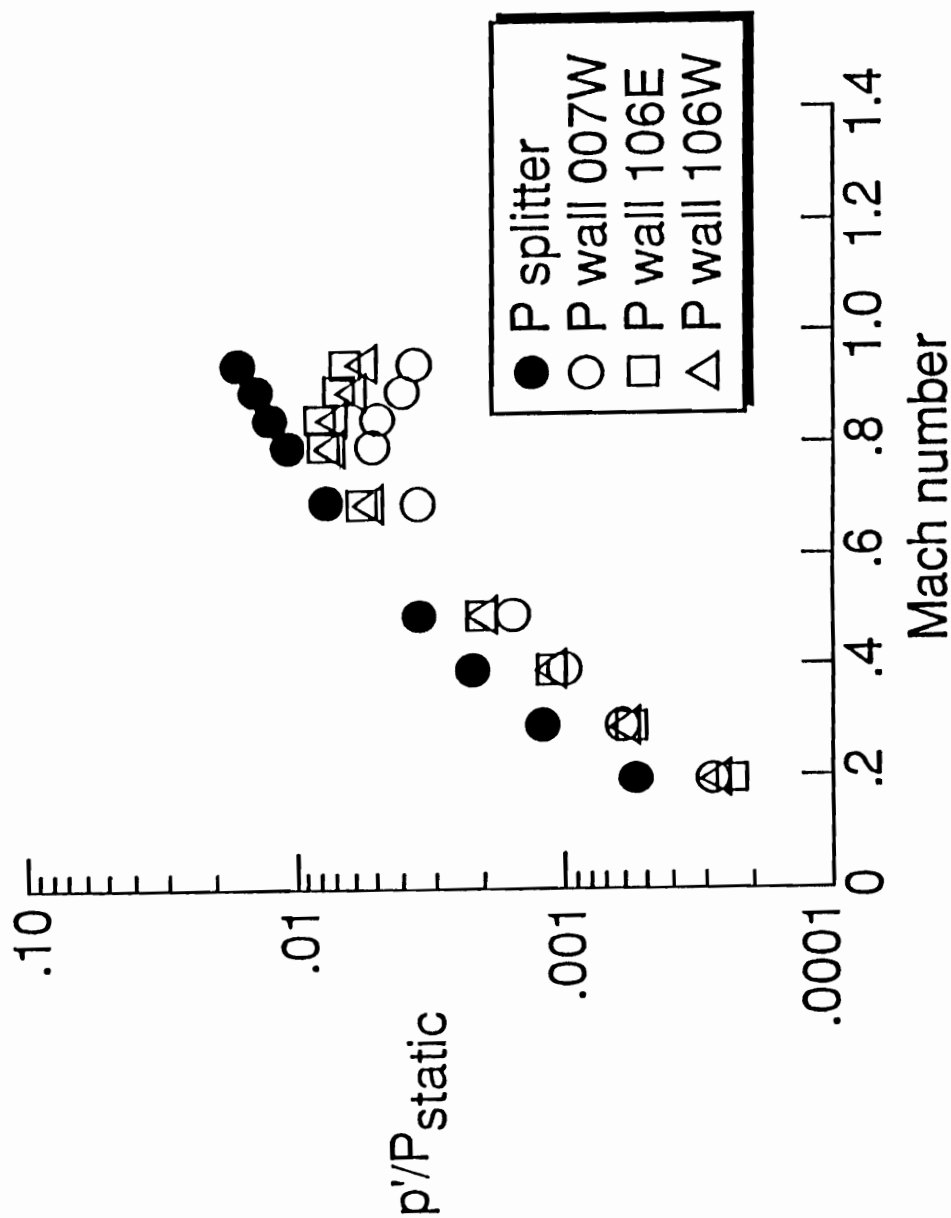


Figure 4.43 Static pressure fluctuations at different locations in the empty wind tunnel for different Mach numbers
Po 3180 psf

to similar data obtained at 0.5 atmospheres (figure 4.42), and 1.5 atmospheres (figure 4.43), no appreciable increases in magnitude could be observed. These data also correspond very well to similar data acquired in other transonic wind tunnel as shown in figure 4.44, Harvey (1980).

When comparing the wall fluctuating pressures to those measured in the freestream, it is important to recognize that the turbulent wall boundary layer influence the measurements made at the wall. However, the trends of the fluctuating pressure data measured at the wall seems to track to freestream data well. The differences are in a higher rms levels measured at the wall. The pressure fluctuations measured at the entrance of the test section (007W) were always less than the measurements obtained at the station corresponding to the streamwise model location (106E & 106W). This difference grew as the Mach number increased. One anomaly that was observed at all total pressures was an increase in mean temperature and fluctuating static wall pressure on the east wall.

As seen in figure 4.41, the trends of the wall boundary layer are similar to both the free stream fluctuating static and total pressures, yet at a higher level. When comparing the spectra of the freestream total and static pressures as a function of Mach number (figure 4.45 and 4.46 respectively), it is noted that the magnitude of the static fluctuations are higher than the total pressure fluctuations at the higher Mach numbers and higher frequencies. Figure 4.47 compares the freestream total and static fluctuating pressure at a Mach number of 0.4. Both of the fluctuating pressures seem well correlated up to the approximately 10kHz beyond which there is a significant decrease in the magnitude of in the static pressure

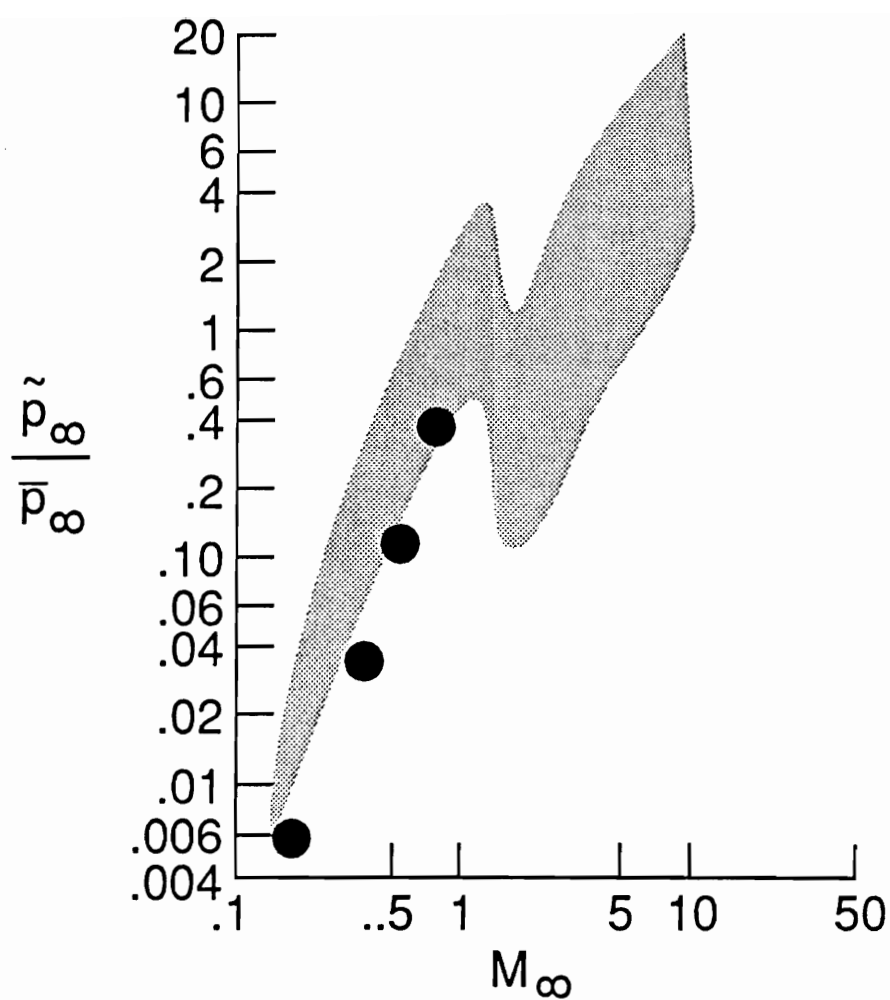


Figure 4.44 Comparison of 8'TPT static pressure fluctuations to other large scale transonic wind tunnels

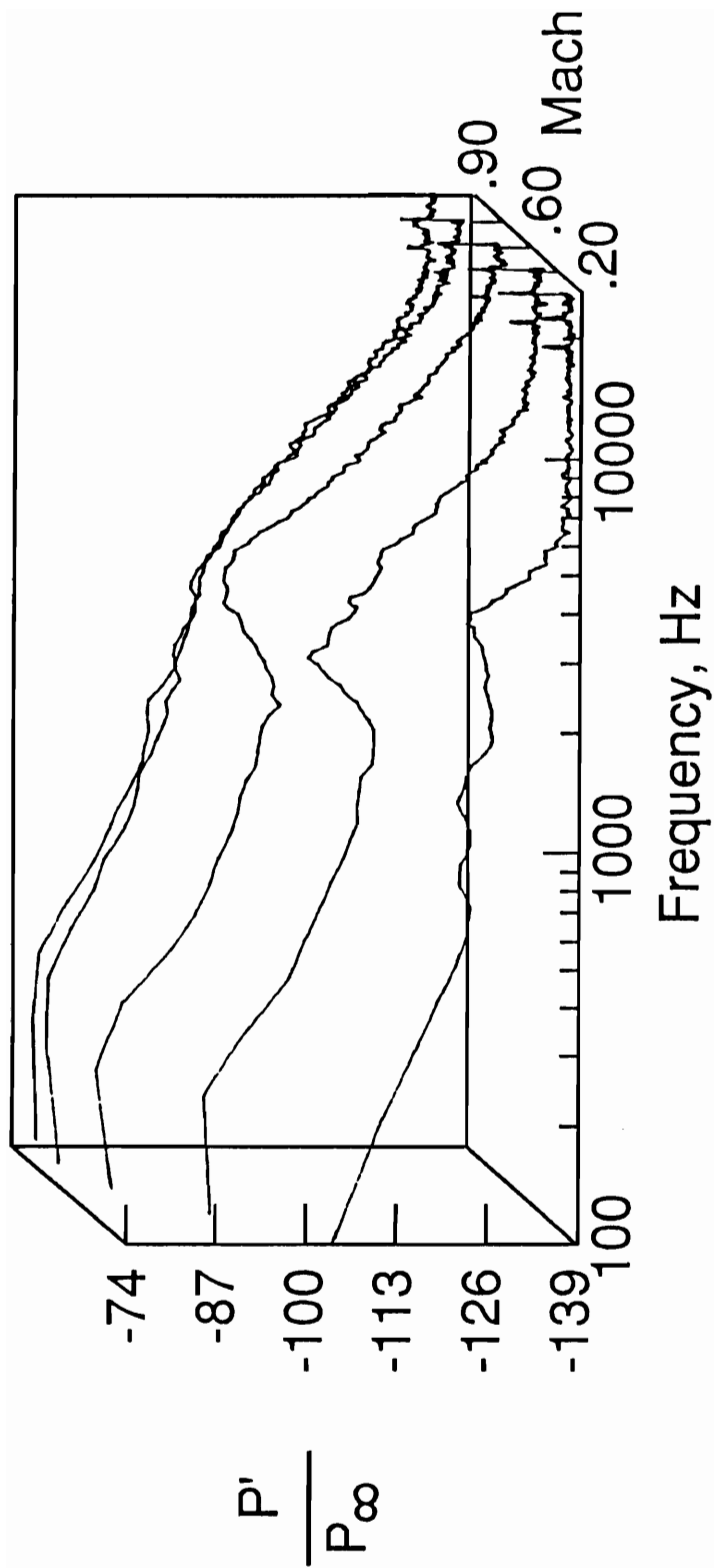


Figure 4.45 Total pressure spectra for different Mach numbers
P₀ 2125

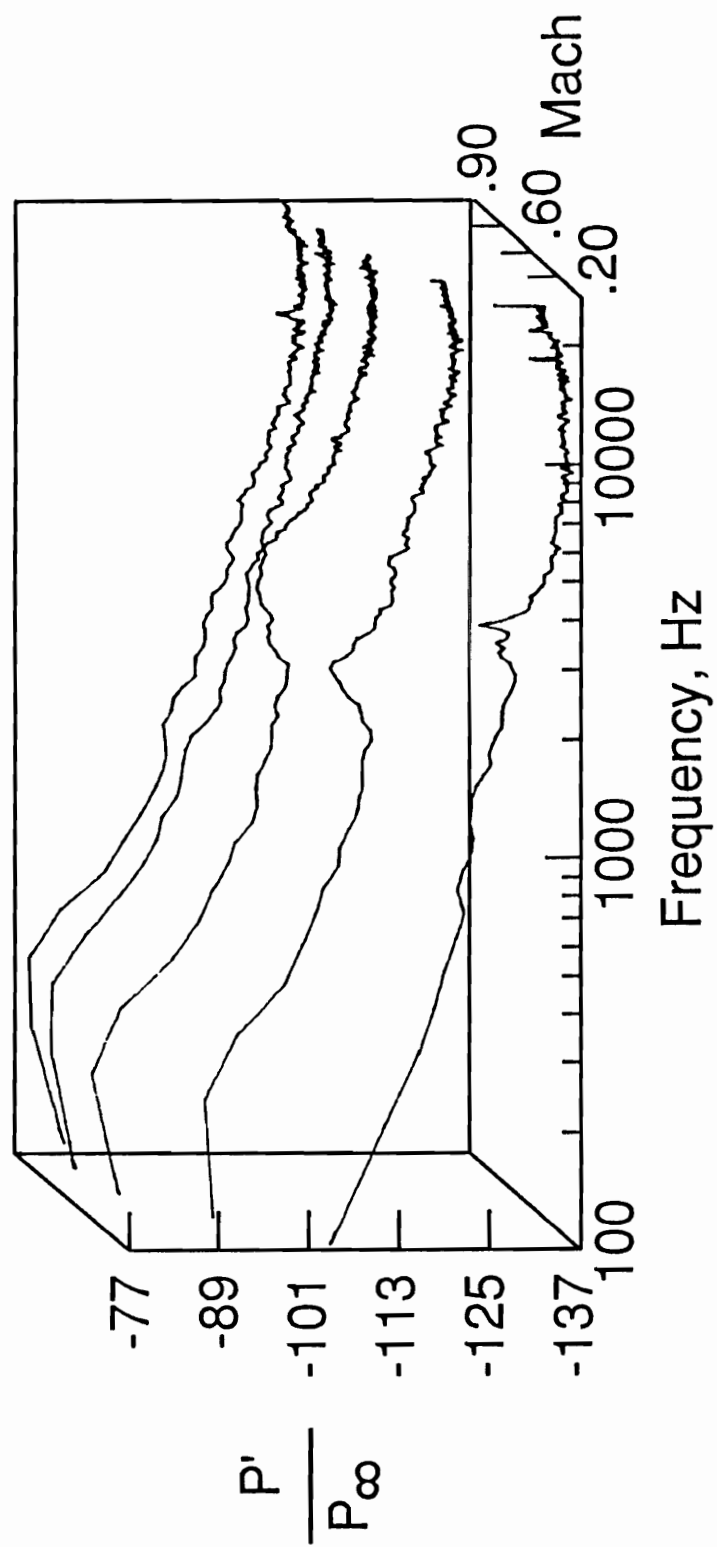


Figure 4.46 Static pressure spectra for different Mach numbers
Po 2125

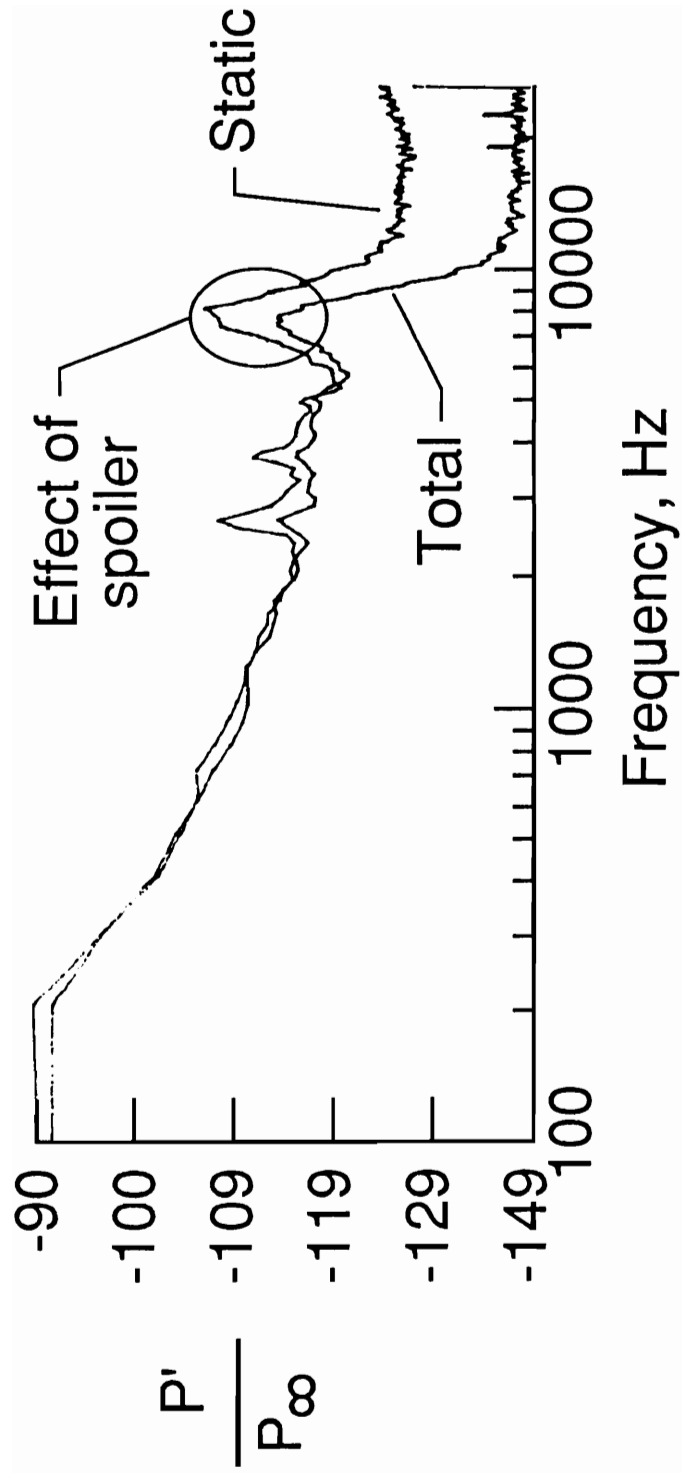


Figure 4.47 Comparison of the total and static pressure spectra
Mach number: 0.4, P_o 2125 psf

fluctuation. As the Mach number is increased the high frequency static perturbation increase at a greater rate than the total pressure perturbations.

The presence of a sonic region between the measurement and the diffuser become evident between a Mach number of 0.9 and 1.0. This is denoted by a decrease in the magnitude in the pressure fluctuations as shown in figures 4.48 - 4.50 which is indicative of eliminating the upstream moving sound from the diffuser. The effectiveness of this sonic region may be influenced by any wake or the non uniformity of the flow into the diffuser.

Acoustic tones were generated by guy wires which supported the sting. They can be identified by their spectral signatures in figure 4.51 for a Mach number of 0.2 and figure 4.52 for a Mach number of 0.9. When the guy wires were removed the tone disappeared. Another source of noise in the empty tunnel configuration was the implementation of the spoilers. The effect of spoiler noise can be identified by the spectral signature of the broad peak at approximately 8 kHz in figure 4.53.

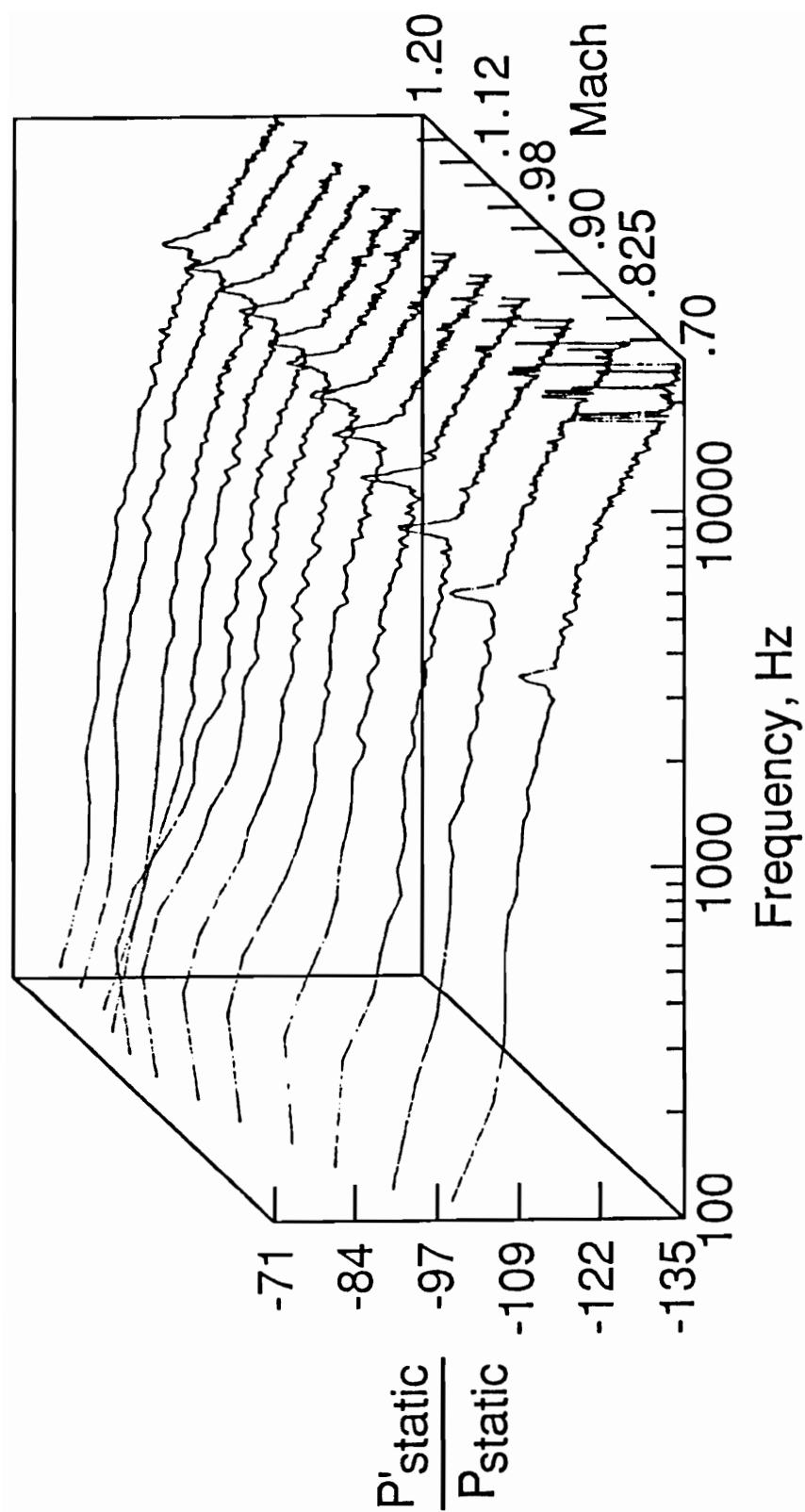


Figure 4.48 The effect of choking the tunnel on wall static pressure spectra for different Mach numbers, P_o 1060 psf

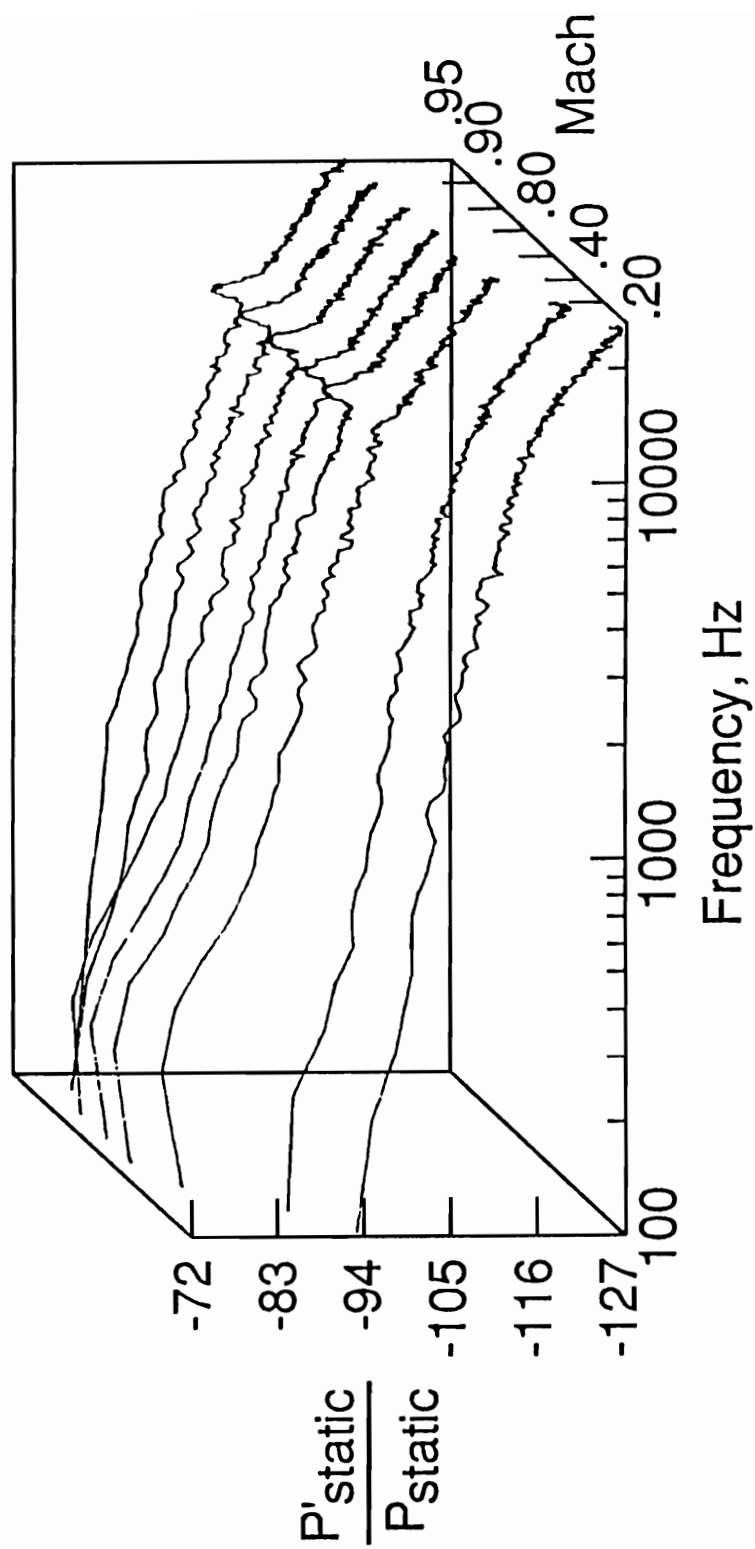


Figure 4.49 The effect of choking the tunnel on wall static pressure spectra for different Mach numbers, P_o 2125 psf

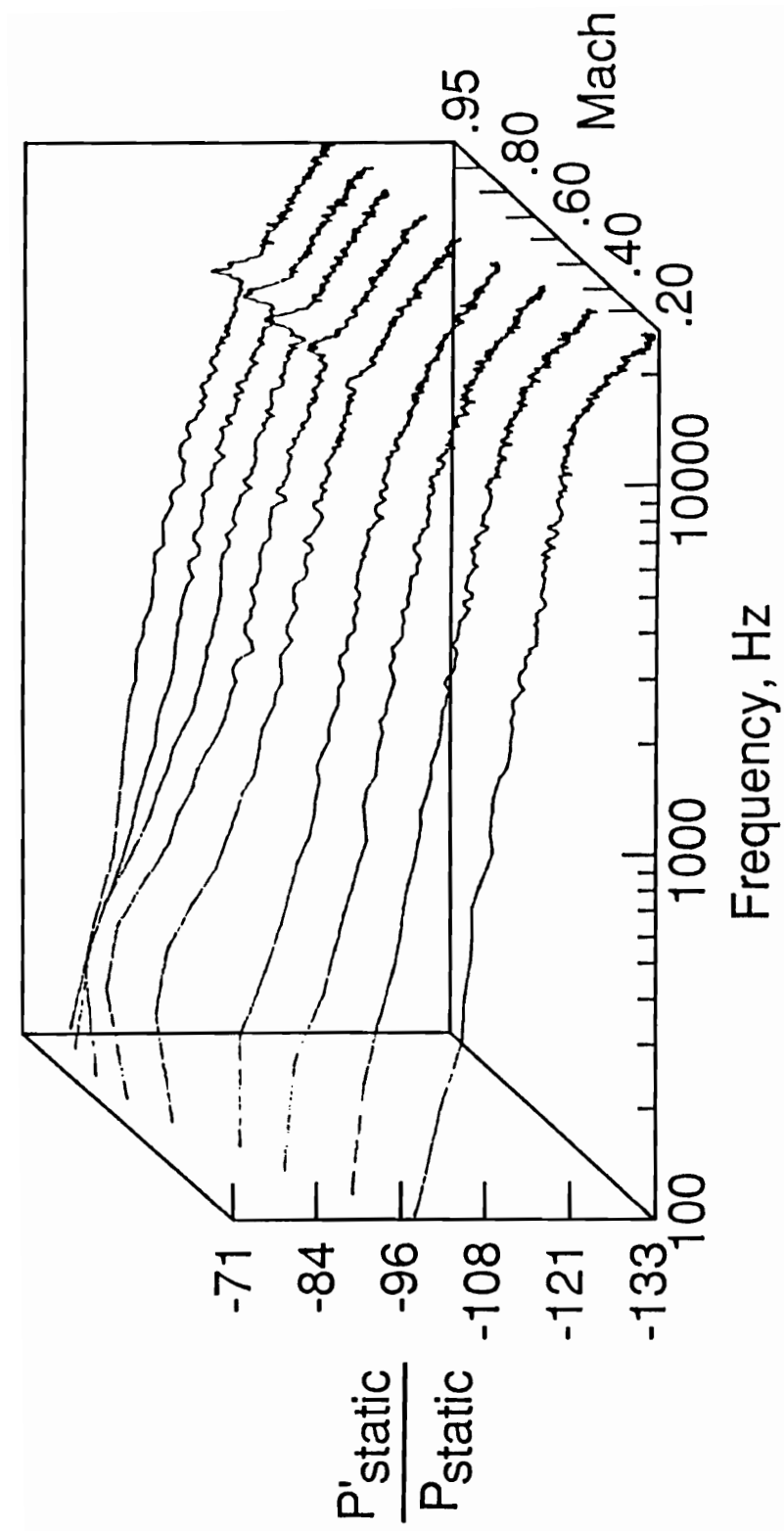


Figure 4.50 The effect of choking the tunnel on wall static pressure spectra for different Mach numbers Po: 3180 psf

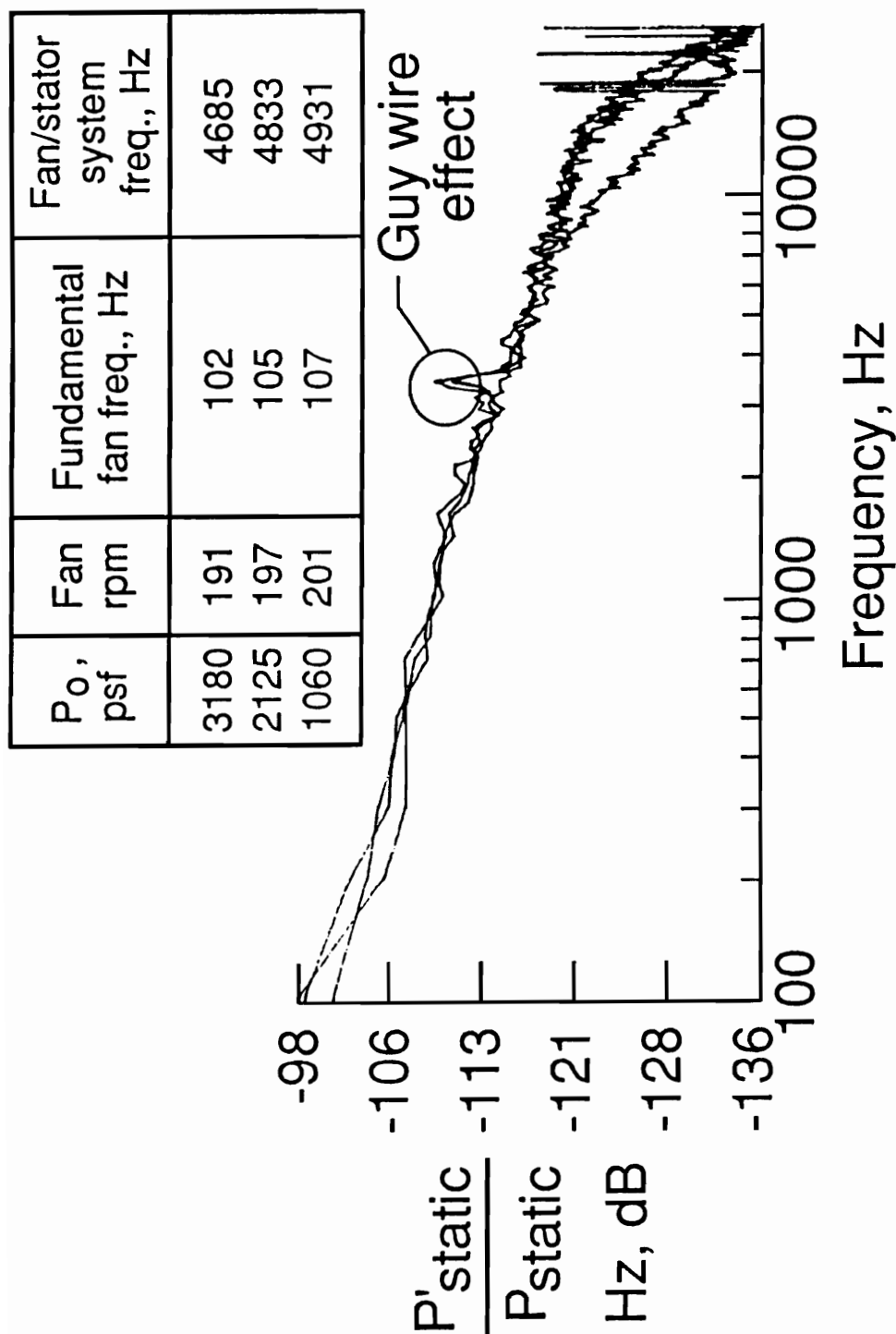


Figure 4.51 Comparison of wall static pressure fluctuations at different total pressures at Mach number of 0.2

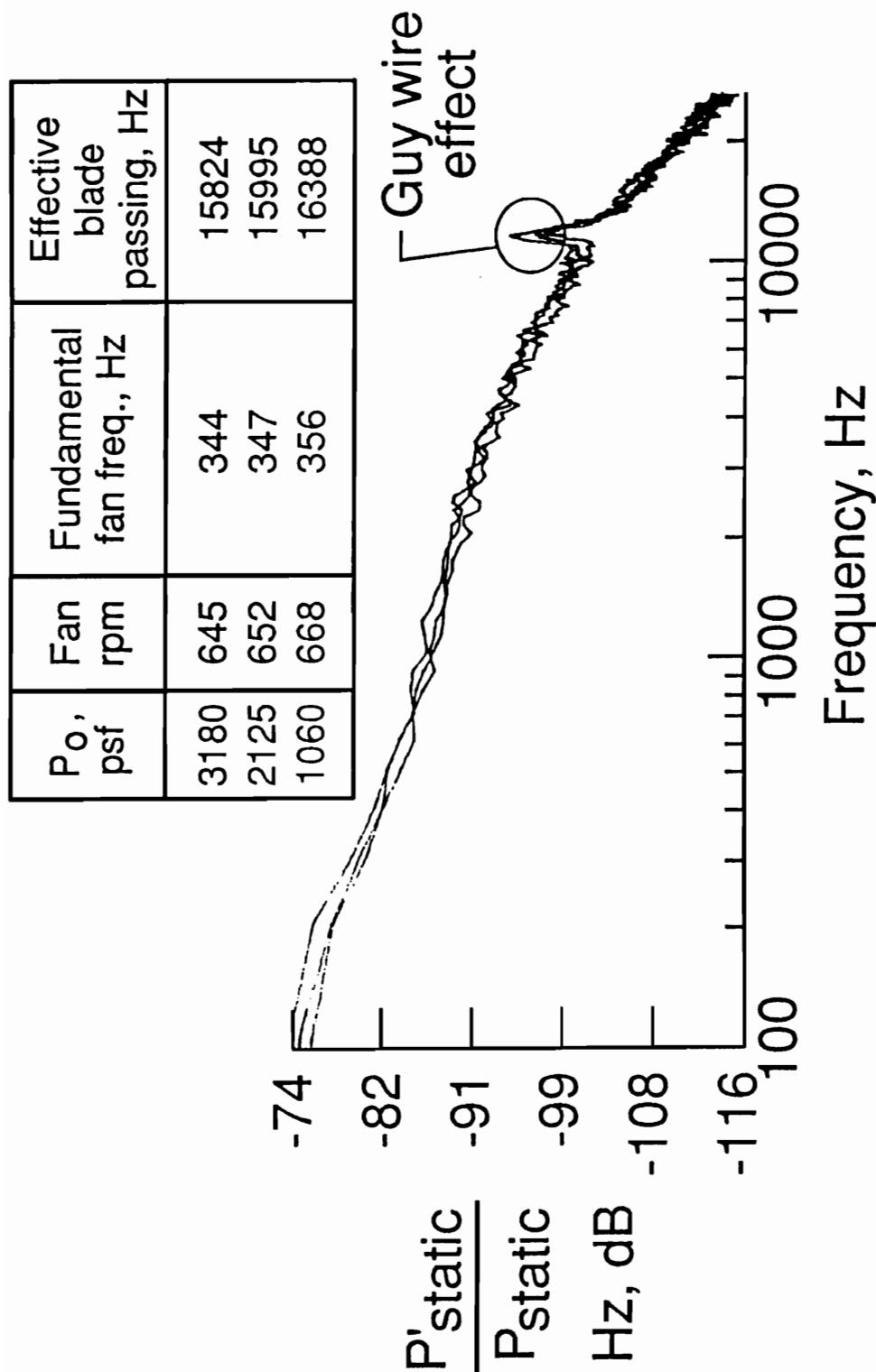


Figure 4.52 Comparison of wall static pressure fluctuations at different total pressures at Mach number of 0.9

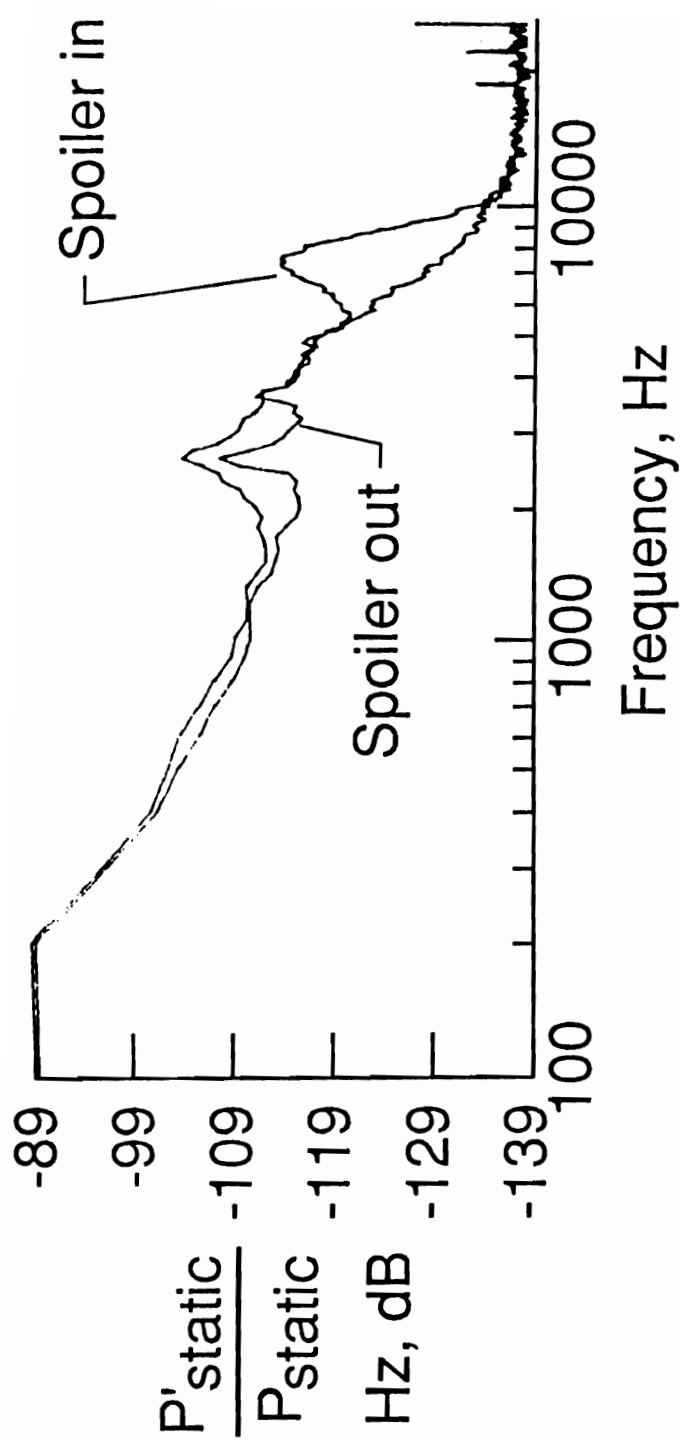


Figure 4.53 Effect of wind tunnel spoiler on static fluctuation pressure measurement at Mach number of 0.4

4.4.2 LFC Fluctuating Pressure Results - Having now established the baseline pressure levels in the empty tunnel, the influence of the LFC model and liner can now be determined. The liner covered the transonic slots and spoiler system which eliminated them as sound sources. Not only did this reduce the noise from these devices but it also isolated the test section from compressors located in the plenum. The removal of the sting and the arc sector also reduced the noise by eliminating the guy wires and strut wake. However, the addition of the large LFC model created it's own sound sources. The boundary layer suction system and the non-uniform or contoured wall liner are thought to be new sources of noise.

Figures 4.54 and 4.55 are examples of the static pressure fluctuation spectra with the LFC model in place. The spectra are generally broadband and compare very well to the empty tunnel configuration. There are some signatures between 20 kHz and 25 kHz that cannot be identified. The rms magnitudes corresponding to these data are compared to the empty tunnel results in figure 4.56. Comparing the empty tunnel and LFC configuration results it can be seen that there is an increase in the fluctuating pressure levels for the LFC model. When the tunnel was choked with the LFC model installed, the fluctuating pressures were reduced to the value approaching the empty tunnel slots closed data, (Harvey, Stainback & Owen 1980).

The uniformity of the unsteady flow field was spot checked because of the inability to survey the entire region. An example of the spectral signatures from two different locations measured in a plane upstream of the model, figure 4.57, indicated the the unsteady flow field was uniform.

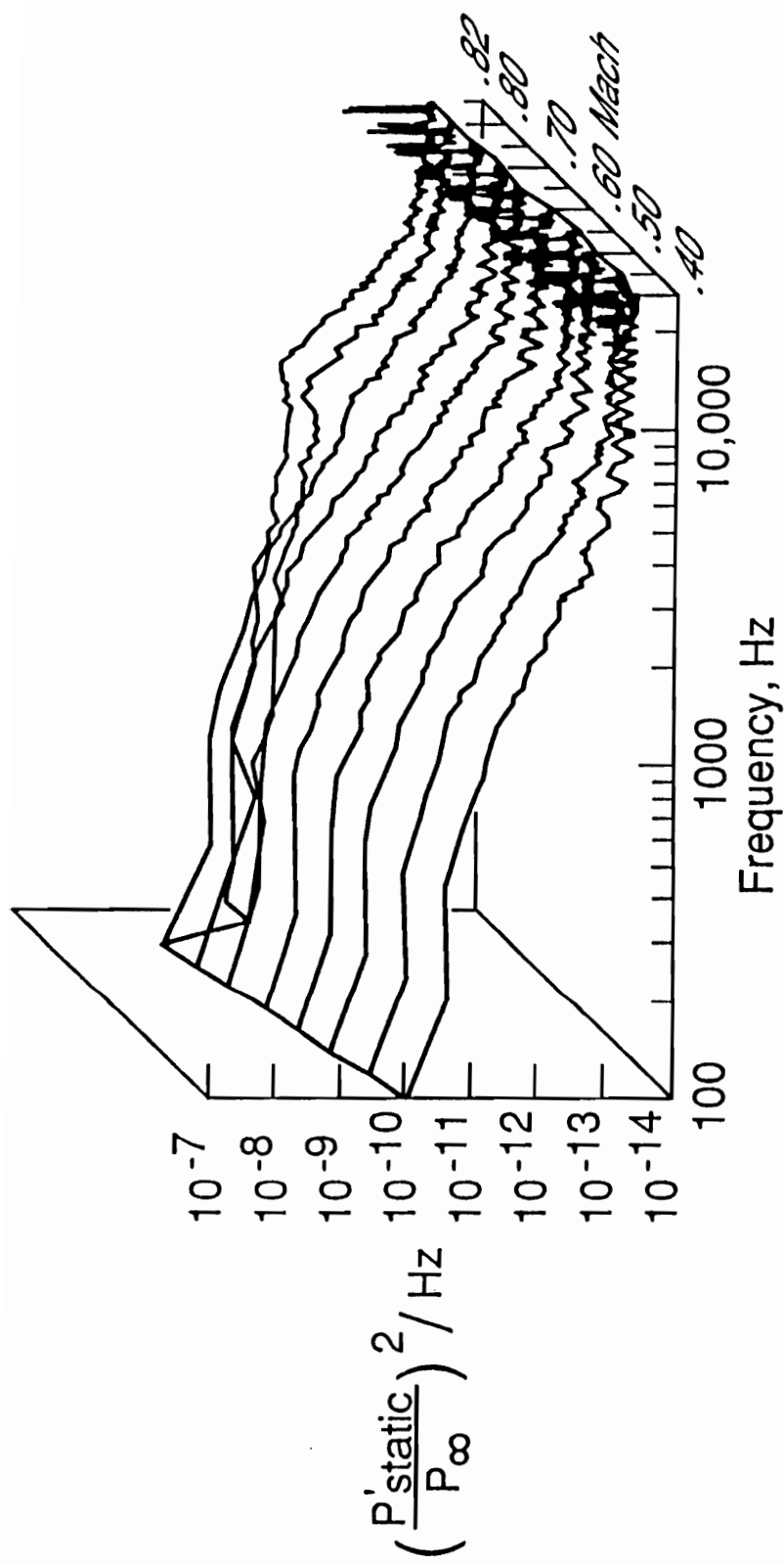


Figure 4.54 Static pressure spectra for different Mach numbers with the LFC model, P_o 1430 psf

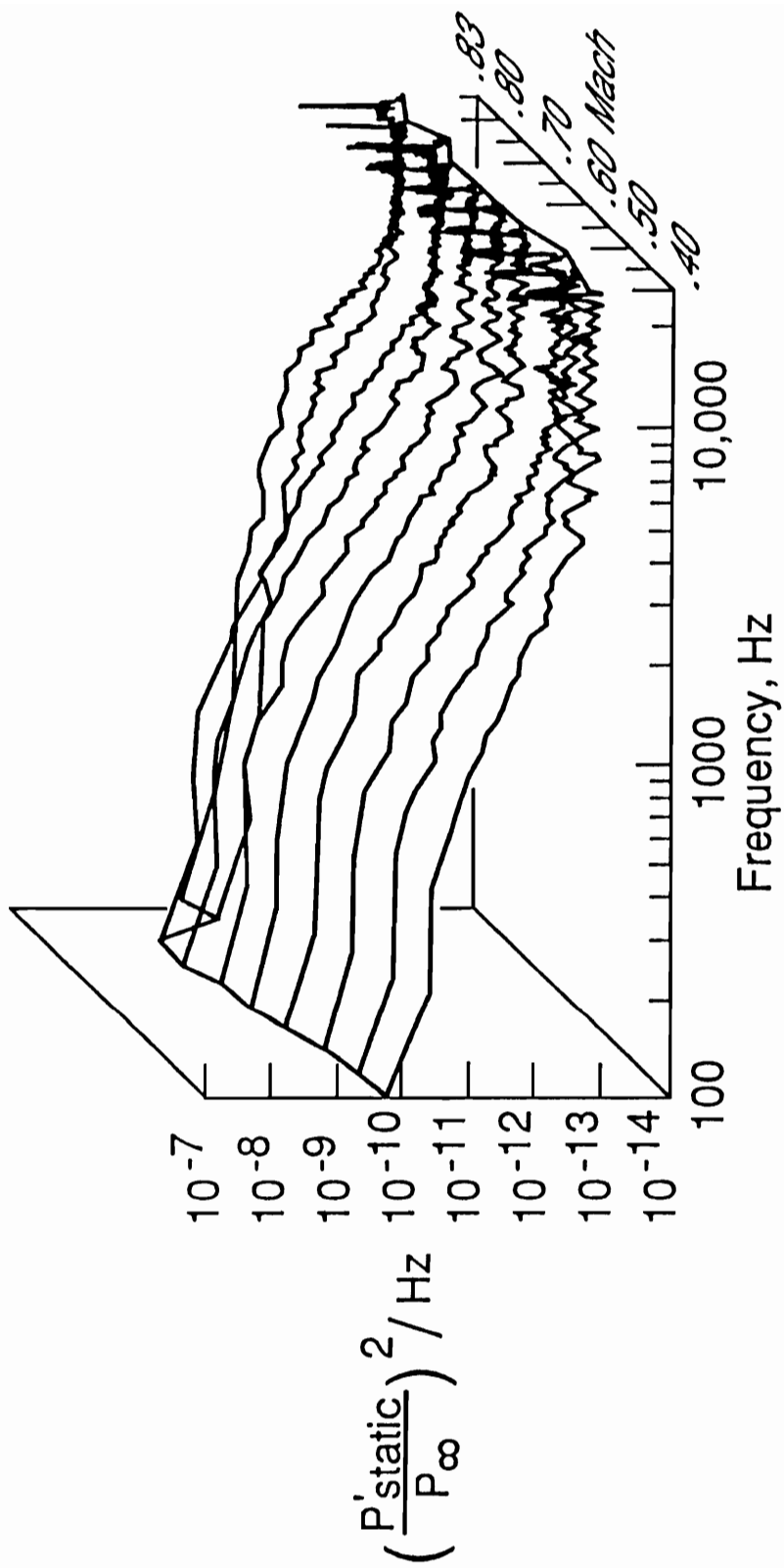


Figure 4.55 Static pressure spectra for different Mach numbers with the LFC model, P_o 710 psf

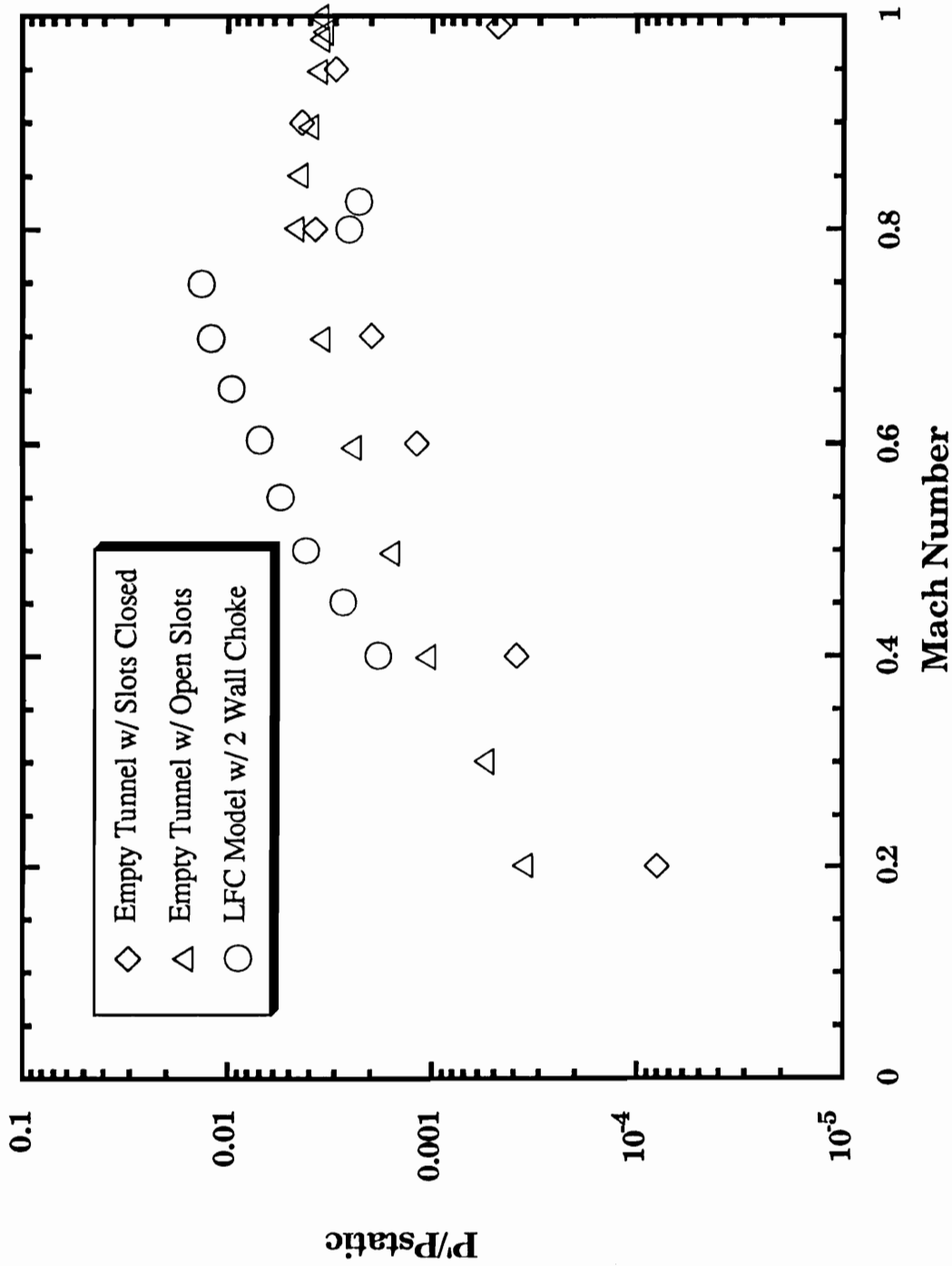


Figure 4.56 Comparison of static pressure levels for the empty tunnel configuration and the LFC configuration, P_o 2125 psf

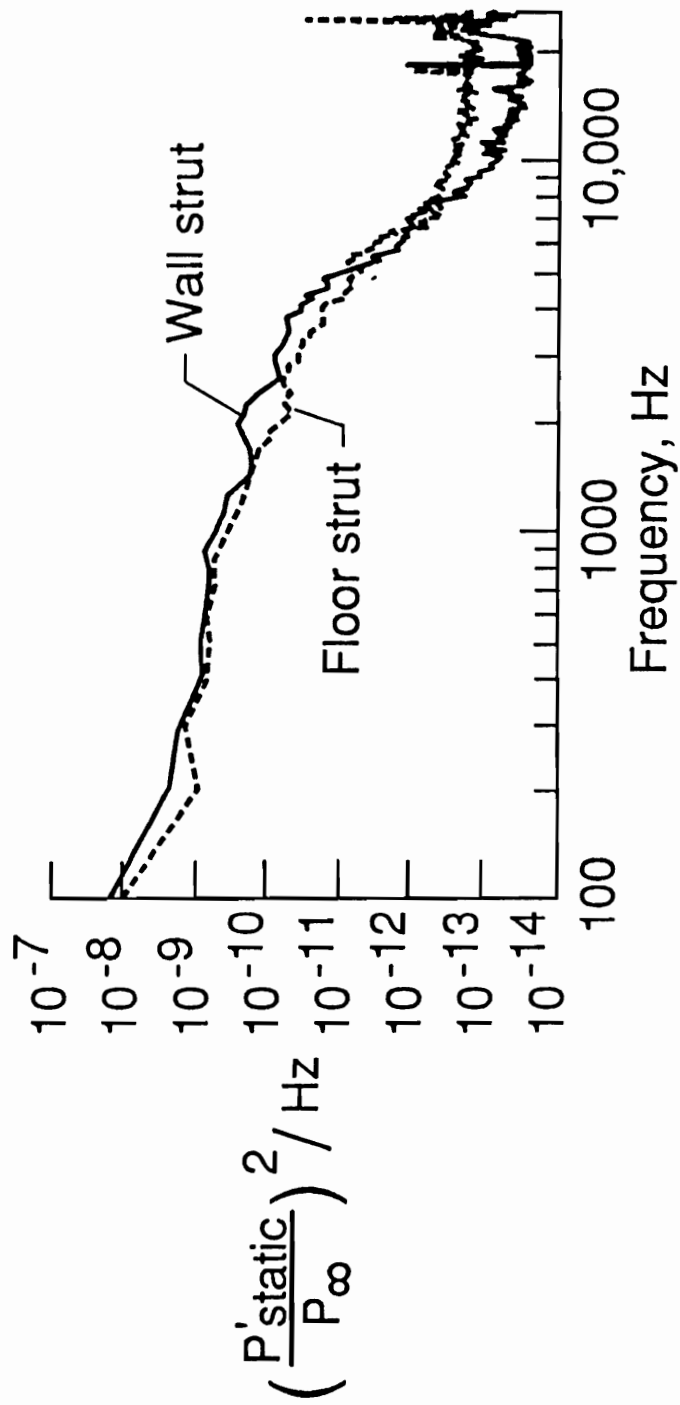


Figure 4.57 Comparison of the static pressure spectra for different locations in the wind tunnel with the LFC model, P_o 710 psf, Mach number of 0.827

It has been suggested by Rose & McDaid (1976) that the pressure fluctuations can normally be neglected for most transonic wind tunnels when hot wire anemometry data is obtained and analyzed. This implies that the sound pressure levels of the tunnel are insignificant. Yet at the same time many researchers will make the opposite assumption and calculate velocity fluctuation levels from the measured pressure fluctuation information. Both of these assumptions are extreme. Comparing the test section pressure fluctuation data, figure 4.56, to the velocity fluctuation data, figures 4.9 - 4.12, it is easy to recognize that the two perturbations are of the same order of magnitude, therefore it would be difficult to ignore the contribution of the fluctuating pressure.

4.4.3 Hot wire and Pressure Probe comparison - Comparison of static pressure fluctuation data derived from the hot wire and the fluctuating pressure probe, show good agreement as shown in figure 4.51. The implication is that the individual components of velocity, density, and total temperature must be correct since the calculation of pressure depends not only on the magnitude of the individual components but also their phase. The complexities of the hot wire technique make it difficult to identify absolute errors in calculating the individual components, yet this comparison gives the user confidence that the two results are probably of the right order of magnitude.

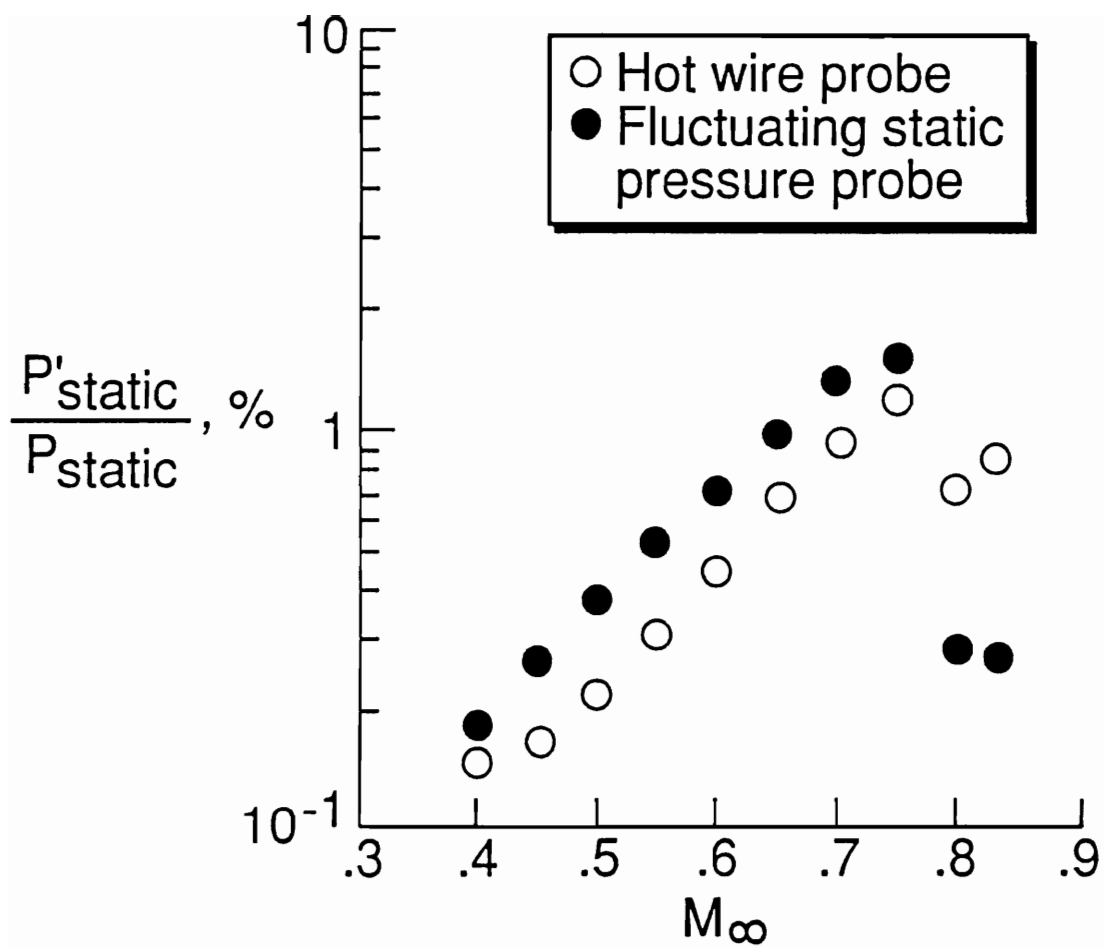


Figure 4.58 Comparison of static pressure fluctuations derived from hot wire probe and fluctuating pressure probe

4.5 LFC Results

Analysis and control of boundary layer stability is especially difficult for high speed flight, particularly for complex geometries. The instabilities that can occur on a high speed model with geometries similar to the LFC model are, leading edge crossflow instabilities, Tollmien-Schlichting instabilities, and Taylor-Gortler instabilities. The scope of this report is to study the freestream flow field and evaluate the potential disturbances that can instigate premature transition through one of these processes. Harris, Harvey, & Brooks (1988) have reported the results of the LFC investigation.

One of the specific objectives of this test program was to investigate the flow quality of the freestream at the design conditions of the LFC model. This would correspond to a Reynolds number of 20×10^6 , a Mach number of 0.82, and a lift coefficient of 0.47. The calibration matrix for the hot-wire probe required the facility to run at many off-design conditions, therefore the fluctuations in the flow were acquired at all times. As previously noted, the tunnel modification was designed for a single condition, therefore, all off-design conditions might be expected to result in higher fluctuation levels. The relationship of the freestream flow quality to the optimum transition conditions were desired, and the discussion of flow quality results will be limited to a Mach number of 0.82 at Reynolds numbers of 10×10^6 and 20×10^6 . The theoretical and experimental pressure distributions over the LFC model which correspond to Reynolds numbers of 10×10^6 and 20×10^6 at a Mach number of 0.82 are shown in figure 4.59. This highlights the regions where the different instabilities may occur.

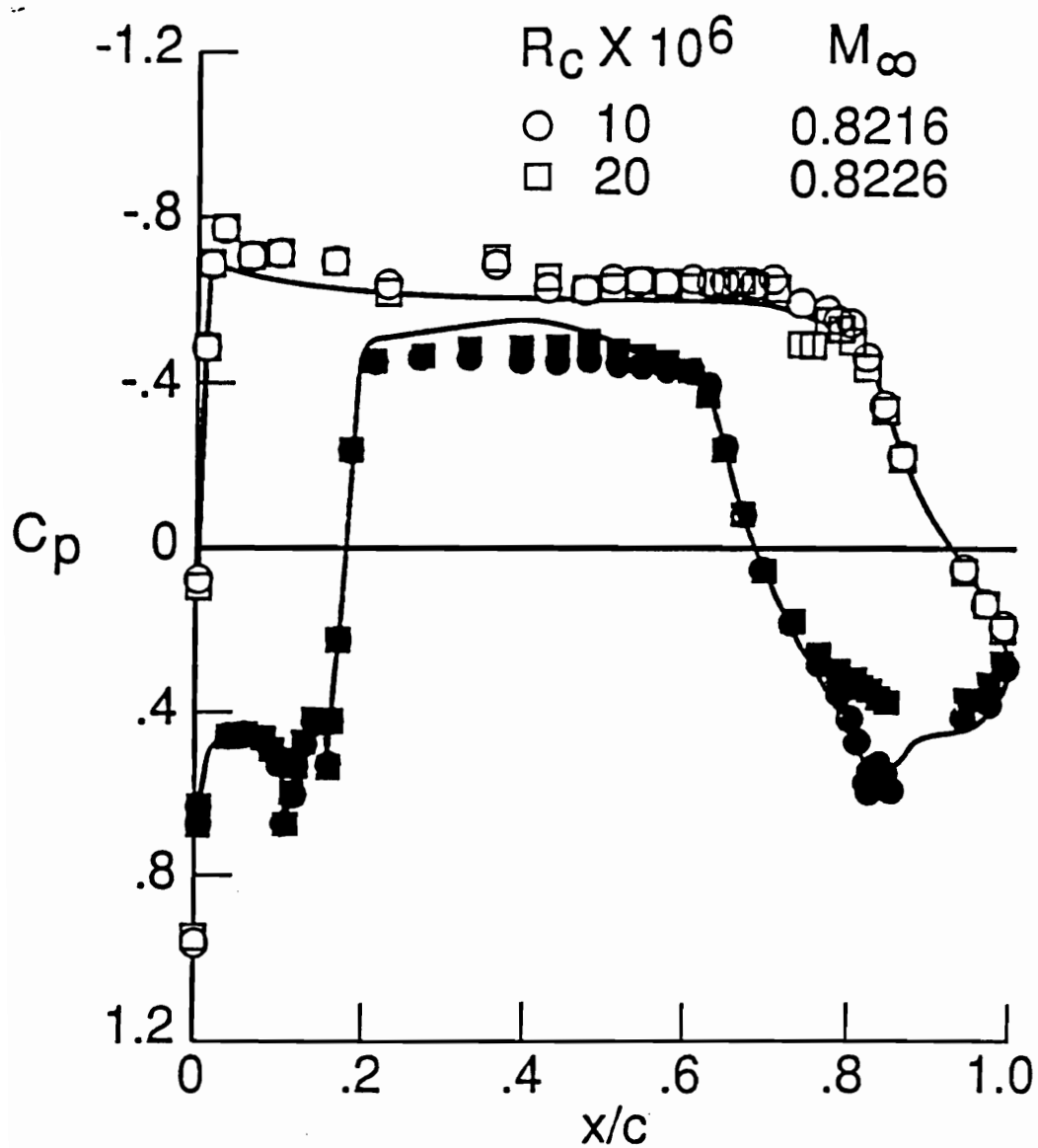


Figure 4.59 Theoretical and experimental pressure distributions on the supercritical LFC model

Harris, Harvey, & Brooks (1988) suggest that the Tollmien-Schlichting (TS) instabilities dominated the transition process for this model, (figure 4.60). Therefore the present study will limit comments to the influence of the outer flow on TS instabilities.

To measure the transition locations on the model, surface mounted thin film gages were located along the span and chord of the model as shown in figure 4.61a. The gages were not calibrated and only qualitative information was available. Dagenhart & Stack (1982) have correlated the voltages from the surface film anemometers to the transition process as can be seen in figure 4.61b. Using this simplified technique, the location of transition can be identified. Two examples of the transition distribution for the LFC model are shown in figure 4.62, for a Mach number of 0.82 and Reynolds numbers of 10×10^6 and 20×10^6 . A more complete set of data can be found in the reference by Harris, Brooks, Stack, and Clukey, (1989).

Once the experimental pressure distribution and transition location were determined, the n-factor and maximum amplified TS frequency could be calculated from linear stability theory. It is recognized that the range of frequencies to be amplified in the boundary layer will vary from condition to condition. Yet for the design condition, this range extends from approximately 6kHz to 26kHz. Based on the measured transition location and measured pressure distribution the most dangerous frequencies are determined from both incompressible and compressible theory to be 11kHz and 7kHz respectively.

The spectra of static pressure fluctuating, figure 4.54 and figure 4.55, measured in the freestream do not indicate any discrete disturbances

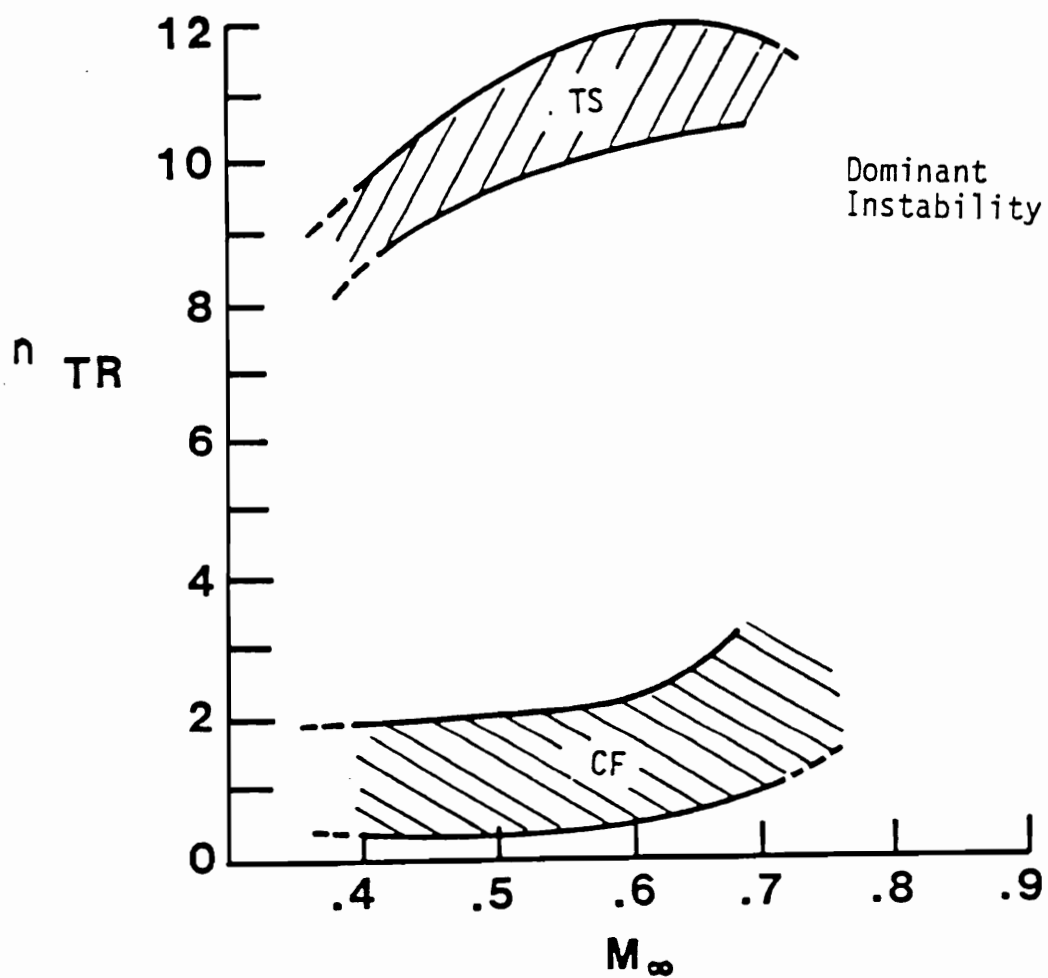


Figure 4.60 Calculated incompressible n -factor at transition for a swept LFC airfoil

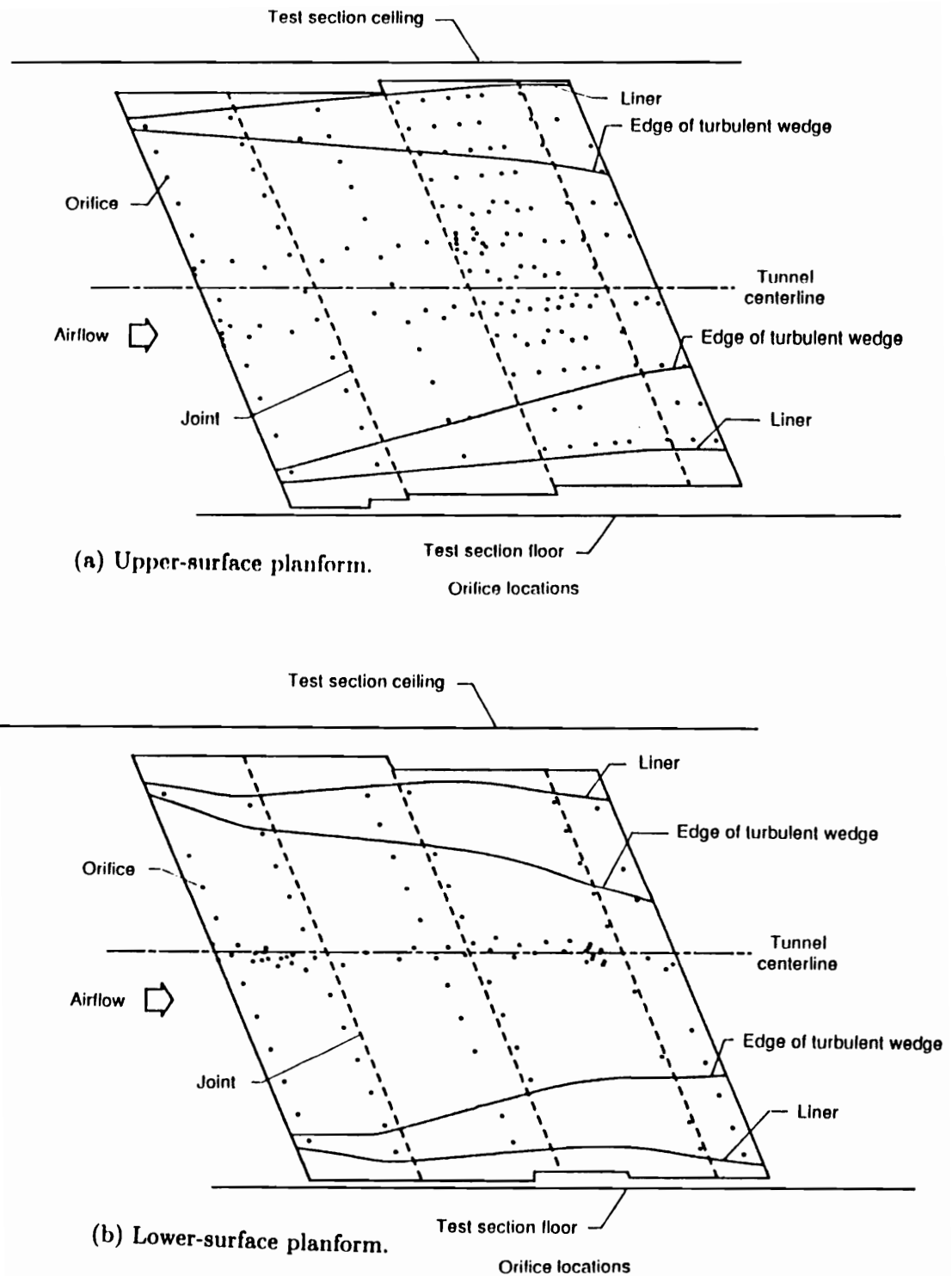


Figure 4.61a Transition detection gage location

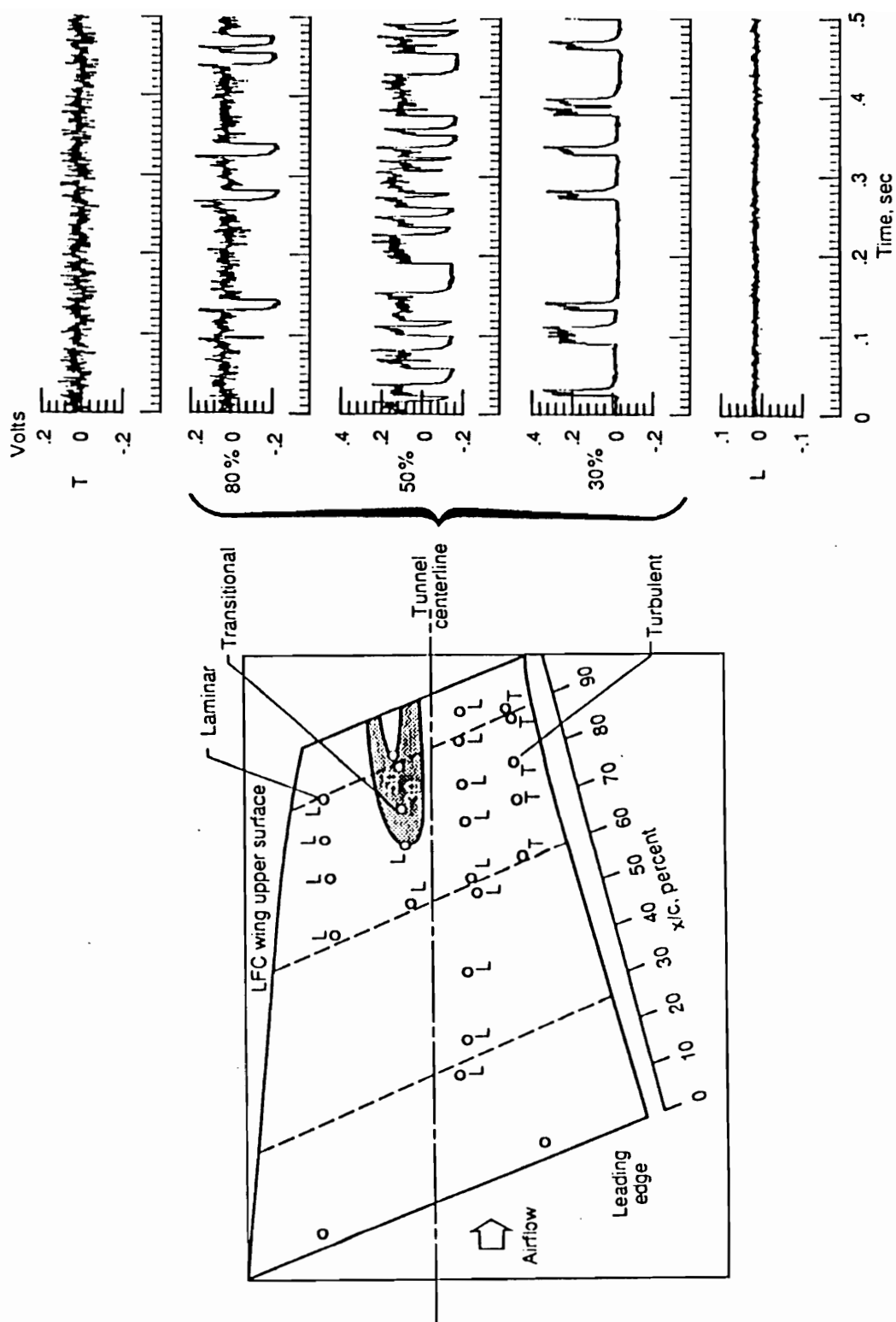


Figure 4.61b Transition detection scheme

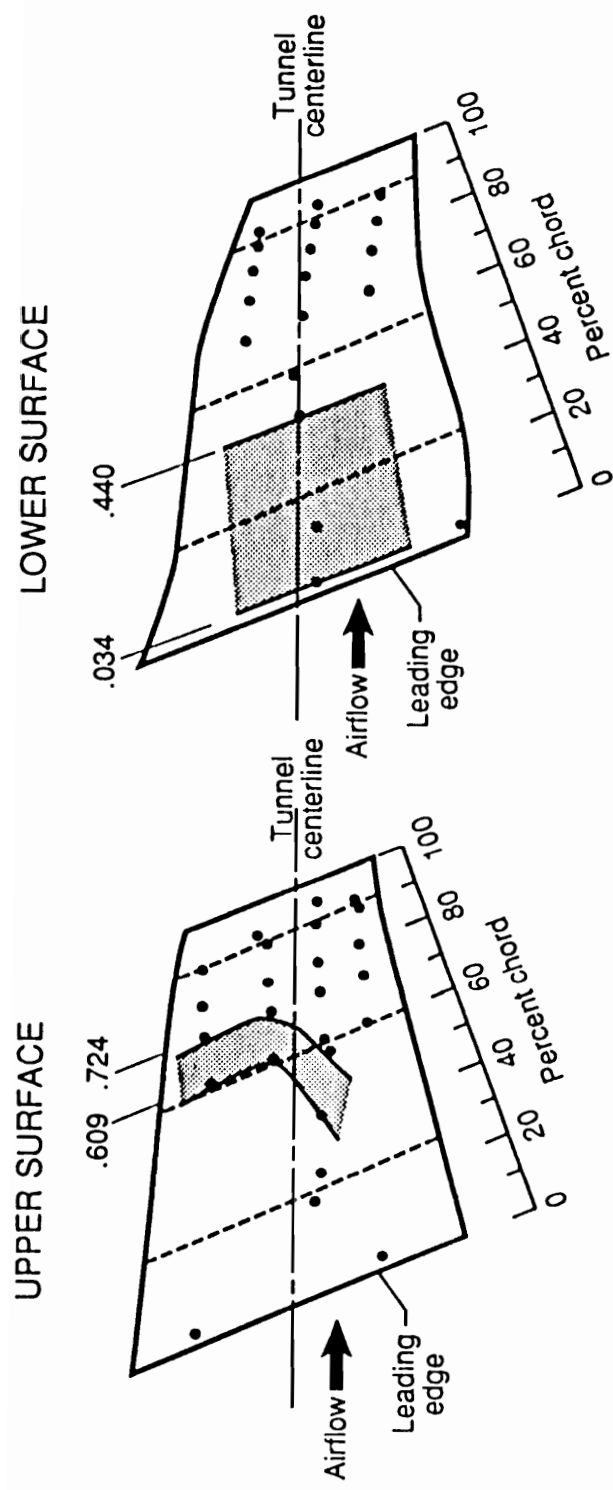


Figure 4.62 Examples of transition distribution for the LFC model

in the frequency range of the predicted TS waves as calculated from linear stability theory. Examining the freestream hot wire spectra, (figure 4.23), in the region of the most dangerous frequencies associated with the maximum amplification of TS waves, several discrete frequencies can be identified. The spectra of the velocity fluctuations was used to determine what perturbation could be identified in the range of frequencies associated with transition. These measured results are compared to the most dangerous frequencies calculated from linear stability theory as shown in figure 4.63. Most of significant spectral signatures from the hot wire velocity data fall on either side of the predicted maximum amplified TS frequency at the design conditions. The amplitude of the broad band fluctuations in the vicinity of the maximum amplified TS frequency are two orders of magnitude less than the other disturbances found in the free stream. This implies that there are no specific spectral signatures that will cause premature transition, especially at the design LFC conditions. Yet this is speculative since the receptivity process is not fully understood. It is possible for disturbances at either lower or higher frequencies identified in the freestream to couple into the boundary layer in such a way as to still cause transition.

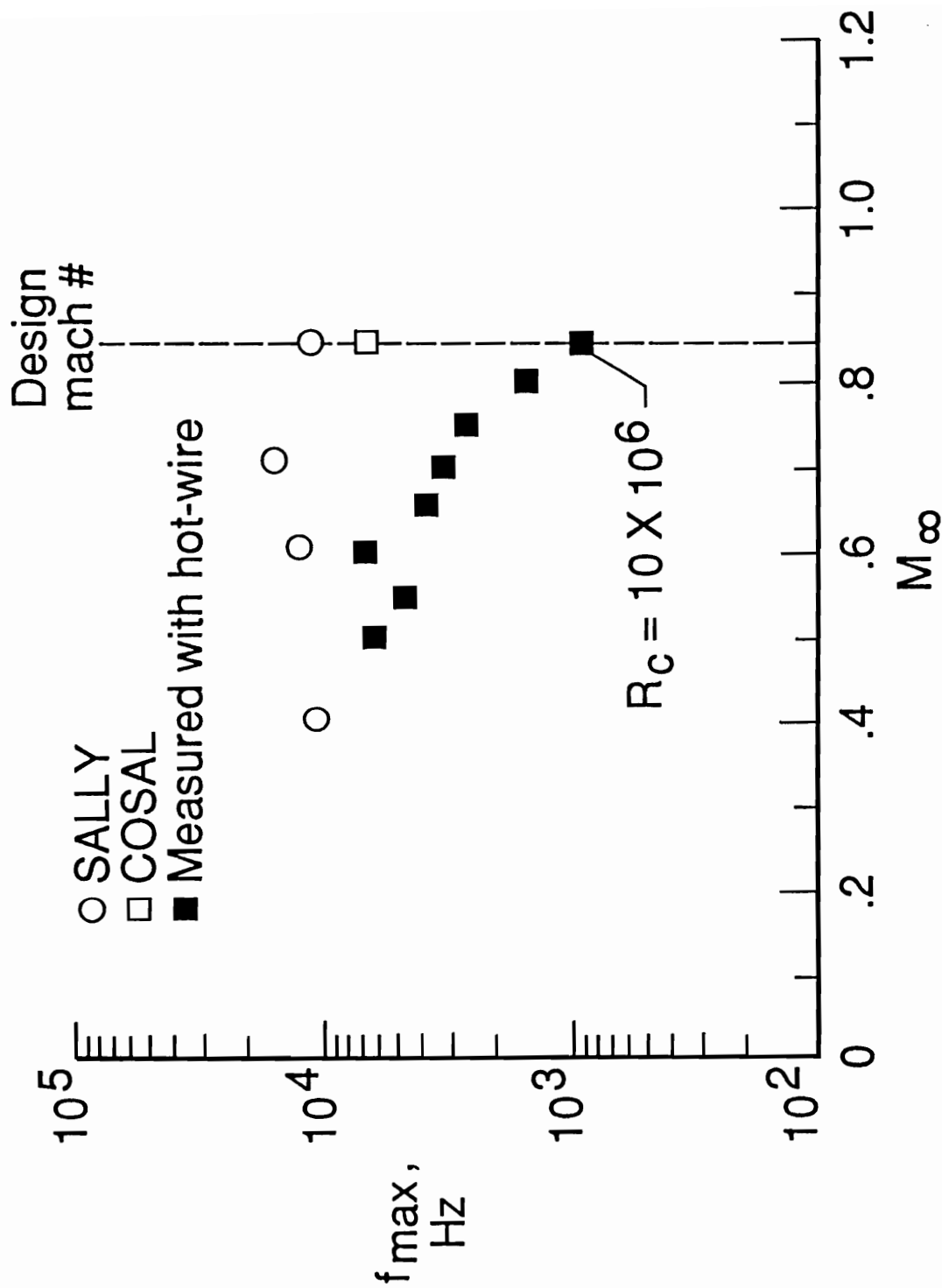


Figure 4.63 Identified spectral velocity signatures that may instigate transition.

5.0 CONCLUSIONS

The experiments described in this dissertation have discussed two primary topics:

- 1.) The measurement of wind tunnel flow quality at transonic speeds, and*
- 2.) The interpretation of the flow quality measurements.*

The conclusions will be divided into these two major topics and will be followed by some general comments which are based on results obtained from the flow quality measurements made in the two configurations of the NASA Langley Research Center 8-foot Transonic Pressure Tunnel:

5.1 Flow quality measurement techniques for transonic flows

The primary instruments for measuring the small disturbances associated with free stream flow quality are the hot wire anemometer and the fluctuating pressure probe. The complexities of hot wire anemometry are centered around the non-linear characteristics of heat transfer of a heated fine wire. Difficulty in calibrating these sensors in compressible flows are compounded by the operation in the slip flow regime. Our findings indicate that in general, the velocity sensitivity and density sensitivity are not the same for the transonic regime. This means that the two sensitivities cannot be coupled to form a mass flow sensitivity. The implication is that the measurement technique must account for the three quantities that are varying in the free stream, i.e. vorticity, entropy, and sound. However, the hot wire anemometer can only measure velocity,

density, and total temperature variables. The lack of information on the direction of sound has limited the ability of the researcher to convert these measured quantities to the desired variables, particularly for the transonic flow regime.

The accuracy of the measured results depends on the calibration of the individual sensor. The two calibration techniques that were evaluated should have resulted in the same sensitivities. Differences between the two methods were identified and are generally attributed to a limited calibration matrix. The calibration data were obtained by varying velocity, density, and total temperature which conformed to the requirements established by the direct calibration technique. However, when this information was non-dimensionalized it was necessary to interpolate and extrapolate the data to meet the requirements of the indirect calibration method. The complexities of the indirect approach were also compounded by several other factors that include:

- the non-linear character of the heat transfer with respect to velocity, density and total temperature. This includes the fact that the conduction and radiation effects of the heated sensor were neglected
- inaccuracies in the measurement of the physical properties of the sensor, which include but are not limited to the sensor length, sensor resistance, lead resistance, and bridge voltage

The direct approach should not be susceptible to these factors, since they will automatically be accounted for in the calibration process. However, the accuracy of the calibration of the direct approach depends on the following factors:

- the general form of the calibration equation has not been optimized
- the limited data set influenced the results of the multiple linear regression used in determining the sensitivities.

Based on the simplicity of the direct calibration method and the factors stated above, it is believed that the direct calibration approach is easier to implement and is less susceptible to error, particularly for the transonic flow regime.

In general, it was found that the velocity and density sensitivity were not equal for the transonic regime. However, it was demonstrated that the velocity and density sensitivities seem to converge for low subsonic Mach numbers and/or high wire Reynolds numbers. When these sensitivities are equal, they can be combined to form a mass flow sensitivity, which significantly simplifies the hot wire analysis process.

Evaluating the mass flow fluctuations as derived from several single and multiple-sensor hot-wire techniques resulted in a good comparison for the low speed conditions. An independent evaluation of the derived hot wire static pressure fluctuations and static fluctuating pressure probe information also resulted in a good comparison. This is an indication that the individual velocity, density, and temperature components are accurately measured. These two comparisons provide confidence that the three-element hot-wire technique is producing reasonable results in both magnitude and phase and confirms the fact that the direct calibration method is an appropriate technique for transonic speeds.

5.2 Flow quality Results for the two wind tunnel configurations

In general the flow quality results for the 8'TPT are considered to be high, however, after careful analysis it is concluded that the levels are consistent with the physics of a transonic wind tunnel. Comparison of fluctuating static pressures are also consistent with other large transonic wind tunnels. This would suggest that if similar multiple sensor measurements were made in these facilities, they would also have high disturbances in the freestream flow field. In fact the 8'TPT has lower fluctuating pressure levels than most of the facilities it has been compared with which indicates that it has good freestream flow quality relative to the other major facilities.

Other hot-wire anemometry techniques typically employed in the measurement of freestream flow quality have been interpreted in an optimistic manner which generally results in low disturbance levels . These hot wire techniques have been shown to be in error up to a factor of 10 for the transonic regime. The levels of the sound being generated in the facility have not been properly accounted for by these hot wire methods because of the simplifying assumptions required of the measurement technique itself. Unfortunately, these erroneous hot wire results have biased the aerodynamic community into believing these low disturbance levels are typical of transonic wind tunnels.

The present results also indicate that the sound generated in the diffuser and fan region of the facility can dominate the perturbation measured in the test section. Therefore one should anticipate that for a typical continuous flow, fan driven, transonic wind tunnel, the flow quality will be degraded with Mach number until a uniform supersonic region is

formed downstream of the test section which will prevent the upstream moving sound from the diffuser to enter the test section.

The impact of the freestream flow quality on the LFC experiment did not seem to adversely affect the boundary layer transition process. There were some discrete disturbances in the freestream that ranged from 5 kHz to 26 kHz that could have been amplified in the boundary layer. Yet no evidence of any influence of the freestream was found in the surface measurements used to detect transition.

5.3 General Comments on flow quality measurement at transonic speeds

The limitations of the current data set can be associated with the operation of a large transonic wind tunnel. The lack of a suitable calibration facility has limited the pursuit of developing this technique. The results of this dissertation indicate that the three-element hot-wire technique is the only viable technique for measuring the complex characteristics that are common to transonic wind tunnels. There is still a need to continue research of the heat transfer characteristics of a heated wire in the transonic flow regime.

REFERENCES

- Allison, D. O., and Dagenhart, J. R., "Two Experimental Supercritical Laminar-Flow-Control Swept-Wing Airfoils," NASA TM 89073, Feb. 1987
- Anders, J. B. Jr., "Turbulence Measurements in Hypersonic, Helium Flow," Masters Thesis, Report 1157, Princeton University, Feb. 1974
- Batchelor, G. K., *The theory of Homogeneous Turbulence*, Cambridge University Press, 1953
- Berry, S. A.: Incompressible Boundary-Layer Stability Analysis of LFC Experimental Data for Sub-Critical Mach Numbers. NASA Contractor Report 3999, Jul. 1986.
- Berry, S. A.; Dagenhart, J. R.; Viken, J. K.; and Yeaton, R. B.: Boundary-Layer Stability Analysis of NLF and LFC Experimental Data at Subsonic and Transonic Speeds. SAE 871859, Long Beach, CA, Oct. 1987.
- Betchov, R.; and Criminale, W. O, Jr.: *Stability of Parallel Flows*. Academic Press, Inc., 1967.
- Bobbitt, P. J.: The Pros and Cons of Code Validation. AIAA 88-2535, Williamsburg, VA, June 1988.
- Bobbitt, P. J.; Waggoner, E. G.; Harvey, W. D.; Dagenhart, J. R.: A Faster "Transition" to Laminar Flow. SAE 851855, Aerospace Technology Conference and Exposition, Anaheim, CA, Oct. 1988.
- Cebeci T., Bradshaw, P., *Physical and Computational Aspects of Convective Heat Transfer*, Springer-Verlag Press 1984
- Clukey, S. J.; Jones, G. S.; Stainback, P. C.: A High Speed Data Acquisition System for the Analysis of Velocity, Density, and Total Temperature Fluctuations at Transonic Speeds. SAE Aerotec 88, Anaheim, CA, Oct. 1988
- Dagenhart, J. R.: Amplified Crossflow Disturbances in the Laminar Boundary Layer on Swept Wings with Suction. NASA TP-1902, Nov. 1981.
- Edwards, A.L.: Multiple Regression and the Analysis of Variance and Covariance. W.H. Freeman and Co., San Francisco, 1979.
- Kovasznay, L. S. G.: Turbulence in Supersonic Flow. Journal of the Aeronautical Sciences, Vol. 20, No. 20, Oct. 1953.

Haftka, R. T., "Stiffness-Matrix Condition Number and Shape Sensitivity Errors," AIAA Journal, vol. 28, no. 7, July 1990

Harris, C. D.; and Brooks, C. W., Jr.: The NASA Langley Laminar-Flow-Control Experiment on a Swept, Supercritical Airfoil. NASA TP 2809, May 1988.

Harris, C. D.; and Brooks, C. W., Jr.: Modifications to the Langley 8-Foot Transonic Pressure Tunnel for the Laminar Flow Control Experiment. NASA TM 4032, May 1988.

Harris, C. D.; Brooks, C. W., Jr.; Stack, J. P.; and Clukey, P. G.: The NASA Langley Laminar Flow Control Experiment on a Swept, Supercritical, Airfoil - Basic Results for Slotted Configuration. NASA TM 4100, June 1989

Harvey, W.D., Stainback, P.C., Owen, F.K.: Evaluation of Flow Quality in Two Large NASA Wind Tunnels at Transonic Speeds. NASA TP-1737, December 1980.

Harvey, W. D.; Pride, J. D.: The NASA Langley Laminar Flow Control Experiment. AIAA Paper No. 82-0567, Mar. 1982.

Harvey, W. D.: Boundary-Layer Control for Drag Reduction. 1st International Pacific Air and Space Technology Conference, Melbourne, Australia, Nov. 1987.

Harvey, W. D.; El-Hady, N. M.: Experimental Transition and Boundary-Layer Analysis of a Swept Laminar Flow Control Airfoil. Fourth Symposium on Numerical and Physical Aspects of Aerodynamic Flows, Long Beach, CA, Jan. 1989.

Hefner, J. N.; Bushnell, D. M.: Applications of Stability Theory to Laminar Flow Control. AIAA Paper 79-1493, July 1979.

Hinze, J. O., *Turbulence*, 2nd edition, 1975

Horstman, C. C., Rose, W. C.: Hot Wire Anemometry in Transonic Flow. AIAA Journal, vol. 15, no. 3, page 395-401, March 1977

Johnson, C. B.; Carraway, D. L; Stainback, P. C.: A Transition Detection Study using a Cryogenic Hot-Film System in the Langley 0.3-Meter Transonic Cryogenic Tunnel. AIAA 87-0049, Reno, NV, Jan. 1987.

Johnson, D. A. and Rose, W. C.: Turbulence Measurements in a Transonic Boundary Layer and Free-Shear Layer Flow Using Laser Velocimeter and Hot Wire Anemometer Techniques. AIAA Paper 76-399, San Deigo, Calif., June 1976.

Jones, G. S.; Stainback, P. C.: A New Look at Wind Tunnel Flow Quality for Transonic Flows. SAE 881452 Aeospace Technology Conference and Exposition, Anaheim, CA, Oct. 1988.

King L.V., "On the Convection of Heat from Small Cylinders in a Stream of Fluid: Determination of the Convection Constrants of Small Platinum Wires with Applications to Hot-Wire Anemometry, Phil. Trans. Royal Society of London, ser. A, Vol 214, no. 14, pp 373-432 (Nov 1914)

Kovasznay, L. S. G.: NACA TM 1130 (1947)

Kovasznay, L. S. G., and Tormarck, S. I. A., "Heat Loss of Hot Wires in Supersonic Flow. Bumblebee Rep. No. 127, Dept. Aero., The Johns Hopkins Univ., April 1950

Kovasznay, L. S. G.: Turbulence in Supersonic Flow. Journal of the Aeronautical Sciences, vol. 20, no. 20, October 1953

Laufer, J. and McClellan, R., "Measurements of Heat Transfer from Fine Wires in Supersonic Flows," Journal of Fluid Mechanics, Vol. 1, Pt. 2, Jan. 1956, pp 276-289

Lawrence, J.C. and Landus, L.G. NACA TN 2843 (1952)

Lomas, C. G., *Fundamentals of Hot Wire Anemometry*, Cambridge University Press, 1986

Marcolini, M. A., Lorber, P. F., Miller, W. T., Jr., Covino, A. F., Jr., "Frequency Response Calibration of Recess-Mounted Pressure Transducers," NASA TM 104031 Feb 1991

McAdams W. H., *Heat Transmission*, Third edition, McGraw Hill (1954)

Morse, P. M., *Vibration and Sound*, McGraw Hill Book Company 1948

Morkovin, M. V.: Fluctuations and Hot-Wire Anemometry in Compressible Flows. AGARD-ograph 24, 1956.

Morkovin, M. V., and Phinney, R. E., "Extended Applications of Hot-Wire Anemometry to High-Speed Turbulent Boundary Layers. AFOSR TN-58-469

Otten, L. J., Pavel, A. L., Finley, W. E., Rose, W. C.: A Survey of Recent Atmospheric Turbulence Measurements from a Subsonic Aircraft. AIAA 19th Aerospace Sciences Meeting, St Louis, Mo. January 1981.

Owen, F. K., Stainback, P. C., and Harvey, W. D., "An Evaluation of Factors Affecting the Flow Quality in Wind Tunnels," AGARD Wind Tunnels and Testing Techniques no 348

Reshotko, E., Panel discussion, AGARD Conference Proceeding, No. 429, Aerodynamic Data Accuracy and Quality: Requirements and Capabilities in Wind Tunnel Testing," Oct. 1987.

Pfenniger, W.; Reed, H.L.; and Dagenhart, J.R., "Design Considerations of Advanced Supercritical Low-Drag Suction Airfoils," Symposium on Viscous Drag Reduction, Dallas Texas, Nov 1979

Prandtl, L., Attaining a Steady Air Stream in Wind Tunnels, NACA TM 726, 1933

Rose, W. C. and McDaid, E. P.: Turbulence Measurement in Transonic Flow. AIAA 9th Aerodynamic Testing Conference, Arlington, Texas, June 1976.

Sandborn, V. A.: *Resistance Temperature Transducers*. Metrology Press, Fort Collins, CO, 1972

Spangenberg W. G., "Heat Loss Characteristics of Hot-Wire Anemometers at Various Densities in Transonic and Supersonic Flow NACA TN 3381 (1955)

Stainback, P. C., Johnson, C. B., and Basnett, C. B.: Preliminary Measurements of Velocity, Density, and Total Temperature Fluctuations in Compressible Subsonic Flow. AIAA 21st Aerospace Sciences Meeting, Jan. 1983.

Stainback, P. C.; A Review of Hot-Wire Anemometry in Transonic Flows. ICIASF '85', pp. 67-78, Stanford, CA, Aug. 1985.

Stainback, P. C.: Some Influences of Approximate Values for Velocity, Density, and Total Temperature Sensitivities on Hot-Wire Anemometer Results. AIAA 24th Aerospace Sciences Meeting, Jan. 1986.

Stainback, P. C., Nagabushana, K. A., Jones, G. S., and Clukey, S. J., "Heat Transfer from Heated Cylinders in Subsonic Flows," ASME - JSME Fluids Engineering Conference, June 1991

Tan-atichat, J., Nagib, H. M., and Loehrke, R. I., "Interaction of Freestream Turbulence with Screens and Grids: A Balance between Turbulence Scales," Bull. American Physical Society, 17, 1097, 1972

Uberoi, M. S., "Effect of Wind-Tunnel Contraciton on Free-Stream Turbulence," Journal of Aeronautical Sciences, Aug. 1956

Vrebalovich, T., "Heat Loss From Hot Wires in Transonic Flow," Research Summary No 36-14, Jet Propulsion Lab., Pasadena, Calif., 1962

Appendix A

Useful Formulas Related to the Derivation of the Hot wire Theory

The fundamental information needed to derive the theory for hot wire anemometry in compressible flow can be related to the heat transfer of a heated cylinder operating in a viscous, compressible gas. To experimentally determine the functional relationship of heat transfer to relevant physical parameters it is necessary to define several general relationships. Since heat conductivity and viscosity vary with temperature, it is necessary to specify a reference temperature to be used in the definition of the Reynolds number and Nusselt number. Total temperature will be used as a reference temperature for this study, unless otherwise noted.

Overheat Ratio

The concept of a sensor operating temperature is probably the most fundamental concept in hot wire anemometry. It is important because it influences the sensitivities and the life of the sensor. The sensor temperature is usually expressed as a ratio, called the *overheat ratio* and can be expressed in terms of sensor temperature and total temperature:

$$\theta \equiv \text{Overheat Ratio} = \frac{T_w}{T_o} \quad (\text{A.1})$$

When an unheated sensor is placed in a compressible flow, aerodynamic heating will cause the sensor temperature to change from its ambient

temperature to an equilibrium temperature. Equilibrium temperature in terms of the recovery temperature is expressed:

$$\text{Recovery Temperature} \equiv T_{\text{Recovery}} = \eta T_o \quad (\text{A.2})$$

It should be noted that the recovery temperature ratio (η) is in general a function of Knudsen number (or Reynolds number) and Mach number.

Data obtained from Vrebalovich (1962), figure A.1 can be used to determine the value of η . For most general subsonic applications ($M < 1$) the influence of Knudsen number can be neglected resulting in an equation that is a function of Mach number alone.

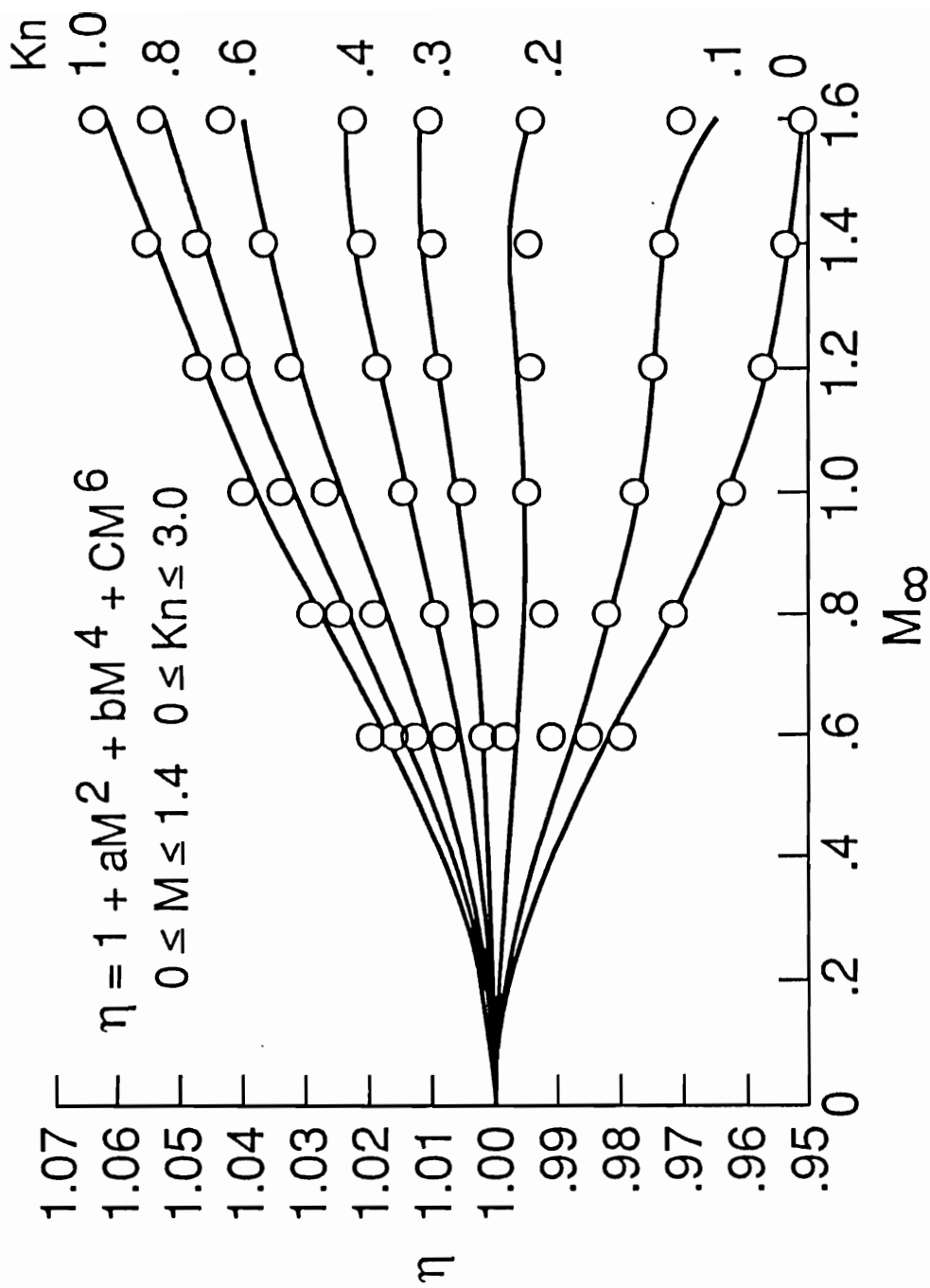
$$\eta \equiv \frac{T_{\text{Recovery}}}{T_o} = \left[1 + B_1 (M)^2 + B_2 (M)^4 + B_3 (M)^6 \right] \quad (\text{A.3})$$

where

$$B_1 = -0.061812670$$

$$B_2 = 0.028677610$$

$$B_3 = -0.004740918$$



Recovery temperature ratio (reference Vrebalovich 1962)

Thermal Loading

It is often useful to represent the recovery temperature and overheat ratio in a non-dimensional form which is called thermal loading:

$$\tau \equiv \text{THERMAL LOADING} = \frac{T_w - T_{\text{Recovery}}}{T_o} \quad (\text{A.4})$$

or

$$\tau = \frac{T_w - \eta T_o}{T_o} \quad (\text{A.5})$$

or

$$\tau = \theta - \eta \quad (\text{A.6})$$

Other useful thermal relationships are

$$\frac{\eta}{\tau} = \frac{\eta T_o}{T_w - \eta T_o} \quad (\text{A.7})$$

$$\frac{\theta}{\tau} = \frac{T_w}{T_w - \eta T_o} \quad (\text{A.8})$$

Resistance - Temperature Relationships

One of the most important relationships in hot wire anemometry is the relationship of temperature to resistance and can be written in terms of

electrical parameters and the ambient temperature. An empirical expression for this relationship is:

$$R_w = R_{ref} \left[1 + \alpha_{ref}(T_w - T_{ref}) + \beta_{ref}(T_w - T_{ref})^2 \right] \quad (A.9)$$

Ignoring the second order effects and this equation becomes:

$$T_w = \left(\frac{1}{\alpha} \right) \left[\left(\frac{R_w}{R_{ref}} \right) - 1 \right] + T_{ref} \quad (A.10)$$

where:

$$R_{ref} = \frac{R_{w(COLD)}}{\left[1 + \alpha_{ref}(T_{Q(WIND \ OFF)} - T_{ref}) \right]} \quad (A.11)$$

For Platinum plated tungsten sensors: $\alpha_{ref} = 0.0036/^{\circ}\text{C}$ at $T_{ref} = 20^{\circ}\text{C}$

For Fiber Film sensors: $\alpha_{ref} = 0.0040/^{\circ}\text{C}$ at $T_{ref} = 20^{\circ}\text{C}$

Other Useful Relationships

Reynolds number $Re = \frac{\rho U d}{\mu_o}$ can be written:

$$d \log Re = d \log \rho + d \log U - \chi_{\mu} d \log T_o$$

where

$$\chi_{\mu} = \frac{\partial \log \mu_o}{\partial \log T_o}$$

Mach number can be written:

$$M^2 = \frac{\left(\frac{U^2}{a^2}\right)}{\left(1 - \left(\frac{\gamma - 1}{2}\right)\left(\frac{U^2}{a^2}\right)\right)}$$

$$d \log M = \frac{1}{\alpha} \left[d \log U - \frac{1}{2} d \log T_o \right]$$

where

$$\alpha = \frac{1}{1 + \left(\frac{\gamma - 1}{2}\right) M^2}$$

APPENDIX B

Derivation of the Basic Linearized Hot Wire Equations

To describe the heat transfer concepts within the scope of this research it is necessary to make several simplifying assumptions. In the first part of this appendix we examine basic principles of the Constant Temperature Bridge circuit which is followed by an analysis of the infinite, one dimensional, steady state, non-radiative energy balance of a heated fine wire, placed normal to the flow.

Constant Temperature Bridge

To make accurate heat transfer measurements it is desirable to keep the sensing element at a constant temperature, which is accomplished by the use of a "Constant Temperature Anemometer". When discussing the theory of a heated wire, it is also important to understand how the anemometer controls the sensor temperature. This can be accomplished in constant temperature anemometry by holding the resistance of the heated element constant through the use of a Wheatstone Bridge, figure 2.1. Balancing the bridge is achieved by varying the current to the sensing element through the negative feedback amplifier. Details of the operation of a Wheatstone Bridge network in a constant temperature anemometer has been described by several researchers, Morkovin & Phinney (1958), Hinze (1959), Sandborn (1972), and Lomus (1986) to name a few.

The speed which the negative feedback amplifier can hold the bridge in balance will determine the "time constant" of the electronic system. Since this feedback occurs almost instantaneously it is necessary to define the resulting small change in the resistance of the wire as the *transresistance* of the electronic circuit. Transresistance is defined as the change in bridge unbalance due to a change in heating current.

$$R_{\text{TR}} \equiv \frac{\Delta E'}{\Delta I} \quad (\text{B.1})$$

It is also important to define the *transconductance* , as the rate of change of the compensating current with the input voltage to the feedback amplifier.

$$G_m \equiv - \frac{\partial(i)}{\partial(IR_{\text{TR}})} = - \frac{\partial(i)}{\partial(e)} \quad (\text{B.2})$$

This allows us to write

$$\Delta I = -G_m(e) \quad (\text{B.3})$$

Transconductance has the dimension of electrical conduction or one over resistance. While it is not necessary to measure transresistance or transconductance directly, the two parameters are related to the time constant of the electronic system. These parameters are optimized through the compensating network of the anemometer system. These factors play a role in the frequency response of the heated wire.

Energy Balance of a Heated Wire

The major application of the hot wire anemometer is the measurement of fluctuating flows. In order to derive a general equation relating the fluctuating wire voltage to the fluctuating gas properties for compressible flows it is necessary to express in symbols the equation of the conservation of energy.

$$\left[\begin{array}{c} \text{Time Rate of Change of} \\ \text{Heat Stored in a Hot Wire} \end{array} \right] = \left[\begin{array}{c} \text{Thermal Energy} \\ \text{Generation Rate} \end{array} \right] - \left[\begin{array}{c} \text{Rate of Heat} \\ \text{Lost to Gas} \end{array} \right]$$

Using Morkovin's convention this can be written

$$\frac{dE}{dt} = W - H \quad (B.4)$$

where

$$E \equiv C(T_w) = \text{Heat Stored}$$

$$W \equiv I^2 R_w = \text{Rate of Heat Generation}$$

$$H \equiv q = \text{Rate of Heat Loss}$$

Each of the variables in equation B.4 have both a mean and a fluctuating component.

$$E = \bar{E} + \Delta E$$

$$W = \bar{W} + \Delta W$$

$$H = \bar{H} + \Delta H$$

Substituting this into equation B.4 and dropping the steady state terms, we have:

$$C \frac{d\Delta T_w}{dt} = \Delta W - \Delta H \quad (B.5)$$

The heat generation rate depends on the current and resistance, or the current and temperature of the wire

$$W = W(I, R) = W(I, T_w) \quad (B.6)$$

and thus

$$\Delta W = \frac{\partial W}{\partial I} \Delta I + \frac{\partial W}{\partial T_w} \Delta T_w \quad (B.7)$$

The convective heat loss is a function of velocity, density, total temperature, and wire temperature:

$$H = f(U, \rho, T_o, T_w) \quad (B.8)$$

and

$$\Delta H = \frac{\partial H}{\partial U} \Delta U + \frac{\partial H}{\partial \rho} \Delta \rho + \frac{\partial H}{\partial T_o} \Delta T_o + \frac{\partial H}{\partial T_w} \Delta T_w \quad (B.9)$$

Substituting Equation B.6 and B.9 into equation B.5 results in:

$$C \frac{d\Delta T_w}{dt} = -\frac{\partial H}{\partial U} \Delta U - \frac{\partial H}{\partial \rho} \Delta \rho - \frac{\partial H}{\partial T_o} \Delta T_o + \left(\frac{\partial W}{\partial T_w} - \frac{\partial H}{\partial T_w} \right) \Delta T_w + \frac{\partial W}{\partial I} \Delta I \quad (B.10)$$

Using the first order terms of the Resistance - Temperature relationship (A.9) on the left hand side of (B.10) results in:

$$C \frac{d\Delta T_w}{dt} = \frac{C}{\alpha_{ref} R_{ref}} \left(\frac{d\Delta R_w}{dt} \right) \quad (B.11)$$

recall that Ohm's law gives

$$\Delta R_w = \frac{\Delta e}{\bar{I}} - \frac{\bar{R}_w \Delta I}{\bar{I}} \quad (B.12)$$

which in differential form becomes

$$\frac{d\Delta R_w}{dt} = \frac{1}{\bar{I}} \left(\frac{d\Delta e}{dt} \right) - \frac{\bar{R}_w}{\bar{I}} \left(\frac{d\Delta I}{dt} \right) \quad (B.13)$$

Substituting B.3, B11, and B.13 into B.10 results in

$$\Delta e + [1 + G_m(R_w)] \left(\frac{c}{\sigma} \right) \frac{\partial \Delta e}{\partial t} = -\frac{R_{ref} \bar{I}}{\sigma} \frac{\partial H}{\partial U} \Delta u - \frac{R_{ref} \bar{I}}{\sigma} \frac{\partial H}{\partial \rho} \Delta \rho - \frac{R_{ref} \bar{I}}{\sigma} \frac{\partial H}{\partial T_o} \Delta T_o \quad (B.14)$$

where

$$\sigma = \left(\frac{\partial H}{\partial T_w} - \frac{\partial H}{\partial T_w} \right) + G_m \left[\overline{R_{ref}} \overline{I} \left(\frac{\partial W}{\partial I} \right) + \overline{R_w} \left(\frac{\partial H}{\partial T_w} - \frac{\partial H}{\partial T_w} \right) \right] \quad (B.15)$$

If we collect the non fluctuating terms we can define

$$\Delta e_u = \frac{\overline{U} \overline{R_{ref}} \overline{I}}{\sigma} \frac{\partial H}{\partial U} \quad (B.16)$$

$$\Delta e_\rho = \frac{\overline{\rho} \overline{R_{ref}} \overline{I}}{\sigma} \frac{\partial H}{\partial \rho} \quad (B.17)$$

$$\Delta e_{T_o} = - \frac{\overline{T_o} \overline{R_{ref}} \overline{I}}{\sigma} \frac{\partial H}{\partial T_o} \quad (B.18)$$

Rewriting equation B.14

$$\Delta e + [1 + G_m(R_w)] \left(\frac{c}{\sigma} \right) \frac{\partial \Delta e}{\partial t} = - \Delta e_u \frac{\Delta u}{U} - \Delta e_\rho \frac{\Delta \rho}{\rho} + \Delta e_{T_o} \frac{\Delta T_o}{T_o} \quad (B.19)$$

If the time constant is made small by appropriate electronic compensation then B.19 becomes

$$\frac{\Delta e}{E} = - \Delta e_u \frac{\Delta u}{U} - \Delta e_\rho \frac{\Delta \rho}{\rho} + \Delta e_{T_o} \frac{\Delta T_o}{T_o} \quad (B.20)$$

This can be written in a general form:

$$\frac{e'}{\bar{E}} = S_u \left(\frac{u'}{\bar{U}_\infty} \right) + S_\rho \left(\frac{\rho'}{\bar{\rho}_\infty} \right) + S_{T_o} \left(\frac{T_o'}{\bar{T}_o} \right) \quad (\text{B.21})$$

Note that the sign of S_{T_o} is negative of S_u and S_ρ .

Appendix C

Derivation of Hot Wire Sensitivities in terms of Mach number, Reynolds Number, and Thermal Loading

When an unheated wire is placed into a compressible flow there is aerodynamic heating which causes the sensor temperature to rise above the ambient temperature. When the wire temperature reaches an equilibrium temperature it is said to have reached its recovery temperature (T_e). If the wire is then heated electrically, its temperature rises to its heated temperature (T_w).

The equation for the conservation of heat for a heated wire is

$$\frac{dE}{dt} = W - H \quad (C.1)$$

where W is the thermal energy generated (or dissipated) per unit time, and H is the rate of heat lost to the fluid, and E can be related to the heat stored in the wire ($E = CT_w$). Imposing the requirement of an instantaneous wire response gives $\frac{dE}{dt} = 0$. Therefore we can equate W and H . Here W can be expressed in terms of electrical power parameters (Ψ_w) and H in terms of fluid and heat transfer.

$$W \equiv (\Psi_w) = \frac{E^2}{R_w} \quad (C.2)$$

$$H \equiv \pi L k_f (T_w - T_o) Nu \quad (C.3)$$

so

$$\Psi_w = \pi L k_f (T_w - T_o) Nu \quad (C.4)$$

Expanding Equation C.4

$$\Psi_w = [\pi L k_t (T_w) Nu] - [\pi L k_t (\eta T_o) Nu] \quad (C.5)$$

and taking the derivative of both sides results in

$$d\Psi_w = \left\{ \begin{array}{l} \left[\begin{array}{l} (\pi L k_t T_w) dNu \\ + (\pi L Nu T_w) dk_t \\ + (\pi L Nu k_t) dT_w \end{array} \right] \\ - \left[\begin{array}{l} (\pi L k_t \eta T_o) dNu \\ + (\pi L Nu \eta T_o) dk_t \\ + (\pi L k_t Nu \eta) dT_o \\ + (\pi L k_t Nu T_o) d\eta \end{array} \right] \end{array} \right\} \quad (C.6)$$

Collecting terms and dividing through by Equation C.4

$$\frac{d\Psi_w}{\Psi_w} = \left\{ \begin{array}{l} \left[\begin{array}{l} \frac{[\pi L k_t (T_w - \eta T_o)]}{[\pi L k_t (T_w - \eta T_o)]} \frac{dNu}{Nu} \\ + \frac{[\pi L Nu (T_w - \eta T_o)]}{[\pi L Nu (T_w - \eta T_o)]} \frac{dk_t}{k_t} \end{array} \right] \\ + \left[\begin{array}{l} (\pi L k_t Nu) \\ (\pi L k_t Nu) (T_w - \eta T_o) \end{array} \right] dT_w \\ - \left[\begin{array}{l} (\pi L k_t Nu) \eta \\ (\pi L k_t Nu) (T_w - \eta T_o) \end{array} \right] dT_o \\ - \left[\begin{array}{l} (\pi L k_t Nu) T_o \\ (\pi L k_t Nu) (T_w - \eta T_o) \end{array} \right] d\eta \end{array} \right\} \quad (C.7)$$

Simplifying in terms of logarithmic variables this becomes:

$$d\log \Psi_w = \left[\begin{array}{c} d\log Nu \\ +d\log k_t \\ -\left(\frac{\eta T_o}{T_w - \eta T_o}\right) d\log \eta \\ -\left(\frac{\eta T_o}{T_w - \eta T_o}\right) d\log T_o \\ +\left(\frac{T_w}{T_w - \eta T_o}\right) d\log T_w \end{array} \right] \quad (C.8)$$

Substituting Overheat and Thermal Loading parameters (See Appendix A), this results in:

$$d\log \Psi_w = \left[d\log Nu + d\log k_t - \left(\frac{\eta}{\tau}\right) d\log \eta - \left(\frac{\eta}{\tau}\right) d\log T_o + \left(\frac{\theta}{\tau}\right) d\log T_w \right] \quad (C.9)$$

It is desired to express all of the terms of this equation in terms of the logarithmic derivatives of U , ρ , T_o , and T_w in order to satisfy the linearized hot wire equations derived in Appendix B. The left-hand side of this equation and the first three terms on the right hand side will be handled individually and put in terms of velocity, density, total temperature and wire temperature.

Beginning with the first term on the right side of equation C.9 , we can find that Nusselt number can be expressed in terms of Mach number, Reynolds number, and overheat ratio, (Morkovin 1954). Nusselt number can also be written in terms of Mach number, Knudsen number, and Thermal Loading, (Baldwin 1958). Using Morkovin's approach

$$\mathbf{dlog\,Nu} = \frac{\partial \log \text{Nu}}{\partial \log M} \mathbf{dlog\,M} + \frac{\partial \log \text{Nu}}{\partial \log \text{Re}} \mathbf{dlog\,Re} + \frac{\partial \log \text{Nu}}{\partial \log \theta} \mathbf{dlog\,\theta} \quad (\text{C.10})$$

Recall from Appendix A that

$$\mathbf{dlog\,M} = \frac{1}{\alpha} \left[\mathbf{dlog\,U} - \frac{1}{2} \mathbf{dlog\,T_o} \right]$$

$$\mathbf{dlog\,Re} = \mathbf{dlog\,\rho} + \mathbf{dlog\,U} - \chi_\mu \mathbf{dlog\,T_o}$$

$$\mathbf{dlog\,\theta} = \mathbf{dlog\,T_w} - \mathbf{dlog\,T_o}$$

Substituting these relationships, equation C.10 we obtain:

$$\mathbf{dlog\,Nu} = \left[\begin{array}{l} \frac{\partial \log \text{Nu}}{\partial \log M} \left[\frac{1}{\alpha} \left(\mathbf{dlog\,U} - \frac{1}{2} \mathbf{dlog\,T_o} \right) \right] \\ + \frac{\partial \log \text{Nu}}{\partial \log \text{Re}} (\mathbf{dlog\,\rho} + \mathbf{dlog\,U} - \chi_\mu \mathbf{dlog\,T_o}) \\ + \frac{\partial \log \text{Nu}}{\partial \log \theta} (\mathbf{dlog\,T_w} - \mathbf{dlog\,T_o}) \end{array} \right] \quad (\text{C.11})$$

Combining like logarithmic terms

$$\mathbf{dlog\,Nu} = \left[\begin{array}{l} \left[\frac{1}{\alpha} \left(\frac{\partial \log \text{Nu}}{\partial \log M} \right) + \left(\frac{\partial \log \text{Nu}}{\partial \log \text{Re}} \right) \right] \mathbf{dlog\,U} \\ + \left[\frac{\partial \log \text{Nu}}{\partial \log \text{Re}} \right] \mathbf{dlog\,\rho} \\ - \left[\frac{1}{2\alpha} \left(\frac{\partial \log \text{Nu}}{\partial \log M} \right) + \chi_\mu \left(\frac{\partial \log \text{Nu}}{\partial \log \text{Re}} \right) + \frac{\partial \log \text{Nu}}{\partial \log \theta} \right] \mathbf{dlog\,T_o} \\ + \left[\frac{\partial \log \text{Nu}}{\partial \log \theta} \right] \mathbf{dlog\,T_w} \end{array} \right] \quad (\text{C.12})$$

The second term of equation C.9 is the thermal Conductivity term, $d\log k_t$, and can be written directly in terms of total temperature:

$$d\log k_t = \left[\frac{\partial \log k_t}{\partial \log T_o} \right] d\log T_o \quad (C.13)$$

Moving on to the thermal loading term of equation C.9, $d\log \eta$, we can determine that it can be expressed in terms of Mach number and Reynolds number.

$$d\log \eta = \frac{\partial \log \eta}{\partial \log M} d\log M + \frac{\partial \log \eta}{\partial \log Re} d\log Re \quad (C.14)$$

Substituting in the relationships for Mach number and Reynolds number

$$d\log \eta = \left[\begin{aligned} & \frac{\partial \log \eta}{\partial \log M} \left[\frac{1}{\alpha} \left(d\log U - \frac{1}{2} d\log T_o \right) \right] \\ & + \frac{\partial \log \eta}{\partial \log Re} (d\log \rho + d\log U - \chi_\mu d\log T_o) \end{aligned} \right] \quad (C.15)$$

Collecting like logarithmic terms:

$$d\log \eta = \left[\begin{aligned} & \left[\frac{1}{\alpha} \left(\frac{\partial \log \eta}{\partial \log M} \right) + \left(\frac{\partial \log \eta}{\partial \log Re} \right) \right] d\log U \\ & + \left[\frac{\partial \log \eta}{\partial \log Re} \right] d\log \rho \\ & - \left[\frac{1}{2\alpha} \left(\frac{\partial \log \eta}{\partial \log M} \right) + \chi_\mu \left(\frac{\partial \log \eta}{\partial \log Re} \right) \right] d\log T_o \end{aligned} \right] \quad (C.16)$$

The left hand side of equation C.9 is the "Electrical Power" term.

$$\mathbf{dlog} \Psi_w = \mathbf{dlog} \left(\frac{E^2}{R_w} \right) \quad (\text{C.17})$$

Expanding this becomes

$$\mathbf{dlog} \Psi_w = 2(\mathbf{dlog} E) - (\mathbf{dlog} R_w) \quad (\text{C.18})$$

For constant temperature anemometry, the wire resistance is held constant resulting in the vanishing of $\mathbf{dlog} R_w$. Equation C.18 is simplified to:

$$\mathbf{dlog} \Psi_w = 2(\mathbf{dlog} E) \quad (\text{C.19})$$

Rewriting equation C.9 with substitutions of C.12, C.13, C.16, and C.19 results in:

$$2(d\log E) = \left\{ \begin{aligned} & \left[\frac{1}{\alpha} \left(\frac{\partial \log Nu}{\partial \log M} \right) + \left(\frac{\partial \log Nu}{\partial \log Re} \right) \right] d\log U \\ & + \left[\frac{\partial \log Nu}{\partial \log Re} \right] d\log \rho \\ & - \left[\frac{1}{2\alpha} \left(\frac{\partial \log Nu}{\partial \log M} \right) + \chi_\mu \left(\frac{\partial \log Nu}{\partial \log Re} \right) + \frac{\partial \log Nu}{\partial \log \theta} \right] d\log T_o \\ & + \left[\frac{\partial \log Nu}{\partial \log \theta} \right] d\log T_w \\ & + \left[\left(\frac{\partial \log k_t}{\partial \log T_o} \right) d\log T_o \right] \\ & - \left(\frac{\eta}{\tau} \right) \left[\begin{aligned} & \left[\frac{1}{\alpha} \left(\frac{\partial \log \eta}{\partial \log M} \right) + \left(\frac{\partial \log \eta}{\partial \log Re} \right) \right] d\log U \\ & + \left[\frac{\partial \log \eta}{\partial \log Re} \right] d\log \rho \\ & - \left[\frac{1}{2\alpha} \left(\frac{\partial \log \eta}{\partial \log M} \right) + \chi_\mu \left(\frac{\partial \log \eta}{\partial \log Re} \right) \right] d\log T_o \\ & - \left(\frac{\eta}{\tau} \right) d\log T_o \\ & + \left(\frac{\theta}{\tau} \right) d\log T_w \end{aligned} \right] \end{aligned} \right\} \quad (C.20)$$

Collecting velocity, density, total temperature, and wire temperature terms

$$2(\mathbf{dlog E}) = \left\{ \begin{aligned} & \left[\left(\frac{\partial \log Nu}{\partial \log Re} \right) + \frac{1}{\alpha} \left(\frac{\partial \log Nu}{\partial \log M} \right) - \frac{1}{\alpha} \left(\frac{\eta}{\tau} \right) \left(\frac{\partial \log \eta}{\partial \log M} \right) - \left(\frac{\eta}{\tau} \right) \left(\frac{\partial \log \eta}{\partial \log Re} \right) \right] \mathbf{dlog U} \\ & + \left[\left(\frac{\partial \log Nu}{\partial \log Re} \right) - \left(\frac{\eta}{\tau} \right) \left(\frac{\partial \log \eta}{\partial \log Re} \right) \right] \mathbf{dlog \rho} \\ & - \left[\begin{aligned} & \chi_\mu \left(\frac{\partial \log Nu}{\partial \log Re} \right) + \frac{1}{2\alpha} \left(\frac{\partial \log Nu}{\partial \log M} \right) - \frac{1}{2\alpha} \left(\frac{\eta}{\tau} \right) \left(\frac{\partial \log \eta}{\partial \log M} \right) \\ & + \left(\frac{\eta}{\tau} \right) - \left(\frac{\partial \log k_t}{\partial \log T_o} \right) + \left(\frac{\partial \log Nu}{\partial \log \theta} \right) - \chi_\mu \left(\frac{\eta}{\tau} \right) \left(\frac{\partial \log \eta}{\partial \log Re} \right) \end{aligned} \right] \mathbf{dlog T_o} \\ & + \left[\left(\frac{\theta}{\tau} \right) + \frac{\partial \log Nu}{\partial \log \theta} \right] \mathbf{dlog T_w} \end{aligned} \right\} \quad (C.21)$$

Equation C.21 is now in the form of the linearized hot wire equation derived in Appendix B and can be written:

$$\mathbf{dlog E} = \{ Su \mathbf{dlog U} + Sp \mathbf{dlog \rho} + ST_o \mathbf{dlog T_o} + ST_w \mathbf{dlog T_w} \} \quad (C.22)$$

where:

$$Su = \frac{1}{2} \left[\left(\frac{\partial \log Nu}{\partial \log Re} \right) + \frac{1}{\alpha} \left(\frac{\partial \log Nu}{\partial \log M} \right) - \frac{1}{\alpha} \left(\frac{\eta}{\tau} \right) \left(\frac{\partial \log \eta}{\partial \log M} \right) - \left(\frac{\eta}{\tau} \right) \left(\frac{\partial \log \eta}{\partial \log Re} \right) \right] \quad (C.23)$$

$$S_p = \frac{1}{2} \left[\left(\frac{\partial \log Nu}{\partial \log Re} \right) - \left(\frac{\eta}{\tau} \right) \left(\frac{\partial \log \eta}{\partial \log Re} \right) \right] \quad (C.24)$$

$$ST_o = -\frac{1}{2} \left[\begin{aligned} &\chi_\mu \left(\frac{\partial \log Nu}{\partial \log Re} \right) + \frac{1}{2\alpha} \left(\frac{\partial \log Nu}{\partial \log M} \right) - \frac{1}{2\alpha} \left(\frac{\eta}{\tau} \right) \left(\frac{\partial \log \eta}{\partial \log M} \right) \\ &+ \left(\frac{\eta}{\tau} \right) - \left(\frac{\partial \log k_t}{\partial \log T_o} \right) + \left(\frac{\partial \log Nu}{\partial \log \theta} \right) - \chi_\mu \left(\frac{\eta}{\tau} \right) \left(\frac{\partial \log \eta}{\partial \log Re} \right) \end{aligned} \right] \quad (C.25)$$

$$ST_w = \frac{1}{2} \left[\left(\frac{\theta}{\tau} \right) + \frac{\partial \log Nu}{\partial \log \theta} \right] \quad (C.26)$$

These sensitivity equations have been derived for a constant temperature anemometer but may be simplified with the implementation of assumptions regarding the effect of "Slip Flow", "Continuum Flow", and "Free Molecular Flow".

Appendix D

Cross Flow Hot Wire Anemometry

The design of an X-wire probe implements the concepts of two yawed sensors which is described by Sandborn (1972). The response of the yawed sensors are used to evaluate the u and v components of the velocity field, (or u and w components depending on the orientation of the yawed sensors). The output voltage from the two X-wires may be written as

$$\frac{e'}{E} = S_u \frac{u'}{U} \pm S_\alpha \frac{v'}{U} \quad (D.1)$$

where S_u is the velocity sensitivity and S_α is the sensitivity to flow angle.

The solution of the equations for a X-wire probe is:

$$\left(\frac{u'}{U}\right)^2 = \frac{S_{\alpha_2}^2 \left(\frac{e'}{E}\right)_1^2 + S_{\alpha_1}^2 \left(\frac{e'}{E}\right)_2^2 + 2 |S_{\alpha_1}| |S_{\alpha_2}| \left(\frac{e'}{E}\right)_1 \left(\frac{e'}{E}\right)_2}{(|S_{\alpha_2}| S_{\alpha_1} + S_{\alpha_1} |S_{\alpha_2}|)^2} \quad (D.2)$$

$$\left(\frac{v'}{U}\right)^2 = \frac{S_{u_2}^2 \left(\frac{e'}{E}\right)_1^2 + S_{u_1}^2 \left(\frac{e'}{E}\right)_2^2 + 2 |S_{u_1}| |S_{u_2}| \left(\frac{e'}{E}\right)_1 \left(\frac{e'}{E}\right)_2}{(|S_{u_2}| S_{\alpha_1} + S_{u_1} |S_{\alpha_2}|)^2} \quad (D.3)$$

where:

$$(e')_1 (e')_2 = \frac{[(e')_1 + (e')_2]^2 - [(e')_1 - (e')_2]^2}{4} \quad (D.4)$$

S_u , $+S_\alpha$, and $-S_\alpha$ were determined for the atmospheric conditions of the low speed regime of the settling chamber of the 8'TPT using a small atmospheric calibration facility.

Appendix E

Table of Bridge Voltages for different Probes

The following tables are intended to provide the basic hot wire calibration information for several three element probes. The wind tunnel conditions and anemometer voltage outputs are tabulated. The dimensions and resistance characteristics of the platinum coated tungsten sensors are also listed.

Test 934 - 8" TPT FLOW QUALITY - Probe 2.1

Wire #	<i>HOT</i> Resistance	<i>COLD</i> Resistance	Wire Dia microns	Length inches	L/Dia	Overheat
1	5.39	2.89	5.0800	0.0450	225.0	1.75
2	3.93	2.59	5.0800	0.0450	225.0	1.50
3	5.32	2.46	5.0800	0.0450	225.0	2.00

Run #	Point #	Po	To	Mach #	Volt 1	Volt 2	Volt 3
16	4	1724.1	539.5	0.6991	5.9814	5.6957	6.6872
16	6	1724.2	539.3	0.6500	5.9670	5.6862	6.6808
16	7	1724.1	539.5	0.5979	5.9510	5.6687	6.6664
16	8	1724.2	539.9	0.5499	5.9238	5.6370	6.6344
16	9	1724.0	539.3	0.4997	5.8917	5.6116	6.5992
16	10	1724.1	539.6	0.4502	5.8373	5.5592	6.5415
16	11	1724.1	540.0	0.3988	5.7684	5.4957	6.4679
17	2	708.9	540.5	0.8276	4.8062	4.6675	5.3929
17	7	709.5	540.2	0.8276	4.8120	4.6699	5.3922
17	8	709.5	540.3	0.8002	4.8240	4.6786	5.4076
17	9	709.4	539.8	0.7498	4.8462	4.7032	5.4375
17	10	709.3	539.4	0.7007	4.8631	4.7168	5.4567
17	11	709.3	539.3	0.6493	4.8708	4.7226	5.4678
17	12	709.4	539.5	0.5979	4.8690	4.7186	5.4681
17	13	709.3	539.6	0.5507	4.8586	4.7057	5.4597
17	14	709.4	539.7	0.5500	4.8572	4.7027	5.4580
17	15	709.3	539.6	0.4987	4.8383	4.6874	5.4403
17	16	709.3	539.9	0.4474	4.8050	4.6537	5.4066
17	17	709.2	539.5	0.3991	4.7680	4.6196	5.3663
18	2	862.7	539.8	0.8257	5.0615	4.9022	5.6433
18	3	862.8	539.9	0.7998	5.0679	4.9070	5.6577
18	4	863.0	539.5	0.7492	5.1024	4.9211	5.6757
18	5	863.0	539.4	0.6984	5.1204	4.9376	5.6966
18	6	863.0	539.7	0.6486	5.1263	4.9364	5.7028
18	7	863.0	539.7	0.6007	5.1211	4.9272	5.6992
18	8	863.1	539.8	0.5496	5.1092	4.9120	5.6887
18	9	863.0	539.8	0.4999	5.0827	4.8924	5.6631
18	10	863.1	540.2	0.4994	5.0809	4.8887	5.6601
18	10	863.1	540.0	0.4501	5.0499	4.8534	5.6296
18	11	863.0	539.9	0.3997	5.0009	4.8044	5.5806
19	12	1431.1	539.9	0.4005	5.5960	5.3223	6.1886
19	13	1431.1	540.1	0.4509	5.6552	5.3786	6.2495
19	14	1431.2	540.1	0.5002	5.7028	5.4250	6.2956
19	15	1431.1	540.2	0.5498	5.7386	5.4592	6.3280
19	16	1431.2	540.4	0.6039	5.7660	5.4876	6.3499
19	17	1431.2	539.9	0.6514	5.7821	5.5098	6.3600
19	18	1431.2	540.3	0.6982	5.7854	5.5148	6.3581
19	19	1431.0	539.7	0.7486	5.7856	5.5181	6.3509
19	20	1431.3	541.7	0.8003	5.7631	5.4926	6.3212
19	21	1431.4	543.1	0.8266	5.7371	5.4583	6.2937

20	22	1499.5	557.3	0.8264	5.7221	5.3908	6.2920
20	24	1499.9	558.6	0.7997	5.7108	5.3813	6.2954
20	24	1499.4	556.8	0.7518	5.7299	5.3968	6.3161
20	26	1498.1	560.6	0.6971	5.7096	5.3606	6.3043
20	26	1499.2	561.2	0.6506	5.7011	5.3523	6.3025
20	27	1499.2	561.0	0.6011	5.6838	5.3328	6.2910
20	28	1499.4	561.4	0.5487	5.6549	5.3034	6.2627
20	29	1499.4	561.1	0.4997	5.6166	5.2665	6.2276
20	30	1499.3	559.4	0.4501	5.5820	5.2445	6.1920
20	31	1499.2	559.5	0.4010	5.5168	5.1804	6.1272
21	4	750.1	560.4	0.8259	4.7734	4.5732	5.3239
21	5	751.0	560.7	0.8259	4.7790	4.5720	5.3229
21	7	750.1	560.7	0.8002	4.7855	4.5769	5.3347
21	8	750.0	560.2	0.7503	4.8138	4.5912	5.3618
21	9	750.0	560.1	0.6995	4.8354	4.6100	5.3862
21	10	750.0	560.2	0.6490	4.8424	4.6127	5.3958
21	11	750.0	560.2	0.5974	4.8404	4.6143	5.3997
21	12	750.0	560.1	0.5500	4.8308	4.6010	5.3916
21	13	749.9	560.0	0.4990	4.8107	4.5792	5.3734
21	14	749.9	560.2	0.4504	4.7785	4.5531	5.3420
21	15	749.9	560.0	0.3991	4.7386	4.5146	5.2994
22	16	904.0	560.4	0.4005	4.9360	4.6830	5.5104
22	17	903.9	561.0	0.4519	4.9795	4.7278	5.5538
22	18	903.9	560.9	0.5008	5.0174	4.7635	5.5882
22	19	904.0	561.0	0.5510	5.0401	4.7857	5.6059
22	20	903.9	561.0	0.5989	5.0554	4.8016	5.6155
22	21	904.0	561.4	0.6513	5.0590	4.8000	5.6123
22	22	904.0	561.3	0.7012	5.0554	4.7996	5.6026
22	23	904.0	561.2	0.7504	5.0428	4.7915	5.5819
22	24	904.0	561.0	0.8005	5.0184	4.7579	5.5464
22	25	903.9	561.0	0.8263	5.0146	4.7604	5.5361
23	26	1809.6	560.8	0.6999	5.9394	5.5836	6.5445
23	27	1808.6	559.8	0.6507	5.9300	5.5714	6.5381
23	28	1809.2	559.3	0.6013	5.9151	5.5617	6.5247
23	29	1808.0	559.7	0.5509	5.8771	5.5234	6.4924
23	30	1807.8	559.5	0.4995	5.8367	5.4840	6.4506
23	31	1808.0	559.8	0.4497	5.7805	5.4292	6.3962
23	32	1808.1	559.6	0.4000	5.7076	5.3692	6.3281

Test 934 - 8" TPT FLOW QUALITY - Probe 7.1

Wire #	HOT Resistance	COLD Resistance	Wire Dia microns	Length inches	L/Dia	Overheat
1	7.72	3.74	5.0800	0.0400	200.0	1.75
2	5.04	3.38	5.0800	0.0400	200.0	1.50
3	6.30	3.62	5.0800	0.0400	200.0	2.00

Run #	Point #	Po	To	Mach #	Volt 1	Volt 2	Volt 3
25	3	1396.2	530.9	0.7999	5.1611	4.3904	4.7691
25	5	1396.1	531.5	0.7998	5.1541	4.3834	4.7596
25	6	1396.1	531.7	0.8272	5.1251	4.3520	4.7311
25	7	1396.1	527.4	0.7517	5.1735	4.3883	4.7738
25	8	1396.0	525.8	0.6954	5.2013	4.4150	4.7999
25	9	1396.0	524.4	0.6483	5.2103	4.4186	4.8067
25	10	1396.0	522.7	0.5998	5.2114	4.4179	4.8062
25	11	1396.0	521.6	0.5505	5.2021	4.4074	4.7957
25	12	1396.0	520.0	0.4998	5.1817	4.3890	4.7771
25	13	1395.8	518.5	0.4502	5.1502	4.3619	4.7490
25	14	1395.8	517.2	0.4014	5.1059	4.3233	4.7059
26	15	698.5	513.4	0.4014	4.3771	3.7745	4.0824
26	16	698.8	513.5	0.4503	4.4075	3.8100	4.1148
26	17	699.2	513.7	0.5002	4.4253	3.8317	4.1333
26	18	698.8	514.2	0.5512	4.4332	3.8463	4.1436
26	19	699.2	514.8	0.6013	4.4328	3.8531	4.1435
26	20	698.2	515.4	0.6510	4.4201	3.8483	4.1335
26	23	710.1	520.1	0.7991	4.3656	3.8182	4.0855
26	24	702.8	520.5	0.8266	4.3340	3.7917	4.0559
27	25	842.1	522.5	0.8265	4.5309	3.9350	4.2215
27	26	842.1	522.5	0.8000	4.5523	3.9521	4.2417
27	27	842.0	520.1	0.7483	4.5794	3.9636	4.2646
27	28	842.1	519.0	0.6973	4.6065	3.9853	4.2907
27	29	842.1	518.1	0.6493	4.6220	3.9937	4.3016
27	30	842.1	517.1	0.6000	4.6300	3.9966	4.3080
27	31	842.1	516.0	0.5507	4.6299	3.9922	4.3069
27	32	842.1	515.1	0.5012	4.6199	3.9793	4.2965
27	33	842.1	514.4	0.4506	4.5982	3.9549	4.2740
27	34	842.1	513.5	0.4001	4.5646	3.9225	4.2420
28	35	1685.3	524.0	0.7480	5.4399	4.6019	5.0021
28	36	1685.2	523.2	0.6971	5.4538	4.6085	5.0135
28	37	1685.2	522.1	0.6504	5.4598	4.6117	5.0178
28	38	1685.1	521.1	0.5993	5.4552	4.6029	5.0138
28	39	1684.9	520.0	0.5487	5.4413	4.5906	5.0009
28	40	1685.0	518.6	0.5008	5.4171	4.5694	4.9791
28	41	1685.2	517.3	0.4503	5.3791	4.5350	4.9433
28	42	1685.1	516.2	0.3999	5.3273	4.4902	4.8966

Test 1005 - 8TPT FLOW QUALITY - Probe 2.2

Wire #	<i>HOT</i> Resistance	<i>COLD</i> Resistance	Wire Dia microns	Length inches	L/Dia	Overheat
1	4.93	2.63	5.0800	0.0400	200.0	1.80
2	4.80	2.31	5.0800	0.0400	200.0	2.00
3	4.98	3.00	5.0800	0.0400	200.0	1.60

Run #	Point #	Po	To	Mach #	Volt 1	Volt 2	Volt 3
13	1	2121.6	580.2	0.8996	6.3809	6.7997	6.3783
13	2	2122.5	580.1	0.8919	6.3836	6.7979	6.3813
13	3	2122.1	578.9	0.7988	6.4236	6.8374	6.4146
13	4	2121.7	580.5	0.6020	6.3789	6.8293	6.3416
13	5	2121.6	582.9	0.4015	6.1437	6.6244	6.0755
13	6	2121.7	569.8	0.4015	6.2517	6.7066	6.2139
13	7	2121.6	569.6	0.6005	6.4689	6.8898	6.4571
14	12	1002.0	569.3	0.9007	5.3136	5.6351	5.3527
14	13	1005.0	569.1	0.8040	5.3777	5.7074	5.4032
14	14	1005.0	569.7	0.5994	5.4110	5.7735	5.4092
14	15	1004.7	569.6	0.3997	5.2765	5.6641	5.2448
14	16	1004.8	579.5	0.8974	5.2477	5.5822	5.2696
14	17	1004.8	579.2	0.7992	5.3062	5.6512	5.3163
14	18	1004.8	578.1	0.6015	5.3517	5.7257	5.3356
14	19	1004.4	578.5	0.4044	5.2311	5.6323	5.1872
15	20	1003.8	589.5	0.8999	5.1759	5.5318	5.1813
15	21	1004.2	589.2	0.8003	5.2382	5.6035	5.2307
15	22	1004.1	588.6	0.6019	5.2767	5.6717	5.2395
15	23	1005.6	588.6	0.3955	5.1492	5.5702	5.0813
16	24	1602.6	590.3	0.8998	5.8467	6.1597	5.8348
16	25	1604.3	589.1	0.8028	5.9019	6.2263	5.8787
16	26	1603.8	589.1	0.6028	5.9006	6.2486	5.8450
16	27	1603.2	589.0	0.4014	5.7214	6.0908	5.6388
16	28	1603.5	579.8	0.4058	5.7955	6.1515	5.7357
16	29	1604.2	580.7	0.6013	5.9668	6.3083	5.9342
16	30	1603.8	579.7	0.8001	5.9849	6.3023	5.9825
16	31	1604.1	580.2	0.9003	5.9430	6.2499	5.9584
16	32	1603.8	568.8	0.9020	6.0285	6.3208	6.0705
16	33	1604.2	568.4	0.7990	6.0825	6.3814	6.1062
16	34	1603.0	570.1	0.5983	6.0653	6.3882	6.0605
16	35	1603.0	568.4	0.4023	5.8930	6.2357	5.8699
17	36	2124.0	569.5	0.4013	6.2572	6.6201	6.2233
17	37	2124.7	571.4	0.6011	6.4537	6.8036	6.4411
17	38	2124.1	570.8	0.8011	6.4904	6.8179	6.5059
17	39	2124.3	589.2	0.7983	6.3366	6.6534	6.3111
17	40	2124.3	589.5	0.6035	6.3103	6.6471	6.2499
17	41	2124.6	589.9	0.3977	6.0824	6.4377	5.9926

Test 1005 - 8'TPT FLOW QUALITY - Probe 3.2

Wire #	HOT Resistance	COLD Resistance	Film Dia microns	Length inches	L/Dia	Overheat
1	7.55	4.92	25.400	0.0500	50	1.50
2	7.52	5.23	25.400	0.0500	50	1.40
3	8.00	4.93	25.400	0.0500	50	1.60

Run #	Point #	Po	To	Mach #	Volt 1	Volt 2	Volt 3
13	1	2121.6	580.2	0.8996	7.4328	6.8243	7.9342
13	2	2122.5	580.1	0.8919	7.4336	6.8174	7.9349
13	3	2122.1	578.9	0.7988	7.4970	6.8327	6.7811
13	4	2121.7	580.5	0.6020	7.4042	6.7211	6.6920
13	5	2121.6	582.9	0.4015	7.0413	6.3623	6.3308
13	6	2121.7	569.8	0.4015	7.1486	6.5003	6.4764
13	7	2121.6	569.6	0.6005	7.5021	6.8419	6.8215
14	12	1002.0	569.3	0.9007	6.2992	4.8152	5.7440
14	13	1005.0	569.1	0.8040	6.3440	4.8352	5.7607
14	14	1005.0	569.7	0.5994	6.2808	4.7266	5.6797
14	15	1004.7	569.6	0.3997	5.9757	4.4624	5.3855
14	17	1004.8	579.2	0.7992	6.1245	4.7244	5.5988
14	18	1004.8	578.1	0.6015	6.2175	4.6364	5.6050
14	19	1004.4	578.5	0.4044	5.9424	4.3579	5.3379
15	20	1003.8	589.5	0.8999	6.1485	4.5692	5.5578
15	21	1004.2	589.2	0.8003	6.1946	4.5747	5.5777
15	22	1004.1	588.6	0.6019	6.1392	4.4818	5.5047
15	23	1005.6	588.6	0.3955	5.8438	4.2119	5.2254
16	24	1602.6	590.3	0.8998	6.8727		6.2182
16	25	1604.3	589.1	0.8028	6.9441		6.2569
16	26	1603.8	589.1	0.6028	6.8790		6.1773
16	27	1603.2	589.0	0.4014	6.5732		5.8710
16	28	1603.5	579.8	0.4058	6.6565		5.9736
16	29	1604.2	580.7	0.6013	6.9551		6.2716
16	30	1603.8	579.7	0.8001	7.0320		6.3678
16	31	1604.1	580.2	0.9003	6.9839		6.3554
16	32	1603.8	568.8	0.9020	7.0873		6.4767
16	33	1604.2	568.4	0.7990	7.1384		6.5058
16	34	1603.0	570.1	0.5983	7.0635		6.4124
16	35	1603.0	568.4	0.4023	6.7604		6.1128
17	36	2124.0	569.5	0.4013	7.1711		6.5038
17	37	2124.7	571.4	0.6011	7.4998		6.8198
17	38	2124.1	570.8	0.8011	7.5884		6.9077
17	39	2124.3	589.2	0.7983	7.3872		
17	40	2124.3	589.5	0.6035	7.3114		
17	41	2124.6	589.9	0.3977	6.9596		

Test 1005 - 8 TPT FLOW QUALITY - Probe 7.2

Wire #	<i>HOT</i> Resistance	<i>COLD</i> Resistance	Wire Dia microns	Length inches	L/Dia	Overheat
1	5.26	2.45	5.0800	0.0450	225.0	2.00
2	5.68	3.34	5.0800	0.0450	225.0	1.60
3	5.31	2.77	5.0800	0.0450	225.0	1.80

Run #	Point #	Po	To	Mach #	Volt 1	Volt 2	Volt 3
19	5	1005.4	578.7	0.8999	5.8093	4.7027	5.2944
19	6	1004.1	578.9	0.8022	5.8788	3.4563	5.3333
19	7	1004.8	573.5	0.6014	5.9632	3.4883	5.4038
19	8	1004.4	576.7	0.4002	5.8153	3.2719	5.2322
19	9	1004.6	575.9	0.2089	5.3767	2.9467	4.8077
20	10	1003.6	588.5	0.8896	5.6990	3.3148	5.2432
20	12	1005.4	588.6	0.6016	5.8299	3.2191	5.3012
20	13	1005.3	587.4	0.4002	5.6977	3.0598	5.1583
20	14	1005.2	585.9	0.2051	5.2583	2.7609	4.7284
21	15	1005.1	569.3	0.2073	5.3473	2.9866	4.8421
21	16	1005.6	568.2	0.4072	5.8004	3.4238	5.2974
21	17	1005.7	568.5	0.6043	5.9190	3.5944	5.4398
21	18	1005.0	570.7	0.8029	5.8457	3.6248	5.4075
21	19	1005.5	569.8	0.8982	5.7775	3.6555	5.3684
22	24	1602.7	569.5	0.8993	6.5612	4.0389	6.0075
22	25	1603.6	569.3	0.7958	6.6048	4.0254	6.0480
22	26	1604.1	566.5	0.6125	6.6336	3.9863	6.0523
22	27	1603.8	570.6	0.6001	6.6090	3.9167	6.0195
22	28	1603.8	568.4	0.4015	6.4351	3.7438	5.8377
22	29	1603.3	565.9	0.2027	5.9140	4.6295	5.3424
23	30	1603.7	580.1	0.8950	6.2981	4.7321	5.2447
23	31	1604.1	578.8	0.8014	6.5319	5.2768	5.9654
23	32	1603.1	577.9	0.6005	6.5347	5.1381	5.9612
23	33	1605.0	578.8	0.3968	6.3629	4.8834	5.7566
23	34	1605.2	577.6	0.2017	5.8165	4.5271	5.2345
24	36	1604.9	570.2	0.4037	6.4097	5.1202	5.8197
24	37	1605.0	571.6	0.5997	6.5871	5.3174	6.0101
24	38	1605.3	570.8	0.8001	6.5795	5.3808	6.0393
24	39	1604.9	570.2	0.9037	6.5256	5.3733	6.0101
25	40	1605.9	590.0	0.8924	6.4128	5.1482	5.8627
25	41	1605.3	589.1	0.8017	6.4710	5.1734	5.9020
25	42	1605.1	588.0	0.6015	6.4916	5.1406	5.8905
25	43	1605.2	588.8	0.3966	6.2926	4.9117	5.6763
25	44	1605.6	589.3	0.3967	6.2885	4.9039	5.6709
25	45	1604.7	587.6	0.1979	5.7520	4.4268	5.1616
26	1	1007.6	569.8	0.8985	5.8131	4.7946	5.3510
26	2	1008.0	569.4	0.8014	5.8876	4.8363	5.4094
26	3	1008.2	568.8	0.5993	5.9429	4.8262	5.4318
26	4	1008.5	566.8	0.4043	5.8248	4.6815	5.3011
26	5	1008.1	567.1	0.2030	5.3805	4.2510	4.8681

27	6	1007.6	579.5	0.9042	5.7457	4.6979	5.2802
27	7	1008.1	578.5	0.7986	5.8345	4.7449	5.3479
27	8	1007.7	579.3	0.6008	5.8854	4.7218	5.3612
27	9	1008.3	578.9	0.4039	5.7600	4.5637	5.2200
27	10	1007.7	578.3	0.2037	5.3245	4.1497	4.7983
28	11	1008.3	589.3	0.9002	5.7311	4.6024	5.2277
28	12	1008.8	589.7	0.8005	5.7924	4.6323	5.2726
28	13	1007.8	589.2	0.5972	5.8445	4.6189	5.2913
28	14	1008.3	589.3	0.4014	5.7076	4.4231	5.1441
28	15	1007.8	586.5	0.2017	5.2795	4.0378	4.7375
29	16	2124.4	586.7	0.2019	6.1419	4.7483	5.5127
29	17	2125.1	590.5	0.3993	6.6944	5.2136	6.0263
29	18	2125.2	588.7	0.6041	6.9430	5.4747	6.2805
29	19	2125.2	590.3	0.8009	6.9493	5.5242	6.3130

Appendix F

Example of Heat Transfer for a Hot-Wire Probe being operated in the Slip Flow Regime

This table is intended to provide the reader with an example of the information necessary to calibrate a hot wire sensor using the indirect approach.

Test 834 - 8TPT FLOW QUALITY - Probe 2.1

Run	Point	Pb	Tb	Mach	Re #	η	Ka	θ 1	θ 2	θ 3	Nu 1	Nu 2	Nu 3
23	26	1809.6	560.4	.5999	54.63	0.9761	.01896	1.6503	1.3519	1.9057	4.3011	5.2376	3.7475
23	28	1809.2	558.9	.6013	49.03	0.9786	.01804	1.6546	1.3553	1.9106	4.2924	5.2452	3.7438
23	27	1808.6	559.4	.6007	51.95	0.9814	.01848	1.6532	1.3543	1.9091	4.2994	5.2345	3.7493
23	32	1808.1	559.2	.4000	34.81	0.9838	.01673	1.6538	1.3547	1.9097	4.0557	5.0217	3.5589
23	29	1808.0	559.3	.5509	45.70	0.9863	.01768	1.6534	1.3544	1.9092	4.2554	5.2154	3.7176
23	31	1808.0	559.4	.4497	38.57	0.9886	.01701	1.6532	1.3542	1.9090	4.1471	5.1074	3.6274
23	30	1807.8	559.1	.4995	42.19	0.9909	.01731	1.6539	1.3548	1.9099	4.2121	5.1734	3.6797
16	6	1724.2	538.9	.6500	51.91	0.9896	.01867	1.7159	1.4056	1.9815	4.2729	5.1458	3.8964
16	8	1724.2	539.5	.5499	45.57	0.9896	.01787	1.7142	1.4042	1.9795	4.2428	5.1262	3.8626
16	4	1724.1	539.1	.6991	54.65	0.9709	.01914	1.7153	1.4051	1.9808	4.2794	5.1347	3.8940
16	7	1724.1	539.1	.5979	48.73	0.9735	.01823	1.7155	1.4053	1.9810	4.2661	5.1487	3.8902
16	10	1724.1	539.2	.4502	38.58	0.9760	.01720	1.7151	1.4049	1.9805	4.1461	5.0397	3.7733
16	11	1724.1	539.6	.3988	34.64	0.9787	.01692	1.7137	1.4038	1.9789	4.0631	4.9583	3.6976
16	9	1724.0	538.9	.4997	42.18	0.9814	.01750	1.7161	1.4057	1.9816	4.2092	5.1023	3.8308
20	24	1499.9	558.2	.7997	49.65	0.9838	.02404	1.6568	1.3572	1.9132	3.9382	4.7688	3.4467
20	22	1499.5	556.9	.8264	50.77	0.9838	.02437	1.6605	1.3602	1.9174	3.9418	4.7529	3.4371
20	24	1499.4	556.4	.7518	47.92	0.9863	.02335	1.6619	1.3614	1.9191	3.9721	4.8022	3.4767
20	28	1499.4	561.0	.5487	37.64	0.9887	.02136	1.6485	1.3504	1.9036	3.9472	4.8351	3.4614
20	29	1499.4	560.7	.4997	34.88	0.9909	.02093	1.6494	1.3511	1.9046	3.9070	4.7951	3.4315
20	30	1499.3	559.0	.4501	32.03	0.9897	.02050	1.6544	1.3552	1.9104	3.8655	4.7590	3.3990
20	26	1499.2	560.8	.6506	42.92	0.9710	.02235	1.6491	1.3508	1.9043	3.9798	4.8522	3.4855
20	27	1499.2	560.6	.6011	40.47	0.9735	.02183	1.6497	1.3514	1.9050	3.9699	4.8470	3.4823
20	31	1499.2	559.1	.4010	28.93	0.9761	.02018	1.6540	1.3549	1.9099	3.7886	4.6732	3.3362
20	28	1498.1	560.2	.6971	45.11	0.9787	.02286	1.6507	1.3522	1.9062	3.9750	4.8275	3.4778
19	21	1431.4	542.7	.8266	50.12	0.9812	.02488	1.7040	1.3958	1.9677	3.9138	4.6880	3.4289
19	20	1431.3	541.3	.8003	49.31	0.9838	.02444	1.7084	1.3994	1.9728	3.9519	4.7445	3.4627
19	14	1431.2	539.7	.5002	34.98	0.9863	.02112	1.7135	1.4036	1.9787	3.9463	4.7788	3.4870
19	16	1431.2	540.0	.6039	40.67	0.9863	.02206	1.7126	1.4029	1.9776	4.0063	4.8331	3.5290
19	17	1431.2	539.5	.6514	43.10	0.9886	.02253	1.7142	1.4042	1.9795	4.0136	4.8374	3.5312
19	18	1431.2	539.9	.6982	45.24	0.9908	.02308	1.7128	1.4031	1.9779	4.0063	4.8240	3.5207
19	12	1431.1	539.5	.4005	28.87	0.9908	.02039	1.7143	1.4042	1.9796	3.8229	4.6472	3.3948
19	13	1431.1	539.7	.4509	32.03	0.9886	.02074	1.7136	1.4037	1.9788	3.8929	4.7233	3.4441
19	15	1431.1	539.8	.5498	37.79	0.9863	.02154	1.7132	1.4033	1.9783	3.9828	4.8124	3.5143
19	19	1431.0	539.3	.7486	47.48	0.9838	.02367	1.7146	1.4045	1.9799	3.9908	4.7937	3.5034
22	16	904.0	560.0	.4005	17.39	0.9810	.03351	1.6514	1.3528	1.9070	3.0358	3.8300	2.6992
22	19	904.0	560.6	.5510	22.79	0.9786	.03544	1.6496	1.3513	1.9049	3.1338	3.9311	2.7728
22	21	904.0	561.0	.6513	25.89	0.9761	.03709	1.6485	1.3504	1.9036	3.1342	3.9045	2.7639
22	22	904.0	560.9	.7012	27.29	0.9735	.03801	1.6489	1.3507	1.9040	3.1172	3.8752	2.7466

22	23	904.0	560.8	.7504	28.57	0.9709	.03900	1.6490	1.3508	1.9043	3.0899	3.8353	2.7188
22	24	904.0	560.6	.8005	29.78	0.9696	.04008	1.6496	1.3513	1.9050	3.0481	3.7543	2.6770
22	17	903.9	560.6	.4519	19.31	0.9697	.03412	1.6495	1.3512	1.9048	3.0811	3.8877	2.7358
22	18	903.9	560.5	.5008	21.08	0.9710	.03473	1.6500	1.3516	1.9054	3.1168	3.9196	2.7626
22	20	903.9	560.6	.5989	24.33	0.9734	.03618	1.6495	1.3512	1.9048	3.1414	3.9316	2.7749
22	25	903.9	560.6	.8263	30.34	0.9762	.04069	1.6497	1.3513	1.9050	3.0378	3.7459	2.6634
18	8	863.1	539.4	.5496	22.81	0.9786	.03569	1.7145	1.4045	1.9799	3.1560	3.8916	2.8399
18	10	863.1	539.8	.4994	21.07	0.9812	.03501	1.7133	1.4035	1.9785	3.1328	3.8817	2.8187
18	10	863.1	539.6	.4501	19.29	0.9839	.03438	1.7138	1.4039	1.9791	3.1041	3.8454	2.7948
18	4	863.0	539.1	.7492	28.66	0.9863	.03925	1.7163	1.4051	1.9807	3.1032	3.8102	2.7979
18	5	863.0	539.0	.6984	27.34	0.9886	.03821	1.7155	1.4053	1.9811	3.1360	3.8584	2.8258
18	6	863.0	539.3	.6486	25.92	0.9908	.03730	1.7147	1.4046	1.9801	3.1549	3.8826	2.8394
18	7	863.0	539.3	.6007	24.46	0.9937	.03648	1.7146	1.4045	1.9800	3.1594	3.8914	2.8429
18	9	863.0	539.4	.4999	21.10	0.9967	.03499	1.7144	1.4044	1.9798	3.1339	3.8836	2.8214
18	11	863.0	539.5	.3997	17.38	0.9709	.03381	1.7142	1.4042	1.9795	3.0533	3.7872	2.7525
18	3	862.8	539.5	.7998	29.85	0.9734	.04040	1.7142	1.4042	1.9796	3.0516	3.7693	2.7733
18	2	862.7	539.4	.8257	30.42	0.9761	.04101	1.7144	1.4043	1.9797	3.0386	3.7506	2.7557
21	5	751.0	560.3	.8259	25.22	0.9787	.04894	1.6504	1.3519	1.9058	2.7586	3.4530	2.4622
21	4	750.1	560.0	.8259	25.21	0.9814	.04897	1.6513	1.3527	1.9069	2.7512	3.4514	2.4628
21	7	750.1	560.3	.8002	24.71	0.9838	.04828	1.6504	1.3519	1.9058	2.7712	3.4717	2.4764
21	8	750.0	559.8	.7503	23.75	0.9863	.04693	1.6519	1.3531	1.9075	2.8130	3.5113	2.5080
21	9	750.0	559.7	.6995	22.66	0.9886	.04568	1.6522	1.3534	1.9079	2.8491	3.5635	2.5379
21	10	750.0	559.8	.6490	21.48	0.9909	.04456	1.6520	1.3533	1.9077	2.8686	3.5934	2.5542
21	11	750.0	559.8	.5974	20.18	0.9908	.04351	1.6519	1.3532	1.9076	2.8777	3.6221	2.5653
21	12	750.0	559.7	.5500	18.92	0.9885	.04262	1.6523	1.3535	1.9081	2.8763	3.6233	2.5642
21	13	749.9	559.6	.4990	17.47	0.9862	.04177	1.6525	1.3536	1.9082	2.8631	3.6130	2.5539
21	14	749.9	559.8	.4504	16.00	0.9837	.04105	1.6519	1.3532	1.9075	2.8352	3.5967	2.5305
21	15	749.9	559.6	.3991	14.39	0.9813	.04035	1.6525	1.3537	1.9082	2.7970	3.5558	2.4963
17	7	709.5	539.8	.8276	25.03	0.9786	.04995	1.7131	1.4033	1.9782	2.7470	3.4061	2.5158
17	8	709.5	539.9	.8002	24.53	0.9760	.04917	1.7128	1.4031	1.9779	2.7659	3.4303	2.5336
17	9	709.4	539.4	.7498	23.56	0.9734	.04779	1.7145	1.4044	1.9798	2.7998	3.4823	2.5680
17	12	709.4	539.1	.5979	20.05	0.9709	.04431	1.7154	1.4052	1.9809	2.8559	3.5675	2.6173
17	14	709.4	539.3	.5500	18.76	0.9697	.04342	1.7146	1.4046	1.9800	2.8521	3.5665	2.6141
17	10	709.3	539.0	.7007	22.52	0.9760	.04654	1.7157	1.4054	1.9812	2.8282	3.5197	2.5925
17	11	709.3	538.9	.6493	21.33	0.9786	.04537	1.7159	1.4056	1.9815	2.8473	3.5498	2.6100
17	13	709.3	539.2	.5507	18.79	0.9812	.04343	1.7151	1.4050	1.9806	2.8533	3.5650	2.6157
17	15	709.3	539.2	.4987	17.31	0.9837	.04255	1.7151	1.4049	1.9805	2.8396	3.5	2.6038
17	16	709.3	539.5	.4474	15.77	0.9863	.04178	1.7142	1.4042	1.9794	2.8105	3.5	2.5780
17	17	709.2	539.1	.3991	14.27	0.9886	.04111	1.7152	1.4050	1.9807	2.7747	3.4986	2.5450
17	2	708.9	540.1	.8276	24.99	0.9908	.05002	1.7122	1.4026	1.9772	2.7409	3.4049	2.5165

VITA

Gregory S. Jones was born on October 2, 1951 in Jeffersonville, Indiana. He graduated from Jacksonville Arkansas high school in May of 1970. After serving six years in the military as an electronic technician, he was discharged with honors as a disabled veteran. He obtained a Batchlors degree from the Mechanical Engineering department of VPI & SU in 1979, then transfered to the Engineering Science and Mechanics department of VPI & SU where he graduated with a master of science degree in 1980. As an instructor in the Engineering Science and Mechanics department he entered the Ph.d program in 1980. He then transfered to the Aerospace department at Georgia Tech when he relocated as a Associated Scientist working in the Advanced Flight Sciences department of Lockheed Georgia Corp. He specialized in advanced measurement techniques that included 3-D laser velocimetry, laser interferometry, hot wire anemometry, and flow visualization. He transfered back to VPI & SU in 1986, as a part time student. when he relocated to NASA Langley Research Center as a Research Scientist. He specializes in flow diagnostics focusing on basic fluid mechanics that includes transitional flows, separated flows, and unsteady flows.

He is currently involved in AIAA and ASME. He is also actively involved in the Boys Scouts of America as a Scoutmaster, and Williamsburg Community Chapel.